ADVECTION, DIFFUSION AND SETTLING IN THE COASTAL ZONE OF LAKE ERIE

BY

ALAA ELDIN ELZAWAHRY, B.Sc, M.Eng.

A Thesis

Submitted to the School of Graduate Studies in

Partial Fulfillment of the Requierments

for the Degree

Doctor of Philosophy

Mcmaster University

ADVECTION, DIFFUSION AND SETTLING IN THE COASTAL ZONE OF LAKE ERIE

ADVECTION, DIFFUSION AND SETTLING IN THE COASTAL ZONE OF LAKE ERIE

BY

ALAA ELDIN ELZAWAHRY

DOCTOR OF PHILOSOPHY (1985)
(Civil Engineering)

McMASTER UNIVERSITY
Hamilton Ontario

TITLE: Advection, Diffusion and Settling in the Coastal Boundary Layer of Lake Erie.

AUTHOR: Alaa Eldin Elzawahry B.Sc. (Cairo University)
M.Eng. (McMaster University)

SUPERVISOR: Dr. W. James

NUMBER OF PAGES: XVI, 251

To My Parents,

My Wife and My Daughters.

ABSTRACT

Pollution in the coastal zones of the Great Lakes has become more serious in recent years. This is due to increased use of coastal water as a result of population and industrial growth. A substantial portion of the contaminants that enters a lake do so from the shoreline via discharges from sewer overflows, industrial outfalls and runoff. Such discharges contain particulates and other materials of density greater than that of lake water. Many heavy metals with toxic components are present in these fractions. The dynamic behavior of these particles in the coastal and offshore waters is thus of great importance. The principal removal processes for these materials are transport and particle settling. An understanding of the characteristics of nearshore currents, diffusion and temperature patterns is essential to determine their effect on removal processes, and in turn, on coastal biological and chemical processes. This study is limited to the physical fluid mechanics of coastal zones.

The structure of the nearshore flow in the vicinity of Cleveland, Ohio is analyzed in detail in this study. The impact of Cleveland, one of the largest urban and industrial agglomerations on the shoreline of Lake Erie, in terms of additional loading is thought to be considerable. A computer program (ADVDIFF) was developed to calculate the mean flow, horizontal turbulent length and time scales, horizontal diffusivities and kinetic energy. ADVDIFF uses filtering techniques, spectral analyses and

statistical analyses. Five episodes representing three different flow regimes which may exist in the coastal zone were chosen for special analyses.

To generate the coastal currents, a rigid-lid, channel-type model with fine grid size in the coastal zone was used. A model originally developed by Simons (1983) was modified to include nonlinear acceleration terms and two different forms of the vertical eddy viscosity. Also, a two dimensional x-y model developed by Simons and Lam (1982) was modified and used to explain some of the observations. Both new models (ERCH, ONELAY) were verified, calibrated and applied to Lake Erie.

A computer program (SEDTRAN) was developed to predict the inflow sediment concentration distribution within the coastal zone. SEDTRAN solves numerically the three dimensional time-dependent mass transport equation including the settling term. The model uses the currents and diffusivities computed by ERCH and ONELAY and the statistical analyses, respectively. SEDTRAN was verified using several test examples, and partially validated using the available data set. The model was applied to many cases of settling activity that may take place in the coastal zone. The results were used to define a representative influence zone for a pollutant source at Cleveland.

ACKNOWLEDGEMENTS

I wish to acknowledge with deep and sincere gratitude the assistance, guidance and encouragement of my advisor Dr. W. James. I am thankful to my supervisory committee members, Dr. C.R. Murthy, Dr. W. Snodgrass and Dr. J. Vlachopoulos for their assistance and continuing intreset in the work.

Special thanks are due to Dr. D.C.L. Lam and T.J. Simons for the use of their hydrodynamic models. In addition I wish to thank J.A. Bull and F. Chiocchio for producing some of the plots used in this study.

The author is grateful to the National Water Research Institute (Burlington, Ontario) and the Great Lakes Environmental Research Laboratory (Ann Arbor, Michigan) for providing the current meter data used in this study.

I am grateful to the Civil Engineering Department, McMaster University for providing the support during the study period. I am also thankful to the Irrigation and Hydraulics Department, Cairo University for having provided study leave.

Finally, I must thank my wife Faten, my daughters Ola and Yomna and my family for their assistance, support and patience during my study.

TABLE OF CONTENTS

LIST OF FIGURES

LIST OF TABLES

CHAPTER 1

SCOPE AND OBJECTIVES OF THE STUDY

1.1 INTRODUCTION

Coastal zones of Great Lakes are very complex environments. Investigations of these nearshore regions have become important in recent years due to increased demands on coastal zones caused by population and industrial growth. A substantial portion of contaminants enters a lake from the shoreline via discharges from sewers, industrial outfalls and runoff. The principal removal processes for these materials are transport and particle settling. An understanding of the characteristics of nearshore currents, diffusion and temperature patterns is essential to determine their effect on the removal processes, and in turn, on coastal biological and chemical processes.

Sediment is considered to be one of main indices of water pollution. All discharges into the coastal zones contain particulate and other materials of density greater than lake water. Many heavy metals with toxic components are present in these fractions. The dynamic behavior of these heavy particles in both coastal and offshore waters is thought to be of great importance.

The sediment distribution in the coastal zone is influenced by the coastal current regime, the mixing processes and thermal structure. Three types of current structure can be readily identified: (1) strong shore-parallel current regimes persisting for several days, (2) episodes of reversals of currents and (3) episodes of weak currents. The mixing processes govern the passage of sediment through the coastal boundary layer where the diffusive eddies are limited to the proximity of the shoreline. The thermal structure in the coastal zone is complicated. It is commonly observed that a strong thermocline acts as a "diffusive floor" suppressing the vertical turbulence and inhibiting diffusion of material into the hypolimnion. However the wind stress and associated water currents move the thermocline vertically (upwelling and downwelling); if the wind stress is great enough the thermocline may intersect the water surface. Complete mass exchange of water between the coastal and offshore waters may then occur.

The question is frequently asked whether a shoreline or nearshore source of contaminants is a problem only to the immediate area surrounding the outfall, or whether the entire basin is affected by the material. The answer may be determined by the interplay between two time-scales, one characterized by the settling of the sediment and the other characterized by the transport and mixing of nearshore parcels of water with the main body of the lake. The mixing processes in turn are governed by two scales: (i) a time-scale which governs the transport of materials through the coastal boundary layer where the diffusion eddies are limited by the proximity of the shoreline and (ii) a time-scale which governs the diffusion of material through the main body of the lake.

The starting point of this work is the observational program undertaken by Canada Centre for Inland Waters (CCIW) and the National Oceanic and Atmospheric Administration (NOAA) in the vicinity of Cleveland, Ohio, in Lake Erie, during 1979. The city of Cleveland represents one of the largest urban and industrial agglomerations on the lake.

1.2 OBJECTIVES

The main objectives were: (i) to obtain a satisfactory definition of the Lake Erie coastal boundary layer and to reveal the transport and mixing characteristics within that zone using the available wind, current and temperature observations; (ii) to compute the currents within the coastal zone using hydrodynamic models; (iii) to obtain the time and spatial distribution of urban sediments within the coastal zone by solving the sediment transport equation, using results from (i) and (ii); (iv) by identifying and simulating different flow regimes in the coastal zone, define the critical (worst) cases from a pollution disposal point of view; and (v) as a conclusion, to define the influence zone of a nearshore source based on the 3-d transient mass transport model and typical coastal current episodes. The objectives are shown in Figure 1.1, which also identifies the three main phases of this study: (1) data analysis, (2) hydrodynamic modeling and (3) transport modeling. Each phase is discussed below.

1.3. OUTLINE OF THE STUDY

(1) Data analysis

Using the observed flow data, the flow and dispersion properties within the coastal zone in the vicinity of Cleveland, were studied in detail (Chapters 3 and 4). Using filtering techniques and statistical

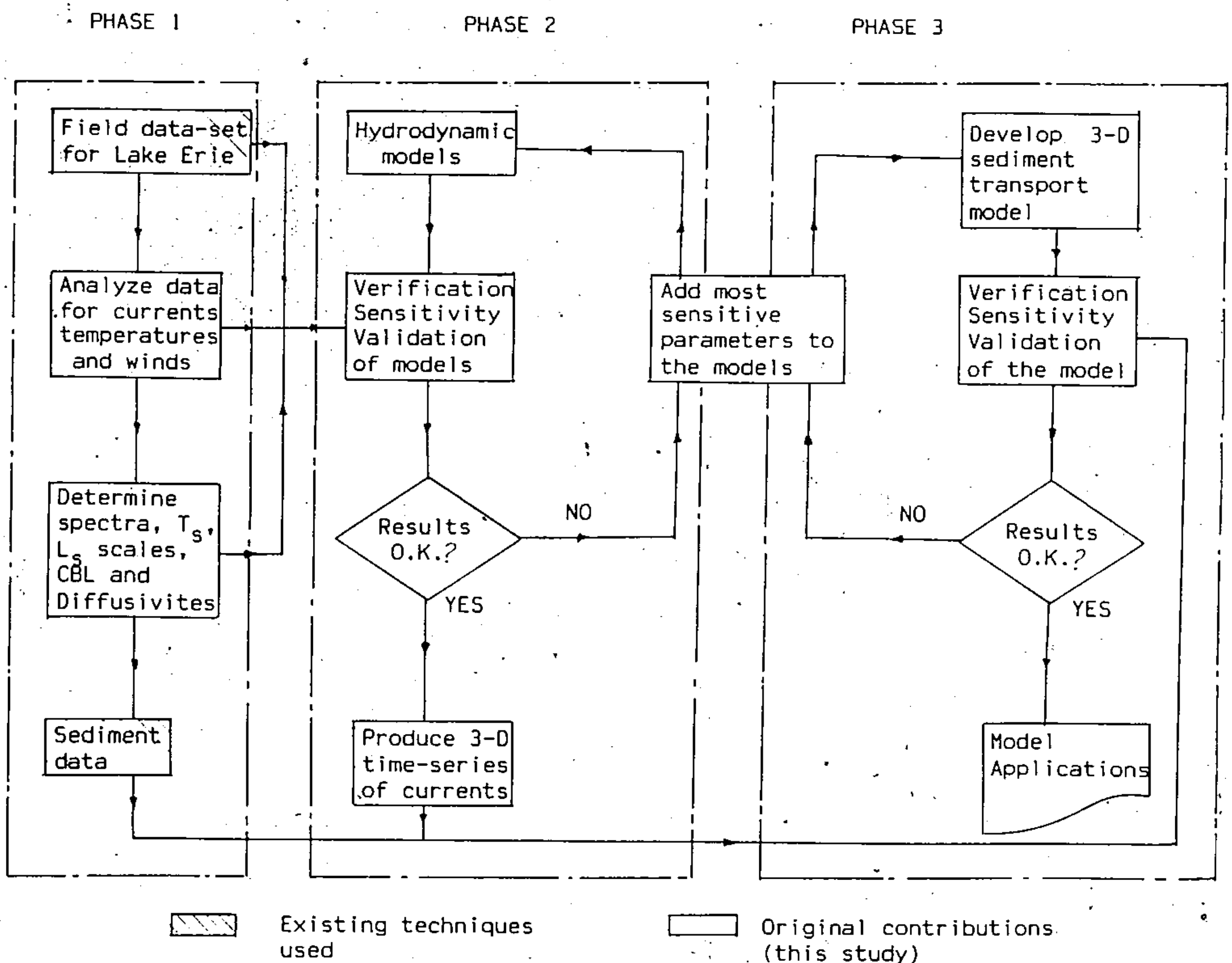

Figure 1.1 Study scope and objectives

and spectrum analyses, the mean flow, horizontal turbulent length and time scales, horizontal diffusion coefficients and the kinetic energy properties were computed. The horizontal turbulent length and time scales were used to define the time and space increment in the numerical solution of the momentum and the mass transport equations (Chapters 5 and 6). The horizontal diffusivities were used to define the diffusion law to solve the mass transport equation (Chapter 6).

(2) Hydrodynamic models

Currents in the nearshore region differ markedly from those in the offshore regions. Stratification, nonlinear accelerations, bottom topography and friction may all be of great importance in the coastal boundary layer. To resolve the small time and length scales of the coastal zone eddies, a fine numerical grid size is required. To resolve the entire lake using such a fine grid is very expensive in terms of computer resources. Pollutant transport within the coastal boundary layer is highly sensitive to the vertical current structure and to the magnitude of the vertical current, especially during upwelling and downwelling episodes.

To generate coastal currents, including the vertical structure of the currents, a rigid-lid channel-type model, with fine grid in the coastal zone developed by Simons (1983) was modified to include the non-linear acceleration terms. Two different forms of the vertical eddy viscosity, representing two different hypotheses concerning the vertical transfer of momentum were added. The model is called ERCH herein. Also, a two dimensional x-y model developed by Simons and Lam (1982) was modified and used to explain some of the observations. The new model is called ONELAY. ERCH and ONELAY were verified, calibrated and applied to Lake Erie (Chapter 5).

(3) Transport model

Most, if not all, existing mass transport models are two dimensional (x-y). The mass transport equation is solved in the x and y co-ordinate directions using vertically integrated currents to obtain vertically integrated pollutant concentrations. These models do not account for the vertical oscillation of the thermocline (upwelling and downwelling) which take place quite frequently within the coastal boundary layer. They also do not account for the vertical variability of the horizontal currents. The three dimensional time dependent sediment transport equation is solved in Chapter 6. The model is called SEDTRTAN. The currents computed by the channel model (Chapter 5) were used to compute the sediment plume or patch. The horizontal diffusivities are assumed to be constant or a function of time based on each individual case. The values of the diffusivities were obtained from the statistical analysis in Chapter 4. SEDTRAN was verified using many test examples, and partially validated using the available sediment data set. SEDTRAN was applied to many of the cases of settling activity that may take place in the coastal zone. The results of all the simulated cases were used to define a representative influence zone for a pollutant source at Cleveland.

CHAPTER 2

BACKGROUND REVIEW

2.1 INTRODUCTION

As mentioned earlier, this study covers three different but interrelated topics: data analysis, hydrodynamic modeling and transport modeling. A considerable literature on each topic exists. This chapter furnishes the ground work for the the three topics. A background review and a literature survey of relevant studies in each topic is presented.

2.2 DATA ANALYSIS

Several extensive data bases from long term observational programs in the coastal waters of the Great Lakes are in existence. However mathematical models capable of synthesizing the many ~~different~~ flow regimes and the turbulence characteristics into a general predictive scheme do not exist. A statistical descriptive analysis of the characteristics of the coastal zone is needed.

2.2.1 Diffusion

1. Horizontal diffusion

Okubo (1971) discussed two fundamental diffusion diagrams on the basis of the analysis of data obtained from the sea. The two diagrams are: (a) the variance of the horizontal distribution of the pollutant versus the diffusion time, and (b) the horizontal diffusivity versus the diffusion length scale. To obtain the diffusion diagrams, he used 20 sets of data from instantaneous dye releases in the upper mixed layer of the sea. The data covered a time scale of diffusion ranging from 2 hours to 1 month and length scale from 30 m to 100 km. Bowden et al. (1974) suggested a theoretical framework to explain the relation between the two diffusion diagrams. The horizontal eddy diffusivity may be represented by:

$$K = \frac{1}{2} \frac{d\sigma^2}{dt} \qquad [2.1]$$

where K is a diffusion coefficient, σ is the standard deviation of the concentration, and t is time. A log-log plot of the variance against the diffusion time produces a straight line of the form:

$$\sigma^2 = a\, t^m \qquad [2.2]$$

where a and m are constants. From [2.1] and [2.2], K is given by:

$$K = (ma/2)\, t^{m-1} \qquad [2.3]$$

so that K can be computed for a given diffusion time from the constants a and m. It follows from [2.2] and [2.3] that

$$K = c\sigma^n \qquad [2.4]$$

where $c = (m/2)\, a^{1/m}$ and $n = 2(m-1)/m$. Bowden et al. (1974) summarized the relation between the index m and the theoretical diffusion characteristics. If m=1, the variance grows linearly with the diffusion time [2.2]. This corresponds to Fickian diffusion with constant K, [2.3]. If m=2, K increases linearly with t, while σ grows as the square of t. This corresponds to linear length scale diffusion. The case of m=3, corresponds to K being proportional to $\sigma^{4/3}$, σ growing as the cube of t, and K growing as the square of t. This corresponds to the classical Richardson "four-thirds power law". Table 2.1 summarizes the diffusion models. In the Okubo (1971) study m = 1.15.

Table 2.1 Summary of diffusion models

m [2.3]	n [2.4]	Diffusion Law	Diffusion Parameters	Diffusion Model
1	0	K = const.	Constant diffusivity (cm/s)	Fickian diffusion
2	1	$K \propto qL$	q diffusion velocity (cm/s) L length scale (cm)	Linear length scale diffusion
3	4/3	$K \propto \varepsilon^{1/3} L^{4/3}$	ε energy dissipation rate (cm^2/s^3) L length scale (cm)	Inertial sub-range diffusion

Murthy (1971) investigated the diffusion characteristics of the hypolimnion in the Lake Erie central basin. The investigation was carried out to define the peak concentration and the vertical and horizontal spread of a dye patch at different times. The thermocline acted as a diffusion floor inhibiting the upward flux, hence the vertical spread was restricted to the hypolimnion. The horizontal spread was small, at least one order of magnitude smaller than surface layer diffusion for a comparable time scale.

Murthy (1972) studied the horizontal diffusion from dye plume experiments in Lakes Ontario and Huron. He calculated the horizontal diffusion due to rapid current changes caused by rapidly changing wind systems. The eddy diffusivities calculated for such cases were enhanced by a factor of 2-4 over those for steady currents. The vertical diffusion of the dye was suppressed significantly due to summer thermal stratification. In the steady currents, the eddy diffusivity attained a constant value at a large distance from the source (up to 2000 m). The conclusions drawn were confirmed by earlier studies (Csanady, 1964, 1968; Bowden, 1965). Csanady (1968) showed that in the early stage of diffusion, within a distance of 300-500 m from the source, the diffusion grows rapidly according to the "4/3 power law". Beyond 2000 m, the accelerated growth is due to the lake current (current shift).

Murthy (1973) also studied large-scale horizontal diffusion in the epilimnion of Lake Ontario. A dye solution was introduced at mid-depth of the epilimnion. The data covered a length scale (patch size) of 100 m to 15 km. The values of the longitudinal and lateral diffusivities were calculated using [2.1] to [2.4]. Longitudinal diffusivities were larger than the lateral by a factor of 2-10. The data surprisingly supported the "4/3 power law". During the initial stage of diffusion (order of hundreds of meters), marked anisotropy of turbulence combined with vertical shear in the longitudinal mean current, gave rise to an apparent increase in the longitudinal diffusion of the patch. For large diffusion times, when the patch grows to the size of kilometers, localized non- uniformities in the flow did not appear to influence the overall diffusion of the patch.

From dye experiments conducted at different locations and depths of Lake Ontario, Murthy (1976) found that the value of m lies between 2 and 3 (shear diffusion and inertial subrange diffusion). The longitudinal eddy diffusivity was greater by a factor of 5-10 than the lateral eddy diffusivity in the early stages of diffusion, and by a factor of 2-3 for large diffusion times. Murthy (1976) and Okubo (1971, 1974) showed that the diffusion in the hypolimnion is smaller than that in the epilimnion. The available turbulent energy for diffusion decreases with depth. Callaway (1974), Kuehnel et al. (1981), Lam and Murthy (1978), Lam and Durham (1984), Lam et al. (1981), Murthy and Kenney (1974) and Murthy and Miners (1978) all showed also that m lies between 2 and 3.

All the previously reviewed studies used a dye tracer either in a patch or plume to investigate diffusion characteristics. The dye experiment seeks the description of particle position as time passes by specifying the particle trajectory (Lagrangian measurements). Another Lagrangian measurement technique commonly used in the Great Lakes uses drogues. The path of individual drogues can be tracked using known reference points. The drogue positions are plotted simultaneously as progressive location plots with time. The current characteristics at the study sites can be described by Lagrangian deformation rates and the deriving turbulence statistics. Literature on the types of drogues, statistical analysis of drogue data and the comparison between drogues, dye and current-meter measurements is available (Bengtsson, 1976; Konyayeve and Merinova, 1983; Molinari and Kirwan, 1975; Murthy, 1973, 1975; Okubo, 1970, 1976; Okubo and Ebbesmeyer, 1976).

The second type of measurement technique is the Eulerian technique. The Eulerian system seeks the description of the velocity at each point in space and time through a direct specification of the velocity. Callaway (1974) analyzed current-meter data obtained off the Oregon coast during the summer of 1972. Callaway (1974) modified and used the computer program presented by Ahn and Smith (1972). The turbulent velocity was computed by dividing the velocity record into segments, fitting a second-order polynomial to these segments and taking the residuals from the fit to be the fluctuational velocity. The time scale was computed by calculating the autocorrelation coefficients and integrating to the point of the first zero crossing. The length scale was computed using the Taylor (1921) hypothesis, which states that, if the mean velocity is much larger than the mean fluctuations at a fixed point of a homogeneous turbulent flow, the flow behaves as if the whole turbulent flow field passes that point with constant mean velocity. The diffusion coefficient was computed using the Hay and Pasquill (1959) assumption. From the observations of crosswind spread of particles 100 m from a continuous ground-level source they showed that the Lagrangian and Eulerian correlograms have similar shapes but different scales (ratio β:1). They reported that β has considerable scatter, with an average of four. Several values of the β coefficient have been reported. Krasnoff and Peskin (1971) summarized some of these and found values ranging from 1.5 to 11.3 for conditions of laboratory experiment grid turbulence and the atmospheric boundary layer respectively. Callaway (1974) showed that a unit power law (linear length scale diffusion) provides reasonable fit between diffusivity and length scale.

Murthy and Dunbar (1981) using current-meter data off Douglas Point, Lake Huron, computed the mean and fluctuations using numerical filtering techniques (Graham, 1963). They used the inertial frequency (16 - 18 hours) as cut-off frequency for the low-pass filter, and the variance of the fluctuations as a quantitative measure of the turbulence level in the flow. They showed that the turbulence index (ratio between fluctuations variance and scalar speed) attains high values close to and far from the shore, with lower values between. These high values are due to the influence of the friction close to the shore and the inertial oscillation far from the shore.

Boyce and Hamblin (1975), followed the approach of Ketchum and Keen (1955) in estimating the horizontal diffusion through a simple balance for the entire basin. They solved analytically the advection diffusion equation using the central basin of Lake Erie as a channel with a point source at the Grand river. Using the distribution of chloride ions, they showed that the best representative value for the horizontal diffusion coefficient is 1.5×10^6 cm^2/s.

2. Vertical diffusion

Several values of vertical eddy viscosity/diffusivity covering a wide range (0.001 - 350 cm^2/s) were reported. Usually the eddy viscosity coefficient which represents the transfer of momentum is larger than that of material transfer (eddy diffusivity coefficient). The momentum is transfered by the pressure fluctuation and translation of mass, while the diffusion of material is accomplished only by the latter. The vertical eddy viscosity A_z is usually estimated from measurements of horizontal current as a function of time and depth, while that of diffusivity K_z is estimated from measurments of temperature/concentration as a function of time and depth. In the case of A_z, the vertical transfer of momentum may be written as:

$$\frac{\tau_{zx}}{\rho} = A_z \frac{\partial u}{\partial z} \qquad [2.5]$$

where τ_{zx} is the stress in the x direction across a plane perpendicular to the vertical axis z, u is the velocity in the x direction and ρ is water density. Simons (1973a) analyzed data from vertical current meter strings located in Lake Ontario, 1972. To compute A_z, he assumed that the shear stress between adjacent layers follows [2.5]. Most of the time, A_z at 10 m depth averaged 50 cm^2/s, a value reported earlier by Platzman (1963). During high wind speeds, A_z increased by a factor of 7. Several assumptions appear in the literature about the vertical eddy viscosity (Ekman, 1905; Gonella, 1971; Csanady, 1972a; Pollard and Millard,1970). An excellent review has been given by Boyce (1974).

In general there are two hypotheses concerning the vertical transfer of momentum during stratified periods. The first idea states that the turbulence is generated at or near the air/water interface and is suppressed at the thermocline by the sharp temperature gradient. Therefore A_z in the hypolimnion is much smaller than that of the epilimnion and may be as small as that of the thermocline (Walters et al., 1978; Simon, 1980a and Lam et al., 1983). The second idea states that the turbulence in the hypolimnion is generated by internal waves as well as the air/water interface. Hence, A_z in the epilimnion is much greater than that of the thermocline (Heinrich et al., 1981). Detailed derivation, discussion and comparison between the two approaches is given in Chapter 5.

In the case of the vertical eddy diffusivity K_z, the vertical transport of material can be written :

$$F = K_z \frac{\partial C}{\partial z} \qquad [2.6]$$

where F is the material vertical flux per unit area, C is the material concentration (C can be replaced by temperature in the case of vertical transport of heat). To relate the time and space derivative, the following form may be used:

$$A(z) \frac{\partial C(z,t)}{\partial t} = \frac{\partial}{\partial z} \left(A(z) K_z(z) \frac{\partial C(z,t)}{\partial z}\right) \qquad [2.7]$$

where A is the cross-sectional area of the lake as a function of z. Equation [2.7] can be used to estimate K_z as a function of depth. The time and space derivatives can be computed from a concentration or temperature survey, (for example, Blanton, 1973). Kullenberg (1969, 1971), using tracer measurements in stratified shallow water and vertical current shear, computed the vertical diffusion coefficient. The values of K_z varied between 0.09 and 60 cm^2/s. He proposed a semi-empirical equation relating K_z to stratification (vertical density gradient), wind velocity and the vertical gradient of horizontal current. Murthy (1972) using dye measurements in the coastal waters of Lakes Huron and Ontario, calculated K_z in the presence of a sharp thermocline. The vertical standard deviation of the dye was estimated from the concentration profile. K_z was computed using [2.1], and attained a very low value of 0.1 cm^2/s.

Kullenberg et al. (1974) investigated vertical mixing in relation to vertical temperature and current structures, using data from an instantaneous point-source, sub-surface dye experiment. They interpreted the several observed profile structures suggesting many possible processes.

2.2.2 Coastal currents

The current flow regimes in large lakes exhibits special characteristics near the coastal boundary layer. Experimental studies in the Great Lakes have shown that the current regimes are extremely complex (Murthy, 1972 and Murthy and Blanton, 1975). The coastal currents differ from one location to another and from season to season. Based on several detailed experimental studies in a number of locations (Bull and Farooqui, 1976; Bull and Murthy, 1980 and Elzawahry and James, 1981) the following coastal flow regimes may be identified: (i) periods of strong alongshore currents persisting for several days; (ii) periods of current reversals during which shore-parallel currents turn around within a few hours; and (iii) periods of weak currents, sometimes stagnation, with irregular changes in direction. Murthy (1973) analyzed flow data obtained off Oshawa, Lake Ontario. The location has a long and straight shoreline and relatively regular bathymetry, and is known for persistent regular currents (Csanady, 1972b,c). The measurments covered both Lagrangian and Eulerian techniques, using drogues and current meters respectively. Differences between the mean currents computed by the two techniques were due to the progressive flow (Stokes, 1847 and Longuet-Higgins, 1969). The component of Stokes velocity (difference between Lagrangian and Eulerian means) was not computed, but it appeared to be small.

Blanton (1974,1975) analyzed current meter data obtained off Oshawa, Lake Ontario, 1970. The response of the current to the wind lagged about 6 to 36 hours, depending on the season and the distance offshore. Total energy of the currents within each season decreased with distance offshore. The same finding was reported earlier by Bennett (1974), and appeared to be reasonable since faster currents occur in shallow waters. Blanton (1974) noticed an abrupt increase in the inertial band energy in the offshore spectra. The ratio between the energy contained in the inertial band to the total energy reached 50%. This finding was supported earlier by Csanady (1972c); Birchfield and Davidson (1967) and Smith (1974), and shows a nearshore zone with quite different current characteristics. The nearshore zone has more or less rectilinear currents containing little inertial motion energy. Moving offshore, there is an abrupt increase in the rotary current energy due to inertial rotation.

Blanton (1975) and Murthy and Blanton (1975) illustrated the currents variability as a function of distance offshore. They plotted the progressive vector diagram of the currents off Oshawa, Lake Ontario, 1970. About 16 km offshore the current vector rotated completely each 17 hours (inertial period) with irregular displacement. Closer to the shore, about 11 km, the rotation was still defined but the net flow was alongshore. At 6 km offshore, the rotary motion disappeared and the flow was alongshore.

Bull and Murthy (1980) and Murthy and Dunbar (1981), from current meter data in Lakes Ontario and Huron respectively, illustrated the current and energy characteristics within the coastal boundary layer. The variability of the mean current and kinetic energy revealed two distinct boundary layers. The inner boundary layer (3 and 2 km offshore for Lakes Ontario and Huron, repectively) is dominated by bottom friction. The inner boundary layer was defined as the distance to the point where the kinetic energy peaks. The outer boundary (12 and 9 km, respectively) is a consequence of the adjustment of inertial currents to alongshore currents. They also observed a pronounced peak around the inertial period in the energy spectra. This peak decreased inshore due to energy dissipation by bottom and shore friction. Detailed analysis and discussion is given in Chapter 4.

2.2.3 Coastal temperatures

Blanton (1974, 1975) and Murthy and Blanton (1975), using current meter and temperature data, illustrated the mechanism of upwelling and downwelling. During stratification periods, the zone of upwelling and downwelling is confined within the coastal boundary layer. The typical cycle of upwelling and downwelling is about 4-5 days (weather cycle). The upwelling and downwelling takes place at mid point between current reversals. In their study the thermocline intersects the water surface about 10 km offshore. Csanady (1972b) showed that the upwelling and downwelling is correlated with east/west flow along the north shore of Lake Ontario. Boyarinov (1981), from a thermal survey taken in the southern part of Lake Onega, reported a three-dimensional upwelling structure. He observed the intersection of the 8 ^{o}C isotherm, which represent the lower boundary of the thermocline, with the water surface at a distance 4 km offshore. The 15 ^{o}C isotherm which characterized the temperature of the upper layer, moved about 7 km offshore. The upwelling phenomena involved the entire water depth (28 m).

2.3 HYDRODYNAMIC MODELS

Hydrodynamic lake models vary from simple models, in which the lake is represented by one homogeneous layer, to three-dimensional time dependent models with variable density. In studying average water currents in lakes, the linearized, verticallly integrated, steady state equations of motion are employed e.g. Gedney and Lick (1972), Liggett and Hadjitheodoron (1969), Platzman (1963) and Wellander (1957).

The time history of wind is at least as important as the instantaneous value. Csanady (1967, 1968) studied the response of a two-layer lake of constant depth to a uniform wind stress. He solved the unsteady linearized vertically integrated (separately for top and bottom layers) momentum and mass balance equations. The analytical solution was obtained for the alongshore and cross-shore components as function of time and distance offshore for the top and bottom layer (coastal jet). The vertical displacement of the thermocline was related to the coastal jet reversals.

Simons (1976) developed a numerical model to simulate water transport in Lake Erie. A vertically-integrated one-layer model was used to simulate the quasi-homogeneous conditions, and a two-layer model was employed for summer stratification. Simons (1976) solved numerically the unsteady vertically integrated equations of motion and continuity including the effect of earth's rotation, pressure gradients associated with temperature distribution, bottom and internal friction and horizontal diffusion of momentum. The wind stress was assumed to be a function of time and space, and values were obtained from six shore stations. The inflow and outflow due to rivers were included. The water circulation in the shallow western basin was largely dominated by the discharge from the Detroit River. The same finding of Bennett (1974), that the water moves in the same direction of the wind close to the shore and against the wind in the interior of the basin, was also reported by Simons (1976). One- and two-layer models have been extensively used to simulate lake hydrodynamics (Bengtsson, 1973, 1978; Falkenmark, 1973; Gedney, 1971; Gedney and Lick, 1972; Gedney et al., 1973 and Saylor and Miller, 1983).

Bennett (1974) analyzed two-dimensional, time-dependent "vertical cross-section models" or channel-type models. The models were: (1)

linear, frictionless, two-layer model and (2) a numerical model which includes the bottom friction and nonlinear terms. The longshore pressure gradient was computed from the condition that the net flow normal to the cross section is zero. Bennett (1974) applied the two models to Lake Ontario finding that, under homogeneous conditions, the strongest currents (coastal jet) were confined to a region near the shore. The effect of stratification and gentle slopes was (a) to increase and decrease the width and the depth of the coastal jet respectively, and (b) straight forward damping of both quasi-geostrophic and inertial components of the flow. Similar findings for Lake Erie currents are reported in Chapter 5.

Bennett (1974), Heinrich et al. (1981) and Simons (1983) developed and used two-dimensional, channel-type, rigid-lid models. In such models the flow properties are assumed to vary with the vertical and cross-shore directions. The alongshore pressure is included so that the flux normal to the cross section is zero. The rigid-lid approximation or surface gravity wave filtering approximation simply removes the divergent part of the flow, i.e. $\nabla V = \partial\eta/\partial t = 0$, where ∇ is the horizontal gradient operator, V is the horizontal velocity vector and η is the free surface elevation relative to the mean water level. Simons (1980b) showed that the rigid-lid approximation is valid only if $(f^2L^2/gH) << 1$, where f is the Coriolis parameter, L is the characteristic length, g is gravity acceleration and H is water depth. Detailed discussion and model equations are given in Chapter 5. Simons' model (1983) did not include the non-linear acceleration terms but used different numerical grid sizes, finer size near the shore. Heinrich et al. (1981) studied the thermocline formation in Lake Erie. The study period was long (order of months), hence they included the surface heat flux in the thermodynamic equation.

Paul and Lick (1974,1981) and Vasseur et al. (1980) developed and used three-dimensional time-dependent models. Such models require large computer storage and are very expensive.

Simons (1971, 1972, 1973) and Lick (1976) developed time-dependent, multi-layer models. In these models the lake is divided into several layers and the interface between the layers are assumed to be permeable and rigid. The free surface and the thermocline are treated as impermeable moving surfaces. The hydrodynamic and continuity equations are integrated for each layer to obtain a system of equations in terms of layer-average variables. The system of equations is then solved numerically using finite-difference methods. Multi-layer models have been used extensively (Hollan and Simons, 1978; James and Eid, 1978; and Simons et al., 1979)

2.4 TRANSPORT MODELS

The analytical solution of the mass transport equation exists for simple and idealized cases, e.g. Csanady (1973), Fischer et al. (1979) and Lam et al. (1984). The analytical models are easy to use and have some engineering applications to coastal diffusion problems. Several detailed analytical solutions are given in Chapter 6.

Lam and Murthy (1978) developed and used two approaches to simulate a coastal outfall. In the first approach, they used a steady, depth-integrated, two-dimensional cross-plume Gausian distribution. The key parameters controlling the concentration distribution in such cases are the mean current and the lateral eddy diffusivity. The model was applied to two steady-state cases: shore-parallel and current reversals. In the second model, they solved numerically the same cases using an implicit finite-difference scheme (Lam, 1976). The lateral eddy diffusivity was introduced by using [2.1], while the standard deviation was computed from the concentrations in an iterative procedure. They tested four diffusion laws: (i) Fickian diffusion; (ii) shear diffusion; (iii) inertial subrange diffusion; and (iv) a semi-empirical diffusion law (Murthy and Kenney, 1974). The semi-empirical law produced as good an agreement with the analytical solution as did the theoretical models.

Kuehnel et al. (1981) developed a computer program to simulate the two-dimensional dilution contours of an outfall. The computer program was based on an analytical steady-state, depth-integrated, two-dimensional, Gaussian cross-plume model. The model was applied to the Lakeview Water Pollution Control Plant (WPCP) in Lake Ontario. They used several diffusion laws and current episodes, computing the average concentration for each current vector. The model was found to be more sensitive to current direction than current speed.

Lam et al. (1981) used the analytical solution of the steady-state two-dimensional advection/diffusion equation in a form of error function to test several diffusion laws. Zaltev et al. (1983) used several analytical solutions of the advection diffusion equation to verify a numerical model developed to simulate pollutant transport in atmosphere, (the Advection Diffusion Model (ADM) package). Karamchandani snd Peters (1983) simplified the advection/diffusion equation to obtain an analytical solution for simulating point and volume sources in the atmosphere.

The simple and idealized cases where analytical solutions are available do not apply in many practical coastal engineering applications, and so numerical techniques must be employed.

One of the simple conceptual models for simulating lake water quality over a relatively long time scale (season or year) is the input-output box model. In such models the lake is simulated as one box in winter and two or three boxes in summer. For each box the mass balance equation is obtained in a form of an ordinary partial differential equation assuming a well-mixed box (CSTR). Several processes can be allowed between the boxes, such as hydraulic flow, entrainment, water level, eddy diffusivity and interbasin flow. The box model is somewhat limited in its cabability to describe complex lake interactions, but may be profitably used diagnostically when an unknown quantity is obtained as a residual, providing all other quantities are known from observations. For more details refer to Vollenweider (1975), Snodgrass and O'Melia (1975), Simons and Lam (1980), Lam et al. (1983).

Several numerical techniques such as finite element and finite difference methods have been reported in the literature to solve the advection/diffusion equation. The choice of scheme is mainly based on the required accuracy, numerical stability and computer resources. Roache (1972) provides an excellent summary of finite difference techniques.

Walters et al. (1978) solved the unsteady, one-dimensional diffusion equation to simulate Lake Washington temperature variability. They solved the one-dimensional thermocline equation using the Crank and Nicolson (1947) implicit finite difference scheme and Galerkin finite element analysis (Martin and Carey, 1973). A new form of the vertical eddy diffusivity was proposed and applied, as discussed in detail in Chapter 5. Both the finite difference and finite element techniques produced good correlations with observations. At the thermocline the finite element method produced smaller and closer results to the observations than did the finite difference. Lam et al. (1983) simulated Lake Erie temperature by solving the one-dimensional thermocline equation using similar techniques and vertical eddy-diffusivity equations to those used by Walter et al. (1978).

Smith et al. (1973) solved the one and two-dimensional advection diffusion equation using Rayleigh-Ritz and Galerkin finite element techniques. Lam (1976) solved the advection/diffusion equation using several techniques, simulating: (a) one-dimensional plume; (b) rectangular wave (pure advection only, and with both advection and diffusion); (c) Gaussian wave; (d) two-dimensional cone shape distribution (Smith et al., 1973); and (e) an observed dye plume (Murthy, 1976). The above cases used: (1) Galerkin finite element (Price et al., 1968); (2) upstream difference plus flux-corrected transport (Book et al., 1975); and (3) box finite difference scheme (Keller, 1971). The results of the numerical simulation showed that the best simulation was produced by the upstream difference plus flux corrected transport. Lam (1980, 1981) and Hutter et al. (1984) provides more information about the application of numerical techniques to solve the advection/diffusion equation.

The most commonly used two-dimensional models to obtain the time and space distribution of pollutants in a lake are the the x-y models. Such models assume homogeneity in the vertical direction, valid during the winter. The input flow to such models are the depth-integrated transports computed by one-layer hydrodynamic models. During summer, a multi-layer model can be used where the mass balance equation is integrated over the depth of each layer. Vertical advection and diffusion are allowed between layers. Lam and Simons (1976) developed and used one- and two-layer, vertically-integrated mass transport models. The models were applied to Lake Erie to simulate the temporal and spatial distribution of chloride. The currents were previously computed by the Simons (1976) hydrodynamic model. The model used a leap-frog finite difference scheme (Browning et al., 1973; Richtmyer and Morton, 1967). They showed that a diffusion coefficient of 2.5×10^5 cm^2/s produced satisfactory results for the epilimnion.

Lam and Durham (1984) simulated a radioactive tritium patch and waste heat plume observed near the Pickering nuclear power generating station in Lake Ontario. They solved the unsteady, two-dimensional advection diffusion equation. The horizontal currents were computed by an objective analysis technique (Sasaki, 1970; Sherman, 1976), using observed values of discharge rate, intake velocity and the ambient current. The horizontal eddy diffusivity was assumed to be a function of the length scale (standard deviation of concentration), and diffusion laws were obtained from Murthy and Miners (1978) and Lam et al. (1981). The observations were used to estimate the eddy diffusivity in the near and far fields. To simulate the irregular coastal configuration and strong convection in the area, they used a finite element method with variable size (George and Simpson, 1979; and Simpson, 1981). Their length scale dependent eddy diffusivity and objective analysis produced satisfactory results.

PHASE 1: DATA ANALYSIS

CHAPTER 3

THE LAKE ERIE FIELD DATA-SET

3.1 INTRODUCTION

Because the last decade has seen such an increase in the utilization of coastal receiving waters as a buffering zone between the shore and the whole lake, national field resources have also been directed toward aquiring an extensive long-term observational data base for identifying and quantitifying the transport and mixing regimes in coastal waters.

The starting point of this study of advection, diffusion and settling in the coastal boundary layer, is the observational program undertaken by Canada Centre of Inland Waters (CCIW) and the National Oceanic and Atmospheric Adminstration (NOAA) in Lake Erie during 1979. Elzawahry and James (1981) prepared a detailed climatological analysis of Lake Erie winds, water currents and water temperatures for the Cleveland coastal site. Their document provides climatological and statistical summaries of meteorological parameters that are related to this study and documents and displays the observed data in a simple form for decision-making purposes. This chapter summarizes the field program. For more details refer to their report. The detailed statistical analyses are summarized in the next chapter (Chapter 4).

3.2 FIELD PROGRAM

From early May to the end of December, 1979, an extensive field program was undertaken by CCIW and NOAA at several sites, one of which was in the vicinity of Cleveland, Ohio, as shown in Figure 3.1. The program was designed to provide continuous time-series of currents, temperatures and winds over the entire time period.

Figure 3.1 shows the locations of the study area and Figure 3.2 gives details of depth contours and current-meter mooring sites. The current-meters were moored on three transects approximately perpendicular to the local shore line. Transect A-B includes six moorings just west of the study area. Each of the transects C-D and E-F includes two current-meter moorings in the middle and the east of the study area respectively. The closest mooring to the shore (mooring 39) was placed 1.9 km from shore. The minimum horizontal spacing between any two adjacent moorings was 2.6 km, between moorings 37 and 36. The horizontal spacing increases offshore up to about 11 km, between moorings 34 and 11. Figure 3.3 shows profiles along the three transects with the current-meter locations.

The field instrumentation (current-meter arrays) consisted of four types: (i) Plessey current-meter model M021 (Robert's rotor type), suited to near surface installation, 10 to 15 m water depth; (ii) Geodyne current meter installed at a minimum depth of 14 m which was in close proximity to the bottom; (iii) Plessey current-meter (RCM12); and (iv) Vector average current-meter (AMF VACM) used only at all NOAA moorings (11,12,16 and 17). The water temperature and the current speed and direction were recorded continuously at time intervals of 15 minutes (NOAA moorings) and 20 minutes (CCIW moorings). The current meter data

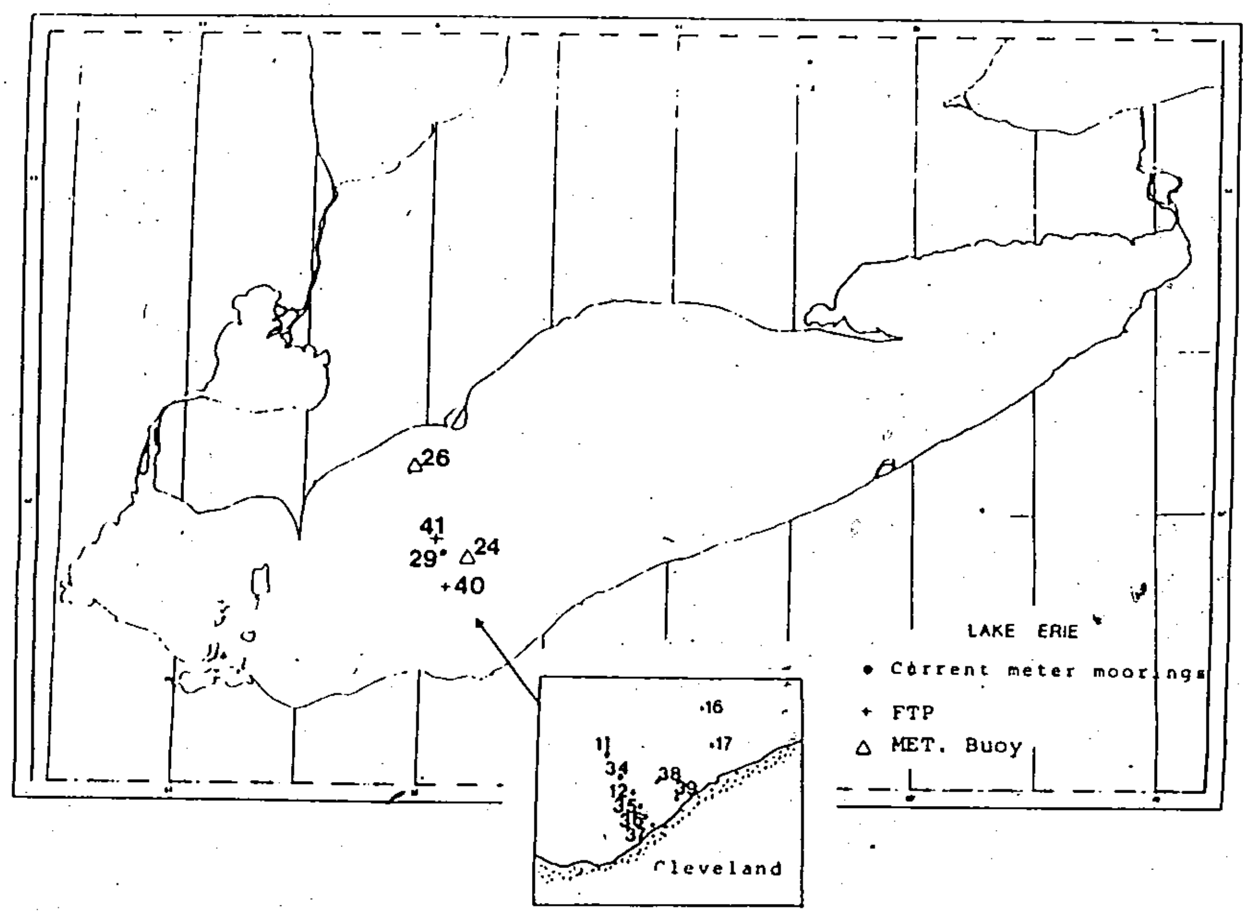

Figure 3.1 Study area in the vicinity of Cleveland, Lake Erie.

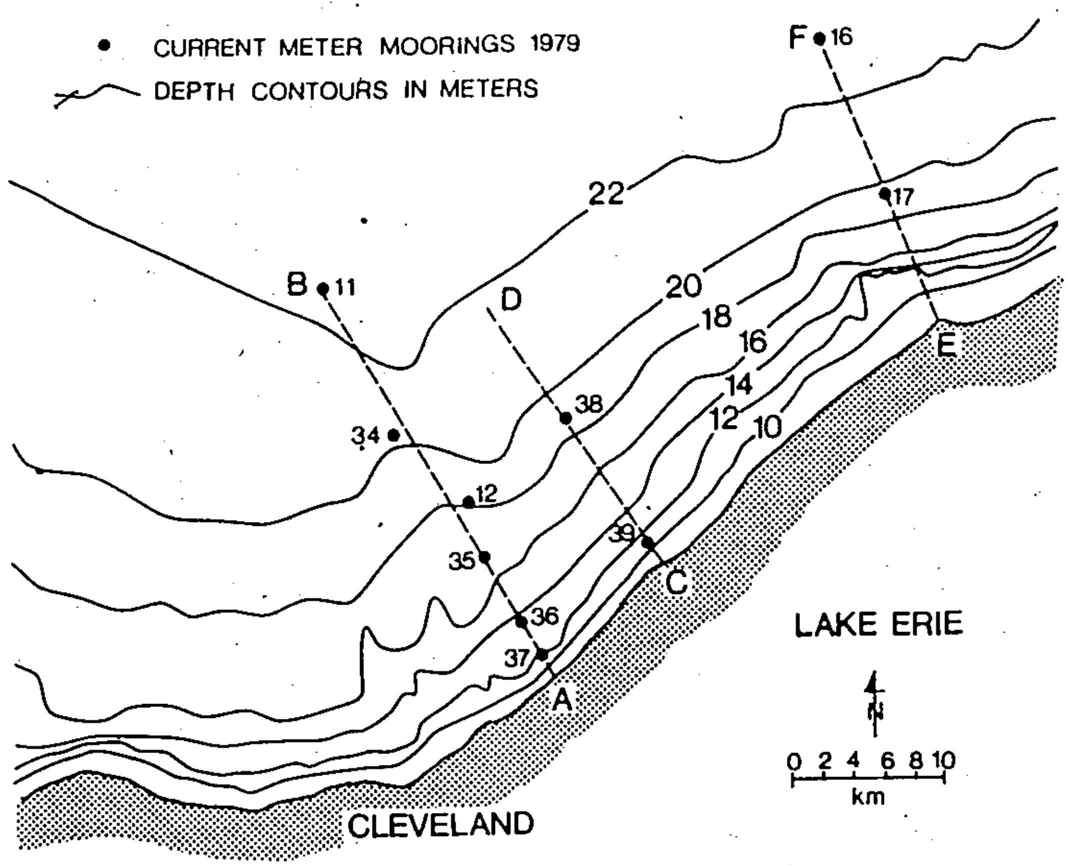

Figure 3.?. Details of depth contours and current-meter mooring sites.

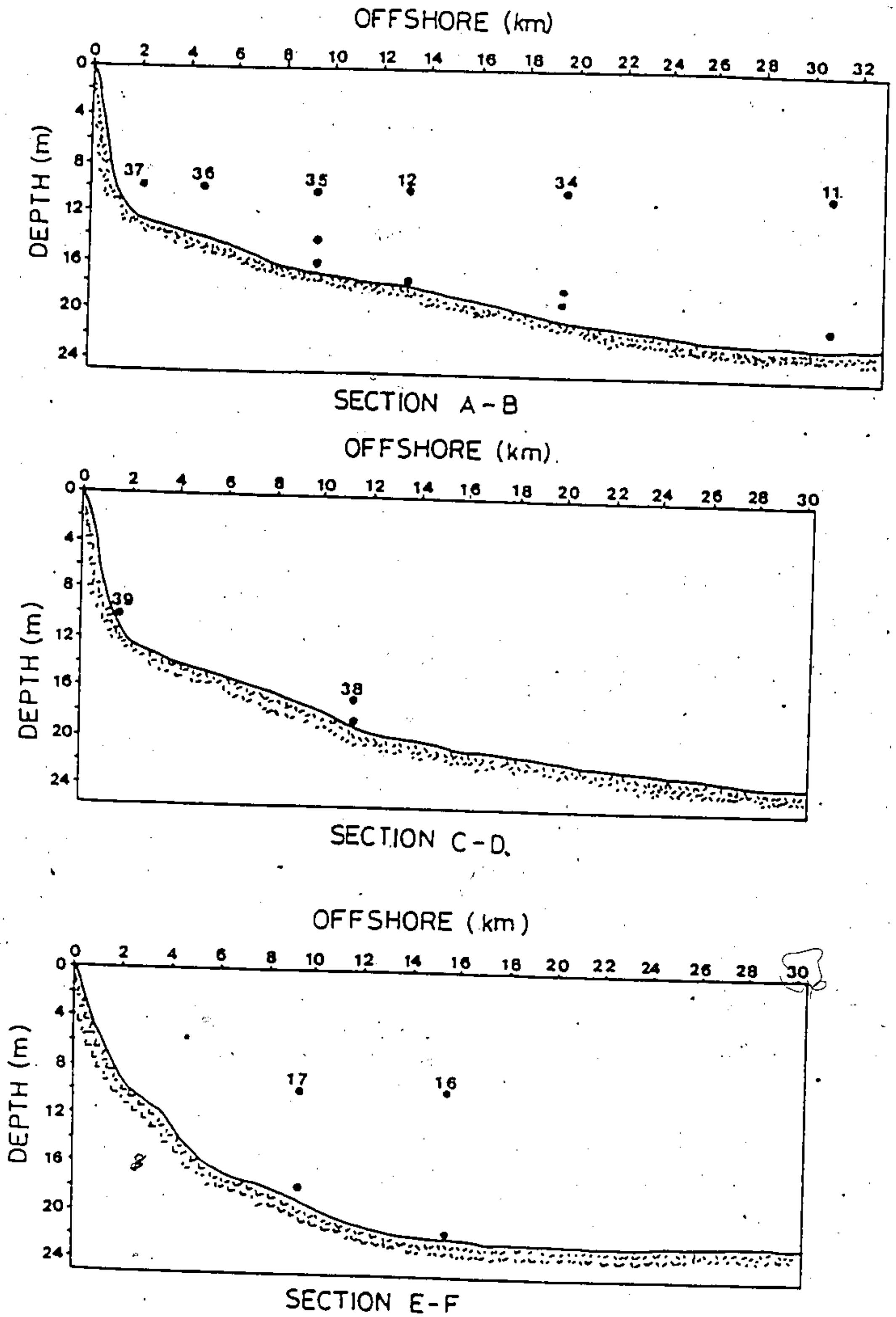

Figure 3.3 Profiles along the main transects with current-meter locations.

is used to identify the transport and mixing characteristics (Chapter 4), to verify, calibrate and validate the hydrodynamic models (Chapter 5) and to generate the sediment plume within the coastal boundary layer (Chapter 6). Figure 3.4 shows a bar chart summary of the current-meter data return. In addition a complete summary of the current-meter data return is presented in Table 3.1.

The data from two meteorological buoys (MET. 24 and MET. 26) located in the study area was used in our study, as shown in Figure 3.1. The main purpose of the collected meteorological data is to obtain estimates of area averages and distributions of surface fluxes of momentum, heat and water vapour in the study area, as discussed in Chapter 5 in more detail. Wind speed, wind direction, air temperature, relative humidity, water temperature, buoy orientation and integrated solar radiation were recorded by the meteorological buoy. The buoys used were Geodyne, torroidal type. A summary of the meteorological data return with latitude and longitude of each buoy is given in Table 3.2.

The data from two fixed temperature profiler (FTP) moorings (40 and 41, see Figure 3.1) were used in our study. The data collected by the FTP is in the form of the water temperature as a function of water depth and time. The FTP data is used to identify cases of upwelling and downwelling by tracking the thermocline location and hence the periods of the maximum water exchange between ~~the~~ coastal and offshore waters, as discussed in Chapter 4. The data is also used to calculate the baroclinic pressure in solving the hydrodynamic equations (Chapter 5). The FTP buoys used were devised by the Mechanical Engineering Unit at

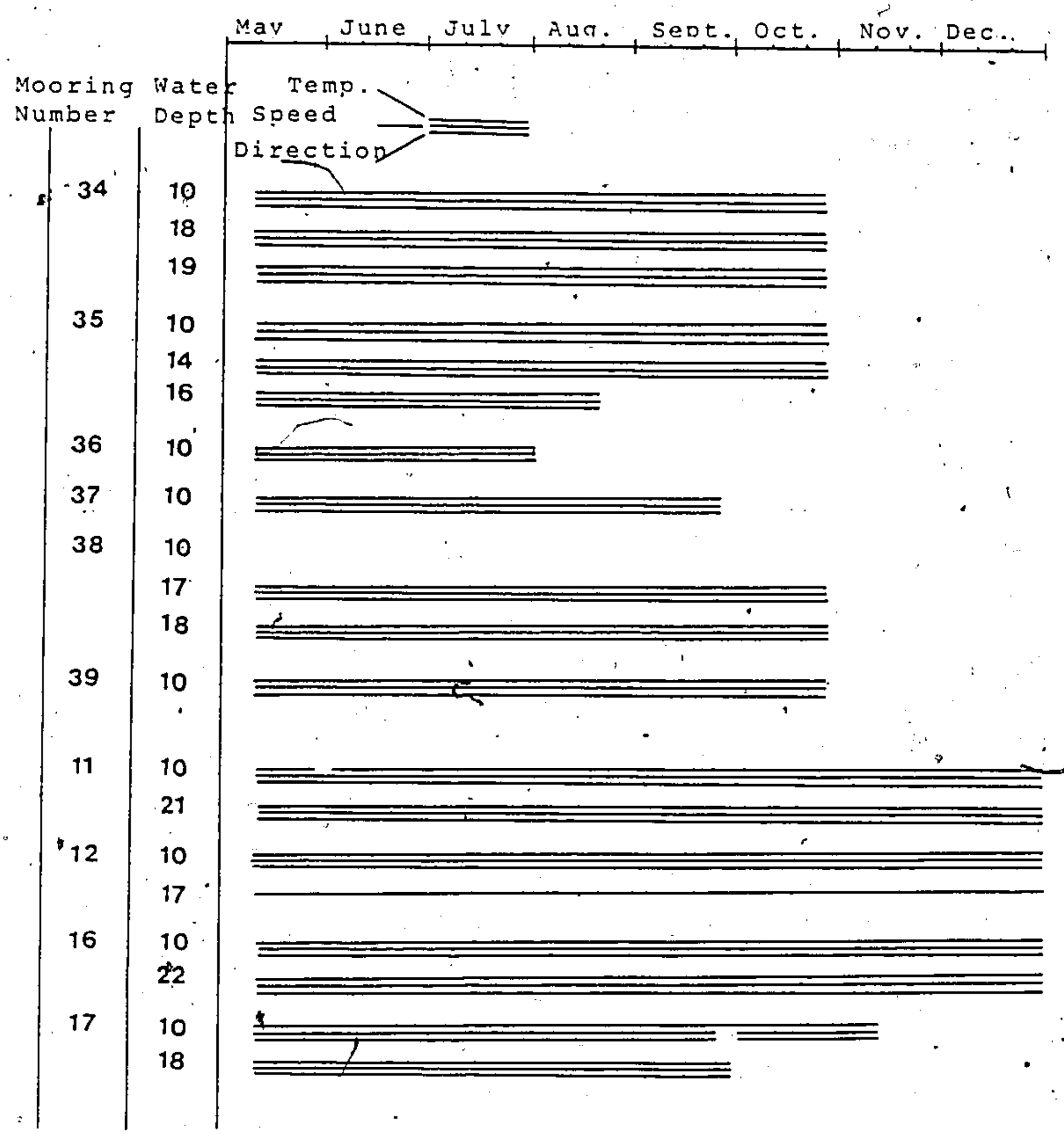

Figure 3.4 Bar chart summary of the current-meter data.

Table 3.1

CURRENT METER SYSTEM SUMMARY 1979

Mooring Number	Site	Latitude N.	Longitude W.	Depth Meters	Dates	Meter	Scan Interval	Data Return T	Data Return S	Data Return D
79-01C-34A	C17	41°42'36"	81°44'08"	10.0	May 10-Oct. 27	H021	20 min.	100	100	100
				17.5	May 10-Oct. 27	Geo	20 min.	100	100	100
				19.2	May 10-Oct. 27	Geo	20 min.	100	100	100
79-01C-35A	C18	41°37'34"	81°40'08"	10.0	May 10-Oct. 29	H021	20 min.	100	100	100
				14.0	May 10-Oct. 29	Geo	20 min.	100	100	100
				15.7	May 10-Oct. 29	Geo	20 min.	58	58	58
79-01C-36A	C19	41°35'11"	81°38'20"	10	May 10-July 30	H021	20 min	100	100	100
				10	July 30-Oct. 29	H021	20 min	0	0	0
79-01C-37A	C20	41°34'03"	81°37'19"	10	May 10-July 30	H021	20 min	100	100	100
				10	July 30-Oct. 29	H021	20 min	60	60	60
79-01C-38A	C21	41°42'47"	81°35'41"	10	May 10-Aug. 1	RCH12	20 min	0	0	0
				10	Aug. 1-Oct. 27	H021	20 min	0	0	0
				17	May 10-Oct. 27	Geo	20 min	100	100	100
				18.7	May 10-Oct. 27	Geo	20 min	100	100	100
79-01C39A	C22	41°37'56"	81°31'53"	10	May 10-Oct. 27	H021	20 min	100	100	100
79-01C-11N	H11	41°46'48"	81°47'24"	10	May 8-Dec. 31	VACH	15 min	97	100	100
				21	May 8-Dec. 31	VACH	15 min	100	100	100
79-01C-12N	H12	41°39'30"	81°40'48"	10	May 8-Dec. 31	VACH	15 min	100	100	100
				17	May 8-Dec. 31	VACH	15 min	100	0	0
79-01C-16N	H16	41°56'29"	81°22'48"	10	May 8-Dec. 31	VACH	15 min	100	100	100
				22	May 8-Dec. 31	VACH	15 min	100	100	100
79-01C-17N	H17	41°50'24"	81°19'48"	10	May 8-Nov. 11	VACH	15 min	100	95	95
				21	May 8-Sept. 30	VACH	15 min	100	100	100

* H021 - plessy current meter, Robert's rator type
* Geo - Geodyne model 920 current meter, savonius rator with vans
*RCH12 - Applied microsystem direction measurements (modified Plessy H021)
*VACH - AHF vector averaging current meter, savonius rator with van follower type

Table 3.2

MET SYSTEM SUMMARY 1979

Mooring Number	Site	Latitude N.	Longitude W.	Date	WS	WD	WT	AT	BC	Scan Interval	Data Return
					SENSORS						
79-01M-24A	C9	$42^{o}07'08"$	$82^{o}03'59"$	May 8 - June 12	25	03	34	35	N.A.		100%
				June 12 - July 12	23	03	34	35	N.A.		100%
				July 12 - July 27	25	03	34	35	N.A.		95%
				July 27 - Aug. 25	25	03	34	35	1641		100%
				Aug. 25 - Sept.25	25	03	34	35	1641		100%
				Sept.25 - Oct. 25	25	03	34	35	1641		100%

Table 3.3

FTP SYSTEM SUMMARY 1979

Mooring Number	Site	Latitude N.	Longitude W.	Depths	Scan Interval	Dates	Data Return
79-01T-40A	C23	$41^{o}45'37"$	$81^{o}53'36"$	0.3-1.2-3.4-3.9-4.9-5.9-6.9 0.9-8.8-9.8-11.8-13.8-15.8-16.8 17.8-18.3-18.8-22-19.8-20.3-20.8	10 min	June 1-July 16	95%
				as above	10 min	July 16-Aug. 26	100%
				0.2-1.1-3.2-3.7-4.8-5.8-6.8 7.8-8.8-9.8-11.8-13.8-15.8-16.7 17.7-18.2-18.7-21.8-19.7-20.2-20.7	10 min	Aug. 26-Oct. 4	100%
				as above	10 min	Oct. 4-Oct. 29	95%
79-01T-41A	US-10	$41^{o}54'06"$	$81^{o}54'50"$	0.6-1.6-4.0-4.5-5.0-6.0-8.0 9.0-10.-11.-12.-13.-14.-15. 16.-17.-18.-21.6-19.5-23.	10 min	June 7-July 19	100%
				.2-1.2-3.6-4.1-4.6-5.6-6.6 7.6-8.6-9.6-10.6-11.6-12.6-13.6 14.6-15.6-16.6-17.6-21.7-19.1-22.6	10 min	July 19-Aug.26	95%
				as above	10 min	Aug. 26-Oct. 2	95%
				as above	10 min	Oct. 2-Oct. 29	95%

CCIW (Healy et al., 1980). Table 3.3 summarizes the FTP data return. Engineering specifications of the instruments deployed have not been included here but have been reported elsewhere (Bull and Farooqui , 1976 and Howarth, 1981).

CHAPTER 4

THE COASTAL BOUNDARY LAYER OF LAKE ERIE

4.1 INTRODUCTION

The physical processes in the coastal regions of large lakes are complex. Unlike the offshore regions, the nearshore areas are subjected to a coastal boundary layer effect, a broad spectrum of turbulent eddies and secondary circulations peculiar to the local bathymetry and shoreline configurations. Into this complex flow regime of the nearshore zone a substantial quantity of nutrients and other contaminants is introduced. Typical sources are sewer overflow, industrial outfalls, urban stormwater runoff and occasional dumpings. Within the nearshore regions, nutrients and pollutants settle out, are diluted, transported and dispersed to the offshore zones. The coastal zone is an important buffering zone, receiving effluent on one edge and dispersing it to the other.

If one turns to the literature on turbulence and turbulent diffusion theory, one finds a multitude of hypotheses. These hypotheses vary, from elegant derivation of statistical theory to verification with data obtained from hydraulic scale models. However, for the purpose of practical application, it is important to substantiate a hypothesis by verification with observed data at an actual coastal site. The complex turbulence characteristics within the coastal boundary layer cannot be reproduced in laboratory models; hence it is desirable to determine empirical coefficients directly from environmental data rather than from laboratory data.

In this chapter the flow and the dispersion properties are described in detail during the stratified period within the coastal zone in the vicinity of Cleveland. A computer program (ADVDIFF) was developed by the author to calculate the mean flow, horizontal turbulent length and time scales, horizontal diffusion coefficients and the kinetic energy properities by using a filtering technique and statistical and spectrum analyses. The results of this part of the work are important to the thrust of the whole study. By identifying the different flow regimes in the coastal zone, the critical (worst) cases from a pollution disposal point of view can be obtained either in the local area (the coastal zone), or lake-wide. The horizontal turbulent length and time scales are used to define the time and space increments for the numerical solution of the momentum and mass balance equations in Chapters 5 and 6. The values of the horizontal diffusivities are used to define the diffusion law and to solve the sediment mass balance equation in Chapter 6. The width of the coastal boundary layer is used to define the domain of the numerical calculations.

4.2 CLIMATOLOGY OF COASTAL CURRENTS

Field experimental programs designed to record long time series records of coastal currents and temperatures over periods of the order of several months, give a time history of the various flow regimes present in the coastal region. Such records usually show an extremely complicated flow situation, varying from season to season and from location to location. Such a record is often difficult to synthesize. As yet, coastal hydrodynamic models are unable to fully predict the complex flow regimes encountered in the coastal zone. Hence the author has attempted to derive a statistical description of the measured flow properties. Application of these results to the hydrodynamic models is discussed in detail in Chapter 5.

In Figure 4.1 are plotted six-hourly average current vectors obtained from 10 m depth current meters of the main transect A-B (Figure 3.2) for the continuous record of measurements (May to July 1979). Despite the apparent complexity of Figure 4.1, there are certain identifiable flow regimes that often repeat themselves. The determination of the relative frequencies of occurrence and the average duration of important flow regimes make up a "climatology" of coastal currents, a direct analogy to the terminology commonly used in desciplines such as geography and meteorology. Several distinct flow regimes can be identified in this plot: (i) episodes of strong alongshore current regimes persisting for several days (for example the periods May 25 to 30 and July 1 to 6); (ii) episodes of current reversals during which shore-parallel currents turn around within eight hours (for example the period June 8 to 21 and July 7 to 31); (iii) episodes of weak currents and sometimes almost stagnation with irregular changes in the direction (for example the periods May 10 to 17 and June 1 to 6).

In Figure 4.2, current rose histograms for the current meter stations in transect A-B, as shown in Figure 3.2, show the joint frequency distribution of speed and direction. The current vectors are separated into compass sectors and speed range frequency of occurrence

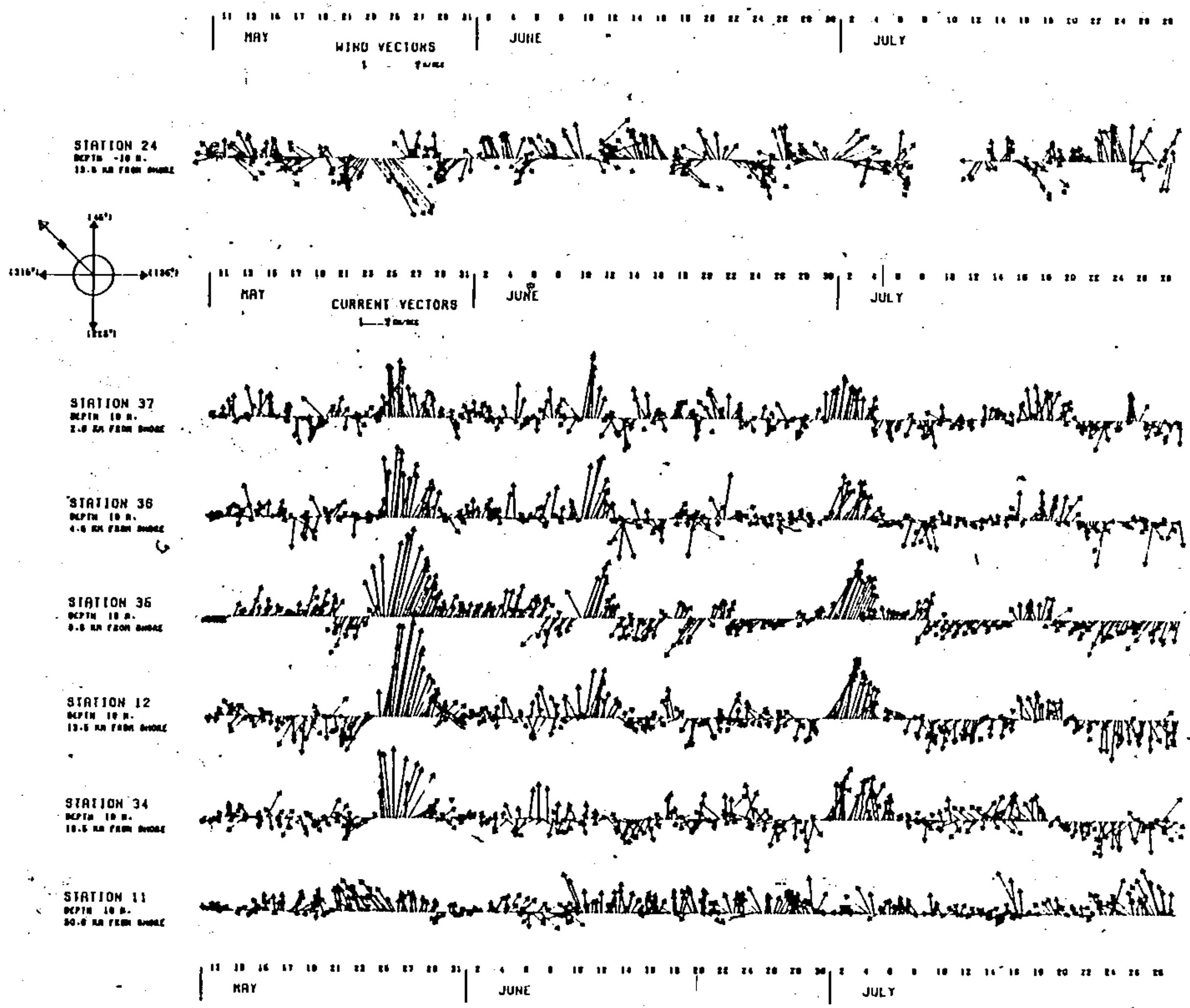

Figure 4.1 Time series vector plots, Cleveland, Lake Erie, May 11 - July 28, 1979.

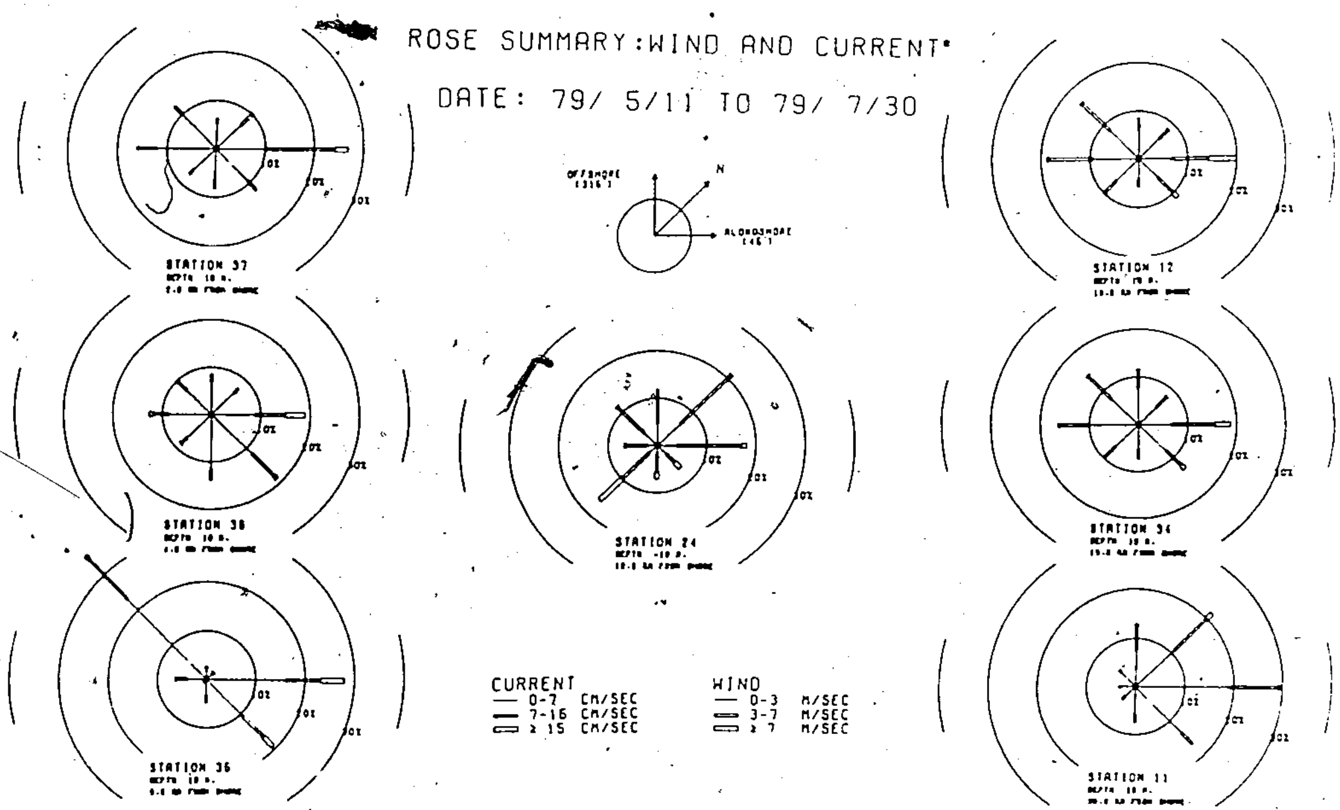

Figure 4.2 Wind and current rose histograms, Cleveland, Lake Erie, May 11 - July 28, 1979.

less than 7, 7 to 15, and greater than 15 cm/s, defined as low, medium and high current speeds respectively. From these plots one can observe that close to the shore (mooring 37), most of the time the flow is shore-parallel. The maximum frequencies of occurrence are 26% and 16% of the total time (May 11 to July 30), in the alongshore direction (45 and 225 degrees from north) respectively. Currents exceeding 15 cm/s are observed for about 3% of the total time but only for currents parallel to the shore. Medium currents are observed for about 30% while the low currents are observed for about 67% of the total time. The shore-perpendicular currents are observed for about 14% of the total time with no currents exceeding 15 cm/s. Moving offshore the effect of the shore and bottom friction decreases, the frequencies of occurrence of the alongshore direction decrease, and the frequencies of occurrence of currents exceeding 15 cm/s increase. For example at mooring 12 the frequencies of occurrence of the alongshore direction and the high currents are about 37% and 10% of the total time respectively. Due to the effect of the inertial rotation far from shore the frequencies of occurrence of the high currents drop to about 3% of the total time at mooring 34.

Due to the dominance of the winds from the south-westerly direction during the summer period, the bias of the flow toward the easterly direction is observed. The mean vector summary plot constructed from the entire data base shows a net easterly flow direction at almost all stations (Figure 4.3). In Figure 4.3 the means of each station are plotted for the depths noted at the arrow-head.

This type of presentation gives the overall picture of the flow pattern. However, it does not represent the single event (episodic)

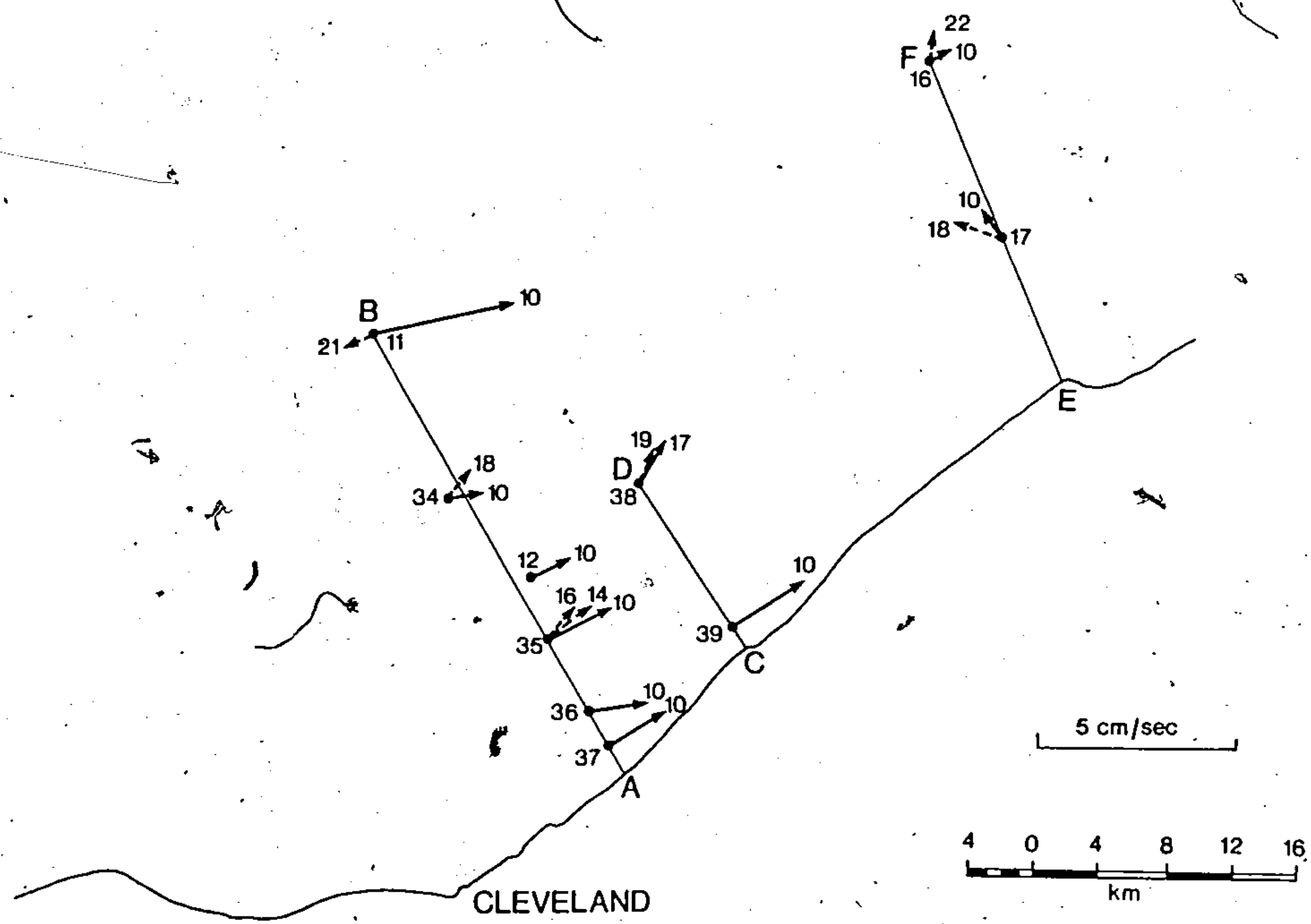

Figure 4.3 Vector-average currents off Cleveland for May11-July 28, 1979. Current-meter depths are noted at the arrow-head.

analysis which is useful for identifying critical pollution situations. Single event analysis is discussed later in this chapter.

4.3 DATA ANALYSES

For long time-series records there is always a need for special techniques to present the physical properties of the record. One of these techniques is to switch from the time domain to the frequency domain by constructing the frequency spectrum and defining the representative mean value of the record based on the spectrum properties. Separation of the mean and the fluctuating components in the original current time series is important for the horizontal turbulence calculations. The mean value can be obtained by assuming a steady or unsteady (moving average) mean. The latter can be computed by using digital numerical filtering techniques.

A computer program called ADVDIFF (ADvection DIFFusion) was developed by the author to calculate the mean flow, horizontal turbulence time and length scales, horizontal diffusion coefficients and the kinetic energy properties. Figure 4.4 shows the program functional flow chart. The time-series current meter data are available in the form of (S_i, θ_i), where S_i is the integrated speed in cm sec^{-1}, and θ_i is the instantaneous direction in degrees measured clockwise from north. The data was resolved into longshore (u_i) and cross-shore (v_i) components, using the following relation:

$$u_i = S_i \cos(\phi - \theta_i)$$
$$v_i = S_i \sin(\phi - \theta_i) \qquad [4.1]$$

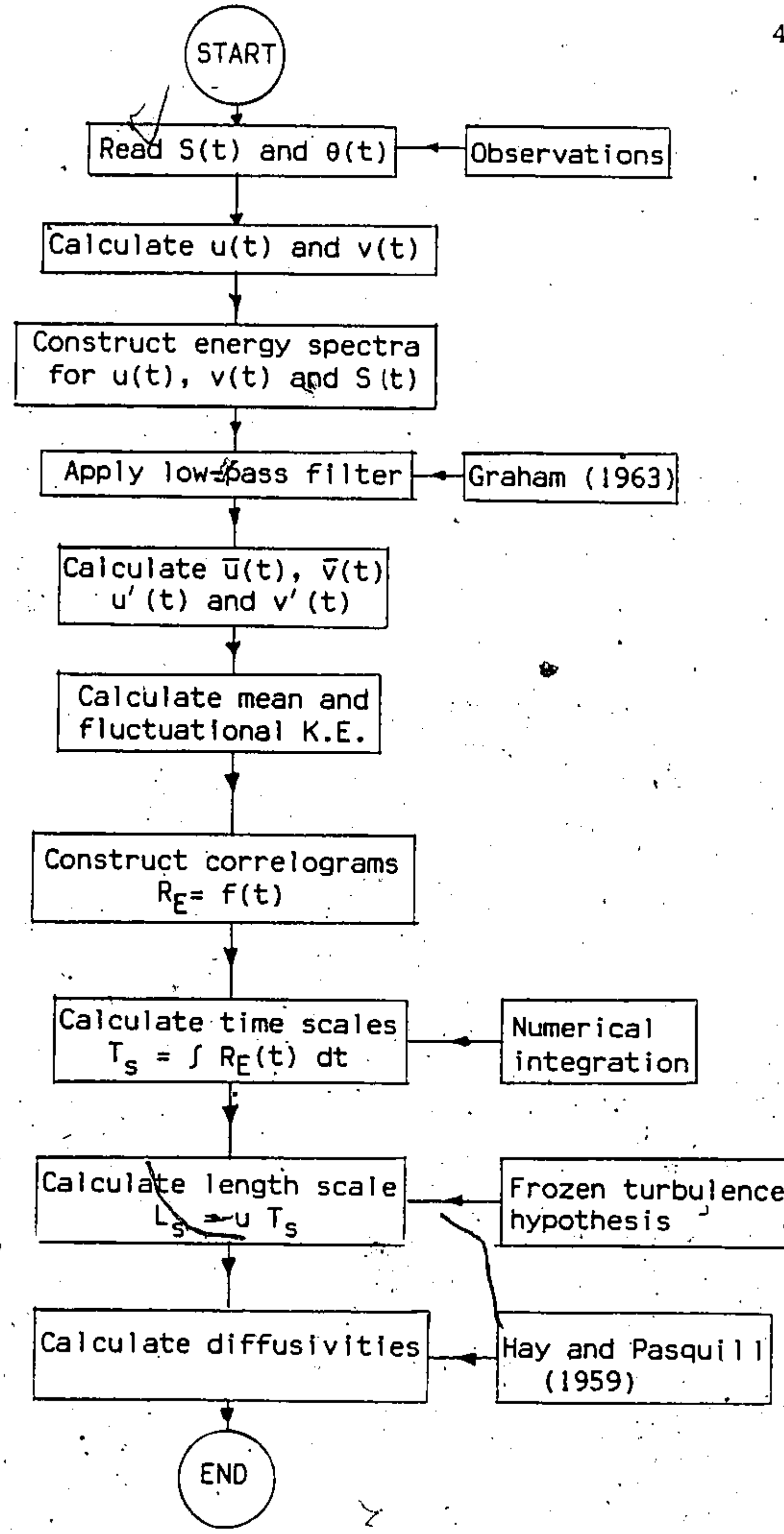

Figure (4.4) Functional flow chart for program ADVDIFF where ϕ is the angle from north of the local shoreline. For Cleveland ϕ is 45°. This preliminary analysis produces two time series, $u_i(t)$ and $v_i(t)$, which are then used as basic data to calculate the rest of the statistical quantities. The energy spectra were constructed following Jones (1957) and summarized in Pasquill (1962). Based on the energy spectra properties (as discussed later) the total current was separated into moving average and fluctuations by using a low-pass digital numerical filter (Graham,1963). The mean and the fluctuational kinetic energies of both components were calculated. The correlograms for u(t) and v(t) were constructed and the corresponding time scales were calculated by integrating the area under the correlograms. The length scales were calculated using the frozen turbulence hypothesis (Taylor, 1921). Finally the horizontal diffusion coefficients were calculated using the Hay and Pasquill (1959) assumption, relating the Eulerian and the Lagrangian correlograms through the β coefficient.

4.4 SPECTRAL CHARACTERISTICS

Spectral analysis is a powerful tool for describing turbulence. It illustrates how the kinetic energy associated with different scales of motions, frequencies and eddy sizes cascade in a turbulence field. A considerable amount of literature is available on the shape and the magnitude of flow field spectra (Jones, 1957; Pasquill, 1962; and Murthy and Dunbar, 1981).

In this study the energy spectra were calculated following Jones (1957) and summarized by Pasquill (1962). See appendix A for detailed calculations. The current kinetic energy spectra were calculated for the entire period (May 11 to July 30) for all moorings, the results of which are presented in Figures 4.5, 4.6 and 4.7. At all moorings the energy spectra cover a wide range of frequencies (time scales), between 2 hours and 1000 hours. Two peaks are observed in all the spectra plots, one at a low frequency band containing energies for periods larger than 8 days, the second at a high frequency band (12-24 hours). The energy associated with the low frequency band is a direct result of the large scale circulation produced by the wind. The large scale oscillation is not characteristic of the coastal boundary layer. The eddies associated with the low frequency band do not contribute to the diffusion of the pollutants; they contribute rather to plume meandering. The energy associated with the high frequency band is probably a direct result of a wave-like oscillation or inertial oscillation. The high frequency peak (inertial peak) is highly pronounced, the same order of magnitude as the low frequency peak, in the offshore spectra (moorings 34/10, 12/10). On the other hand the nearshore spectra (moorings 37/10 and 36/10) show that the inertial peak is considerably less than that observed in the offshore spectra. The gradual decrease of the inertial peaks moving onshore indicates a transition zone where the inertial currents transform into quasi-steady shore parallel currents.

Figure 4.7a shows the kinetic energy spectrum of mooring 11/10; the inertial peak is not as highly pronounced as expected. Boyce (1985) analyzed the entire cross-lake transect data, finding that the cross spectra between mooring 11/10 and mooring 29 at the middle of the lake show no coherence at the 100 to 50 hour period band. On the other hand

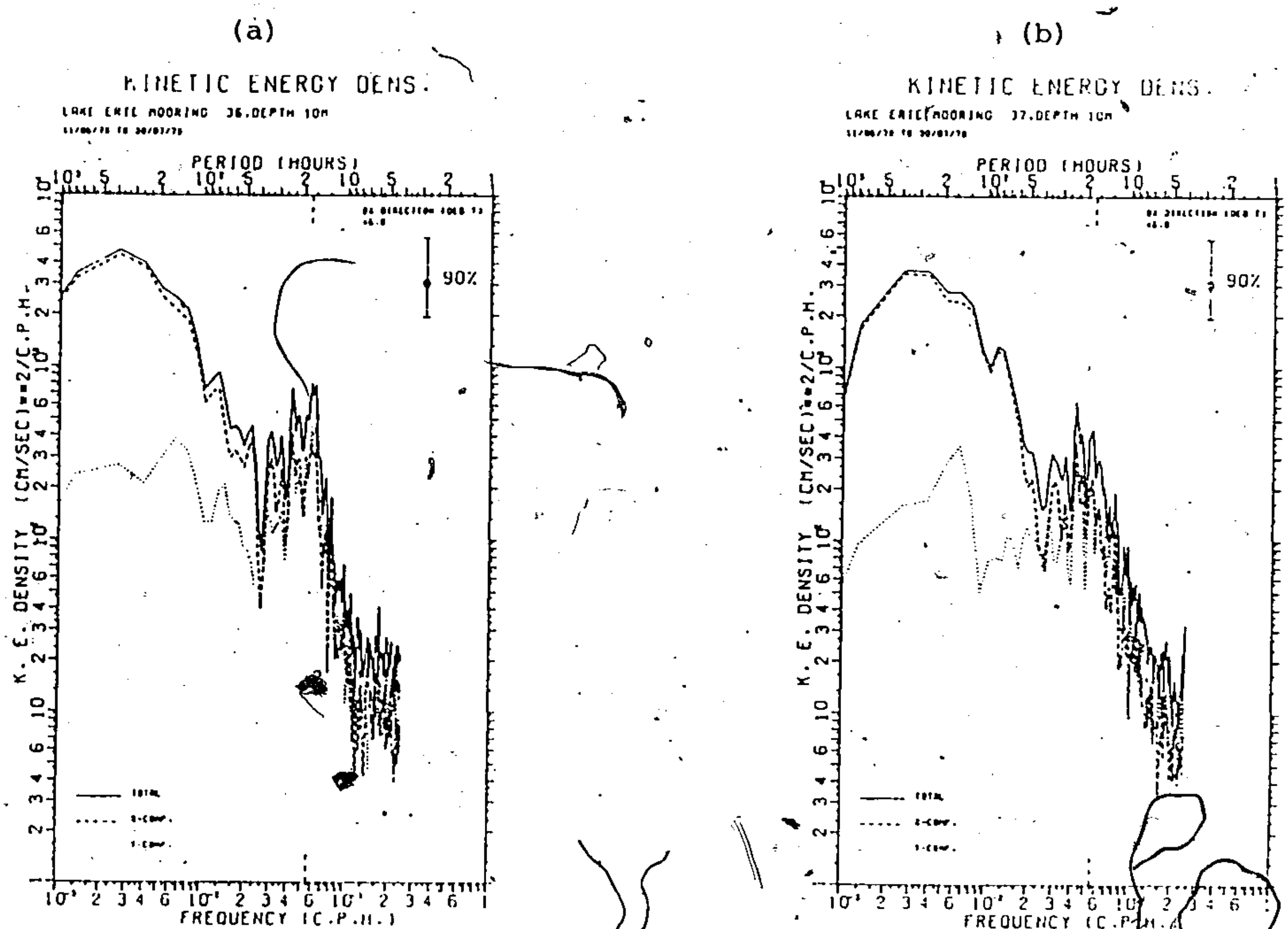

Figure 4.5 Kinetic energy density plot for mooring 37 (a) and mooring 36 (b): Time-series data used from May 11 - July 30, 1979.

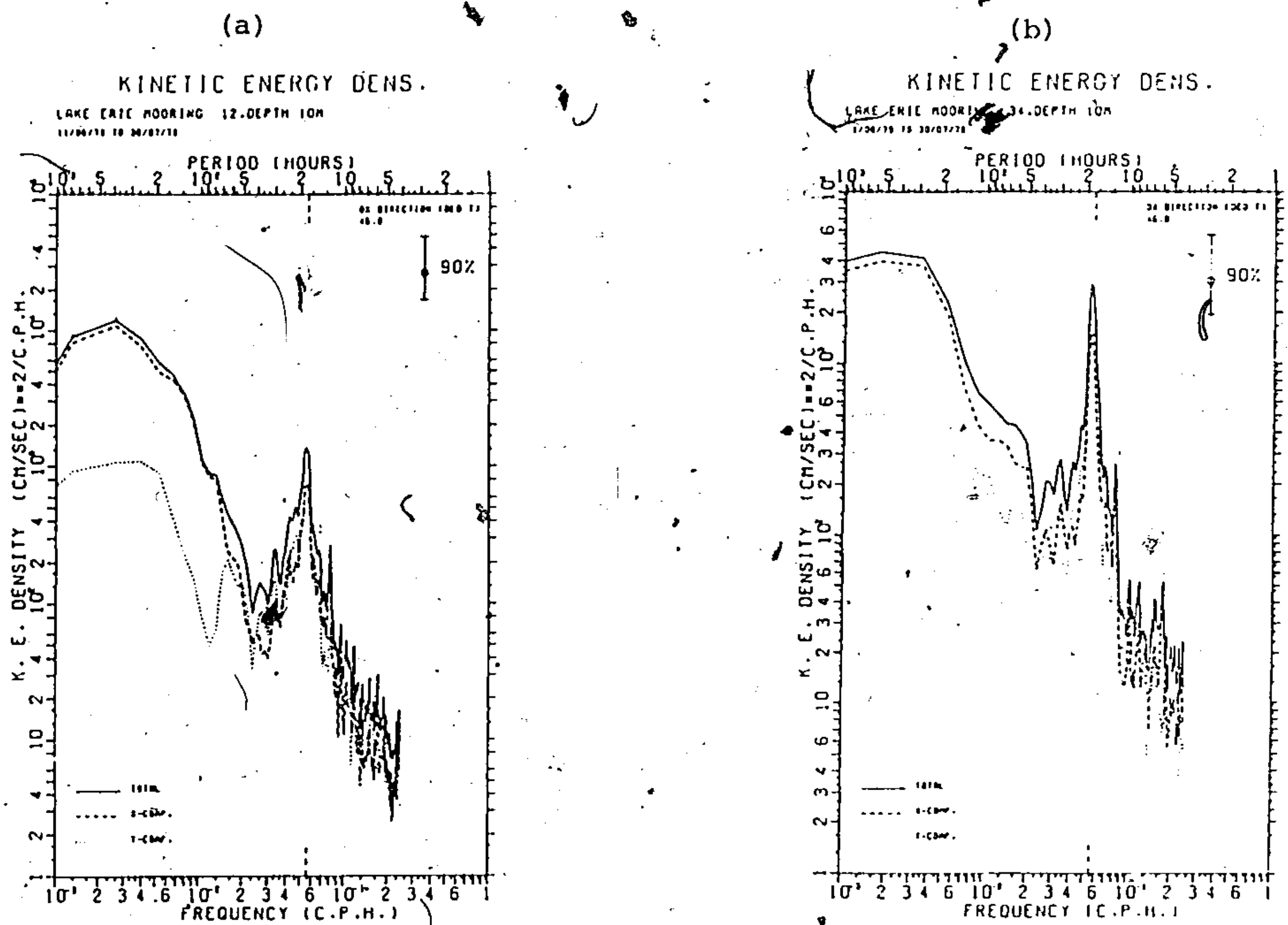

Figure 4.6 Kinetic energy density plot for mooring 12 (a) and mooring 34 (b): Time-series data used from May 11 - July 30, 1979.

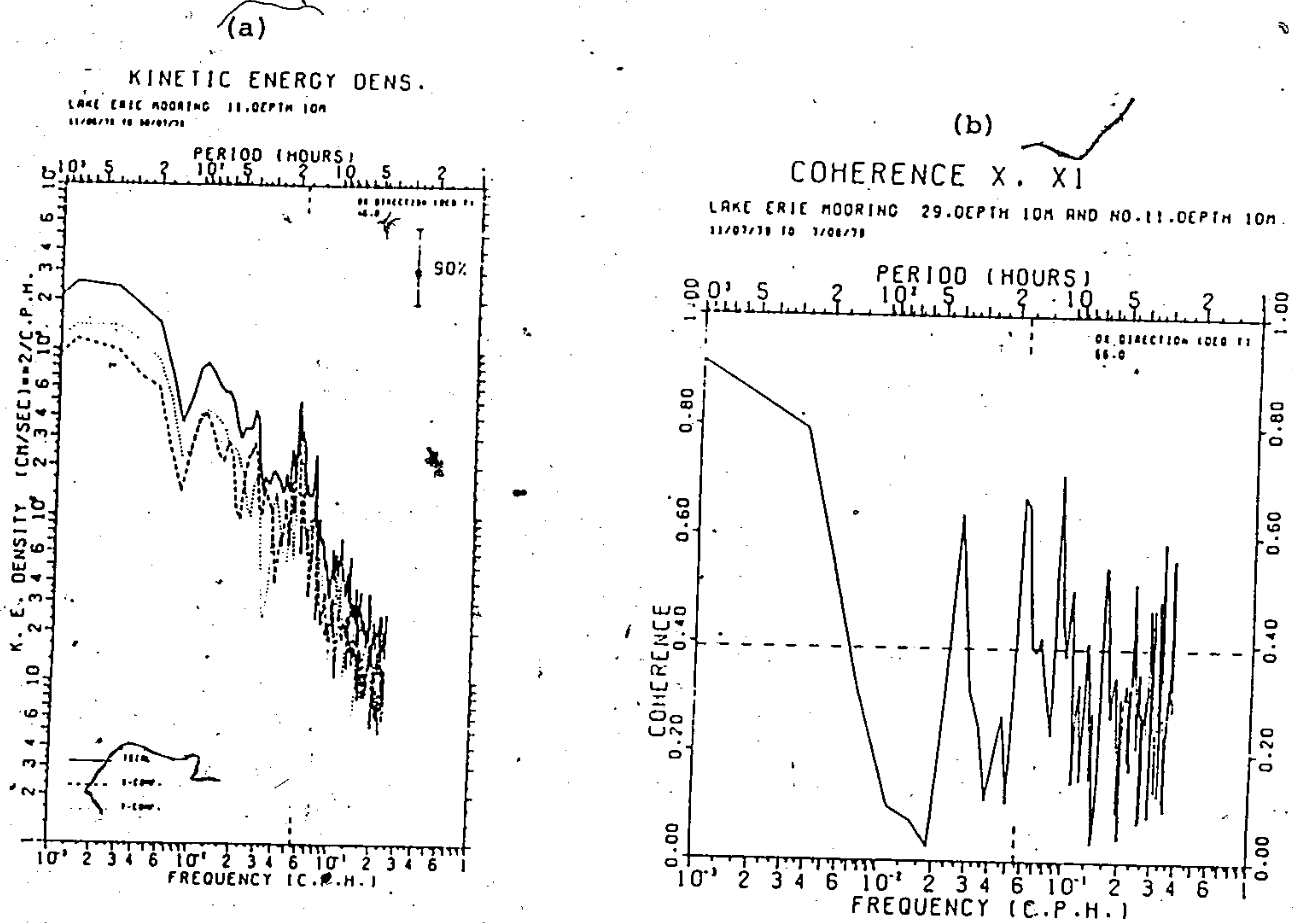

Figure 4.7: (a) Kinetic energy density plot for mooring 37, time-series data used from May11-July30, 1979.
(b) Coherence between moorings 11 and 29.

the coherence between mooring 29 and all other stations appears to be strong in this band. Figure 4.1 also shows that station 11/10 is different from the others. For this reason, although the results from station 11/10 are included, no conclusions are drawn from these data.

4.5 NUMERICAL FILTERING

Separating the mean and the fluctuational flows is an essential step in defining the characteristics of both the transport and the turbulence fields. Based on the characteristics of the energy spectra, digital low-pass filter techniques developed by Graham (1963) and extensively applied to the analysis of time series current-meter data for large lakes (Simon,1974 and Murthy and Dunbar, 1981) were employed. Graham's (1963) techniques are based on identifying frequencies of interest. Once they are determined the gain function must be defined for all frequencies. The value of the gain function at the frequencies that are to be eliminated should be zero, and the value of the gain function where the frequencies are to remain undisturbed should be one. An inverse Fourier transformation is applied to the gain function and the result is a weight function in the time domain. The gain function (filter) derivation is summarized in Appendix B.

Identifying the frequencies that are of interest in applying the numerical filtering techniques is a crucial step in this analysis and requires some physical insight. It is based on the selection of a frequency to divide the energy spectrum into two separate parts. To the left of this frequency the energy contained in the spectrum is considered to be the energy associated with the mean flow. To the right of this frequency the energy contained is considered to be the energy associated with the turbulent motion or small scale motion. The frequency selected is such that the energy associated with the mean motion is to be higher than the energy associated with the turbulent motion. Two low-pass filters with an 18 to 24 hours cutoff range, to retain the inertial oscillation as part of the fluctuations, and a 10 to 14 hours cutoff range, in which the inertial oscillation appears as part of the mean flow, were constructed and applied to the analysis of the current-meter time series data. The mean u-component characteristics derived by the application of the two filters to 20 minute data from the mooring 37/10 record and for the period May 25 - 31 are shown in Figure 4.8. It is clearly seen that the fluctuations around the mean attain higher values in the case of the 18 to 24 hours cutoff range than the 10 to 14 hours cutoff range. In the former the inertial oscillation is considered to be part of the fluctuations.

The running mean values $\bar{u}(t)$ and $\bar{v}(t)$ are subtracted from the original time-series record to define the fluctuations $u'(t)$ and $v'(t)$. The average total kinetic energy per unit mass is calculated using the expression

$$\frac{1}{2}\,\overline{u^2}(t) = \frac{1}{2}\,\overline{[\,\bar{u}(t) + u'(t)]^2}$$

$$= \frac{1}{2}\,\overline{\bar{u}^2}(t) + \frac{1}{2}\,\overline{u'^2(t)} + \overline{\bar{u}(t)u'(t)} \qquad [4.2]$$

The first term on the right hand side of equation [4.2] represents the

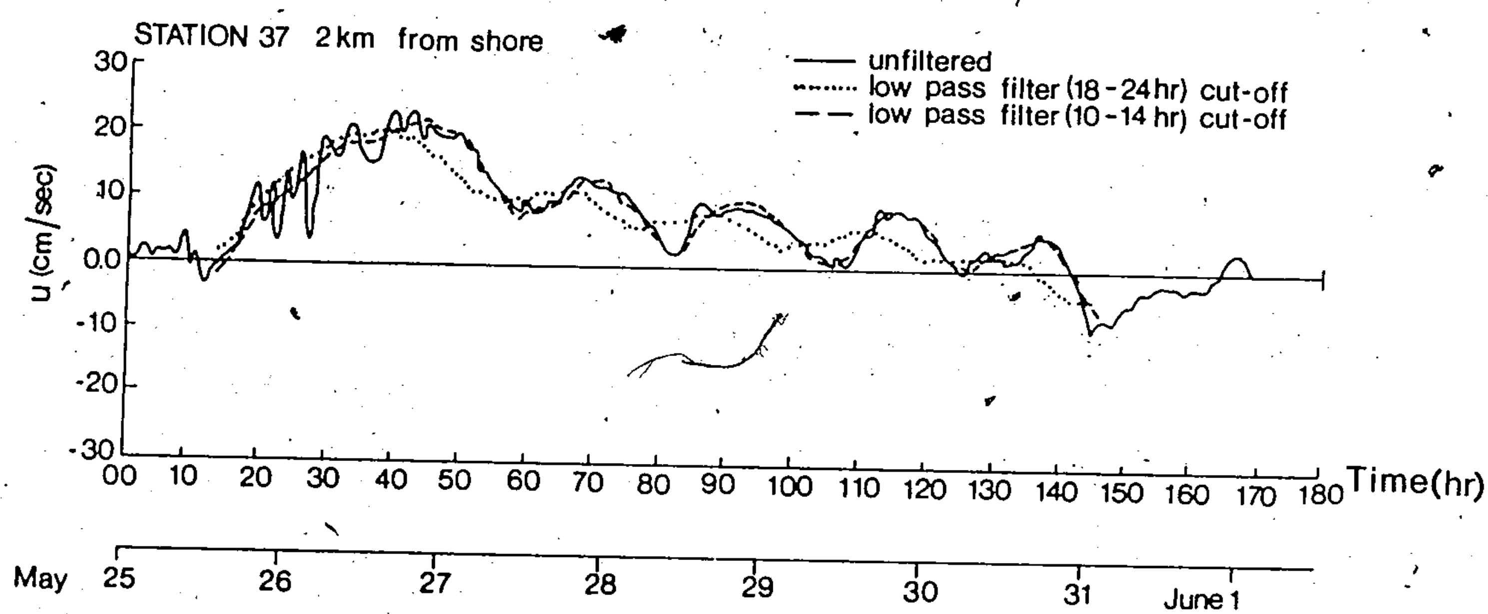

Figure 4.8 Running means for May 25-30 episode obtained by the application of 10-14 and 18-24 cutoff low-pass filter

average mean kinetic energy per unit mass, the second term represents the average fluctuational kinetic energy per unit mass and the third term is the average product of the mean and the fluctuational velocities. The third term gives the residual kinetic energy and by definition is equal to zero. Due to the use of digital numerical filtering techniques in calculating the mean and the fluctuational velocities the residual kinetic energy attained non zero but negligible values in this analysis.

One way of measuring the fluctuational intensity or the turbulence level is to calculate the ratio between the root mean square of the fluctuational velocity and the mean scalar speed (S). These are defined as the turbulence indices (i_x and i_y) for the shore-parallel and shore-perpendicular components respectively, expressed:

$$i_x = \frac{\sqrt{u'^2}}{S}$$

$$i_y = \frac{\sqrt{v'^2}}{S} \qquad [4.3]$$

4.6 EDDY DIFFUSIVITY CALCULATIONS

In studying the transport of particles in the coastal zone it is necessary to assign numerical values to the coefficients which represent the diffusivity. From a practical point of view, turbulent diffusion is still calculated largely from field studies. One method is to obtain the diffusion coefficients by measuring the turbulent properties of the flow using current-meter records (Eulerian measurements). This method is less direct than using Lagrangian measurements such as tracers (dye and drifts). Diffusion by it's nature is Lagrangian and the diffusion coefficients obtained by Eulerian approaches have to be related to the Lagrangian coefficients. In this study the diffusion coefficients are expressed in the terms of Eulerian statistics as

$$K_x = \sqrt{\overline{u'^2}}\, u\, \beta \int_0^{\infty} R_E(\tau)d\tau \qquad [4.4]$$

where u' and u are the fluctuational and the mean velocities obtained by applying the numerical digital filters discussed earlier, τ is a time lag variable and $R_E(\tau)$ is the Eulerian autocorrelation coefficient defined by

$$R_E = \frac{\sum_{t=0}^{T-\tau} u'(t)\, u'(t+\tau)}{\left\{ \sum_{t=0}^{T-\tau} u'^2(t) \quad \sum_{t=0}^{T-\tau} u'^2(t+\tau)\right\}^{1/2}} \qquad [4.5]$$

where T is the total record length. In [4.4] β is a dimensionless coefficient introduced by Hay and Pasquill, 1959. They showed that the Eulerian and the Lagrangian correlograms (the correlation coefficient as function of the time lag) are similar in shape and related to the β coefficient as follows:

$$R_E(t) = R_L(\eta)$$

where

$$\eta = \beta t \qquad [4.6]$$

For the sake of simplicity β has been arbitrarily assumed to be unity since an appropriate value of β is rather difficult to establish. To confirm the value of β, rather difficult Eulerian-Lagrangian field measurements are required at Cleveland or similar sites.

The integral time-scales were then computed by integrating the correlogram to the point of front zero crossing where $R_E(\tau)=0$. It is assumed here that the "turbulent eddies" have forgotten their origin. Thus the time-scale T_s is:

$$T_s = \int_0^{t_0} R_E(\tau)d\tau \qquad [4.7]$$

where t_0 is the time for the front zero crossing of the correlogram.

The length scales were computed using the frozen turbulence hypothesis (Taylor hypothesis,1921). This hypothesis implies that the gradient of the fluctuational velocity u′ in time is related to the gradient:

$$\frac{\delta u'}{\delta t} = -\bar{u} \frac{\delta u'}{\delta x} \qquad [4.8]$$

This relation is valid if the fluctuations occur at a much slower rate than the mean motion, i.e $u' << \bar{u}$. In this study the root mean square of the fluctuations was less than the average scalar speed most of the time. The length scale L_s was calculated using the expression

$$L_s = \bar{u} \cdot T_s \qquad [4.9]$$

4.7 EPISODIC (SINGLE EVENT) ANALYSIS

As remarked earlier, certain flow regimes that repeat themselves can be identified. To examine the structure of coastal currents and the turbulence field properties within the coastal boundary layer "single event" or "episodic" analysis is used here. An episode is defined as a segment of data with somewhat similar characteristics at all moorings. Five episodes were isolated from the total record for detailed analysis. Episodes 1 (May 25-30) and 4 (July 1-6) represent a strong shore-parallel current flow regime, episode 2 (June 1-6) represents a weak current flow regime and episodes 3 (June 8-22) and 5 (July 8-31) represent reversal current flow regime. See Figure 4.1 for more details.

3.8.1 Strong shore-parallel current event

In both episode 1 and episode 4, the flow was parallel to the shore and toward the north-east direction. On average the values of the current speed of episode 1 were higher than episode 4. The total time and spatial averages of the integrated scalar speed obtained from the 10 m depth current-meters along transect A-B were 13 cm/s and 10 cm/s for these episodes. The wind speed corresponding to episode 1 was strong (12 m/s on average) and blowing from the north-northeast direction. During episode 4 the wind speed was weaker (7 m/s on average) and blowing from the north-west direction. In the May episode the lake was unstratified, while in the July episode the lake was strongly stratified, the vertical temperature gradient being 2.5 °c /m at 17 m water depth. Figure 4.9 shows the daily average temperature profile for June and July 1979 recorded at (FTP) mooring number 40. No (FTP) record was available during

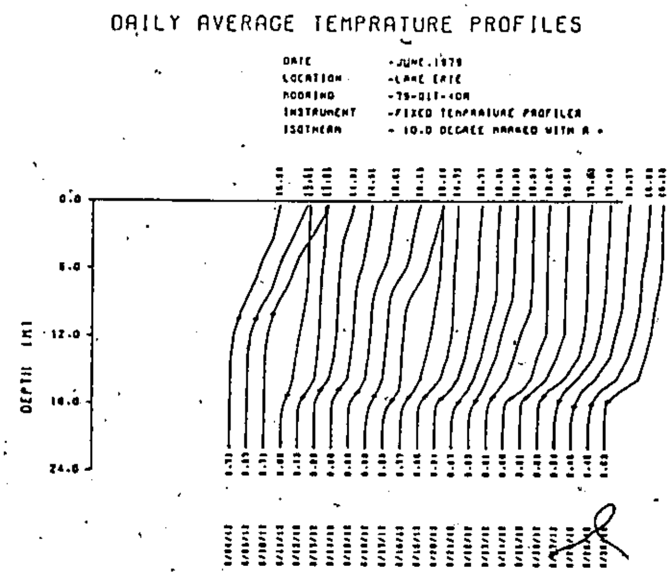

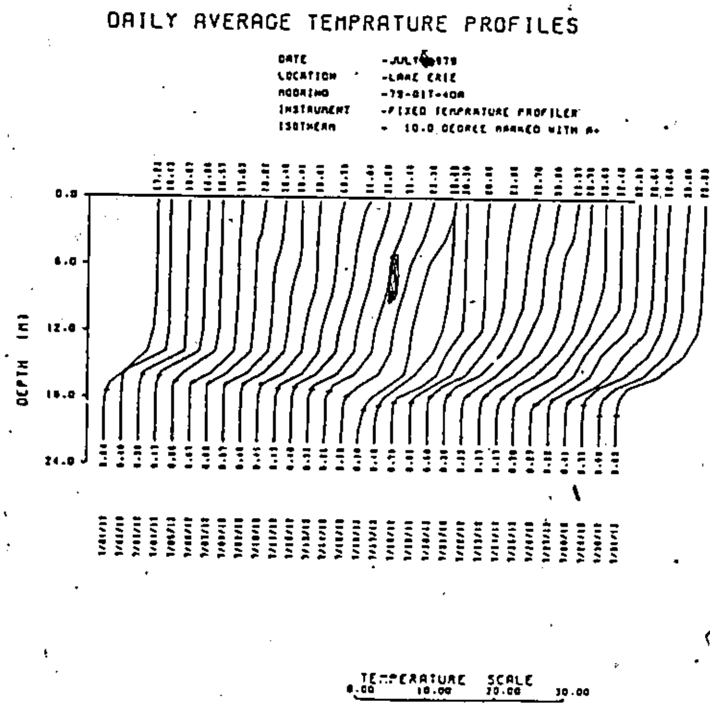

Figure 4.9 Daily average temperature profiles for June and July, 1979, FTP 40.

May, 1979. The maximum wind speed for the 1979 stratified period occurred during episode 1. The NNE wind was blowing along the lake's major axis. Typical return flow at 10 m depth and below was observed at all moorings. This return flow was against the wind and resulted from the high barotropic pressure gradient developed during the wind storm. During the May episode the wind was strong enough to mix the whole water depth, abruptly ending the stratification process started at the beginning of May. This is illustrated by plotting the temperature against the time for moorings 34 and 35 as shown in Figure 4.10.

The definition of the coastal boundary layer is vague, differing according to individual's interests and the objectives of their studies. From the coastal engineering point of view the coastal boundary layer is the area where waves break, generating longshore currents. Wave induced motion and turbulence at the bottom lead to resuspension and redistribution of deposited sediments. From the coastal circulation study point of view, the coastal boundary layer is the area where the currents and the thermocline are highly influenced by the shore and the bottom topography (Csanady, 1972 a,b; Brichfield, 1972; Bennett, 1973; Bennett and Lindstorm, 1977). In this study the definition and the characteristics of the coastal boundary layer are based on the variability of the mean flow, mean and turbulent kinetic energies and the horizontal turbulence as a function of distance from shore during the strong shore-parallel episode. The typical boundary layer characteristics are well exhibited during persistent strong shore-parallel currents.

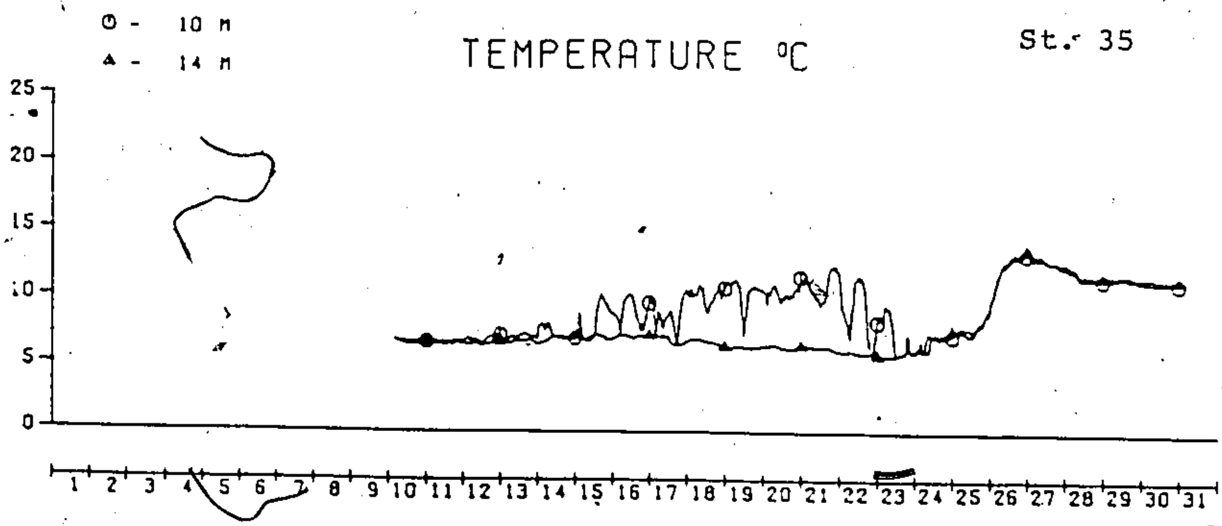

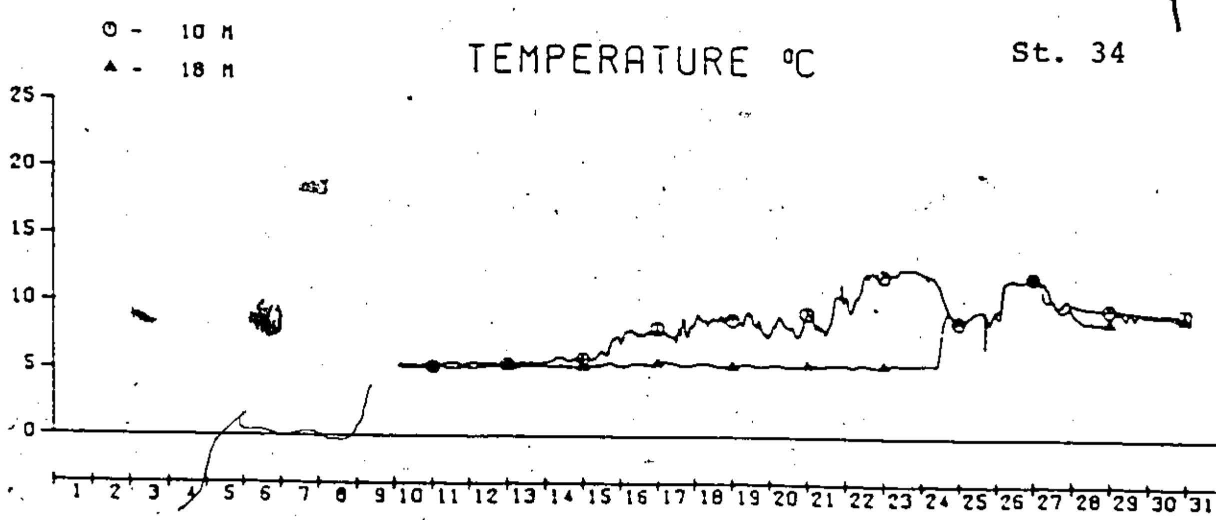

Figure 4.10 Time series of observed temperature for moorings 35 and 34.

The variability of the shore-parallel and onshore/offshore components of the mean current and the total kinetic energy with distance from shore is shown in Figures 4.11 and 4.12. The results are plotted for all 10 m current-meters on the main transect A-B and also station 39 on transect C-D for episodes 1 and 4. Stations 16 and 17 were excluded due to their relative remoteness from the main transect A-B. In both episodes, longshore mean current is directed towards the north-east direction accompanied by an onshore component. The mean current (and therefore the kinetic energy) attain a maximum at a distance of 14 km from shore, characterizing two distinct flow regimes, each of which exhibits typical boundary layer type of flow. Nearshore flow, within a few kilometers from the shore, is a result of the interaction of several physical factors, including bottom friction, which rapidly dissipates the kinetic energy of currents in shallow water. Thus the nearshore flow is designated the frictional boundary layer (FBL). The width is taken to be the distance to the point where the kinetic energy reaches a peak value. For the Cleveland site the FBL width is found to be 14 km. This is greater by a factor of six than the FBL width calculated from similar data at Douglas Point in Lake Huron (Murthy and Dunbar, 1981) and at Pickering in Lake Ontario (Bull and Murthy, 1980). A plausible explanation is that the width of the FBL changes with bottom slope, because friction is depth limited. Thus, where the bottom slopes steeply downward the FBL may be expected to be relatively narrow, and, conversely, where the bottom is relatively flat, relatively wide. At Douglas Point and Pickering the bottom slope is relatively steep (0.015 and 0.01 respectively) whereas at Cleveland the bottom slope is

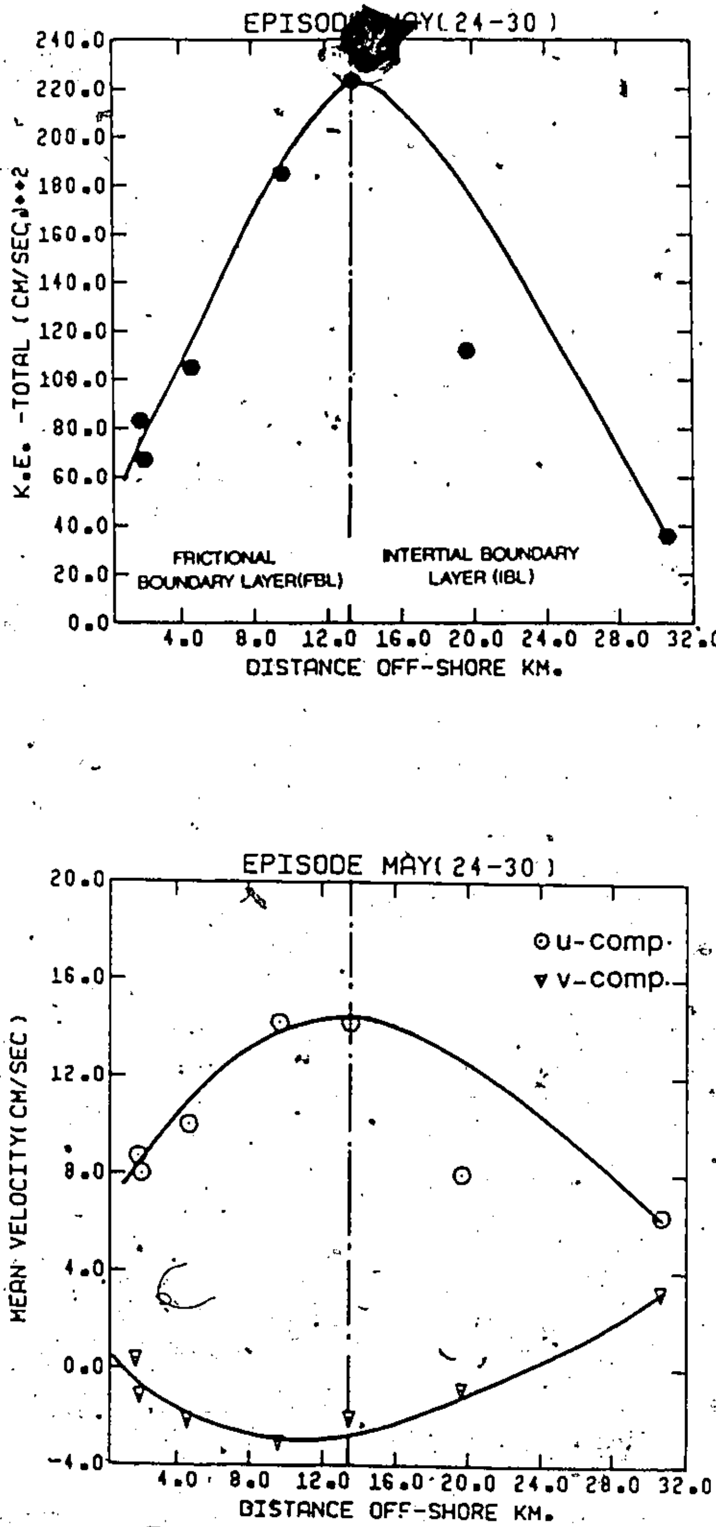

Figure 4.11 Total kinetic energy and mean velocities u and v for May 25-30 episode as a function of distance offshore.

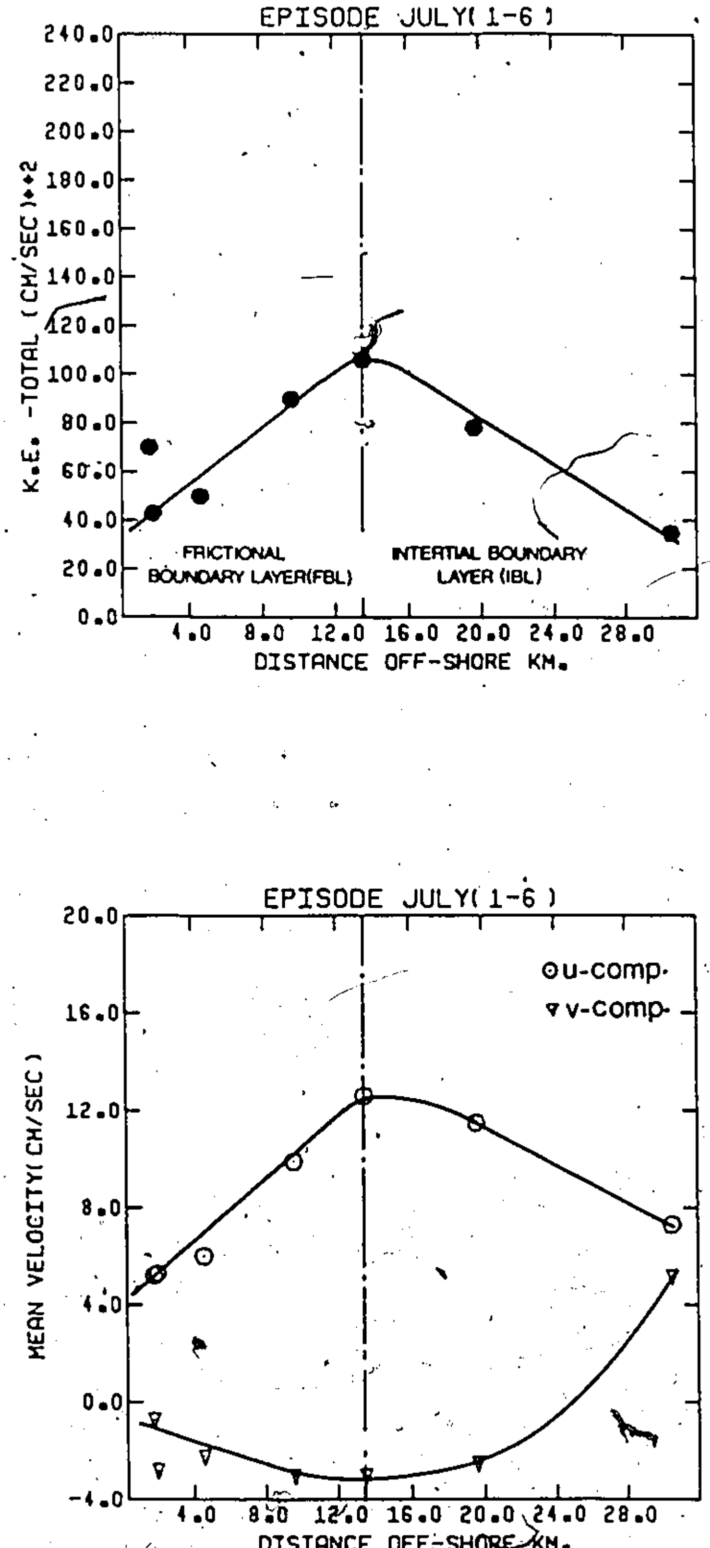

Figure 4.12 Total kinetic energy and mean velocities u and v for July 1 - 6 episode as a function of distance offshore.

relatively flat (0.002), thus accounting for a much larger FBL width.

Further offshore, beyond the zone of frictional influence, the adjustment of the inertial currents to shore-parallel currents takes place. The inertial currents have a nearly rotary motion, as a result of the balance between the local particle acceleration and Coriolis force due to the earth's rotation. This adjustment takes place in water deep enough to be stratified. Blanton (1974), while analyzing similar data off Oshawa in Lake Ontario, defined the width of the coastal boundary layer as the distance from shore where an abrupt increase in the inertial fraction of the kinetic energy is observed. He defined the inertial fraction of the kinetic energy as the ratio between the kinetic energy contained in the inertial band (12-24 hours) and the total kinetic energy of the spectra. He set arbitrarly the width of the coastal boundary layer as the distance offshore where the inertial fraction of the kinetic energy attains 50% or more of the total kinetic energy. In this study the inertial fraction of the kinetic energy did not exceed 26% of the total kinetic energy up to 20 km from shore. At Cleveland the coastal boundary layer (CBL) extends over an offshore distance of 30 km or so, much larger than the northshore of Lake Ontario (Csanady, 1972b; Blanton, 1974; Boyce, 1977) and the Douglas coastal site in Lake Huron (Murthy and Dunbar, 1981).

The distribution of the total kinetic energy per unit mass between the u and v components as a function of distance from the shore is plotted in Figure 4.13 for episodes 1 and 4. The kinetic energy of the u-component dominates everywhere.

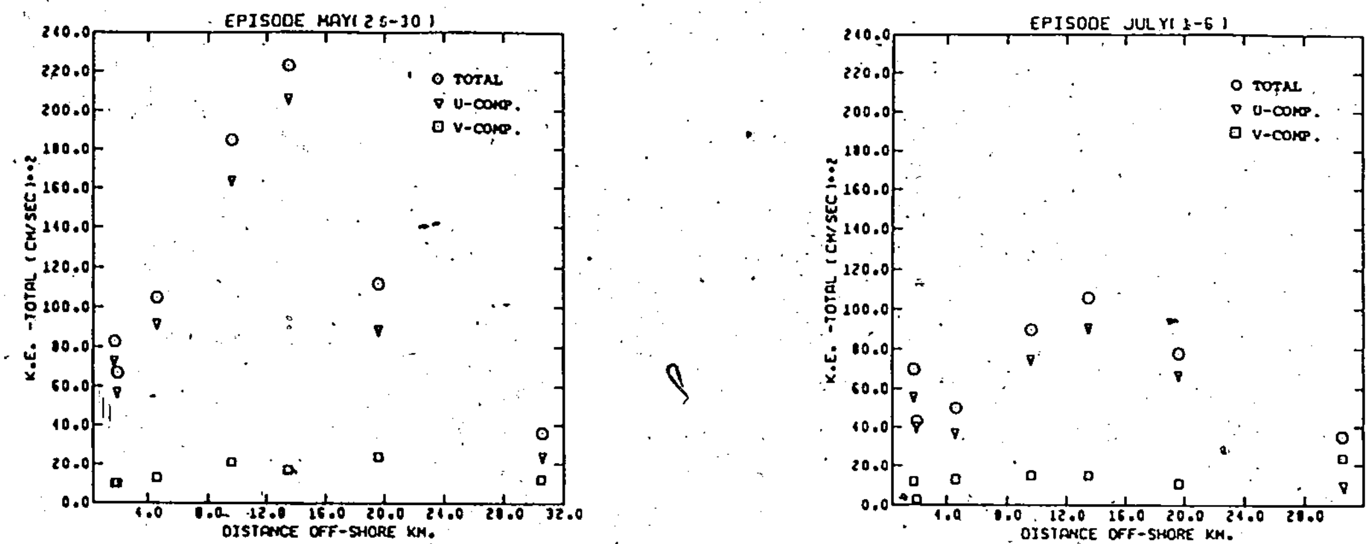

Figure 4.11 Alongshore and onshore/offshore kinetic energy variation as a function of distance from the shore for May 25-30 and July 1-6 episodes.

Figure 4.14 shows plots of the total, the mean and the fluctuational kinetic energies against the distance from shore for episodes 1 and 4. The mean kinetic energy dominates everywhere. In the May episode the fluctuational kinetic energy attains maximum values of 16.4% and 14.2% of the total kinetic energy at moorings 37 and 34 respectively. In the July episode it attains maximum values of 11% and and 7.9% at moorings 36 and 34 respectively. The variability of turbulence indices (i_x and i_y) as a function of distance from shore is plotted in Figure 4.15 for episodes 1 and 4. In the May episode the turbulence indices attain in general higher values than those of the July episode, indicating higher field turbulence during the May episode. Close to the shore and far from the shore the turbulence indices attain high values due to the contribution of the bottom and shore friction and due to the inertial oscillation respectively. Lower values are attained at intermediate distances from the shore.

Figure 4.16 shows some examples of correlograms (autocorrelation coefficient versus time lag) for the u and v components for episode 1 and 4. The correlograms are plotted for stations 37 and 12 up to the first zero intersection.

The mean velocities, total kinetic energies, variances, integral time scales and the horizontal exchange coefficients computed from the available current-meter records in the study area are summarized in Tables 4.1 and 4.2 for episodes 1 and 4 respectively. Moorings 37/10 to 11/10 inclusive represent the upper layer (epilimnion), moorings 35/14, 34/18 and 38/17 represent the lower layer (hypolimnion) and moorings 35/16 to 16/21 inclusive represent the bed characteristics.

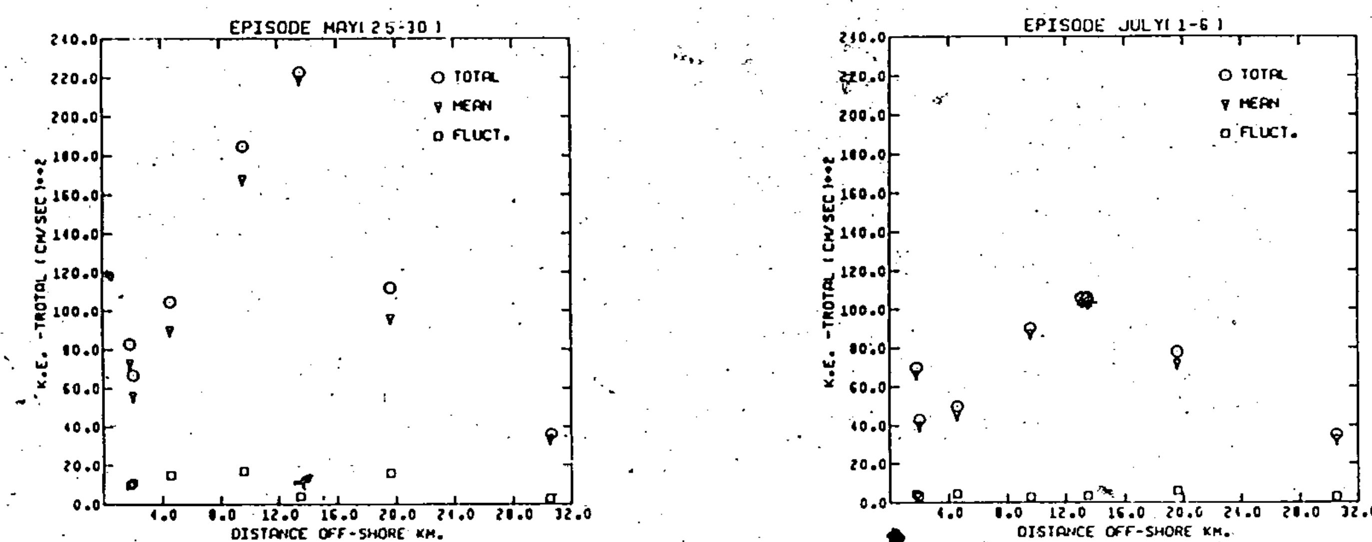

Figure 4.14 Mean, fluctuational and total kinetic energies variation as a function of distance from the shore for May 25-30 and July 1-6 episodes.

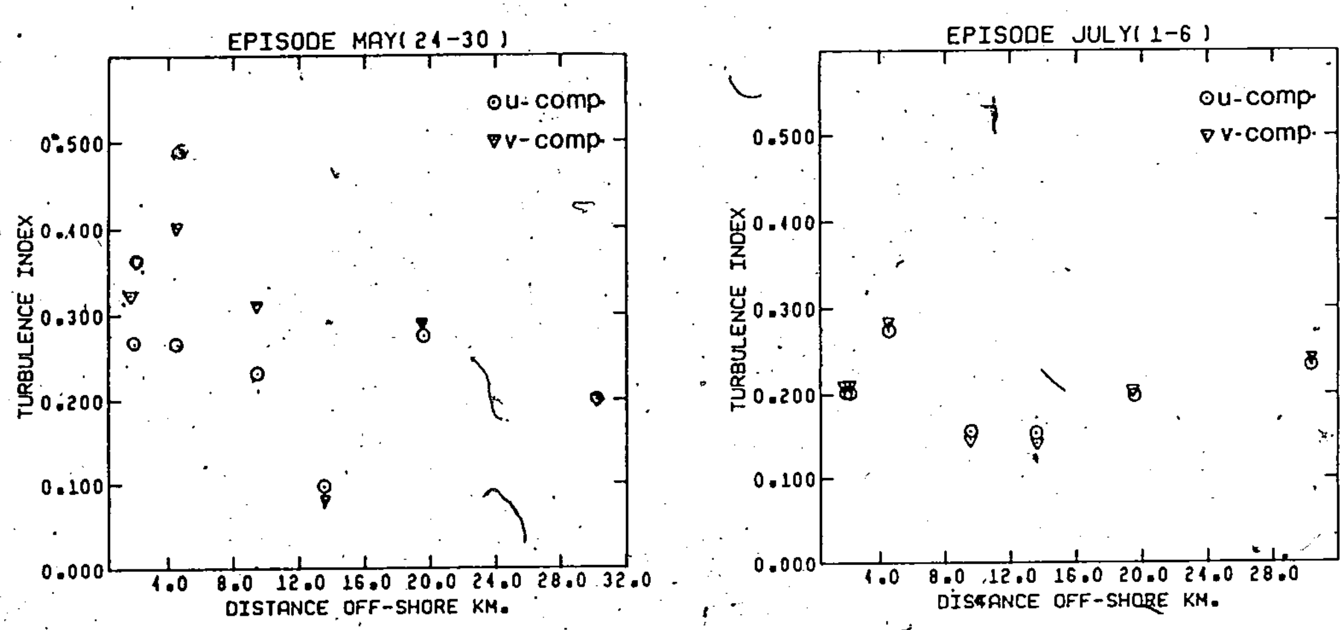

Figure 4.15 Turbulence indices i_x and i_y as a function of distance from the shore.

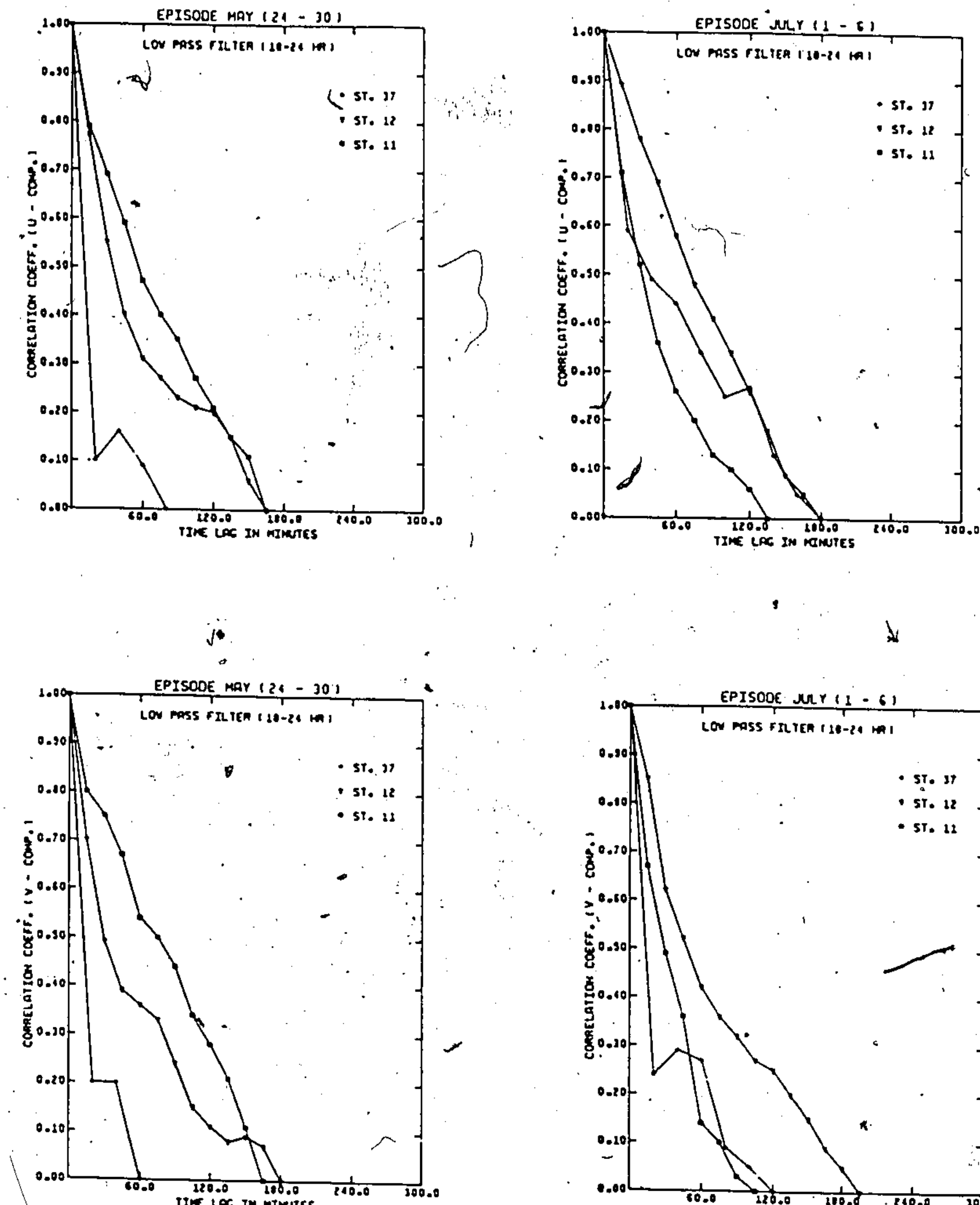

Figure 4.16 Representative Eulerian autocorrelation coefficients for u and v components.

Table 4.1: Computed mean and turbulence parameters using the 18-24 h low-pass filter, May 24 to 30, 1979 episode

St. No. / Depth (m)	Dist. off-shore (km)	Mean velocity cm/s		K.E. Total $(cm/s)^2$		Variance $(cm/s)^2$		Time scale s $\times 10^2$		Horiz. Diffusion $cm^2/s \times 10^4$	
		u	v	u	v	u	v	T_{sx}	T_{sy}	K_x	K_y
37/10	2.0	8.1	0.4	57.	10.	10.3	11.7	15.6	9.0	4.1	0.1
39/10	1.8	8.5	-1.1	73.	10.	8.0	10.7	32.4	14.4	7.9	0.5
36/10	4.6	10.1	-2.1	92.	13.	10.0	20.0	24.0	6.6	7.7	0.6
35/10	9.6	14.2	-3.0	164.	21.	12.2	21.0	24.0	6.0	12.0	0.8
12/10	13.5	14.1	-1.8	206.	17.	5.4	2.4	45.6	37.2	15.0	1.0
34/10	19.6	8.0	-.8	89.	24.	14.0	17.8	14.4	13.8	4.3	0.5
11/10	30.5	6.3	3.2	24.	12.	2.0	2.1	45.6	52.8	4.1	2.5
35/14	9.6	14.1	-1.1	166.	21.	34.0	34.0	11.4	10.2	9.4	0.7
34/18	19.6	7.0	-3.5	97.	40.	50.0	46.0	19.2	6.0	9.5	1.4
38/17	11.5	14.6	0.3	205.	18.	28.0	29.0	9.0	7.2	7.0	0.1
35/16	9.6	12.0	0.8	114.	10.	10.0	8.8	21.0	10.8	8.0	0.3
11/21	30.5	1.9	0.5	19.	17.	9.0	5.0	66.6	56.4	3.8	0.6
38/19	11.5	11.3	1.2	117.	9.	9.0	8.0	21.0	14.4	7.1	0.5
17/18	9.6	5.4	3.0	27.	24.						
16/22	15.6	5.8	2.4	28.	12.	6.0	3.2	64.8	51.6	9.2	2.2

Table 4.2: Computed mean and turbulence parameters using the 18-24 h low-pass filter, July 1 to 6, 1979 episode

St. No. / Depth (m)	Dist. off-shore (km)	Mean velocity cm/s		K.E. Total $(cm/s)^2$		Variance $(cm/s)^2$		Time scale $s \times 10^2$		Horiz. Diffusion $cm^2/s \times 10^4$	
		u	v	u	v	u	v	T_{sx}	T_{sy}	K_x	K_y
37/10	2.0	5.2	-0.8	40.	3.	3.0	3.4	36.6	19.2	3.3	0.3
39/10	1.8	5.3	-2.6	58.	12.	4.0	5.7	29.4	10.8	3.1	0.6
36/10	4.6	6.0	-2.2	37.	13.	5.0	6.0	36.0	13.2	4.8	0.7
35/10	9.6	9.9	-3.2	75.	15.	3.5	2.6	40.8	31.8	7.6	1.6
12/10	13.5	11.0	-3.4	91.	15.	4.0	3.0	46.8	48.0	10.3	2.8
34/10	19.6	10.5	-2.5	67.	11.	6.0	6.2	60.0	46.8	15.4	2.9
11/10	30.5	3.2	5.2	10.	25.	3.0	3.5	52.2	43.8	2.9	4.3
35/14	9.6	10.0	-1.3	75.	10.	7.8	9.3	21.0	19.8	5.9	0.8
34/18	19.6	10.0	-2.0	92.	24.	24.0	21.0	44.4	37.2	21.8	3.4
38/17	11.5	10.0	-1.3	91.	14.	10.0	10.0	26.4	15.6	8.3	0.6
35/16	9.6	7.1	1.0	41.	5.	4.0	5.5	36.6	40.8	5.2	1.0
11/21	30.5	4.1	-1.0	25.	13.	8.6	9.4	84.0	80.4	10.1	2.5
38/19	11.5	7.0	2.0	46.0	6.	3.6	2.5	40.8	22.8	5.4	0.7
17/18	9.6	7.0	-1.5	47.	8.	7.0	4.6	69.6	78.8	12.9	2.5
16/22	15.6	5.7	.3	30.	13.	3.4	4.8	73.2	75.0	7.7	.5

A number of results may be derived from the computed mean and turbulence parameters tabulated in Tables 4.1 and 4.2. The values of the mean velocities and kinetic energies in all moorings and depths indicate a peak around a distance of 12-14 km from the shore. In both episodes the shore-parallel component at all depths is directed toward the north-east. The shore-perpendicular component at the upper layer (10 m) current-meters is directed toward the shore, while at the lower layer and bed current-meters an offshore component is observed, indicating downwelling. The shore-parallel kinetic energy dominates everywhere except far from the shore. The values of the variances in the May episode are higher than those of the July episode. The maximum values of the variances are observed close to the shore and to the thermocline (mooring 35/14). The time scales range from 600 to 8400 seconds. In the May episode the time scales are shorter than those of the July episode. In general the fluctuational kinetic energies of episode 1 are higher than those of episode 4, therefore, the correlograms drop rapidly and the time scales are shorter. Horizontal exchange coefficients range from a low of 10^3 cm^2/sec to a high of 2×10^5 cm^2/sec and order of magnitudes are generally consistent with the values published in the literature using similar calculations (Callaway, 1974). Exchange coefficients in the alongshore direction (K_x) are somewhat greater than the exchange coefficients in the onshore/offshore direction (K_y), indicating that the turbulence structure in the coastal boundary layer is anistropic. In both episodes, close to the shore (mooring 35), the horizontal exchange coefficients attain smaller values in the lower layer (35/14 and 35/16) than those of the upper layer (35/10). Similar results were reported by Murthy (1971). In a diffusion experiment to study dye spread in the central basin of Lake Erie, Murthy (1971) found that the horizontal spread of the dye patch in the hypolimnion was small, at least one order of magnitude less than the epilimnion dye spread.

4.7.2 Weak current event

From the waste disposal point of view the weak current event is one of the worst events. Due to the low transport and mixing associated with the event, very high concentrations are expected within the coastal zone. If the weak current event is followed by an onshore flow regime the high concentration pollutant is advected toward the shoreline creating unfavourable conditions. The weak current regime is represented by episode 2 (June 1-6). The same techniques used in analyzing the strong shore-parallel event were used to analyze the weak current event. Results are summarized in Table 4.3.

The average shore-parallel and shore-perpendicular components of the weak current event are less than those of the strong shore-parallel event by factors of 6 and 2.5 respectively. In episode 2, the two well-defined boundary layers observed during the strong shore-parallel episodes are not strongly exhibited but can still be identified. The u and v kinetic energies associated with episode 2 are less than those of the strong shore-parallel episodes by factors of 10 and 2 respectively. The turbulent kinetic energy level in episode 2 is less than that of episodes 1 and 4 by a factor of 2.5 while the time scales are larger by a factor of 2 on the average. The values of K_x are less by a factor of 5

Table 4.3: Computed mean and turbulence parameters using the 18-24 h low-pass filter, June 1 to 6, 1979 episode

St. No. / Depth (m)	Dist. offshore (km)	Mean velocity cm/s		K.E. Total $(cm/s)^2$		Variance $(cm/s)^2$		Time scale s $\times 10^2$		Horiz. Diffusion $cm^2/s \times 10^4$	
		u	v	u	v	u	v	T_{sx}	T_{sy}	K_x	K_y
37/10	2.0	1.4	0.2	10.	5.	4.4	6.8	56.4	64.2	1.7	0.3
39/10	1.8	2.0	-0.9	10.	7.	5.6	8.6	57.6	57.6	2.7	1.5
36/10	4.6	2.6	-0.9	11.	8.	6.0	8.4	81.6	84.0	5.2	2.2
35/10	9.6	4.9	-2.4	17.	6.	3.6	2.0	52.8	46.2	4.9	1.6
12/10	13.5	0.7	-0.5	7.	10.	6.0	7.0	82.8	85.8	1.4	1.1
34/10	19.6	-0.2	-0.4	6.	9.	4.6	6.0	87.6	92.4	0.5	1.0
11/10	30.5	1.6	-1.3	6.	6.	5.0	3.8	46.2	34.2	1.7	0.9
35/14	9.6	0.8	0.8	7.	7.	5.6	6.8	82.8	79.8	1.5	0.4
34/18	19.6	-0.7	-0.2	4.	7.	3.6	5.0	87.0	88.8	1.2	0.3
38/17	11.5	0.1	0.9	6.	6.	4.5	4.0	77.4	87.0	0.2	1.6
35/16	9.6	0.7	0.2	3.	3.	2.0	2.7	63.0	68.4	0.6	0.2
11/21	30.5	-1.4	0.3	4.	5.	3.5	4.6	43.2	55.2	1.1	0.4
38/19	11.5	-0.4	1.0	4.0	4.	3.0	2.8	67.2	70.8	0.5	1.2
17/18	9.6	-3.7	1.8	19.	17.	7.0	7.4	84.0	83.4	8.2	4.1
16/22	15.6	0.6	.02	5.	5.	2.3	3.4	54.6	69.6	0.5	.03

while the values of K_y are comparable.

4.7.3 Current reversal event

The current reversal event is defined as an episode during which the shore-parallel currents change direction in a matter of six to eight hours. The current reversal regime is of particular significance from the viewpoint of waste disposal. The current reversal regime is usually accompanied by cases of upwelling and downwelling within the coastal boundary layer. During upwelling and downwelling a mass exchange between the coastal and offshore waters takes place. The current reversal regime is represented by episode 3 (June 8-21) and episode 5 (July 7-31). In spite of the fact that the current reversal is not clearly exhibited in some moorings, these two episodes are still the closest episodes to the current reversal regime in the entire data record.

The vertical displacement of temperature with time at a fixed point of measurement indicates a case of upwelling or downwelling. In the case of upwelling a cold mass of water is forced toward the surface from a lower equilibrium level and a temperature drop is to be expected. In the case of downwelling a warm water mass is forced toward the bottom and a temperature rise is expected. Figure 4.17 shows the temperature variability as function of time during the month of June and July, 1979 for moorings 39, 37 and 36. Cases of upwelling and downwelling can be observed, denoted by U and D respectively. By relating Figure 4.17 to the current vector plots in Figure 4.1, one can observe that the cases of upwelling and downwelling occur approximately at mid point between

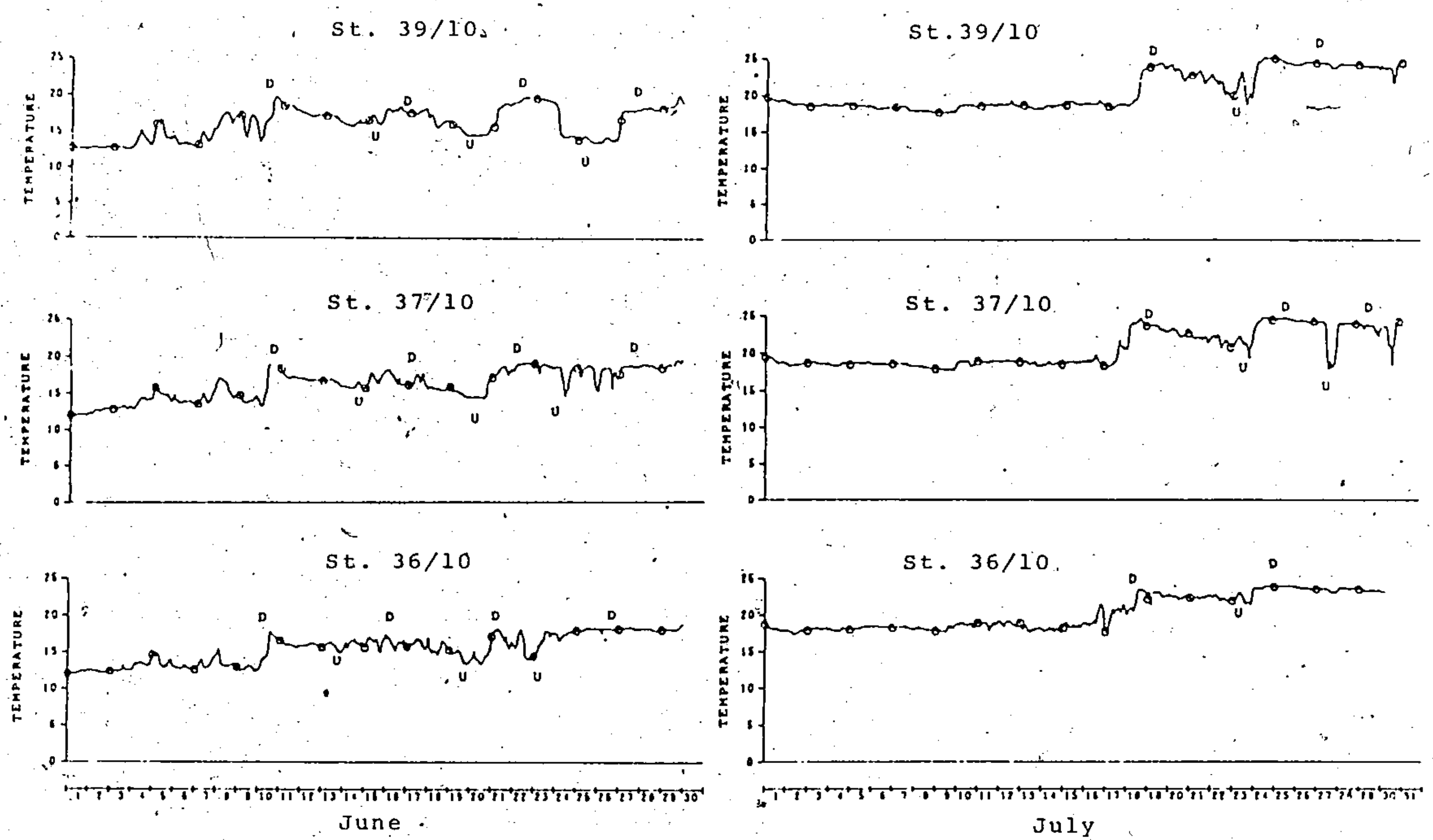

Figure 4.17 Time series of observed temperature for moorings 39/10, 37/10 and 36/10 during June and July, 1979.

current reversal.

The results of applying the same techniques used earlier are tabulated in Tables 4.4 and 4.5 for episodes 3 and 5 respectively. Due to the current reversal the mean velocities are relatively low compared with those of the strong shore-parallel current event. The mean kinetic energy level attains an intermediate range between the strong shore-parallel current and the weak current events. On average the mean kinetic energy level is less than that of the strong shore-parallel current regime by factors of 4 and 2 for u and v respectively. The values of the turbulent kinetic energy are comparable with those of the strong shore-parallel current, while the values of the time scales are comparable with those of the weak current. The values of K_x are less than those of the strong shore-parallel by a factor of 3, while the values of K_y are comparable.

4.8 HORIZONTAL EXCHANGE COEFFICIENTS

In Figure 4.18, the horizontal exchange coefficients are plotted continuously (based on the five episodes calculations) for the top layer current meters. As can be seen, there are periods of high values and periods of low values and these coincide with the turbulent kinetic energy level in the coastal boundary layer. The values of K_x are generally six times larger than K_y, indicating anisotropic turbulence structure within the coastal boundary layer. There is no obvious relation between the diffusivities and the distance from shore.

In Figure 4.19, the eddy diffusivity is plotted against the Eulerian integral length scale for both components at all moorings and

Table 4.4: Computed mean and turbulence parameters using the 18-24 h low-pass filter, June 8 to 22, 1979 episode

St. No. / Depth (m)	Dist. off-shore (km)	Mean velocity cm/s u	v	K.E. Total $(cm/s)^2$ u	v	Variance $(cm/s)^2$ u	v	Time scale s $\times 10^2$ T_{sx}	T_{sy}	Horiz. Diffusion $cm^2/s \times 10^4$ K_x	K_y
37/10	2.0	2.0	0.1	31.	9.	8.3	8.8	56.4	46.2	3.2	0.2
39/10	1.8	2.3	-1.4	37.	11.	13.6	12.5	51.6	40.8	4.4	2.1
36/10	4.6	1.0	-0.6	33.	15.	10.0	13.6	58.2	54.0	1.8	1.2
35/10	9.6	-1.1	1.4	33.	12.	5.4	5.9	39.8	37.8	1.0	1.3
12/10	13.5	1.3	-0.6	27.	10.	9.2	8.4	70.8	62.4	2.9	1.0
34/10	19.6	-1.2	-0.1	16.	10.	10.8	8.5	61.2	51.6	2.4	0.2
11/10	30.5	3.7	0.02	20.	12.	8.5	6.5	40.8	44.4	4.4	0.02
35/14	9.6	0.3	0.6	30.	16.	10.4	16.0	58.2	49.8	0.5	1.3
34/18	19.6	-1.0	0.8	21.	21.	18.5	23.2	45.6	48.6	2.0	1.8
38/17	11.5	-1.0	0.9	27.	18.	12.0	13.5	37.8	62.4	1.3	2.1
35/16	9.6	0.04	0.5	18.	6.	3.6	4.8	32.4	45.6	0.02	0.5
11/21	30.5	-1.8	0.1	11.	9.	6.6	6.4	63.0	68.4	2.9	0.2
38/19	11.5	-0.7	-0.2	13.0	7.	3.6	4.0	36.0	46.8	0.5	0.2
17/18	9.6	-3.1	2.4	30.	14.	9.2	5.4	73.2	69.6	6.9	3.9
16/22	15.6	-1.4	1.3	9.	9.	5.8	5.0	59.4	71.4	2.0	2.1

Table 4.5: Computed mean and turbulence parameters using the 18-24 h low-pass filter, July 7 to 31, 1979 episode

St. No. / Depth (m)	Dist. off-shore (km)	Mean velocity cm/s		K.E. Total $(cm/s)^2$		Variance $(cm/s)^2$		Time scale s $\times 10^2$		Horiz. Diffusion $cm^2/s \times 10^4$	
		u	v	u	v	u	v	T_{sx}	T_{sy}	K_x	K_y
37/10	2.0	0.02	0.1	15.	6.	4.2	5.4	54.0	25.8	0.02	0.05
39/10	1.8	0.5	-0.6	17.	7.	6.2	5.0	54.6	48.0	0.7	0.6
36/10	4.6	-1.0	-0.3	14.	5.	5.4	5.0	58.2	56.4	1.4	0.4
35/10	9.6	-2.1	1.7	14.	7.	3.3	3.0	46.2	50.4	1.8	1.5
12/10	13.5	-3.0	1.0	21.	7.	6.6	4.9	67.2	69.6	5.2	1.5
34/10	19.6	-0.9	1.1	16.	12.	11.2	9.2	67.2	75.0	2.0	2.6
11/10	30.5	3.2	1.6	15.	10.	4.4	5.4	53.4	49.8	3.6	1.9
35/14	9.6	-1.7	0.7	19.	11.	10.0	12.0	68.4	70.2	3.7	1.7
34/18	19.6	-0.5	1.6	31.	29.	30.0	30.0	82.8	85.8	2.3	7.5
38/17	11.5	-2.0	0.8	14.	8.	8.0	10.0	76.2	75.0	4.3	1.9
35/16	9.6	-1.3	0.3	9.	3.	4.0	4.0	66.0	68.4	1.7	0.4
11/21	30.5	-1.3	0.1	11.	8.	4.0	8.0	33.6	54.0	0.9	0.2
38/19	11.5	-1.4	0.5	5.	2.	1.5	2.0	55.8	55.2	1.0	0.4
17/18	9.6	3.4	-0.5	32.	8.	6.0	3.0	59.4	41.3	4.9	0.4
16/22	15.6	-1.4	0.8	8.	5.	6.0	6.0	64.2	73.2	2.2	1.4

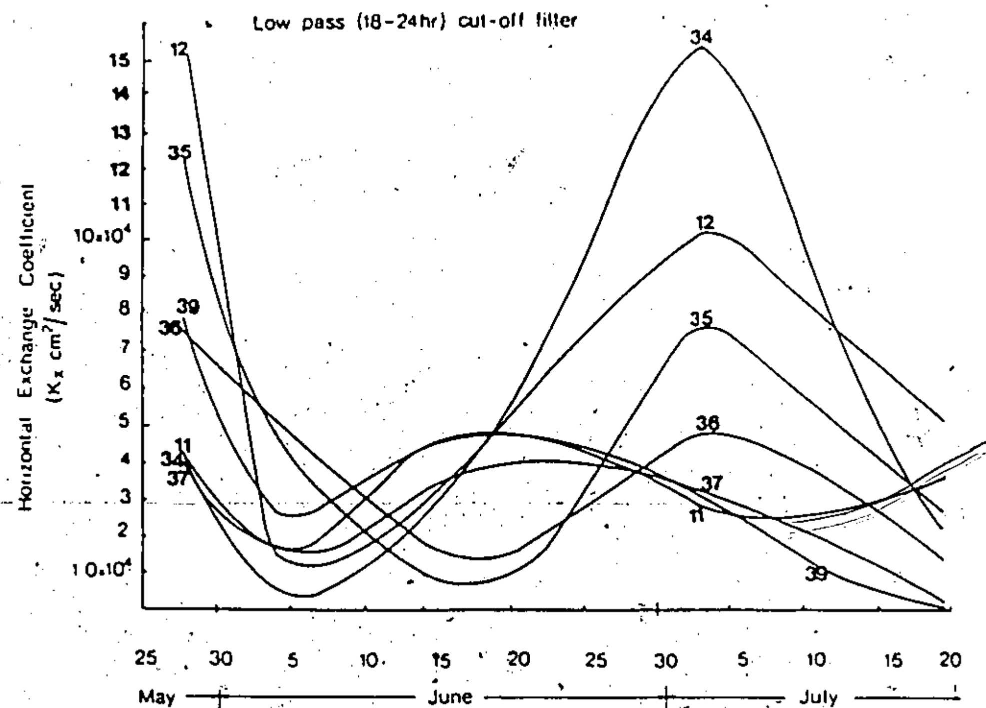

(a)

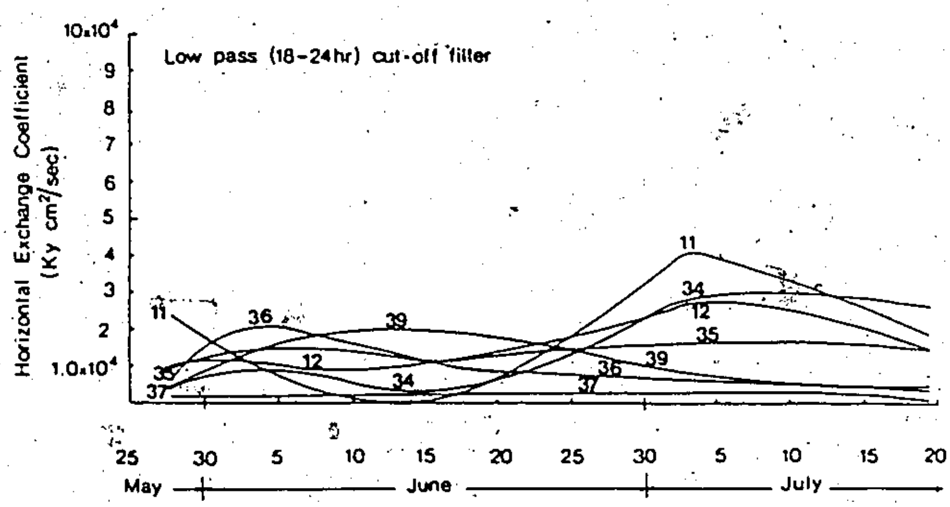

(b)

Figure 4.18 Horizontal exchange coefficients: (a) K_x and (b) K_y as a function of time (all 10 m current meters).

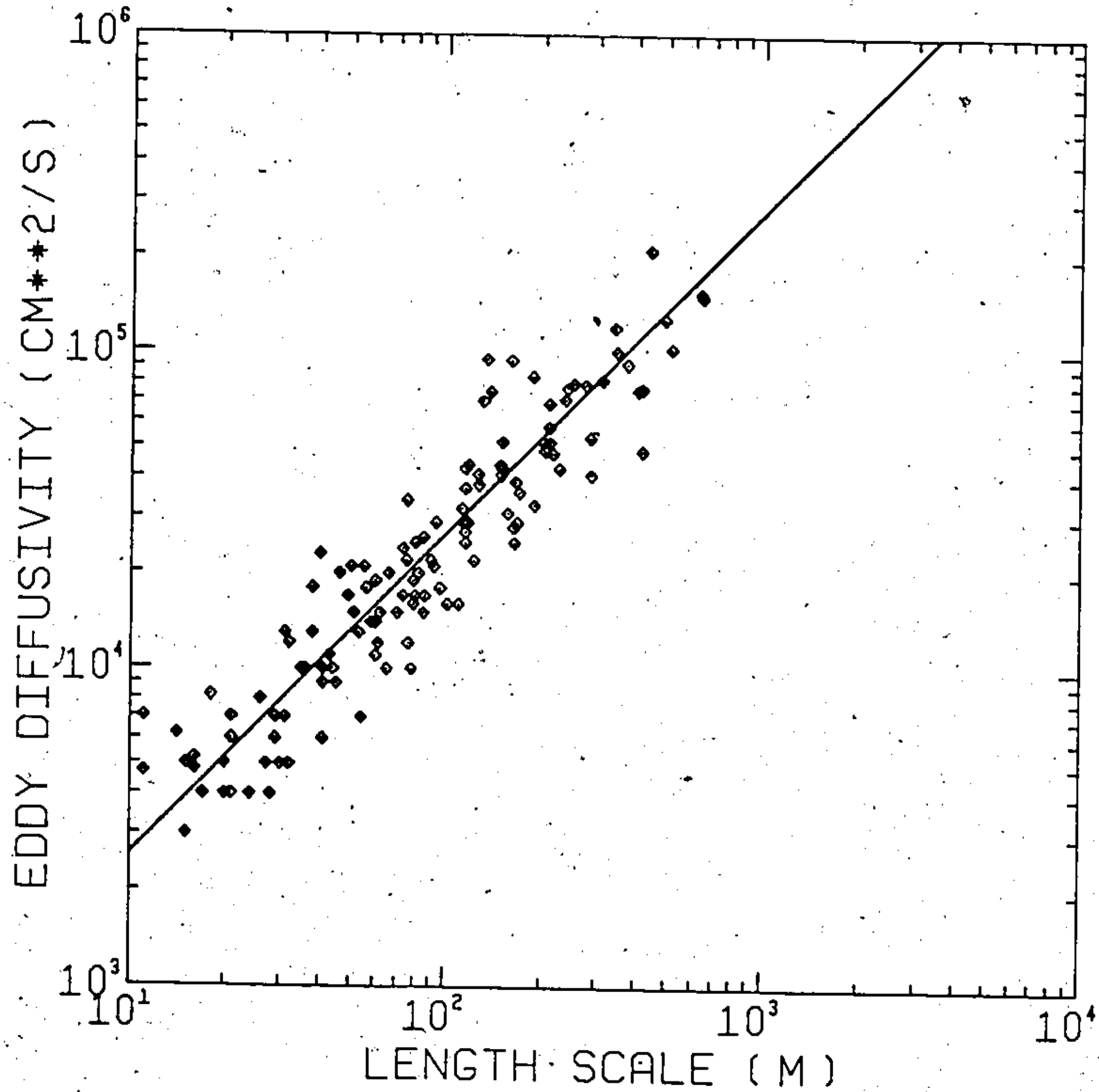

Figure 4.19 Diffusion coefficient as a function of length scale (all moorings both directions).

depths. The reader is refered to Chapter 2 for the detailed discussion of the fundamental diffusion diagrams. A regression analysis was carried out to find the diffusion law:

$$K = 2.5 \times L_s^{1.01} \qquad [4.10]$$

where K is the diffusion coefficient in cm^2/s and L_s is the Eulerian integral length scale in cm. Equation [4.10], indicates that the governing diffusion law in the vicinity of Cleveland is shear diffusion rather than inertial sub-range diffusion. Similar results were obtained by Callaway, 1974 and Murthy, 1976. It is important to note that due to the proximity of the shoreline the Eulerian integral length scale covered in the diffusion diagram does not exceed 700 m.

4.9 DISCUSSION

As mentioned earlier, the results of this part of the study are very important to the whole study thrust. From the waste disposal point of view, five episodes representing three different flow regimes, namely strong shore-parallel currents, weak currents and current reversal regimes were subjected to detailed analyses. The strong shore-parallel current regime showed maximum transport along the shore with high longitudinal exchange coefficient. Due to the anisotropic nature of the turbulence structure within the coastal boundary layer, coastal pollutants are expected to be retained within the coastal zone. During the weak current regime, the currents and the exchange coefficients attained low values, hence a very high pollutant concentration is expected in the immediate vicinity of the source. During the current reversal regime, cases of upwelling and downwelling with mass exchange between the coastal and offshore waters were observed. The currents and the exchange coefficients attained an intermediate range between the strong shore-parallel current and the weak current regimes.

From the results of the five episodes, the average time and the length scales were 4900 seconds and 200 meters respectively. The closest distance between any two adjacent current-meters in the coastal arrays of our study was about 2 km (10 times the average length scale), therefore it is neccessary to generate current data between the stations. The time scale recommended for the numerical solution of the hydrodynamic and the mass transport models is 10 to 15 minutes.

Coastal boundary layer characteristics were exhibited during the strong shore-parallel current episodes. The results showed an inner boundary layer (FBL) about 14 km out from the shore, while the width of the coastal boundary layer (CBL) extends over an offshore distance of 30 km or so.

The regression equation obtained from the diffusion diagram, Figure 4.19, showed that the shear diffusion (linear length scale diffusion) governs the diffusion in the coastal zone of lake Erie in the vicinity of Cleveland.

As there was not enough data available for the analysis of the vertical circulation and the vertical diffusivity, this analysis is carried out using the hydrodynamic models (Chapter 5). The results from this part of the study are used in the next two Chapters, 5 and 6.

PHASE 2: HYDRODYNAMIC MODELS

CHAPTER 5

HYDRODYNAMIC MODELS

5.1 INTRODUCTION

The results obtained from the analysis of the current-meter data (Chapter 4) showed that the width of the coastal boundary layer is about 30 km. Using the inertial frequency to separate the mean and the fluctuation velocities, the average length scale or "eddy size" was found to be 500 meters. Since the smallest distance between any two adjacent current-meters was about 2 km, as shown in Figure 3.2, the spatial resolution of the current-meter data was coarser than the average eddy size. To obtain the flow field for this fine spatial resolution, it is necessary to synthesise, or generate, a conformable field of velocity vectors.

Two approaches may be used: (1) Interpolation and extrapolation (Lam, 1984) based on a two-dimensional grid and a set of observed currents, without satisfying the continuity equation in the first step. This generated flow field will create or destroy mass. To avoid this difficulty the objective analysis method is used in the second step by subjecting the interpolated current field to an optimization procedure with a continuity constraint (Sasaki, 1970; Sherman, 1976). This approach could be generalized to generate three-dimensional flow fields if vertical velocity observations are available. Unfortunately the vertical velocity is very small and beyond the detection capabilities of available direct measurement instruments (1 cm/s). The vertical velocity is effectively zero except close to the shore (within the coastal boundary layer) where upwelling and downwelling takes place. In this study, the detailed vertical structure of the flow and the vertical velocity are significant, so the interpolation and extrapolation approach is not suitable.

(2) The second approach is to use hydrodynamic models to predict the flow field. The models are classified into steady and unsteady models, with respect to time; one, two and three dimensional models with respect to space; and non-stratified and stratified models with respect to temperature profile. The model required in this study is a three dimensional time-dependent, stratified hydrodynamic model. Three dimensional models of flow in a stratified lake are complex, difficult to program and use, and the results are difficult to interpret (Heinrich, et al., 1981). Moreover, to avoid the subgrid diffusion problem the horizontal grid size should be approximately 500 m, and the vertical grid size, about 2 m. As a first step, such a model of Lake Erie could use a coarse grid, say 6 km horizontally, requiring 5000 grid points. In the second step the coastal boundary layer near Cleveland could be resolved using a finer grid of about 0.5 km i.e. 10,000 grid points. Based on the time scale calculations in Chapter 4, the basic time step required is about 15 minutes. An episode lasting one week thus requires 672 time steps. Using usual main frame resources, such a model study is expected to be very expensive. The cross-section of the central basin of lake Erie from 10 km to the east and 10 km to the west of Cleveland does not vary significantly. The wind field is also

considered not to vary over this distance significantly. Therefore the general flow field is not expected to vary much in the east-west direction over this distance.

The rigid-lid channel-type model developed by Simons (1983), has been modified by the writer to include non-linear acceleration terms. Two different forms of the vertical eddy viscosity were also added. To find the parameters which will most significantly affect the simulation results, sensitivity analyses were carried out. The verified and calibrated model was then used to generate the flow field in the coastal zone off Cleveland. Variable flow properties in the vertical direction and in one horizontal direction perpendicular to the shore-line were modelled. An along-shore pressure gradient was included so that the flux perpendicular to the channel cross section is zero. The results were compared to the available current-meter data for several episodes. In addition a two-dimensional X-Y model developed by Simons and Lam (1982) was tested and used to verify some of the results specially for weak, or nonstratified, periods.

5.2 CHANNEL-TYPE MODEL "ERCH"

Simons (1983) developed a model to simulate the channel-type response observed in the Great Lakes, e.g. Lake Ontario (Boyce and Mortimer, 1978). After a strong north-west wind impulse, alongshore baroclinic jets associated with nearshore upwelling and downwelling and wave-like phenomena in open water with periods near the inertial period of the Great Lakes (16-18 h) were observed. Simons assumed that the properties of the flow vary only in two directions: vertical and shore-perpendicular. The along-shore pressure gradient is modelled such that the net along-shore flux is zero. The model uses the rigid-lid approximation whereby surface gravity waves are filtered out. The Boussinesq approximation is used, (the water density is constant except in the hydrostatic equation where the density variations affect the gravitational acceleration i.e. fluid buoyancy). The model computes the flow field and the temperature profile at each time step by solving the whole cross section using a coarse grid size. The values obtained are used to define the off-shore boundary conditions of the coastal boundary layer which is then resolved using a finer grid size. In large-scale circulation, the Rossby number (a measure of the ratio of the nonlinear acceleration term to the Coriolis term) is of the order of 10^{-2}, and so the nonlinear terms may be neglected. In the coastal zone the length scale decreases, the velocity and the velocity gradient increase rapidly, indicating the importance of the nonlinear acceleration terms. Typical values for the coastal zone motions in the coastal zone of Lake Erie (Chapter 4) are U=20 cm/s, $L=10^6$ and $f=10^{-4}$, the Rossby number (R=U/fL) is of the order of 0.2. For these reasons the model was modified to include the vertical and the shore perpendicular nonlinear acceleration terms. The new model is called ERCH (ERie CHannel).

5.2.1 Basic equations and parameters

The basic equations used in ERCH after adding the nonlinear terms are:

$$\frac{\partial u}{\partial x} + \frac{\partial v}{\partial z} = 0 \qquad [5.1]$$

$$\frac{\partial u}{\partial t} = - \frac{\partial (uu)}{\partial x} - \frac{\partial (uw)}{\partial z} + fv - \frac{1}{\rho_o}\frac{\partial P}{\partial x} + \frac{\partial}{\partial x}\left(A_x \frac{\partial u}{\partial x}\right) + \frac{\partial}{\partial z}\left(A_z \frac{\partial u}{\partial z}\right) \qquad [5.2]$$

$$\frac{\partial v}{\partial t} = - \frac{\partial (uv)}{\partial x} - \frac{\partial (vw)}{\partial z} - fu - \frac{1}{\rho_o}\frac{\partial P}{\partial y} + \frac{\partial}{\partial x}\left(A_x \frac{\partial v}{\partial x}\right) + \frac{\partial}{\partial z}\left(A_z \frac{\partial v}{\partial z}\right) \qquad [5.3]$$

$$\frac{\partial P}{\partial z} = - \rho g \qquad [5.4]$$

$$\frac{\partial T}{\partial t} + \frac{\partial uT}{\partial x} + \frac{\partial wT}{\partial z} = 0 \qquad [5.5]$$

$$\rho = \rho (T) \qquad [5.6]$$

where:

t	is time,
z	is vertical distance positive upward,
x,y	shore-perpendicular and shore-parallel distances,
u,v,w	are the fluid velocities in the x, y and z directions respectively,
f	is Coriolis parameter, assumed constant at 10^{-4} 1/s.

ρ is the fluid density,

ρ_o is the reference water density at 4°C,

A_x is the horizontal eddy viscosity,

A_z is the vertical eddy viscosity,

g is the gravitaional acceleration,

T is the temperature

Equation [5.1] is the equation of continuity, using the rigid-lid approximation. It is known that for large-scale circulations in lakes the divergence is so much smaller than the vorticity that it can be neglected. The surface elevation is determined only by the velocity potential of the divergent component. The rigid-lid approximation or the surface gravity wave filtering approximation simply removes the divergent part of the flow, i.e. $\nabla V = \partial\eta/\partial t = 0$ in equation [5.1], where ∇ is the horizontal gradient operator and $\delta\eta$ is the free surface elevation relative to the mean water level. The rigid-lid approximation is justified if

$$\frac{f^2L^2}{g\,H} \ll 1 \qquad [5.7]$$

where L is the characteristic length and H is the water depth. In the central basin of Lake Erie the term in [5.7] is about 0.3, while in the western basin of Lake Erie this term is about 0.5.

Equations [5.2] and [5.3] are the horizontal momentum equations in the x and y directions respectively. Equation [5.3] is the vertical momentum equation, i.e. the balance between the gravitational acceleration and the vertical pressure gradient, or the hydrostatic approximation. In the three momentum equations the pressure is expressed as:

$$P = P_e + P_i$$

$$P_e = P_s + \rho\, g\, \eta$$

$$P_i = \int_z^{\eta} (\rho - \rho_o)\, g\, dz \qquad [5.8]$$

where:

P_e is the external (barotropic) pressure.

P_i is the internal (baroclinic) pressure.

P_s is the atmospheric pressure at the air/water interface.

Equation [5.6] is the equation of state, and gives the water density as function of water temperature as follows:

$$(\rho - \rho_o)/\ \rho_o = -\alpha\ (T - T_o)^2\ ,$$

where the value of the thermal expansion coefficient α is 6.8×10^{-6} $^{o}C^{-2}$ (Simons, 1973).

In this study the value of the horizontal eddy viscosity has been assumed to be constant at 10^5 cm^2/s.

The vertical eddy viscosity plays an important role in the vertical transfer of momentum. As is clear from the review in Chapter 2, the literature is replete with representations of the vertical eddy viscosity. In general there are two hypotheses concerning the vertical transfer of momentum. The first idea states that turbulence is generated at or near the air/water interface and is suppressed at the thermocline by the sharp temperature gradient. Therefore the vertical eddy viscosity in the hypolimnion is much smaller than that of the upper layer epilimnion which is as small as the thermocline vertical eddy viscosity. The second idea states that the turbulence in the hypolimnion is generated by internal waves as well as at the air/water interface. Hence the value of the vertical eddy viscosity in the epilimnion is much greater than in the thermocline.

In this study both approaches have been used to calculate the vertical eddy viscosity. The first approach was applied to Lake Erie by Heinrich et al. (1981). The functional form of the vertical eddy viscosity is given by the product of the eddy viscosity A_o in the absence of stratification and the stability function f which is dependent on stratification:

$$A_z = A_o\, f(R_i) \qquad [5.9]$$

where R_i is the Richardson number, given by:

$$R_i = \frac{g\,\alpha\,(\partial T/\partial z)}{\rho\,(\partial u/\partial z)^2} \qquad [5.10]$$

where u is the magnitude of the horizontal velocity at depth due to the combined action of waves (including internal waves) and currents.

Heinrich et al. (1981) assumed that u is a function of the surface velocity u_o cm/s and decays exponentially with depth as follows:

$$u = u_o \exp(z/D) \quad [5.11]$$

where D is an empirical constant and of the same order of magnitude as the wave length of the surface waves. The surface wave velocity is expressed as function of the wind stress τ_w as follows:

$$\tau_w = \rho \; C_D \; u_o^2 \quad [5.13]$$

where C_D is the drag coefficient.

Heinrich et al. (1981) used the Sundaram et al. (1970) formulation for the thermal expansion coefficient:

$$\alpha = 1.5\times10^{-5} \; (T-4) - 2\times10^{-7} \; (T-4)^2 \quad [5.13]$$

They also used the following form of the stability function (Munk and Anderson, 1948):

$$f = (1+\sigma_1 \; R_i)^{-1/2} \quad [5.13]$$

where σ_1 is an empirical constant. The vertical eddy viscosity in the absence of stratification, A_o was assumed to be a function of the wind stress, distance from surface and wave amplitude:

$$A_o = A_s \; (C_1 + C_2 \; e^{z/D}) \quad [5.14]$$

where C_1 and C_2 are empirical constants and A_s is a function of the wind stress and lake depth. From [5.10] to [5.14], the vertical eddy viscosity is expressed:

$$A_z = \frac{A_s \left(C_1 + C_2 e^{z/D} \right)}{\left(1 + \sigma_1 C_D g \alpha \dfrac{D^2 e^{-2z/D}}{\tau_w} \dfrac{\partial T}{\partial z} \right)^{1/2}} \qquad [5.15]$$

The second approach was recently applied to Lake Erie by Lam et al. (1983). This form of the eddy viscosity was originally proposed and used by Walters et al. (1978) in Lake Washington. Three different vertical eddy viscosities are assumed one for each layer:

$$\text{Epilimnion} \quad A_z = A_o \, (1+\sigma_2 R_i)^{-1} - \gamma \frac{\partial \rho}{\partial z} \frac{g}{\rho} \qquad [5.16]$$

$$\text{Mesolimnion} \quad A_z = A_{TC} \, (N_{TC}^2 \, / \, N^2)^{1/2} \qquad [5.17]$$

$$\text{Hypolimnion} \quad A_z = A_B - \gamma \frac{\partial \rho}{\partial z} \frac{g}{\rho} \qquad [5.18]$$

where A_o is the air/water interface eddy viscosity parameter, N is the Brunt-Vaisala frequency, TC denotes the value at the thermocline, A_B represents the limiting value of the bottom turbulence induced by wind, defined by $A_B = 2A_{TC}$ and σ_2 is an empirical constant. The value of A_o was related to the wind velocity W using the empirical formulation

(Walters et al 1978), developed for the vertical eddy diffusivity:

$$A_o = 5 \times 0.0045\ W \qquad [5.19]$$

where W is in cm/s, A_o is in cm^2/s and the factor 5 is a calibration parameter. Lam et al. (1983) used the following relation for the equation of state:

$$-\delta\rho/\rho = \alpha\ (T-4)\ \delta T \qquad [5.20]$$

where α is the thermal expansion coefficient and is equal to 13.6×10^{-6} $^oC^2$. The second term in the right hand side of [5.16] and [5.18] attains a large positive value for unstable situations in which $\partial\rho/\partial z$ is large but negative. This indicates instantaneous adjustment by rapid mixing. The value of γ has been taken to be constant at 4.6×10^3. The squared Brunt-Vaisala frequency in equation [5.17] has been approximated by:

$$N^2 = \frac{g}{\rho}\ \frac{\partial\rho}{\partial z} = -\ g\ \alpha\ (T - 4)\ \frac{\partial T}{\partial z} \qquad [5.21]$$

The calculation from one layer to another is achieved by the conservation of vertical eddy viscosity.

The turbulent eddies are restricted by the lake bottom, therefore the eddy diffusivity in both approaches is assumed to decrease in proportion to the square of the ratio between the local water depth and the maximum depth. To compute both approaches to the vertical eddy viscosity, two subroutines were written by the writer. the first subroutine (DIFFUSE1) solves [5.15] using a finite difference method for each point in the x-z plan and each time step. The second subroutine (DIFFUSE2) solves [5.10] to [5.18] using a finite difference method. The intersection of two successive vertical eddy viscosity profiles is used as a criterion to switch from one profile to another. The calculations are performed for each point in the x-z plan and each time step.

Boundary conditions:

At the air/water interface where z = 0, the heat flux and the wind stresses are given by:

$$\rho\ K_z\ \partial T/\partial z = q = 0$$

$$\rho\ A_z\ \partial u/\partial z = \tau_{wx}$$

$$\rho\ A_z\ \partial v/\partial z = \tau_{wy} \qquad [5.22]$$

where K_z is the eddy diffusivity coefficient and q is the surface heat flux. The effect of the heat flux on the vertical circulation over a short time period (week or so) can be neglected. The wind stresses in the x and y directions respectively are given by:

$$\tau_{wx} = C_D\ (\rho_a/\rho)\ W\ U$$

$$\tau_{wy} = C_D\ (\rho_a/\rho)\ W\ V \qquad [5.23]$$

where C_D is the surface drag coefficient, ρ_a is air density, U and V are the wind speed components in the x and y directions respectively. Several values have been reported for C_D; in this study a value of 2×10^{-3}

has been used. The rigid-lid approximation implies that the vertical velocity w at the surface z=0, equals zero.

At the bottom, z =-h, the shear stresses τ_{bx} and τ_{by} are given by:

$$\tau_{bx} = 0.002\ u_b\ (u_b^2 + v_b^2)^{1/2}$$

$$\tau_{by} = 0.002\ v_b\ (u_b^2 + v_b^2)^{1/2} \qquad cm^2/s^2 \qquad [5.24]$$

where u_b and v_b are the bed velocities in the x and y direction respectively (at the first grid level above the bottom) in cm/s. The bottom shear stresses are related to the vertical velocity gradients by:

$$\tau_{bx} = \rho\ A_z\ (\delta u/\delta z)$$

$$\tau_{by} = \rho\ A_z\ (\delta v/\delta z) \qquad [5.25]$$

At z=-h, the bottom heat flux is assumed to be zero and the no-slip condition is used i.e. u = v = w = 0. The initial conditions are defined by a known temperature profile and by starting from a state of rest. Program ERCH solves [5.1] to [5.6] numerically using explicit and implicit finite difference schemes. Initially ERCH solves the whole cross section using a coarse grid size and then solves the coastal boundary layer using a finer grid size. The values of the velocities and temperature obtained from the coarse grid calculations are used to define the off-shore boundaries of the fine grid. The functional flow is given in Figure 5.1. The input parameters to ERCH are: the horizontal increments DX and DXX in meters for the coarse and fine grids respectively; the number of the coarse grid horizontal increments covering the whole cross section JT, and the coastal zone JR; the corresponding water depth in meter HV and HVV; the number of the vertical increment corresponding to the maximum water depth KM; the temperature profile corresponding to the maximum depth TO(Z) in ^{o}C; the numerical time step DT in seconds; the number of days of simulation NDAYS and hourly time series of wind speed and direction. The model calculates the shore-perpendicular and shore-parallel components of the wind stress using equation [5.23], and solves the thermodynamic equation [5.5] using a two step Lax-Wendroff scheme (Richtmyer, 1963). The horizontal momentum equations [5.2] and [5.3] are solved in two steps. In the first step the left hand side is solved only for the last term in the right hand side using a backward implicit scheme. The value of the vertical eddy viscosity is calculated using [5.15] or [5.16] to [5.18]. In the second step, [5.2] and [5.3] excluding the last term in both, are solved explicitly. The values obtained from the first step are used as initial values in the term for the time derivative. The horizontal diffusion term is evaluated by centered differences, and the presssure gradient is evaluated by centered differences. The nonlinear terms are evaluated by forward differences when the velocities are negative and backward differences when the velocities are positive. Hence the one-sided difference is always on the upwind side of the point at which the time derivative is evaluated. The upwind differencing is only first-

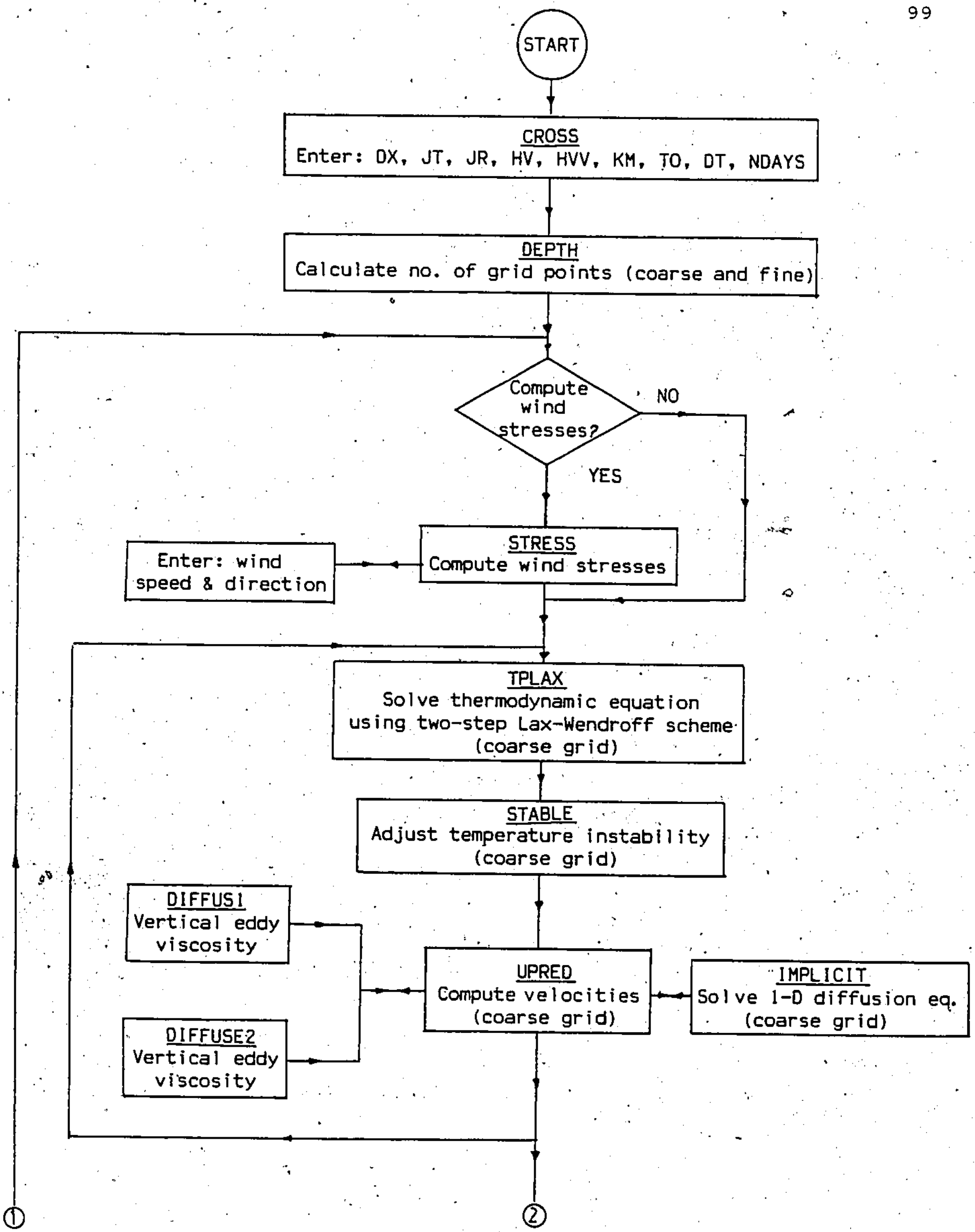
START
CROSS
Enter: DX, JT, JR, HV, HVV, KM, TO, DT, NDAYS
DEPTH
Calculate no. of grid points (coarse and fine)
Compute wind stresses?
NO
YES
STRESS
Compute wind stresses
Enter: wind speed & direction
TPLAX
Solve thermodynamic equation using two-step Lax-Wendroff scheme (coarse grid)
STABLE
Adjust temperature instability (coarse grid)
DIFFUS1
Vertical eddy viscosity
DIFFUSE2
Vertical eddy viscosity
UPRED
Compute velocities (coarse grid)
IMPLICIT
Solve 1-D diffusion eq. (coarse grid)
1
2

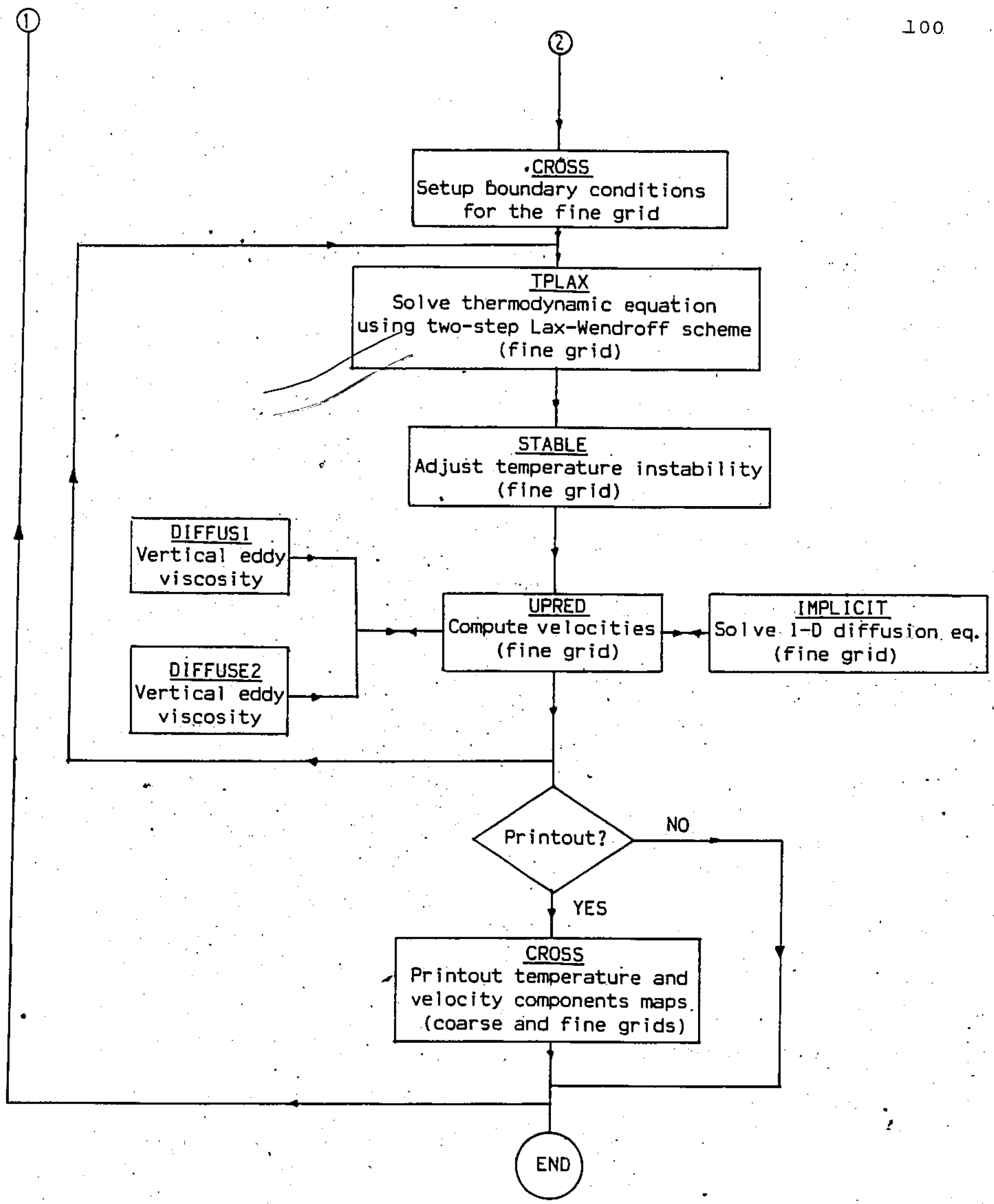

Figure 5.1 Functional flow chart for program ERCH

order accurate but there is no restriction for spatial instability. Chapter 6 provides more details. This procedure is used for solving both the coarse grid and fine grid for each time step.

5.2.2 ERCH verification and sensitivity

There is a degree of uncertainity associated with the estimation of model input and parameters. Each meteorological and limnological parameter will have some effect upon the flow field and temperature distribution, the extent of which varies considerably from parameter to parameter. For example a small variation in an input parameter may cause a large difference in the model output. In this case the model is said to be "sensitive" to this parameter, and vice-versa. Sensitivity analysis allows the modeler to concentrate his data abstraction effort on the parameters which will most significantly affect the model results.

In carrying out sensitivity analysis for program ERCH, a cross-section similar to the Lake Erie cross-section at Cleveland was used, and the following parameters were varied: wind speed, wind direction, horizontal eddy viscosity, vertical eddy viscosity and bottom friction. Table 5.1 summarizes the analyses. The model was run for one prototype day using a 15 minute time step and the effect on the u and v current components were studied. In Figures 5.2 and 5.3 , the results are plotted for six points at distances 2, 7 and 15 km from shore the at both the water surface and 10 m below the water surface.

The initial values and the variability ranges used in carrying out the sensitivity analyses are typical of those used in lake modelling. The wind speed was varied from 0.2 to 3.0 times the initial value of 5

TABLE 5.1 ERCH SENSITIVITY PARAMETERS

Parameter	Initial value	Range of variability
wind speed W (m/s)	5	1-15
Wind direction (degrees from north)	45^{o}	225^{o}-315^{o}
Horizontal eddy viscosity A_x (cm^2 /s)	10^3	0 - 10^6
Surface-vertical eddy viscosity A_z (cm^2 /s)	100	0 - 500
Bottom friction coefficient C_D	0.002	(0.001-0.003)

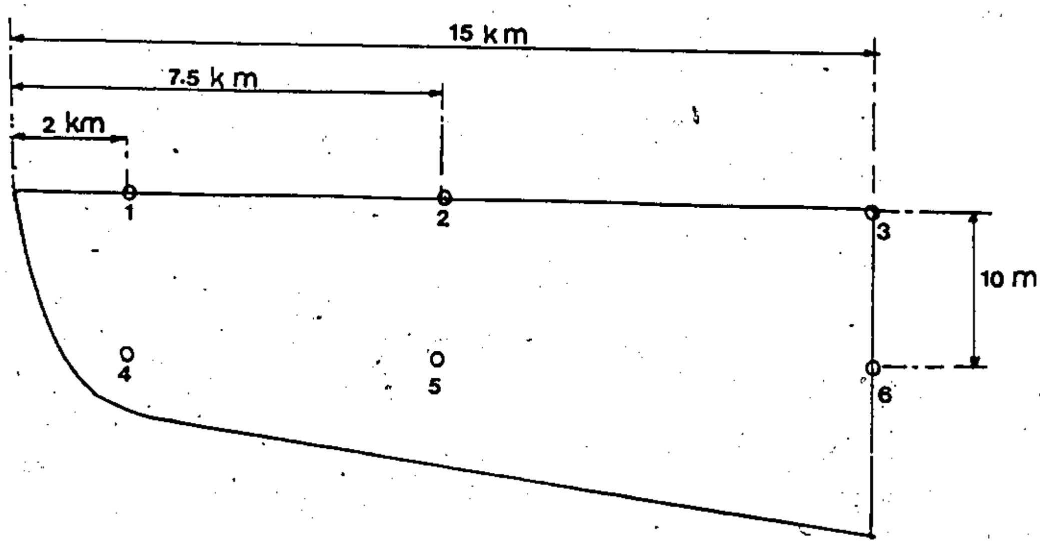

Legend for Figures 5.2 and 5.3

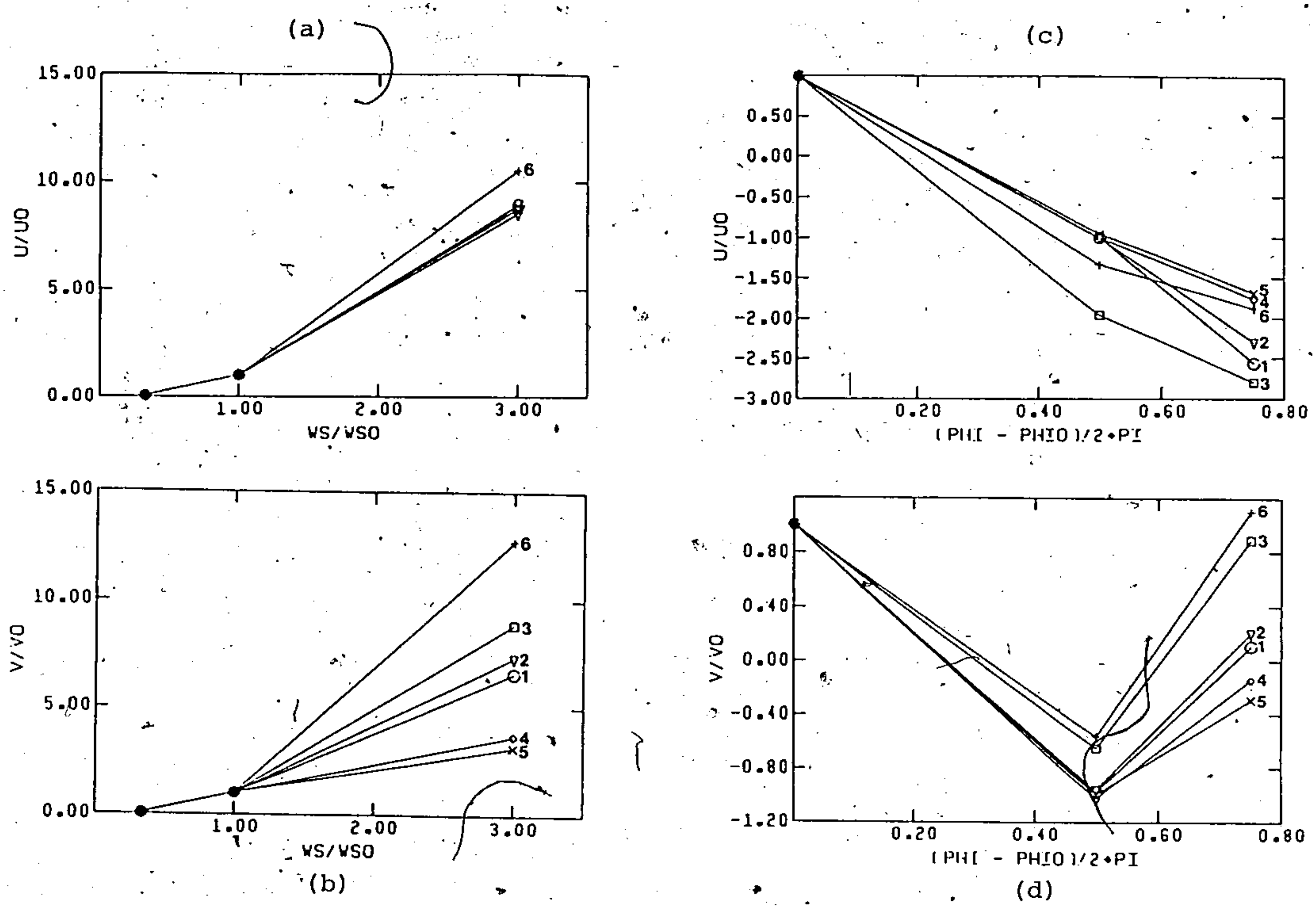

Figure 5.2 ERCH sensitivity analysis.

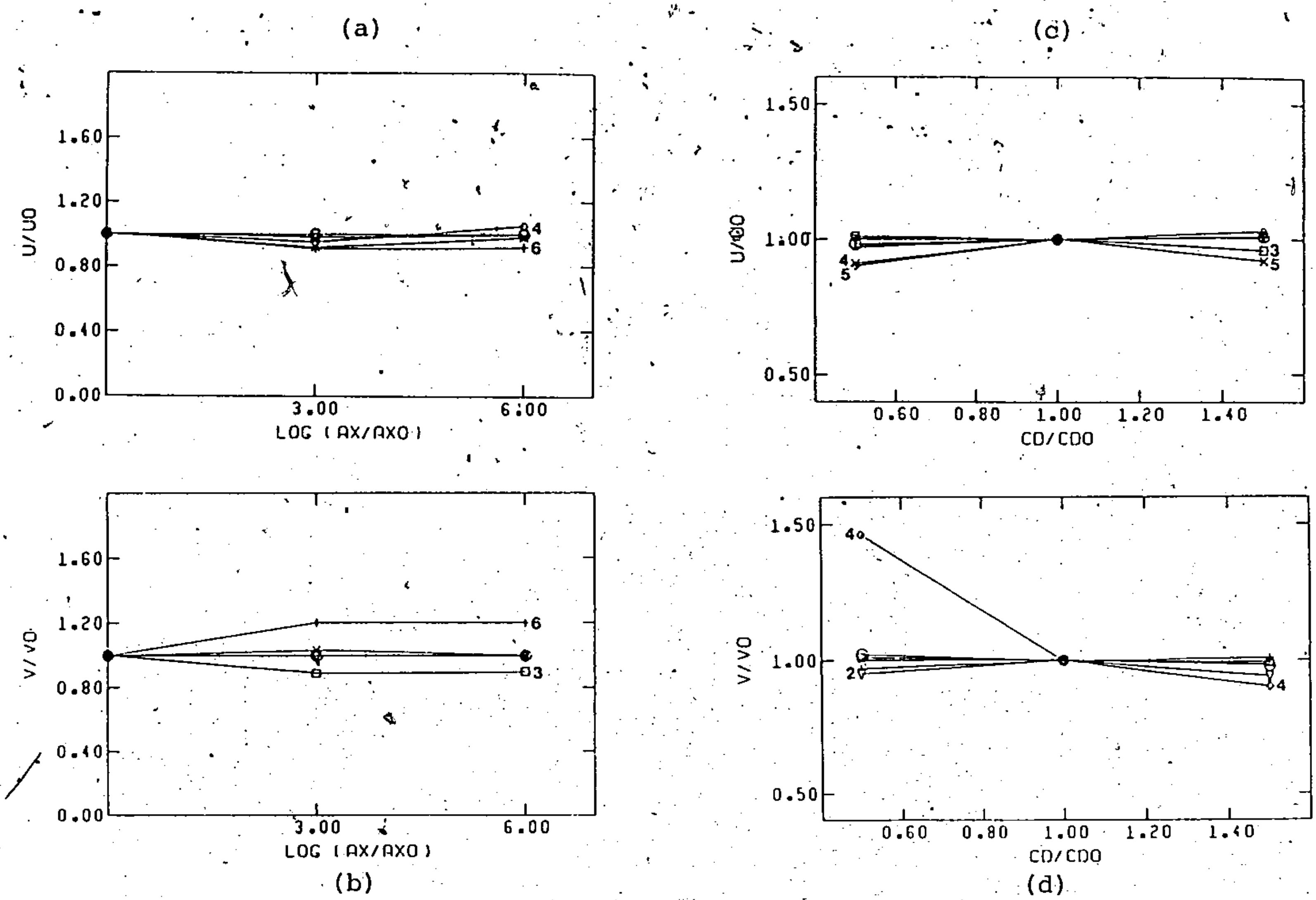

Figure 5.3 ERCH sensitivity analysis (cont.)

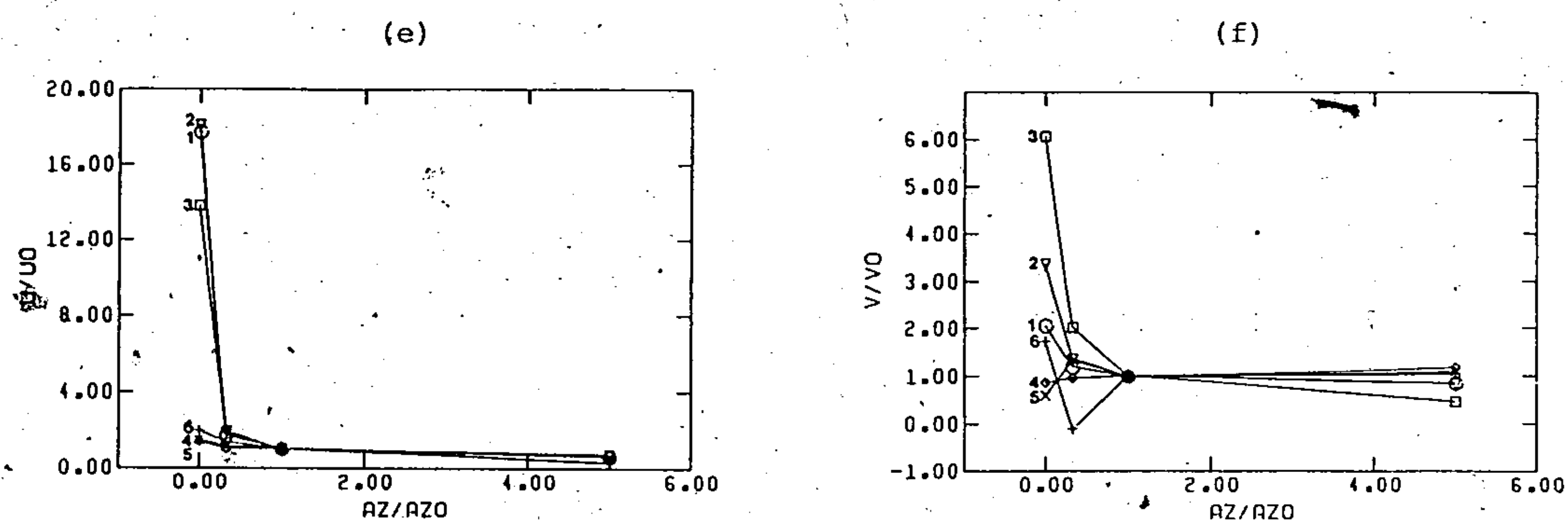

Figure 5.3 continued

m/s. Figures 5.2a and b indicate that, by decreasing the wind speed by a factor 0.2, both the u and v components decreased to almost zero, and by increasing the wind speed by a factor 3, both components increased by a factor of 3 to 13. This indicates that the model is highly sensitive to the wind speed. Figures 5.2c and d show the effect of changing the wind direction. Again the model is found to be highly sensitive to the wind direction.

Figures 5.3a and b show the effect of changing the horizontal eddy viscosity on the u and v components. Changing the horizontal eddy viscosity by 3 to 6 orders of magnitude caused a change of only 10-20% in both components, so the model is in-sensitive to the horizontal eddy viscosity. This is due to the fact that the vertical shear stress in [5.2] and [5.3] is larger than the horizontal shear stress. In Figures 5.3c and d the velocity components u and v were found to be highly sensitive to a decrease in vertical eddy viscosity especially near the surface. A large vertical velocity gradient is developed here to balance the decrease in the vertical eddy viscosity coefficient in accordance with [5.22]. The velocity components were found to be less sensitive to an increase in the vertical eddy viscosity from the initial value. In Figure 5.3e and f the velocity components u and v were found to be insensitive to the variation of the bottom friction stress except at point 4 close to the shore and to the bottom. An increase of 50% in v-component due to 50% decrease in the bottom friction stress at point 4 is observed. The change in the temperature was small with respect to the variation of all stated parameters over this short time.

The channel-type response was tested by inputting a sustained strong wind velocity of 10 m/s from the north-east quadrant for a duration of one day. The results are presented in Figure 5.4. Figure 5.4a shows the isotherm plots in the x-z plane using 1°C intervals. The transport of surface waters due to wind set-up is from the north shore towards the south shore, upwelling the colder water to the surface along the south shore. This can be observed from the tilted isotherm in Figure 5.4a. Figure 5.4b presents a plot of the contour lines of the shore perpendicular component v. The plot shows a strong southward near-surface flow accompanied by a broad return flow at 10 m depth. This flow is due to the effect of the Coriolis force and is an indication of the wind-driven Ekman layer. The increase and decrease of the shore-perpendicular component moving off-shore, is due to the effect of the frictional and inertial boundary layer discussed in Chapter 4. Figure 5.4c presents the same plot as Figure 5.4b, but for the shore-parallel component. The velocity contour lines show that the water in the shallow regions close to the shore is accelerated in the direction of the long-shore component of the wind (coastal jet). Moving off-shore the flow returns at the deeper central lake region. This flow pattern is similar to the results obtained by Bennett (1974) in applying a channel-type model to lake Ontario and is a closed basin analogy to the "bottom slope current" of Weenink and Groen (1958). Figure 5.4d presents the contour lines of the vertical velocity. The vertical velocity is effectively zero at the central region of the lake and non-zero values are observed close to the shore. A downward flow in the south shore and an upward flow at the north shore of the lake are observed indicating downwelling

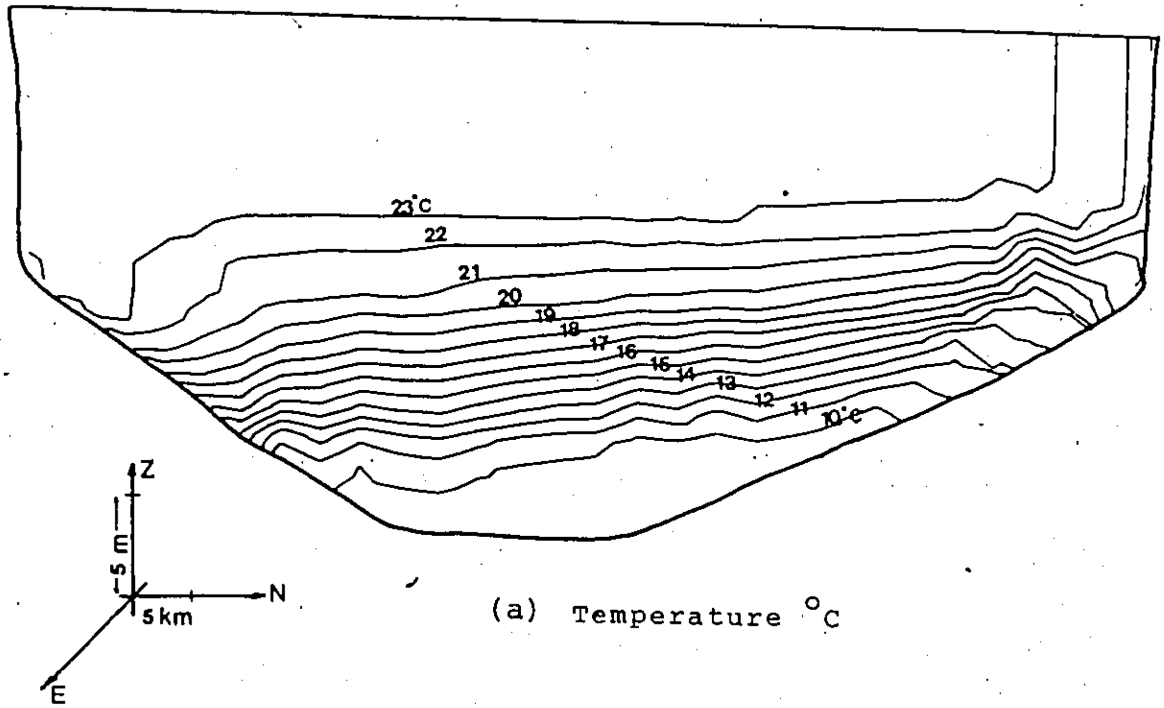

(a) Temperature °C

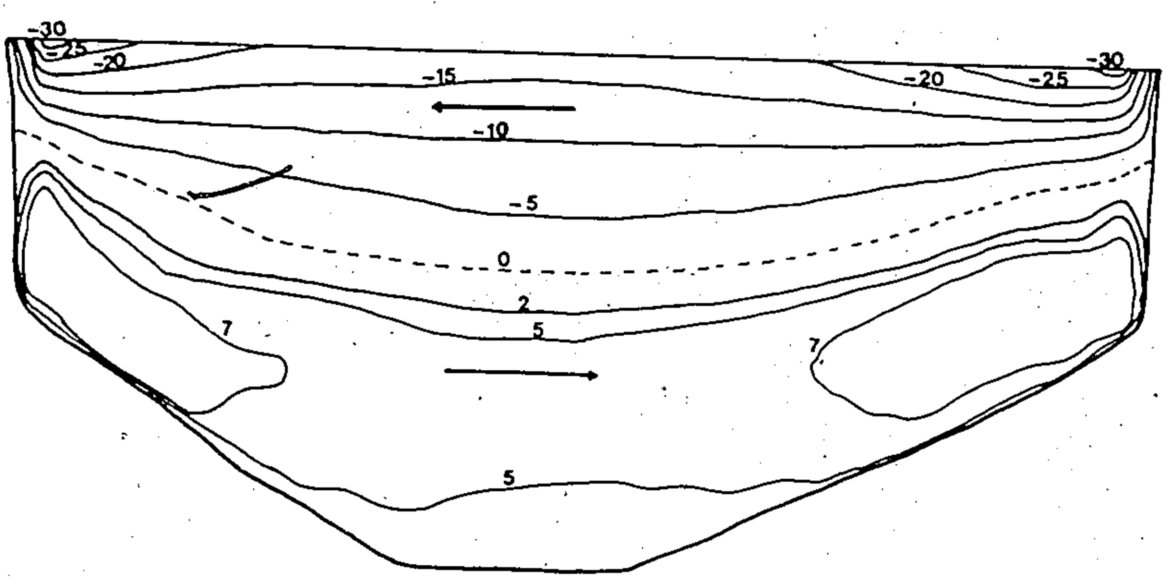

(b) Shore perpendicular component (cm/s)

Figure 5.4 Temperature and flow profiles of the channele-type responce.

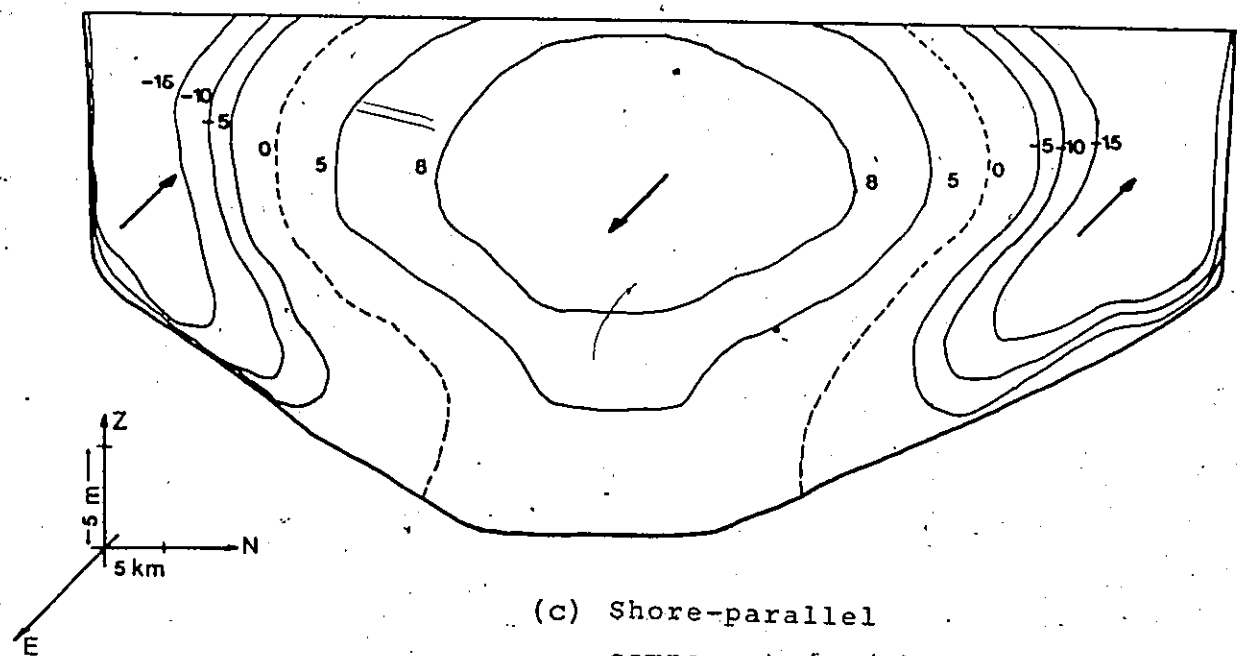

(c) Shore-parallel component (cm/s)

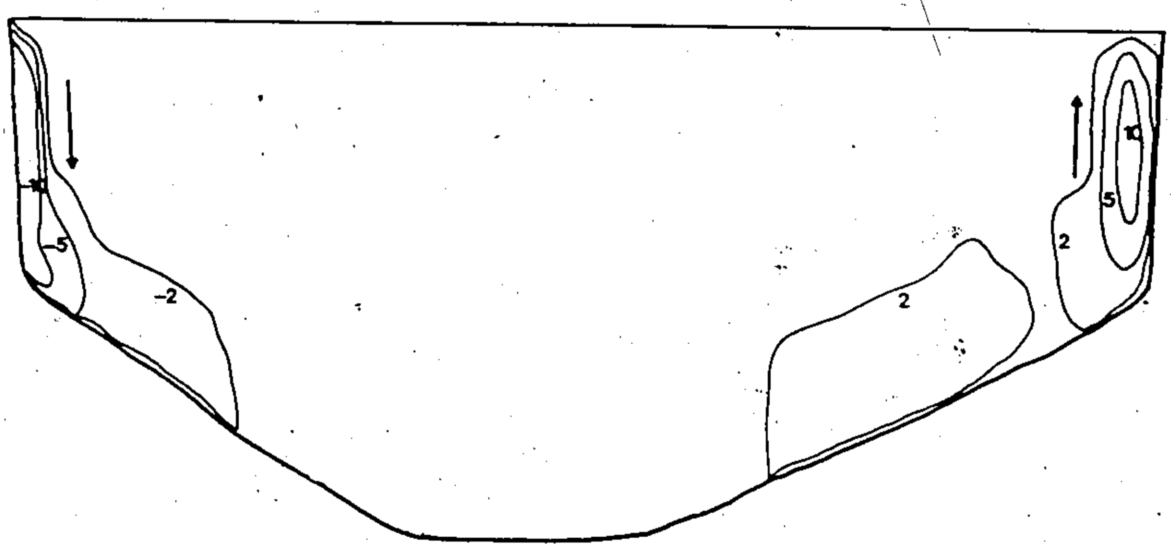

(d) Vertical component (cm/s x 10^3)

Figure 5.4 Continued

and upwelling respectively. The vertical velocity is about 3 orders of magnitude (10^{-3}) smaller than the horizontal velocity.

The effect of stratification on the "coastal jet" was studied by running ERCH using all the above parameters for two different temperature profiles, representing homogeneous and stratified lakes. The results are presented by plotting contours of equal shore-parallel components in the x-z plane. Figure 5.5a presents the homogeneous case and Figure 5.5b the stratified case. The results show that the coastal jet is wider in the stratified case while the jet is deeper in the homogeneous case. The difference between the two cases reaches 5 cm/s at the water surface close to the shore and also at 15 m from the water surface at the lake center.

The effect of using a fine grid in the coastal zone is presented in Figures 5.6a and b. The variation of the u and v components respectively with the distance from shore at the water surface for both fine 0.5 km and coarse 3 km grid sizes is given. It can be seen that close to the shore the velocity difference between the two cases reaches 25 cm/s.

The effect of the nonlinear acceleration terms has been tested by running ERCH with and without the nonlinear terms using the previous parameters. Figures 5.7a and b present the distribution of the shore-parallel component in the x-z plane within the coastal zone including and excluding the nonlinear terms respectively. It can be seen that by including the nonlinear terms the velocity, the width and the depth of the coastal jet are decreased. This result is also observed in Figures

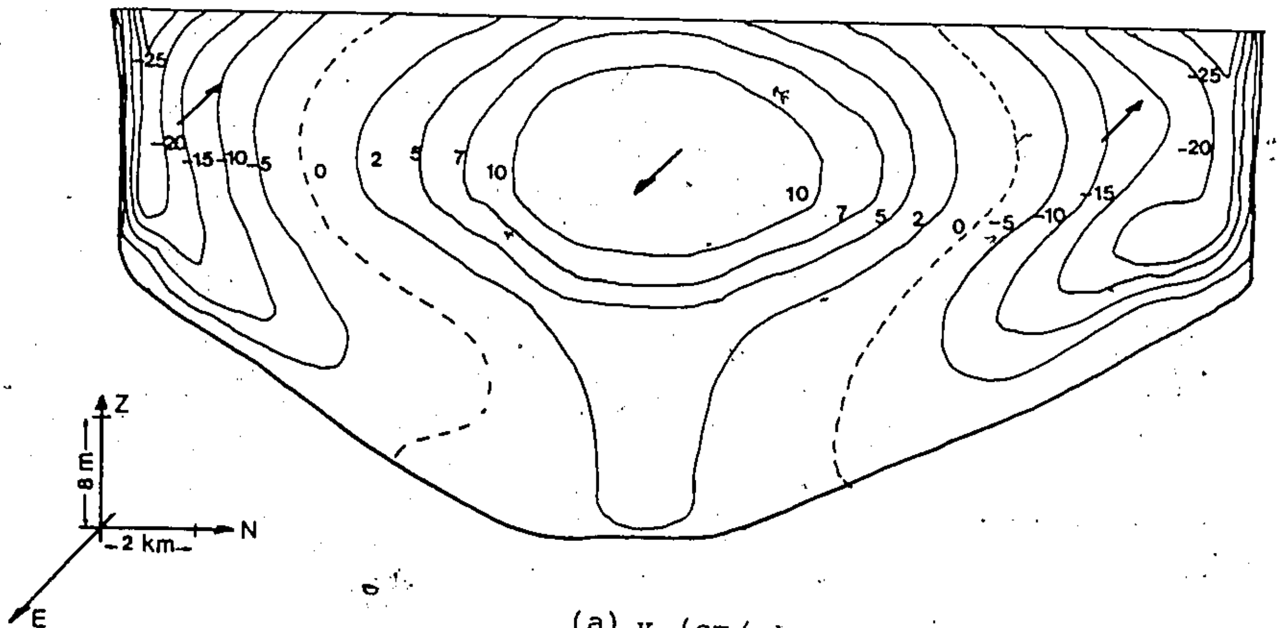

(a) v (cm/s)

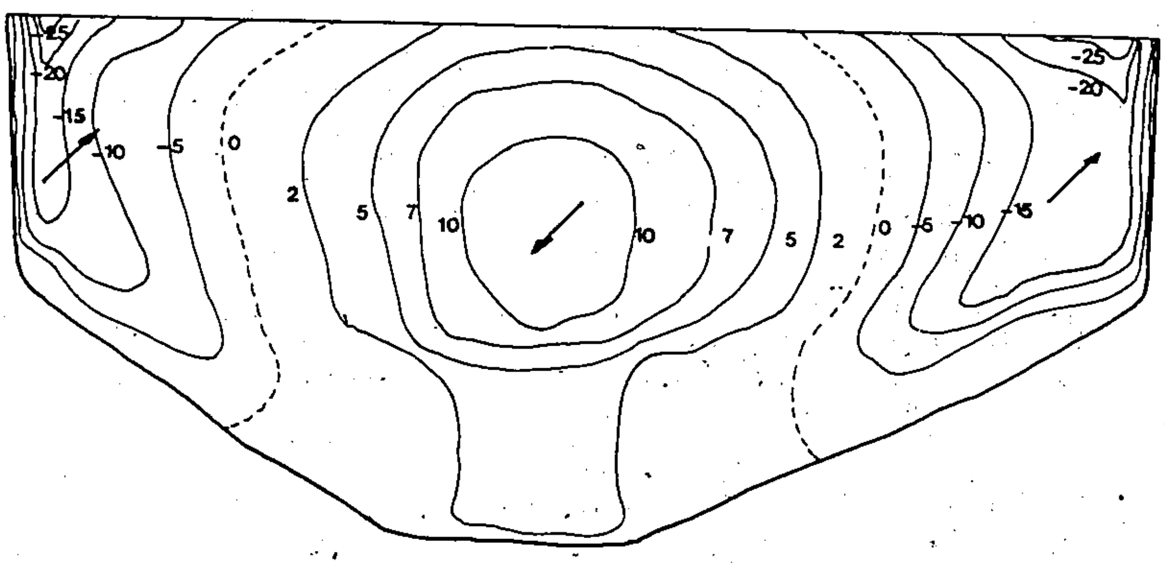

(b)

Figure 5.5 Longshore current profile for a homogeneous lake (a) and a stratified lake (b).

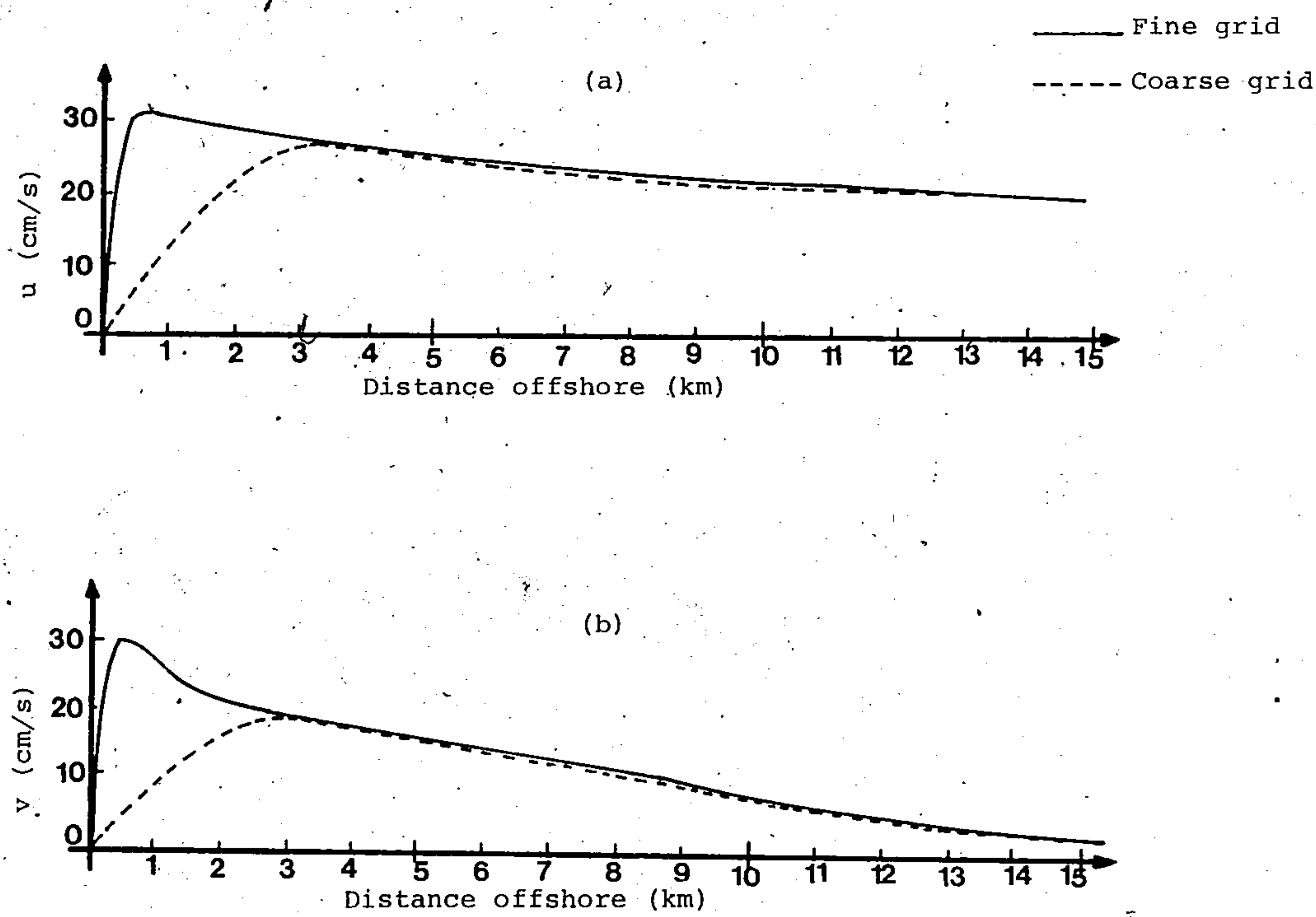

Figure 5.6 Velocity components u and v as a function of distance from the shore for fine and coarse grids.

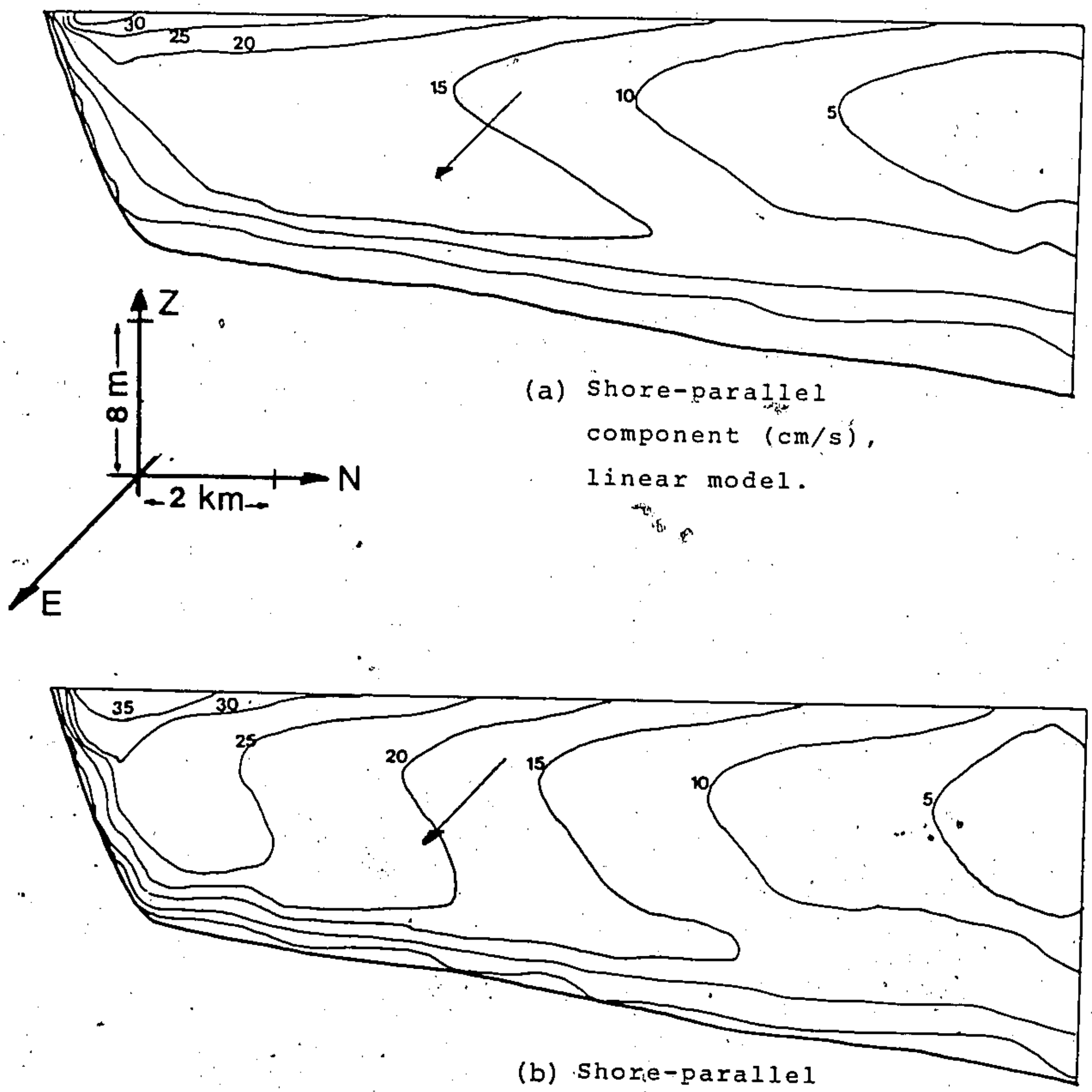

(a) Shore-parallel component (cm/s), linear model.

(b) Shore-parallel component (cm/s), nonlinear model.

Figure 5.7 Longshore current profiles for linear model (a) and nonlinear model (b).

5.8a and b by plotting the variation of the u , v components with distance from shore at the 10 m depth. Including the nonlinear terms caused a reduction of up to 6 cm/s for the u component and 11 cm/s for the v component.

5.2.3 ERCH results and discussion

ERCH was used to simulate one episode of strong shore-parallel currents (May 25 to 31) and one episode of weak currents (June 1-6). The two forms of vertical eddy viscosity discussed earlier (subroutines DIFFUSE1 and DIFFUSE2) were used in simulating both episodes. Table 5.2 lists the constants used. The horizontal increments were 3 Km and 0.5 Km for the coarse and the fine grids respectively, the vertical increment was 1.25 m, and the time increment was varied between 10 and 15 min to achieve numerical stability.

The results for the weak current episode are presented in Figures 5.9 and 5.10 for the shore-perpendicular and shore-parallel components respectively. Figure 5.9 shows the onshore offshore wind velocity together with the observed current and the two computed currents at seven locations covering the coastal boundary layer. At all stations, in the first 12 hours or so, the computed current is quite different from the observed but for the rest of the time the same flow pattern is obtained using both DIFFUSE1 and DIFFUSE2. Close to the shore the thermocline is not formed due to the depth restriction, so the values of the vertical eddy viscosity obtained from both formulations are close. Far from shore the thermocline is formed at 10 m depth. The values of the vertical eddy viscosity obtained from DIFFUSE1 for depths greater than 10 m are

TABLE 5.2 .. ERCH constants

Constants	units	comments
$A_s = 20\ \tau_w$	A_s cm^2/s, τ_w dyne/cm^2	[5.15]
$C_1 = C_2 = 1$	------	[5.15]
$D = 900$	cm	[5.15]
$\sigma_1 C_D = 0.00225$	------	[5.15]
$A_o = 2 \times A_s$	cm^2/s	[5.16]
$\sigma_2 = 0.03$	------	[5.16]
$\gamma = 4.6 \times 10^3$	cm s	[5.16]
$\alpha = 13.6 \times 10^{-6}$	$^oC^{-2}$	[5.20]
$C_D = 2 \times 10^{-3}$	------	[5.23]
$\rho_a = 1.25 \times 10^{-3}$	g/cm^3	[5.23]
$\rho = 1$	g/cm^3	[5.23]
$g = 981$	cm/s^2	

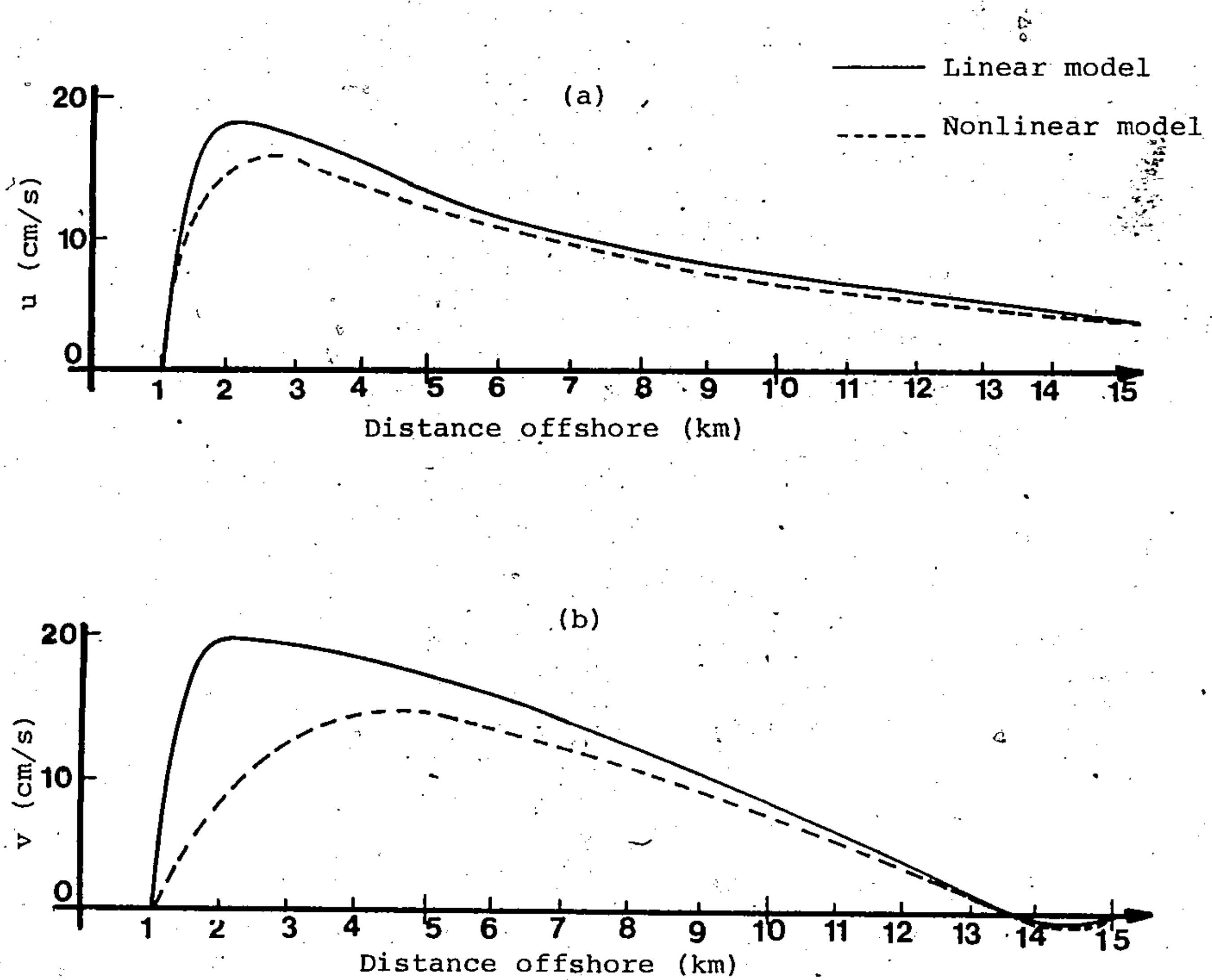

Figure 5.8 Velocity components u and v as a function of distance from the shore for linear and nonlinear models.

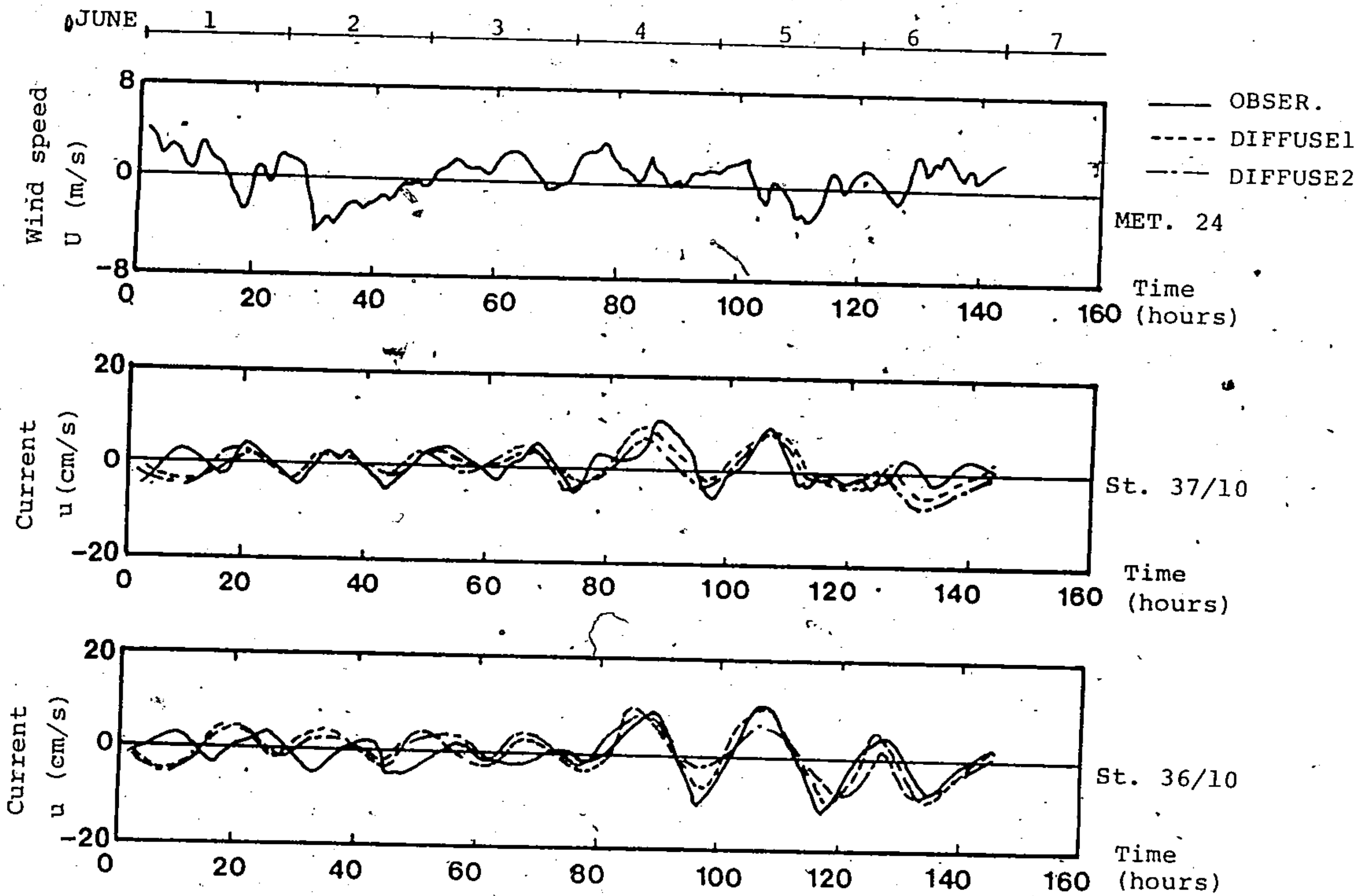

Figure 5.9 Shore perpendicular wind and observed and computed currents (DIFFUSE1 and DIFFUSE2) as a function of time, June 1-6, 1979 episode.

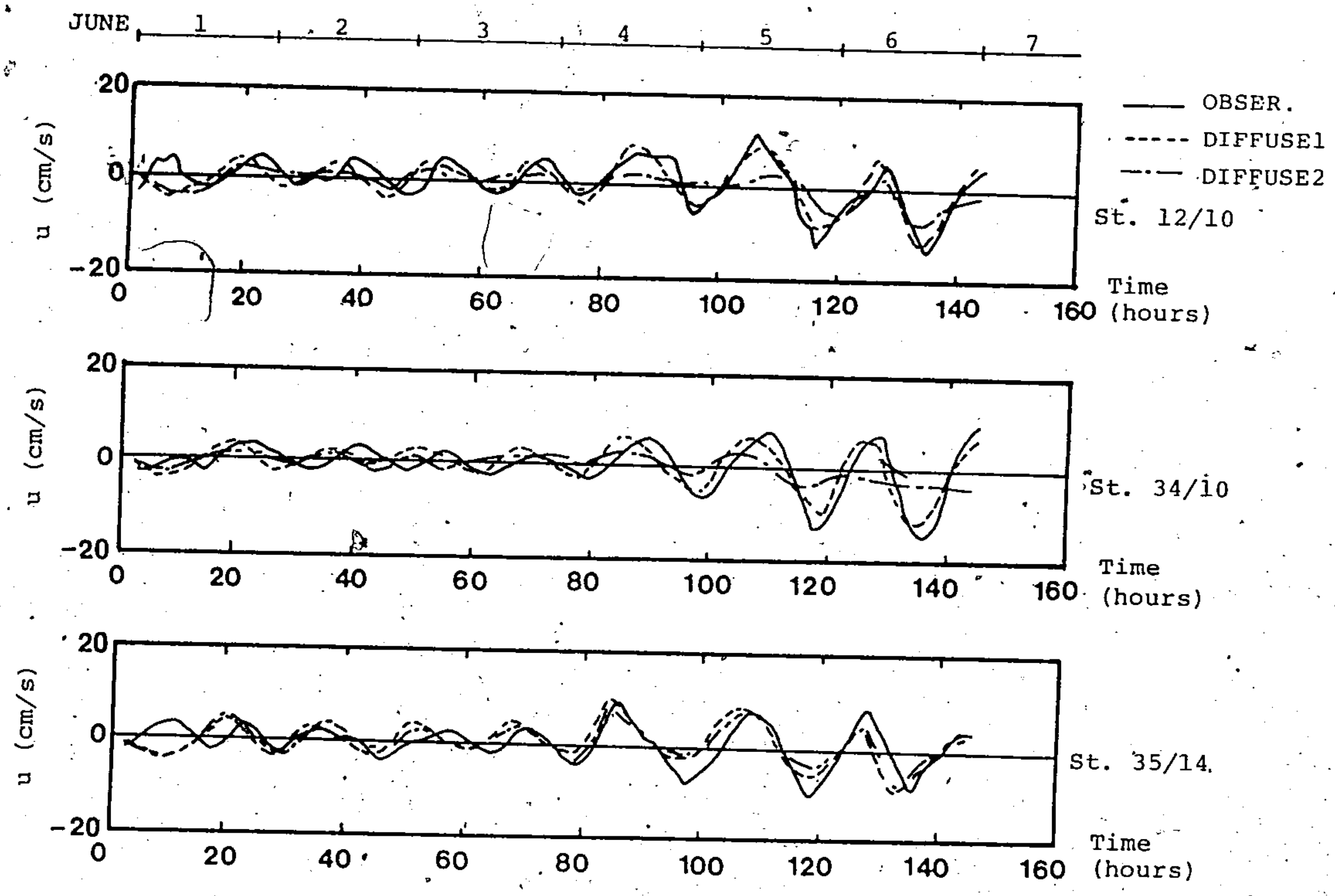

Figure 5.9 Continued

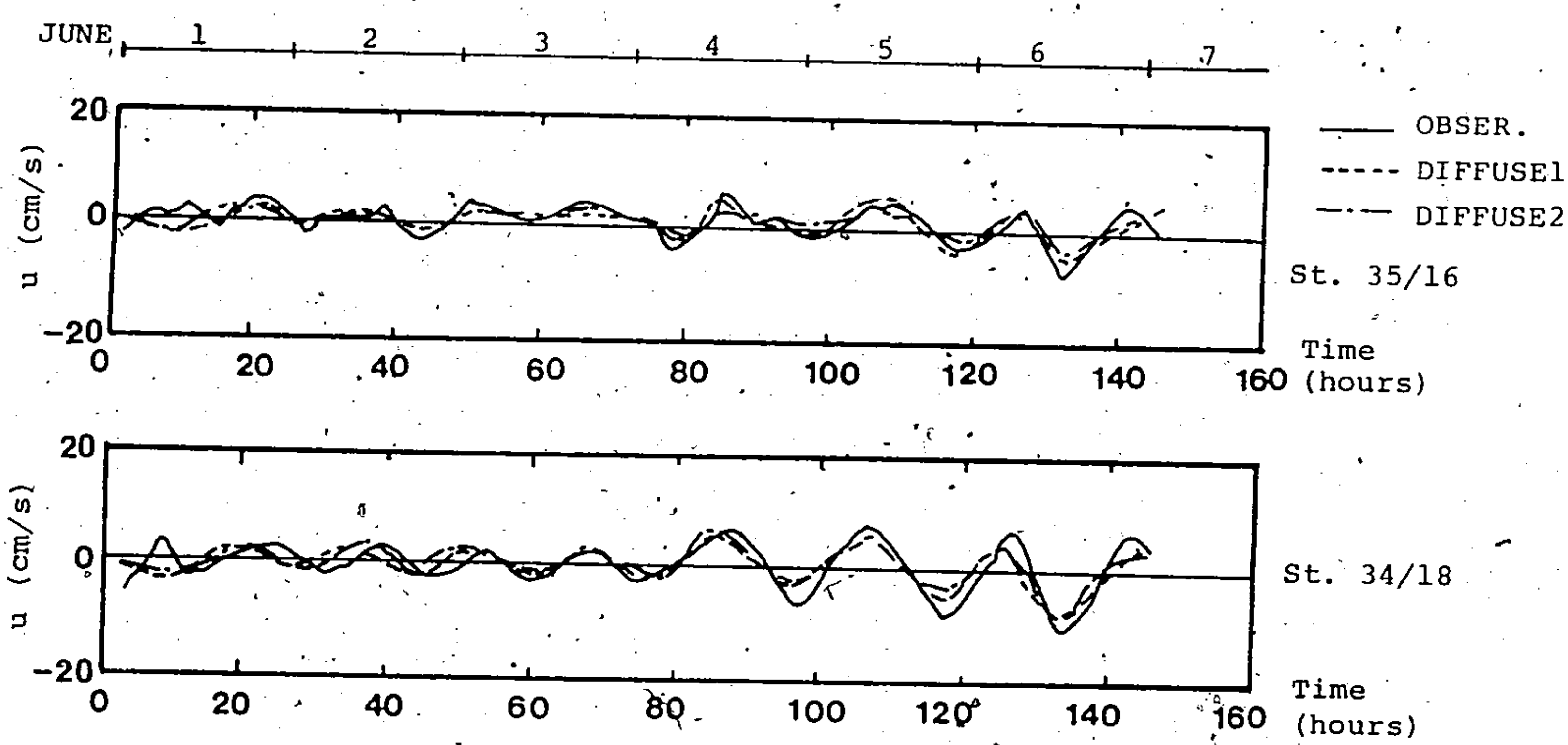

Figure 5.9 Continued

much higher than those from DIFFUSE2. The temperature profile and the vertical eddy viscosity are presented in Figure 5.11. In Figure 5.9, close to the shore at station 37, the currents computed by DIFFUSE1 and DIFFUSE2 are close to the observation. Far from the shore DIFFUSE1 gives higher and closer values to the observations than does DIFFUSE2.

Figure 5.10 is similar to Figure 5.9 but illustrates the shore parallel component and the same remarks apply to Figure 5.10. In this episode, ERCH predicts the currents reasonably well using DIFFUSE1.

In the May episode ERCH was used to simulate the currents using DIFFUSE1. The results obtained are presented in Figures 5.12 and 5.13 for the shore-parallel and shore-perpendicular currents respectively. Figure 5.12 presents the shore-parallel wind velocity together with observed currents using ERCH. Figure 5.12 also presents computed results for the one-layer model which is discussed in the next part of this chapter. The results are presented for four stations within the coastal zone. The computed currents obtained from ERCH are quite different from the observed, occasionally having an opposite sense. The same remarks apply to the shore-perpendicular component plotted in Figure 5.13. In this episode the wind blew from NNE at a velocity approaching 16 m/s and the water built up rapidly in the western basin developing a high barotropic pressure gradient against the wind stress. The pressure gradient developed a strong current at 10 m depth against the wind direction. This strong wind impulse completely mixed the central basin of Lake Erie, as shown in Figure 4.10. For this case a depth integrated two dimensional model may be expected to give better results. The one-layer

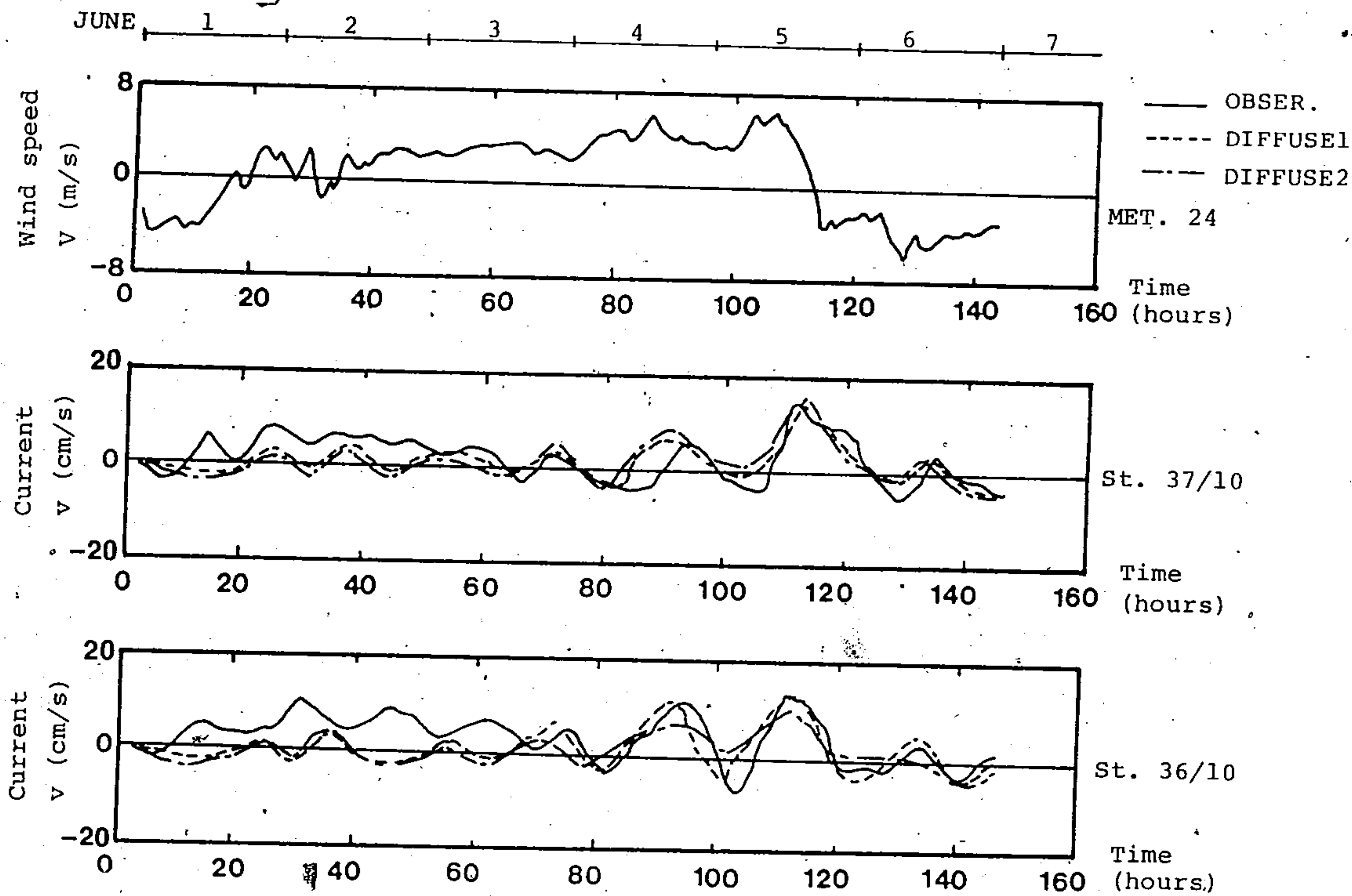

Figure 5.10 Shore Parallel wind and observed and computed currents (DIFFUSE1 and DIFFUSE2) as a function of time, June 1-6, 1979 episode.

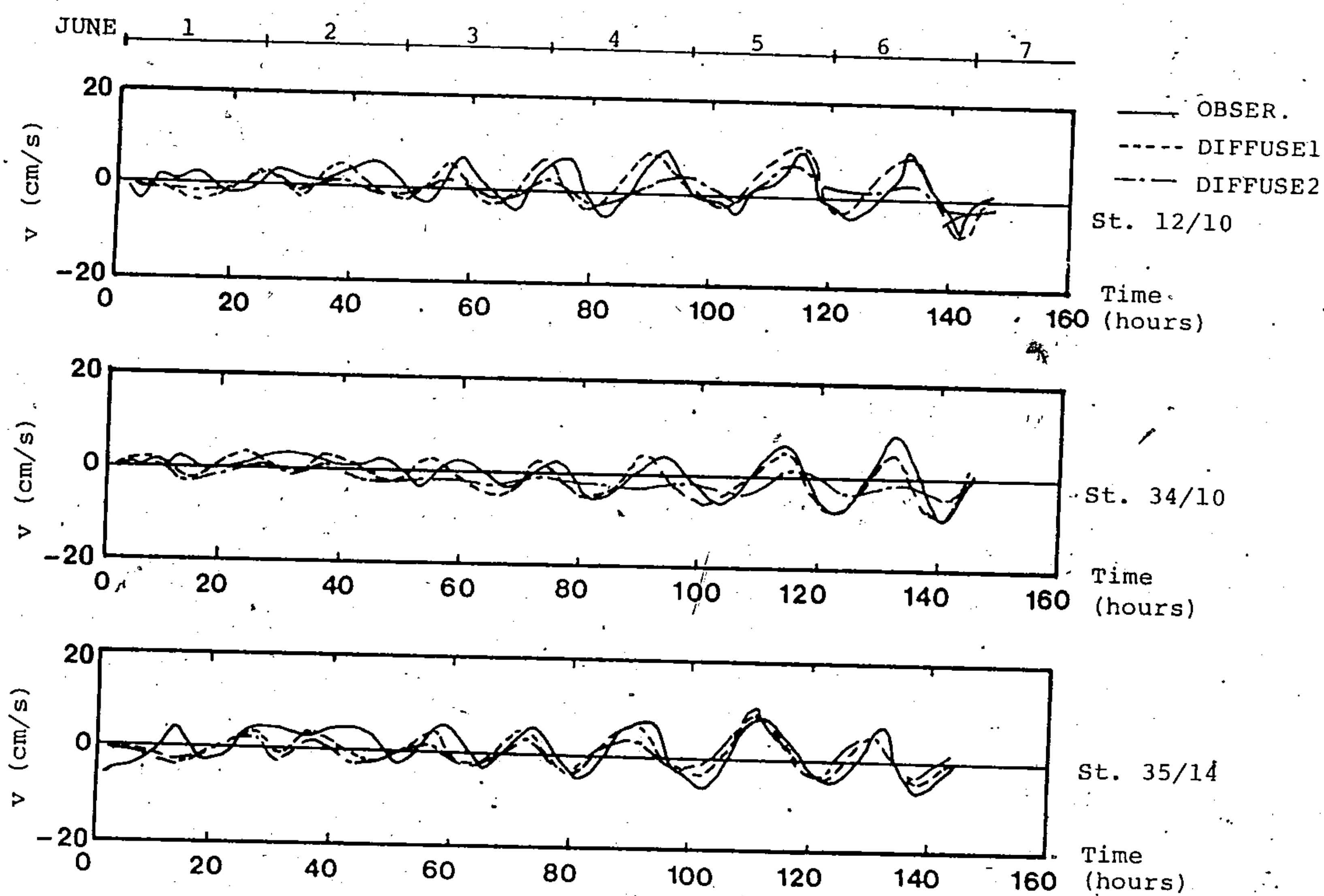

Figure 5.10 Continued

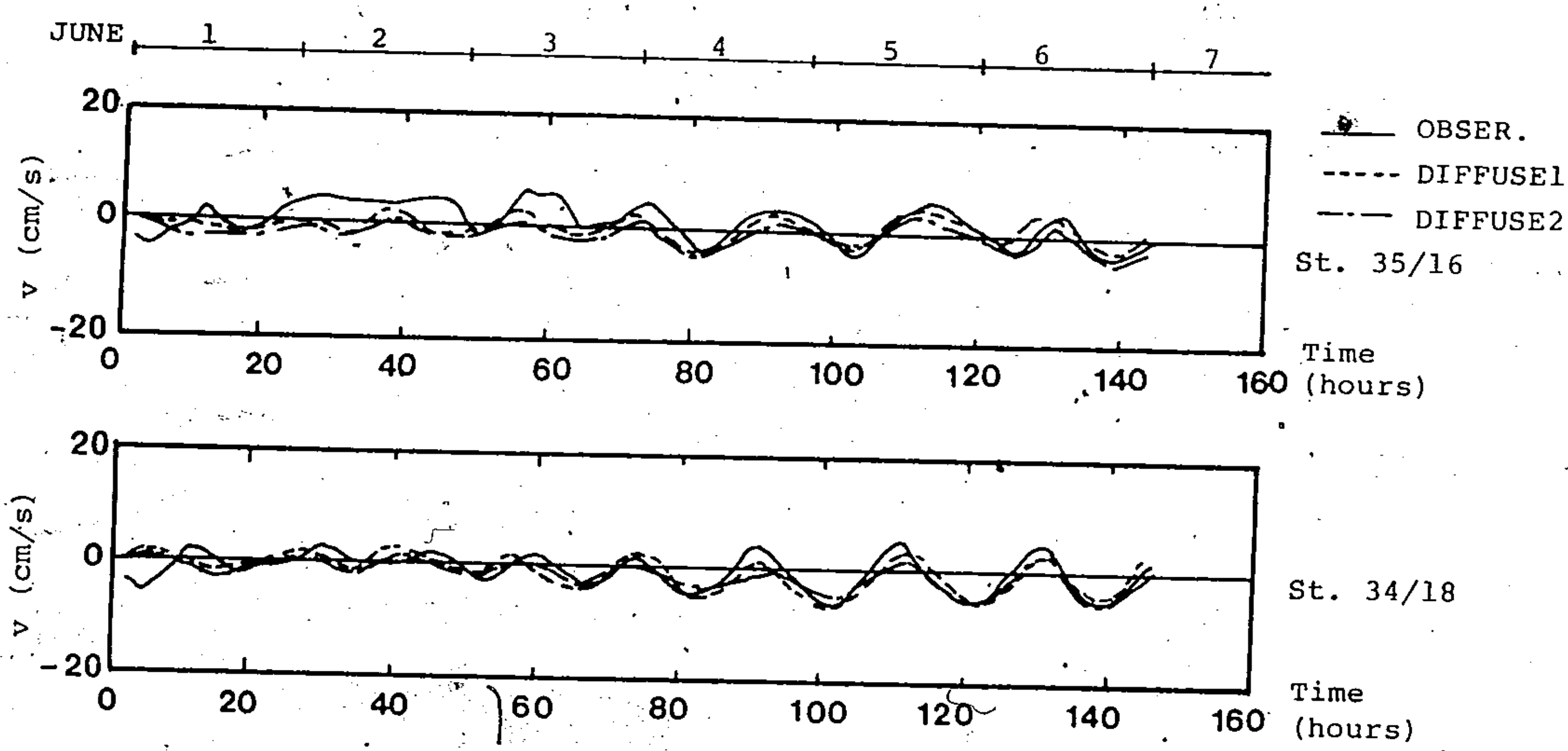

Figure 5.10 Continued

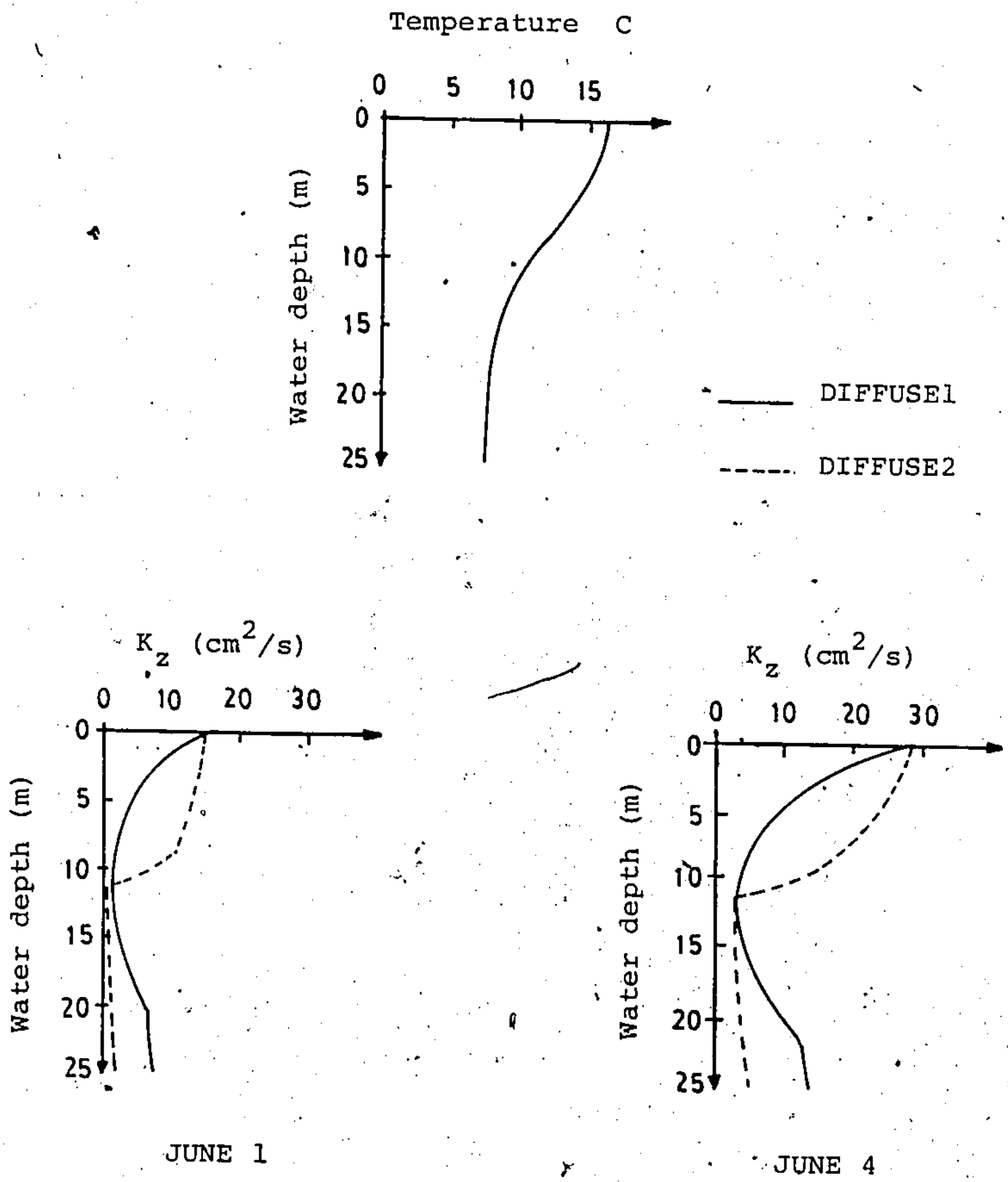

Figure 5.11 Temperature and computed vertical diffusivity (DIFFUSE1 and DIFFUSE2) profiles for June 1 and 4.

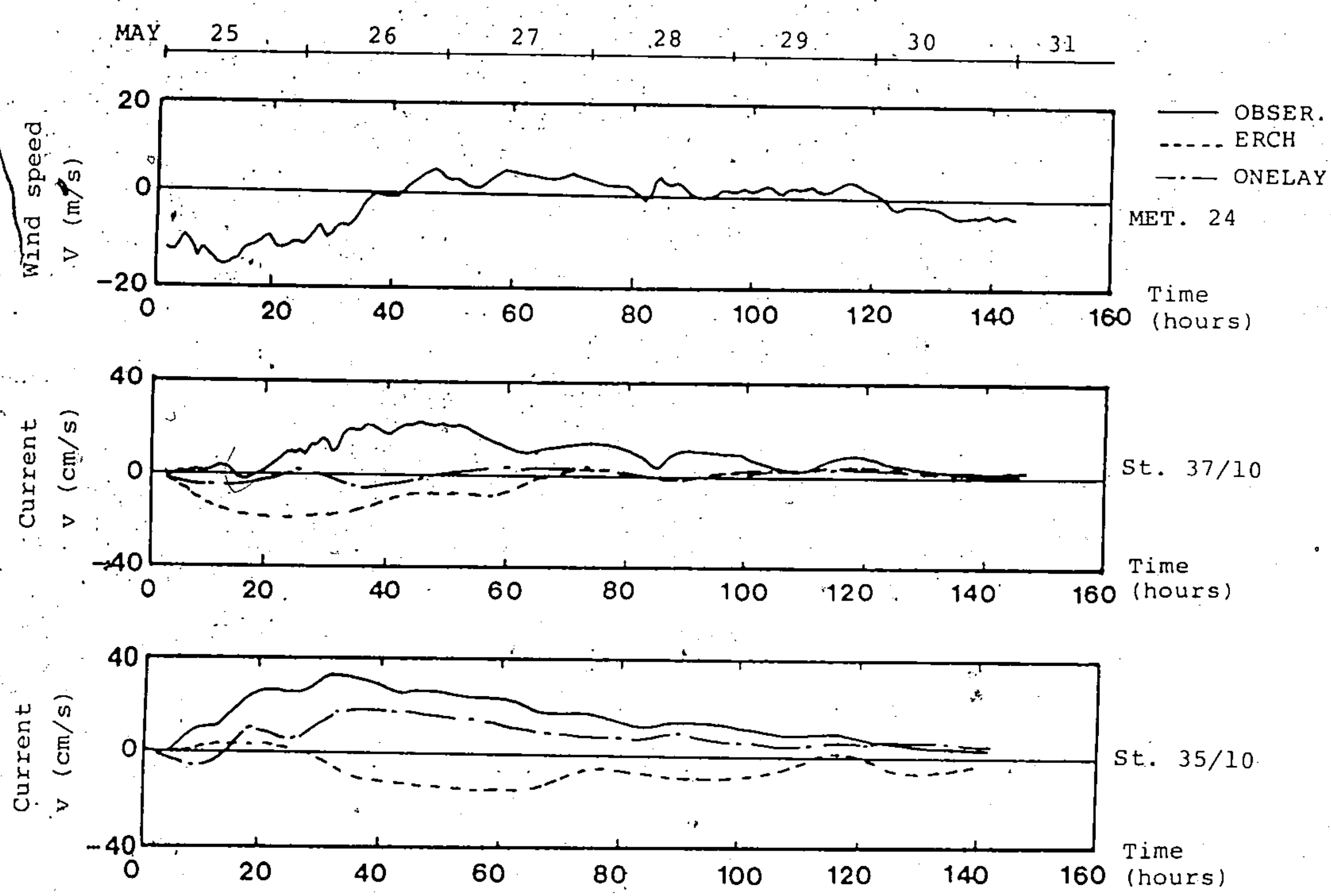

Figure 5.12 Shore-parallel wind and observed and computed currents (ERCH and ONELAY) as a function of time, May 25-30,1979 episode.

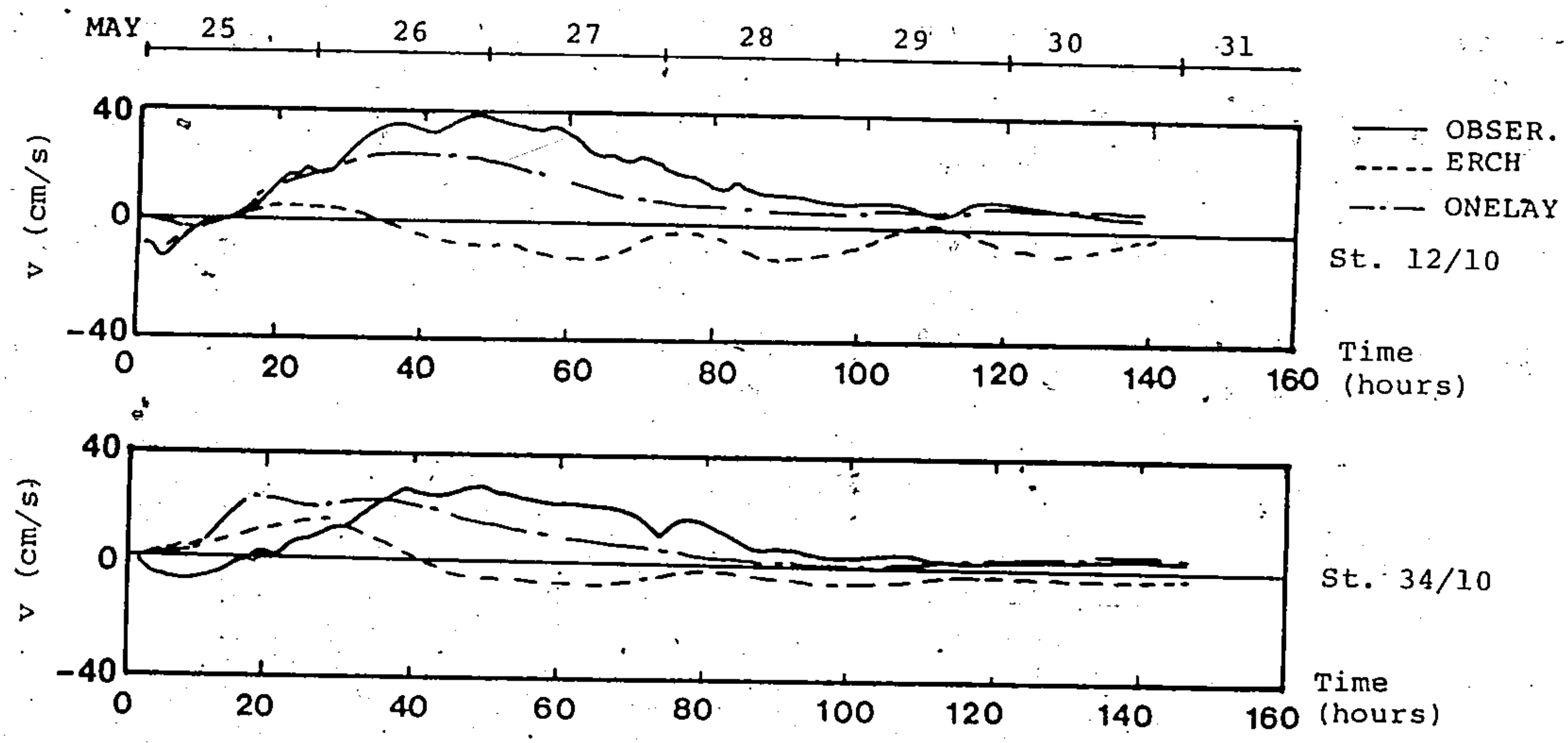

Figure 5.12 Continued

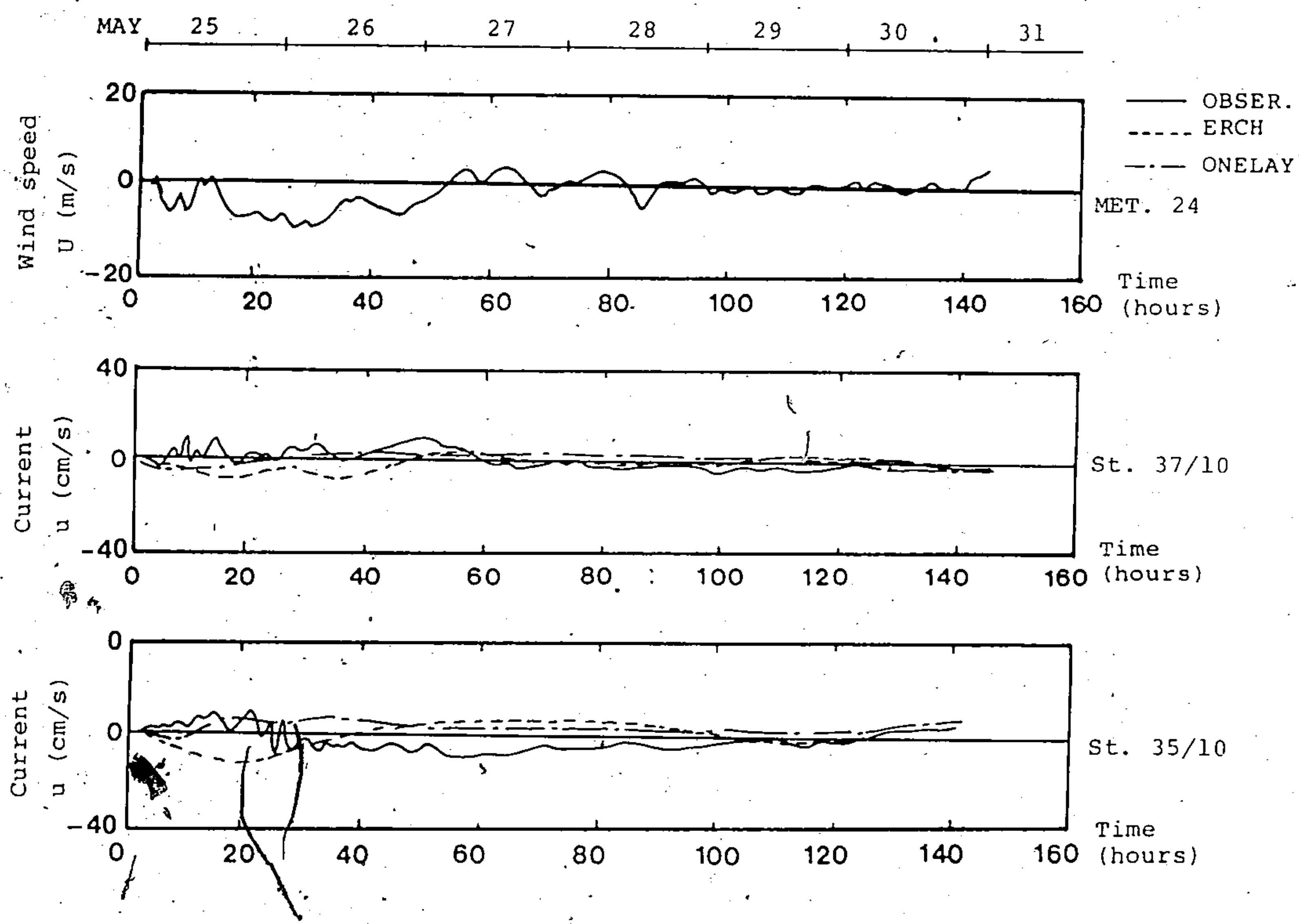

Figure 5.13 Shore-perpendicular wind and observed and computed currents (ERCH and ONELAY) as a function of time, May 25-30, 1979 episode.

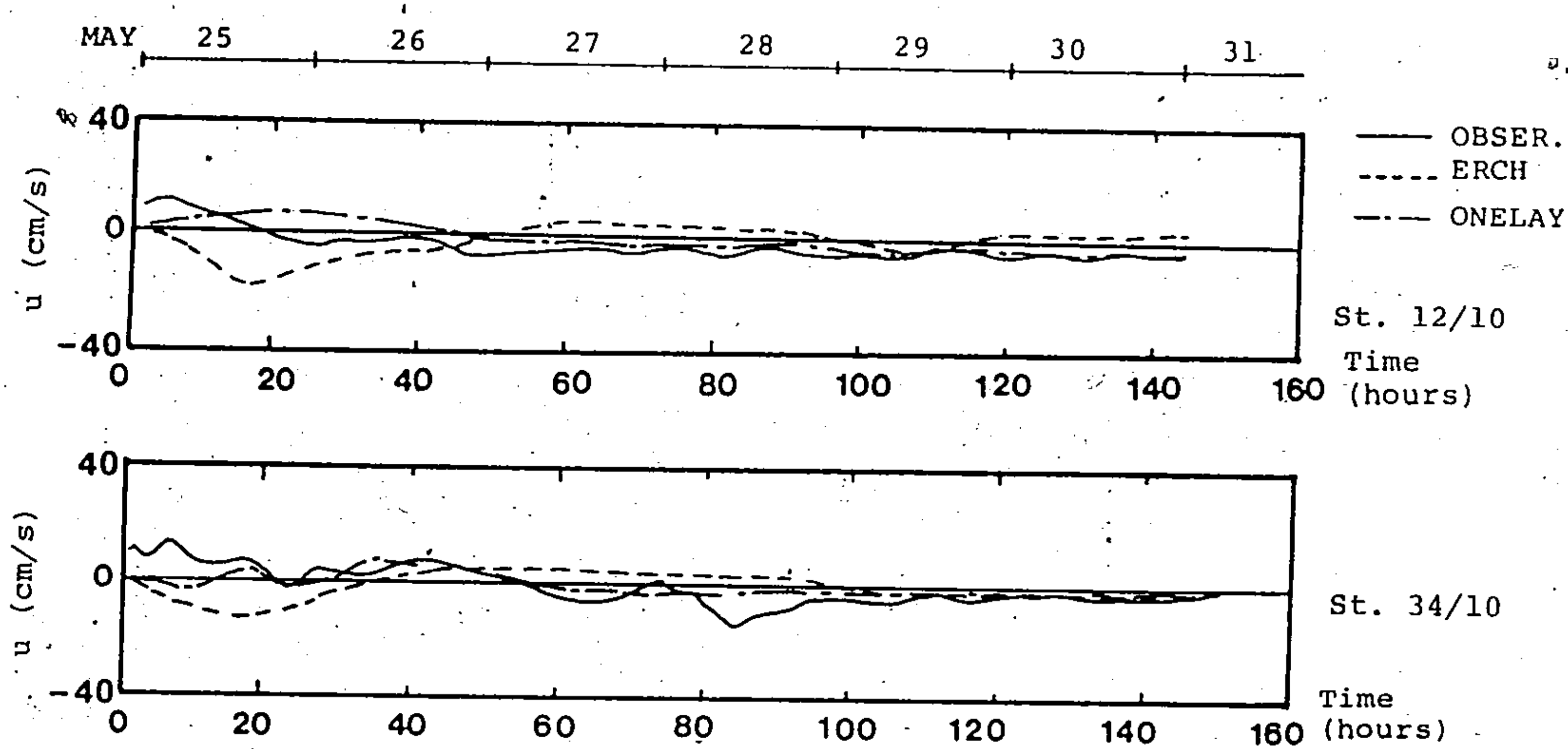

Figure 5.13 Continued

model developed by Simons and Lam (1982) was used to obtain currents for this episode. The model formulation, sensitivity and application are presented in the next part of this dissertation.

5.3 ONE-LAYER MODEL "ONELAY"

The model developed by Simons and Lam (1982) assumes that the basin is relatively well-mixed vertically. The model computes the vertically integrated current and the free surface elevation for a given wind and given inflow and outflow. The non-linear acceleration terms are dropped, the Coriolis term is included, and either linear or nonlinear bottom friction can be modelled.

5.3.1 Basic equations and parameters

The model solves the vertically integrated equations of motion and continuity:

$$\frac{\partial U}{\partial t} = fV - gH\frac{\partial z}{\partial x} - BU + \tau_{wx} \qquad [5.26]$$

$$\frac{\partial V}{\partial t} = -fU - gH\frac{\partial z}{\partial y} - BV + \tau_{wy} \qquad [5.27]$$

$$\frac{\partial z}{\partial t} = -\frac{\partial U}{\partial x} - \frac{\partial V}{\partial y} \qquad [5.28]$$

where t is time, U and V are the vertically integrated current, corresponding to the horizontal coordinates x, y (x clockwise from y) respectively, z is the free surface displacement from a mean level (positive upward), H is the mean depth of the basin, B is a bottom stress coefficient, f is the Coriolis parameter, and τ_{wx} and τ_{wy} are the wind stress components divided by water density.

The bottom stress coefficient B is given by one of the following forms:

$$\text{linear} \quad B = a/H \qquad a = 0.01\text{-}0.05$$

$$\text{Nonlinear} \quad B = C_D\,(U^2 + V^2)^{1/2}/H^2 \qquad C_D = 0.002 \qquad [5.29]$$

The wind stress is computed using [5.23].

The model uses a single staggered grid. The water depth and the free surface elevation above the mean are defined at the centre of a grid square. These values represent averages over this grid. The vertically integrated water transport U is defined at the centre of the left and right sides of the grid square while the V-component is defined at the lower and upper sides.

The model first predicts the free surface elevation, the U-component and then the V-component at all time steps using the last available value of all variables. Numerical stability is achieved if:

$$\Delta t < \Delta S/\sqrt{2gH_{max}} \quad \text{and}$$

$$\Delta t < 1/B_{max}$$

where Δt is the time step and ΔS is the grid size (Platzman, 1963). In this study ΔS = 6.667 Km, H_{max} = 62 m and t = 180 s.

5.3.2 Model sensitivity

Sensitivity analyses were carried out using Lake Erie bathymetry. The effect of the wind stress, wind direction, inflow and outflow transport (Detroit and Niagara rivers), and the bottom friction on the free surface elevation and the current transports were studied. In each case the model was run for one day using a 3 minute time step. The effect of the usual parameters was studied at three locations about 6.7, 13.4 and 27 km off Cleveland. The results are presented in Table 5.3. The results show that the free surface elevation is highly sensitive to the change in the wind speed, wind direction and the inflow transport. The outflow transport has nearly almost no effect due to its remoteness from the study site. The current transports are less sensitive to the parameters than the free surface elevation. The effect of the bottom friction was also found to be significant.

Since the Simon and Lam model uses constant wind stress, the model was modified by the writer to include hourly average wind speed and direction time series for the wind stress calculations. The modifird model is called ONELAY (ONE LAYER).

5.3.3 ONELAY results and discussion:

For the May episode two runs were carried out using linear and nonlinear bottom friction. The results for nonlinear bottom friction were higher and closer to the observed flows than those for the linear

Table 5.3, ONELAY sensitivity parameters

Parameter	Initial value	Range of variability	Max. and min. factors of change		
			z	U	V
Windstress degree/cm	1	0-2	-7.5, 7.5	-1, 2.5	-0.5, 2
Wind direction degree from north	45^{o}	135^{o}-225^{o}	-10, 10	-2.5, 1.0	-1.5, 3.5
Inflow x 10^8 m^3/day	5.07	0.0-10.14	-8, 8	0.2 , 2.0	0.6, 1.2
Outflow x 10^8 m^3/day	5.52	0.0-11.04	--	--	--
Inflow-Outflow x 10^8 m^3/day	5.07-5.52	0.0,0.0 - 10.14,11.04	-8, 8	0.2, 2.0	0.5,1.1
Bottom friction	linear	nonlinear	-2, 7	-1.1, 3.8	1.5, 2

bottom friction. The results are plotted in Figures 5.12 and 5.13. In both cases the results obtained from ONELAY are closer to the observed flows at all moorings than the results obtained from ERCH.

5.4 DISCUSSION

According to a study in Lake Ontario (Bennett, 1974), the wind term in [5.26] has to be greater than the pressure term in the nearshore zone, to produce nearshore flow in the direction of the wind nearshore. The opposite is true in deep water. This was confirmed by ERCH. ONELAY and observed currents do not conform to this. On the other hand ERCH does not account for (a) shore irregularity in the east-west direction (b) the difference in the water depth between the central and western basins, which is large and develops a boundary at the lower 15 m. The effect of such a boundary is increased in the case of north-westerly wind where a high barotropic pressure gradient is developed along the lake's major axis.

In spite of the fact that ONELAY gives better results than the ERCH for the May episode, the model results are not deemed to be appropriate for this study. ONELAY predicts the vertically integrated currents over a relatively coarse grid of about 6.7 km (currents between the grid points were interpolated). ONELAY is adequate for the prediction of the vertically integrated lake circulation during nonstratified periods, where the entire lake is solved.

Close to the shore (st. 37), both ERCH and ONELAY produced results difference from the observations. Sensitivity analysis of both ERCH and ONELAY showed that the shallow central basin is highly sensitive to wind speed and direction. The average wind stresses over the first two days of the May storm were 2.2 and 1.9 dyne/cm^2 for MET. 26 and MET. 24 respectively. For such stress differences between the north shore and (almost) the basin centre, the entire basin may spin anticlockwise forming one cell. Because of the combination of the barotropic return flow in the lake's major axis and the anticlockwise rotation of the central basin, the alongshore flow in the south shore was against the wind. Saylor and Miller (1983), using current-meter data in the central basin of Lake Erie, observed that the two-cell response to the wind described by Gedney (1971) is not formed during significant wind stress impulses. The pattern frequently forms a one-cell circulation where the flow is apparently more barotropic than predicted.

ERCH is used to generate the flow field for several days in Chapter 6, and the results in all cases are in agreement with the observations.

PHASE 3: TRANSPORT MODEL

CHAPTER 6

TRANSPORT MODEL "SEDTRAN"

6.1 INTRODUCTION

The general goal of a water quality model is to predict the concentration of a contaminant over space and time, knowing the boundary conditions, the initial flow structure and the initial contaminant concentration distribution. The contaminant concentration is highly sensitive to the mean current and turbulent fluxes. Truly predictive water quality models necessarily include the prediction of the current and turbulent fluxes as well as the concentration. But it is useful in many cases to use sophisticated water quality models without simultaneously predicting the current and turbulent fluxes. In this case the hydrodynamic model is run first, the appropriate data are stored and then used to run the mass transport model. In the less difficult situations, where the current and turbulent fluxes are known from observations , the mass transport model only is run.

In the present study the hydrodynamic models are run first to generate the current field (Chapter 5), the current field is stored and then used as input to the mass transport model. The field observations are used to verify, calibrate and validate the hydrodynamic models and to estimate the turbulent fluxes by means of the diffusion coefficient calculations (Chapter 4).

To study the effect of the different flow regimes discussed in

Chapter 4 on the sediment distribution within the coastal boundary layer, both the detailed vertical structure of the horizontal flow and the vertical velocity have to be incorporated in the mass transport model. Thus a three-dimensional time dependent mass transport model is required.

Sediment transport and deposition in coastal zones can be divided into two major topics according to the sediment source: (i) sediment discharge from a land source (sewers, industrial outfalls and runoff), and (ii) sediment load generated by erosion and resuspension of the lake shore and bottom.

Sediment resuspension calculations require measurements of a reference concentration for each time step of the simulation period, to construct the logarithmic-suspended load concentration profile. It is very difficult, if not impossible, to establish a reference concentration for each time step. The other alternative is to relate the reference concentration to the shear velocity and the bed load discharge (Einstein, 1950). For more details refer to a previous study (Elzawahry ,1981). Bed load calculations require relating the sediment characteristics to the flow properties through some empirical constants in an iterative procedure. It is not an easy task to develop three-dimensional time dependent sediment transport models capable of computing the sediment bed load, the sediment resuspension distribution and the inflow sediment distribution. Such models are expected to be very costly and the results are expected to be difficult to iterpret. When Chen (1971) formulated a longitudinal dispersion equation for suspended sediment with a moving bed, the work involved many simplifications and formulations. Moreover, the sediment resuspension is highly influenced by thermal stratification.

The thermocline behaves as a diffusive floor preventing the bed sediment from resuspension in the epilimnion.

A computer program called SEDTRAN was developed by the author to predict the inflow sediment concentration distribution within the coastal boundary layer. The program solves numerically the three dimensional time dependent mass balance equation including the settling term. The program solves the sediment transport equation using a forward time difference, central finite difference for the diffusion terms and upwind finite difference with flux-corrected transport technique for the advection and settling terms.

The ability of the numerical model to simulate efficiently one, two or three space variables is illustrated by many numerical test examples. The model was partially validated using the limited suspended sediment measurments collected by the water quality laboratory at Heidelberg college. Part of the data published by the U.S. Geological Survey (USGS) 1979, have also been used in the validation. The program was used to simulate many settling activity cases which may take place in coastal waters. All the simulated cases were used to define: (1) a representative zone influenced by a nearshore source of pollution and (2) the sediment grain size distribution across the coastal boundary layer.

6.2 DEVELOPMENT OF THE THREE DIMENSIONAL MODEL "SEDTRAN"

A computer program called SEDTRAN (SEDiment TRANsport) was written by the author to solve the three-dimensional time-dependent sediment mass balance equation. The sediment concentration is assumed to be a function of the three space coordinates and time. The three velocity components in the alongshore, the cross-shore and the vertical directions previously computed by ERCH (Chapter 5) are input to SEDTRAN which generates a three dimensional sediment plume/patch. The three velocity components are assumed to vary only in the alongshore and the cross-shore directions. The horizontal diffusivities are assumed to be constants or functions of time, the values being obtained from the statistical analysis performed in Chapter 4. The vertical eddy diffusivity is assumed to be a function of time, wind stress, water temperature and water depth. The settling velocity is calculated for each grain size using Stokes law for Reynolds numbers less than 0.1 and the relation reported by Simon and Sentruk (1977) for Reynolds numbers larger than 0.1. SEDTRAN simulates up to 10 sources of sediment with variable locations. The source concentrations can be constant or time dependent. The model simulates a continuous source to generate a plume and a spike to generate a patch. The bottom topography is also accommodated by SEDTRAN.

6.2.1 Basic equation and parameters

The concentration distribution of suspended solids in a turbulent flow field can be shown to follow

$$\underset{(1)}{\frac{\partial C}{\partial t}} = -\underset{(2)}{\frac{\partial (uC)}{\partial x}} - \underset{(3)}{\frac{\partial (vC)}{\partial y}} - \underset{(4)}{\frac{\partial (wC)}{\partial z}} + \underset{(5)}{\frac{\partial}{\partial x}\left(K_x \frac{\partial C}{\partial x}\right)} + \underset{(6)}{\frac{\partial}{\partial y}\left(K_y \frac{\partial C}{\partial y}\right)}$$

$$+ \underset{(7)}{\frac{\partial}{\partial z}\left(K_z \frac{\partial C}{\partial z}\right)} - \underset{(8)}{\bar{w}_s \frac{\partial C}{\partial z}} \qquad [6.1]$$

where

- C is the mean value of suspended solids concentration
- t is time
- x, y are the shore-parallel and the shore-perpendicular coordinates
- z is the vertical coordinate, positive upward
- u is the shore-parallel velocity
- v is the shore-perpendicular velocity
- w is the vertical velocity
- K_x is the shore-parallel diffusion coefficient
- K_y is the shore-perpendicular diffusioin coefficient
- K_z is the vertical diffusion coefficient
- w_s is the settling or fall velocity of suspended solids.

In deriving [6.1] the mass transport due to the molecular diffusion is much less than that due to the turbulent fluctuation, and is neglected.

Equation [6.1] can represent the conservation of any other transferable scalar quantity in a turbulent flow, such as neutral density tracer, heat and energy. The equation yields the balance between the rate of change of concentration, the net transport by fluid mean motion (advection terms), the turbulent net diffusion (diffusion terms) and the net downward flow of suspended solids due to the gravitational force (settling or sink term). In the case of a neutral density tracer such as dye, the fall velocity is set equal to zero.

The velocity components u, v and w are previously computed by ERCH (Chapter 5) and stored to be used in SEDTRAN. The three velocity components are assumed to be functions of the cross-shore and the vertical directions and the variability with the alongshore direction is neglected (channel model). Refer to Chapter 5 for more discussion.

The fall velocity w_s is calculated for each grain size in the sediment inflow distribution using Stokes law for particles less than 0.0625 mm (silt and clay):

$$w_s = \frac{(\rho_s - \rho)\, g\, D_s^2}{18\,\mu} \qquad [6.2]$$

where

ρ_s is the suspended sediment density,

ρ is the water density,

g is gravity acceleration,

D_s is the sediment particle diameter,

μ is the dynamic viscocity of the fluid.

Equation [6.2] is a balance between the particle buoyant weight and the resisting force resulting from the fluid drag, with drag coefficient $C_d=24/R_w$, where R_w is Reynolds number. Equation [6.2] is only applied if $R_w < 0.1$ ($D_s < 0.0625$ mm), where the downward flow of suspended sediment is treated as low Reynolds number flow and hence the inertia term is dropped. For larger Reynolds numbers the inertia term cannot be neglected. Considerable literature on incorporating the inertia force in

[6.2] exists (Proudman and Pearson, 1957; Langlois, 1964; and Happel and Brenner, 1973). In this study, for particle sizes bigger than 0.0625 mm, the experimental relation reported by Rouse (1937), and given in Figure 6.1, is used. A weighted arithmatic mean for the fall velocity is calculated to get the mean fall velocity w_s.

The fall velocity obtained from [6.2] and Figure 6.1 is for a single particle in an infinite fluid. If only a few closely spaced particles are in the fluid, they will fall in a group with higher velocity than that of a single particle. On the other hand, if particles are dispersed throughout the fluid, the interference between neighboring particles will tend to reduce their fall velocity (hindered settling). The theoretical results reported by McNown and Lin (1952) is used with typical concentrations observed in the study area to calculate the effect of the sediment concentration on fall velocity. The results showed a maximum decrease of 4% in the fall velocity, therefore the effect is neglected here.

It is well known that the characteristics of turbulent quantities such as turbulent intensity and diffusion coefficient are affected by the suspension of solid particles. The intensity of turbulence of the flow is damped as a result of increased energy consumption needed to suspend sediment and hence the diffusion coefficient decreases. The ratio between the eddy diffusivities for (a) suspended solids and (b) clear water is a function of sediment and water densities, sediment fall velocity, sediment concentration, water depth, bottom roughness, shear velocity and von Karmen coefficient (Hino, 1963). The mathematical

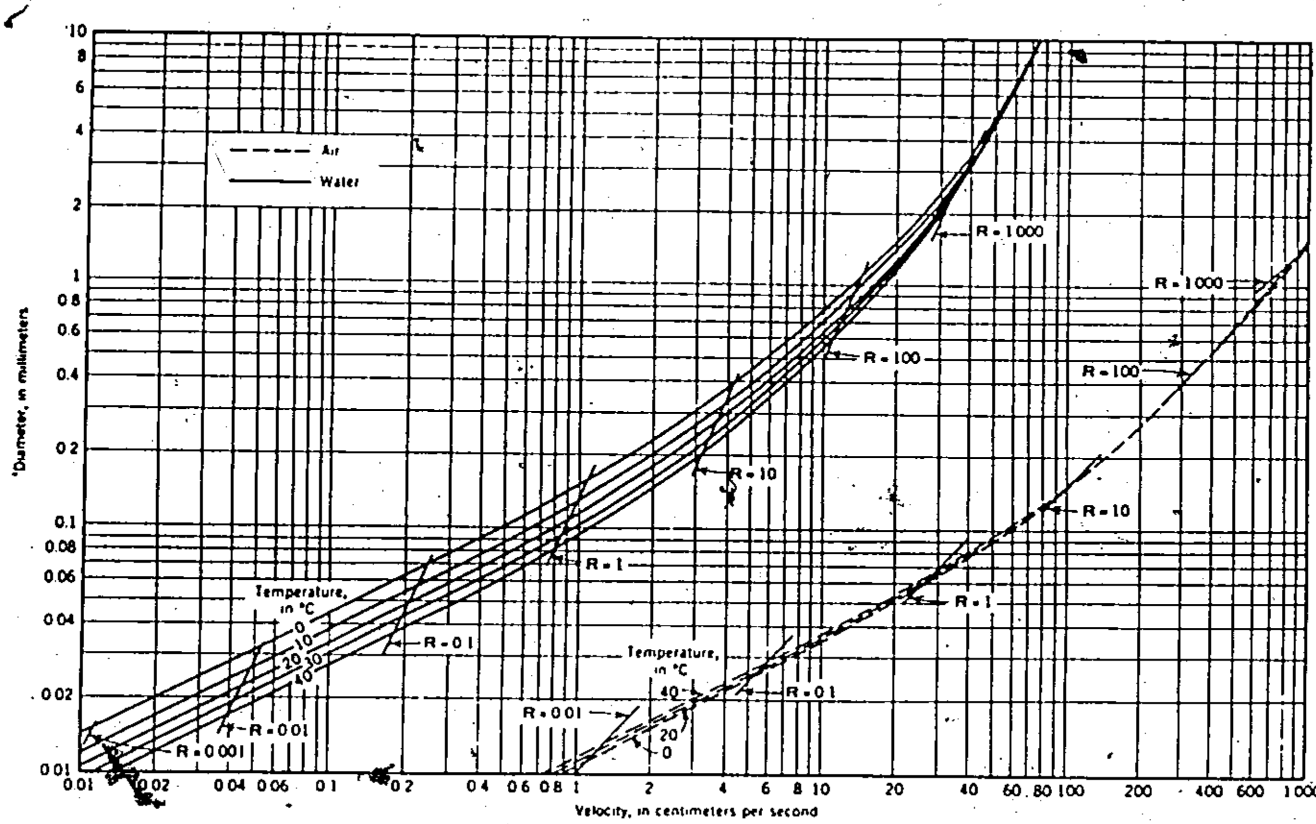

Figure 6.1 Fall velocity as function of particle size (Rouse, 1937).

expression derived by Hino (1963) was used with typical values of the previously mentioned parameters to find the effect of the sediment concentration on the diffusion coefficient. The results showed a maximum decrease of 8% in the diffusion coefficient. In this study the suspended sediment eddy diffusivity is taken to be equal to that of clear water.

The horizontal eddy diffusivities are assumed to be constant and were derived from the statistical analysis in Chapter 4. In the case of a patch the diffusion coefficients are assumed to be a function of time (diffusion time). The values and the diffusion laws used are reported later in this chapter.

The vertical eddy diffusivity is assumed to be a function of the water depth, water temperature and the wind shear stress:

$$K_z = \frac{K_s \; (C_1 + C_2 \; e^{z/D})}{\left(1 + \sigma_1 \; C_D \; g \; \alpha \dfrac{D^2 \; e^{-2z/D}}{\tau w} \dfrac{\delta T}{\delta z}\right)^{3/2}} \qquad [6.3]$$

Equation [6.3] is similar to [5.15] where K_s is assumed to be equal to A_s.

The diffusion of momentum is accomplished by both (a) the pressure fluctuations and (b) the translation of the water particles, whereas the diffusion of material is accomplished only by the latter (b). This is utilized in [6.3] by using a power of 3/2 instead of the power 1/2 used in [5.15].

6.2.2 Numerical techniques

Analytical techniques for solving the transport and diffusion equation [6.1] do not exist except for the simple and idealized cases, used for verification of the SEDTRAN code later in this chapter. Thus finite difference techniques are used to solve [6.1] numerically.

The time derivative (term 1 in [6.1]) is approximated by a finite difference form a using forward difference scheme (FDS), while the second order terms (diffusion terms 5,6 and 7) are approximated using a central difference scheme (CDS).

Approximating the advection terms 2,3,4 and 8 in [6.1] in a simple finite difference form without inviting inaccuracy or instability seems to be impossible. For the moment let us drop terms 3,4,6,7 and 8 from [6.1], i.e.,

$$\frac{\partial C}{\partial t} = - u \frac{\partial C}{\partial x} + K_x \frac{\partial^2 C}{\partial x^2} \qquad [6.4]$$

Let i,j,k and m represent a grid point of space coordinates x,y,z at a time t respectively such that $C_{i,j,k}$ is the suspended sediment concentration at grid point (i,j,k) at time m. Approximating [6.4] in a finite difference form, using forward time difference scheme and central difference scheme for the advection and diffusion terms, yields:

$$\frac{C^{m+1}_{i,j,k} - C^{m}_{i,j,k}}{\Delta t} = - u \frac{C^{m}_{i+1,j,k} - C^{m}_{i-1,j,k}}{2\Delta x} + K_x \frac{C^{m}_{i+1,j,k} - 2\, C^{m}_{i,j,k} + C^{m}_{i-1,j,k}}{\Delta x^2} \qquad [6.5]$$

which can be rearranged as

$$\frac{C^{m+1}_{i,j,k} - C^{m}_{i,j,k}}{\Delta t} = \frac{K_x}{2\Delta x^2} \{(2-R_e)\, C^{m}_{i+1,j,k} - 4\, C^{m}_{i,j,k}$$

$$+ (2+R_e)\, C^{m}_{i-1,j,k}\} \qquad [6.6]$$

where $R_e = u\Delta x/K_x$ is called the cell Reynolds number. Equation [6.6] can be shown (Peyret and Taylor, 1981) to be stable only if R_e less than 2. If R_e is greater than 2, an unstable solution is obtained. This kind of instability is called spatial instability and occurs even when steady state problems are solved. The only way to use CDS and avoid the spatial instability is to use a very fine grid. Typical values for the coastal zone of Lake Erie (Chapter 4) are: u = 20 cm/sec ; $K_x = 10^4$ cm^2/sec; and the spatial increment must be less than 10 meters. To simulate a 15 km by 15 km area, 1500 x 1500 grid points for one level are required. To generate the current and the sediment concentration over this very fine grid, computer memory of at least 1000 and 10000 k bytes are anticipated for ERCH and SEDTRAN respectively. Moreover the computation time is expected to be long: to simulate one day real time, 2000 and 10000 cp seconds are required on a CDC Cyber 170/730, for ERCH and SEDTRAN respectively. It is easy to conclude from these values that the solution will be very expensive. Suitable computers were not available at the time of this research.

To avoid the spatial instability, non-centered difference (one-sided difference) such as upstream difference scheme (UDS) may be used for the advection terms. In the UDS, "backward" and "forward" differencing are used depending on the velocity sign. Backward differences are used when the velocities are positive, and vice-versa. Thus the difference is always on the upstream side of the point which the time derivative is evaluated, i.e.,

$$\frac{C^{m+1}_{i,j,k} - C^{m}_{i,j,k}}{\Delta t} = -u\,\frac{C^{m}_{i,j,k} - C^{m}_{i-1,j,k}}{\Delta x} \qquad \text{for } u > 0$$

$$= -u\,\frac{C^{m}_{i+1,j,k} - C^{m}_{i,j,k}}{\Delta x} \qquad \text{for } u < 0 \qquad [6.7]$$

The UDS can be shown (Mesinger and Arakawa, 1976) to be stable for all R_e. Even though this resolves the spatial instability, the scheme introduces other difficulities. Roach (1972), using Hirt's stability analysis showed that [6.7] is equivalent to

$$\frac{\partial C}{\partial t} = -\frac{\partial uC}{\partial x} + K_{art}\frac{\partial^2 C}{\partial x^2} \qquad [6.8]$$

where

$$K_{art} = \frac{u\Delta x}{2}\,(1 - Cn) \qquad [6.9]$$

where $Cn = u\Delta t/\Delta x$ is known as the Courant number. The method introduces a non-physical diffusion coefficient K_{art}, which is known as numerical or artificial diffusivity. To minimize the artificial diffusion, Cn must be chosen to be as close to 1 as possible. In practice, it is impossible to simultaneously keep Cn in the three directions x, y and z at all points equal to 1. Typical values are u=20 cm/sec, Δt = 15 minutes, Δx = 300 m, Cn = 0.6 and K_{art} = 1.2×10^5 cm^2/sec. The artificial diffusion introduced by the UDS is thus about 10 times larger than the actual diffusivity, which cannot be accepted. Many other finite difference schemes are applicable, but all have the problem of too much diffusion or spatial instability.

The only way to suppress the artificial diffusion and simultaneously achieve the desired accuracy is to add "anti-diffusion" to the scheme to balance the unwanted diffusion. A suitable method was proposed by Chaudri (1971). The general and complete method was developed by Boris and Book (1973) and Book et al. (1975,1981), and is called flux-corrected transport technique (FCT). The method uses two steps: (1) use a scheme which introduces artificial diffusion, such as UDS, and (2) eliminate the artificial diffusion by using the results of the first step as initial values to solve the diffusion equation with negative values of K_{art}, i.e.

$$\frac{\partial C}{\partial t} = - K_{art} \frac{\partial^2 C}{\partial x^2} \qquad [6.10]$$

The antidiffusion as given in [6.10] removes the error introduced in the first step but new maxima and minima are formed where they are physically unreasonable. The new minima is actually negative. In order for the antidiffusion stage to be non-negative, Boris and Book (1973) gave the following qualitative limitation:

"The antidiffusion stage should generate no maxima or minima in the solution, nor should it accentuate already existing extrema."

This qualitative limitation is translated to quantitative form in steps (d) and (f) in the following paragraph.

The FCT algorithm is used to solve equation [6.1]. The sequence of operation is summarized for simplicity only in the x-direction [6.4] with positive velocity as follows:

(a) Diffuse C :

$$C^{m+1}_{i,j,k} = C^{m}_{i,j,k} + \frac{K_x \Delta t}{\Delta x^2} (C^{m}_{i+1,j,k} - 2C^{m}_{i,j,k} + C^{m}_{i-1,j,k})$$

(b) Transport C:

$$C^{m+1}_{i,j,k} = C^{m}_{i,j,k} - \frac{\Delta t}{\Delta x} (u_R C^{m}_{i,j,k} - u_L C^{m}_{i-1,j,k})$$

where

$$u_R = 1/2\ (u^{m}_{i+1,j,k} + u^{m}_{i,j,k})$$
$$u_L = 1/2\ (u^{m}_{i,j,k} + u^{m}_{i-1,j,k})$$

(c) Compute the first differences:

$$\Delta_{i+1/2,j,k} = \frac{\delta C}{\delta x} = \frac{C^{m+1}_{i+1,j,k} - C^{m+1}_{i,j,k}}{\Delta x}$$

(d) Correct the antidiffuse flux:

$$S = \mathrm{sign}\{\Delta_{i+1/2,j,k}\}$$

$$F_{i+1/2,j,k} = S.\max\{0, \min[S.\Delta_{i-1/2,j,k},\ \Delta_{i+1/2,j,k}\ \eta_{i+1/2,j,k},\ S.\Delta_{i+3/2,j,k}]\}$$

where:

$$\eta_{i+1/2,j,k} = 1/2\ Cn_{i+1/2,j,k}(1 - Cn_{i+1/2,j,k})$$

$$Cn_{i+1/2,j,k} = \frac{\Delta t}{\Delta x} \max (u_R, u_L)$$

(e) Antidiffuse:

$$C^{m+1}_{i,j,k} = C^{m+1}_{i,j,k} + F_{i-1/2,j,k} - F_{i+1/2,j,k}$$

(f) Final concentration:

Add results of a and e.

It is important to mention here that step (b) is a finite difference approximation using the second order upwind or "donor cell" method . The "donor cell" method is more accurate than the first order upwind, since it maintains something of the second order accuracy (Roach, 1972). The same procedure is repeated for all advection terms and the settling term. The numerical solution is stable only if:

$$\Delta t \leq \frac{1}{\left(\frac{2K_x}{\Delta x^2} + \frac{2K_y}{\Delta y^2} + \frac{2K_z}{\Delta z^2} + \frac{|u|}{\Delta x} + \frac{|v|}{\Delta y} + \frac{|w-w_s|}{\Delta z} \right)} \qquad [6.11]$$

Equation [6.1] is solved for the following boundary conditions

(1) Open boundary: the open boundaries are assumed to be far from the source where the diffusion flux may be assumed to be zero, i.e.,

$$n_x K_x \frac{\partial C}{\partial x} + n_y K_y \frac{\partial C}{\partial y} = 0 \qquad [6.12]$$

where $n=(n_x,n_y)$ is unit vector to the boundary

(2) Free surface:

$$K_z \frac{\partial C}{\partial z} = 0 \qquad [6.13]$$

(3) Solid boundary: both the advection and diffusion fluxes are assumed to be zero, i.e., $\partial C/\partial n=0$ for lateral boundary and $K_n\ \delta C/\delta x + w_s C=0$ for bottom (deposition boundary).

6.2.3 Operation of the program

The input parameters to SEDTRAN are: the numerical time step; the time increments to input current; wind and source concentrations; number of hours of simulation; the three spatial increments; number of grid points at each direction; number of sources; water depth; vertical temperature profile; sediment grain size distribution; wind velocity; and the three velocity components. SEDTRAN computes the number of vertical increments corresponding to each water depth, the fall velocity using [6.2] or Figure 6.1. The wind stress is computed using [5.23] and the vertical diffusivity is computed using [6.3]. The sediment concentration over the grid points is computed using the FCT procedure discussed earlier. The sediment concentration is printed out level by level for the given printout time increment. Figure 6.2 shows the SEDTRAN functional flow chart.

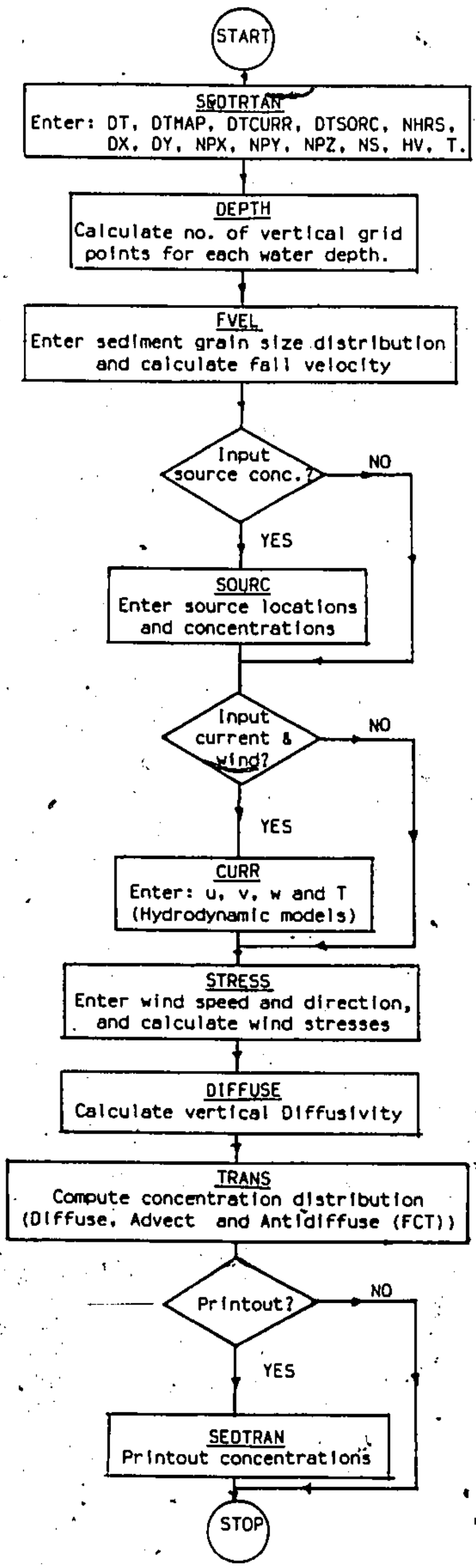

Figure 6.2 Functional flow chart for program SEDTRAN

6.3 SEDTRAN VERIFICATION

Verification implies testing the program code, structure and numerical techniques by comparison of model responses with theoretically anticipated results in as many cases as possible for which the anticipated results are known. As mentioned earlier, analytical solution of [6.1] is possible only for a few special cases. Pasquill (1962), Csanady (1972) and Fisher (1979) give the details. In this study the test examples have been chosen on the following basis: (i) the solution is known and the behaviour of the solution can be prescribed because the physical nature of the problem is known; (ii) the solution is simple so that we may concentrate on the reliability of the results rather than the difficulties of obtaining the solution and (iii) the tests contain as many different practical situations as possible. Seven test examples were chosen to simulate cases of: 1-D advection; 1-D diffusion; 2-D diffusions; 3-D diffusions; 1-D advection/diffusion; and 2-D advection/diffusions as follows:

1. One-dimensional advection: to simulate one dimensional pure advection (terms 1 and 2 in [6.1]), a rectangular wave was chosen. Smith et al. (1973) and Lam (1975) simulated the rectangular wave using different finite element and difference techniques. In this study the rectangular wave is simulated using UDS and UDS+FCT and the results are shown in Figure 6.3 a. Due to the presence of the discontinuities the rectangular wave provokes a large number of short-wave components, hence very accurate results cannot be obtained unless a very small spacing is used (Smith et al., 1973). Figure 6.3a shows the effect of the

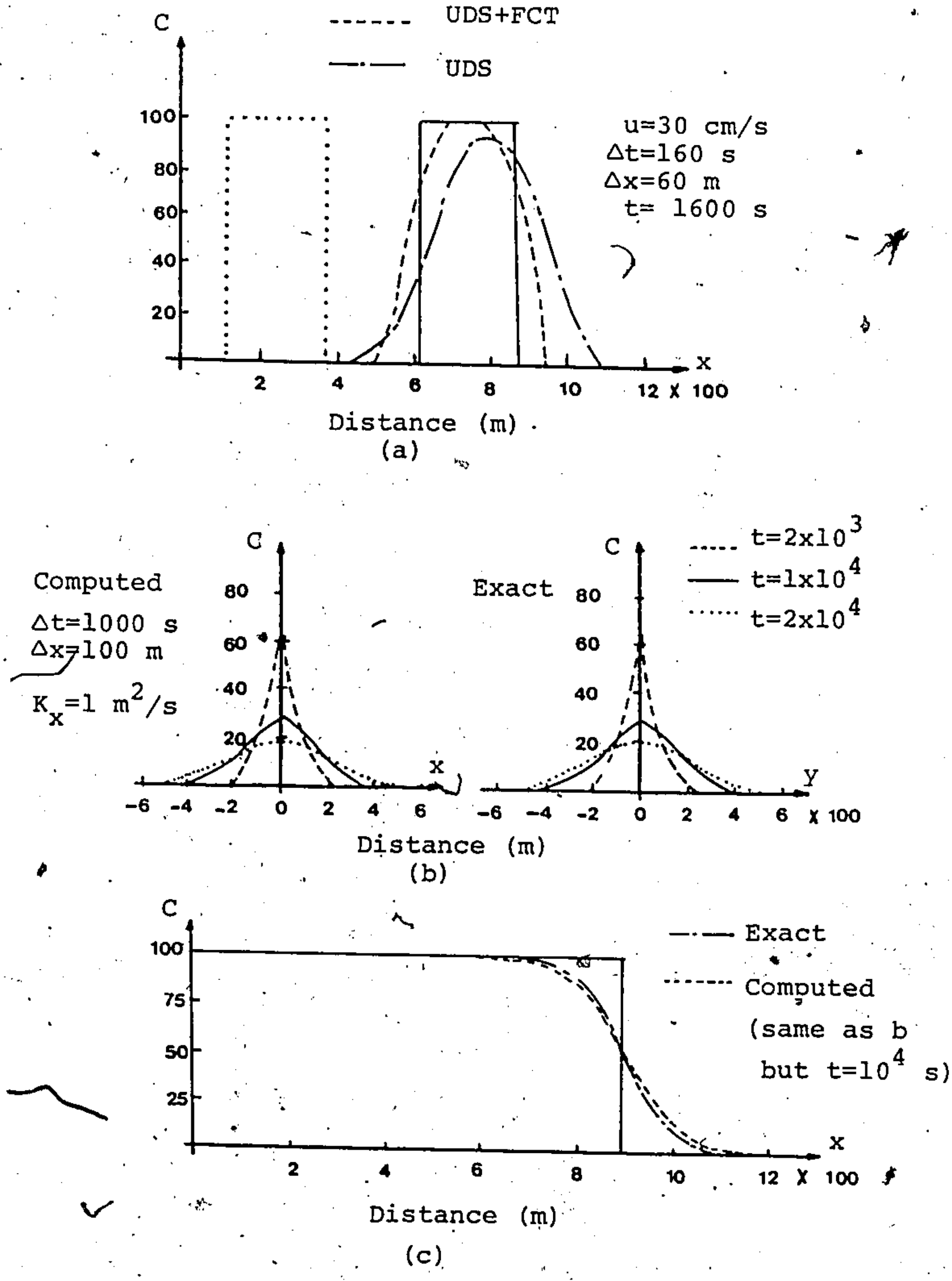

Figure 6.3 SEDTRAN verification, 1-D advection (a) and 1-D diffusion (b and c).

artificial diffusion introduced by UDS, (K_{art} = 1.8×10^4 cm^2/sec) and the improvement introduced by using UDS+FCT when 60% of the error is removed. Smith et al. (1973) reported that even high order finite elements cannot produce satisfactory results. Boris and Book (1973) and Lam (1975), of several finite difference and element schemes, showed that UDS+FCT produce the closest results to the exact solution (refer to Chapter2 for more details).

2. One-dimensional diffusion: the case of one-dimensional diffusion was verified using a delta function (pulse) and step function as follows:

(a) Delta function: In this case the one diffusion equation (terms 1 and 5 in [6.1]) is solved for initial concentration $C(x,0) = M\delta(x)$, where δ is the delta function and M is the pulse strength. The analytical solution is given by:

$$C(x,t) = \frac{M}{\sqrt{4\pi K_x t}} \exp\left(\frac{-x^2}{4K_x t}\right) \qquad [6.13]$$

(b) Step function: In this case the one diffusion equation is solved for initial concentration $C(x,0) = 0$ if $x < x_0$ and $C(x,0) = C_0$ if $x > x_0$. The analytical solution is given by:

$$C(x,t) = \frac{C_0}{2} \{1 - \mathrm{erf}\left(\frac{x - x_0}{\sqrt{4K_x t}}\right)\} \qquad [6.14]$$

Figures 6.3b and c, show a comparison between SEDTRAN results and the exact solution ([6.12] and [6.13]). It can be seen that SEDTRAN predicts the concentration in both cases reasonably well.

3. Two-dimensional diffusions: the two-dimensional diffusions case was verified by solving terms 1, 5 and 6 in [6.1] for the slug case (delta function), using the initial condition $C(x,y,0) = M\delta(x)\delta(y)$. The analytical solution is given by:

$$C(x,y,t) = \frac{M}{4\pi t\sqrt{K_x K_y}} \exp\left(\frac{-x^2}{4K_x t} - \frac{-y^2}{4K_y t}\right) \qquad [6.15]$$

Comparison between SEDTRAN results and the exact solution for x and y directions is shown in Figure 6.4a.

4. Three-dimensional diffusions: the three-dimensional diffusions equation (terms 1, 5, 6 and 7 in [6.1]) is solved for the slug case using the initial condition $C(x,y,z,t) = M\ \delta(x)\ \delta(y)\ \delta(z)$. The analytical solution is given by:

$$C(x,y,z,t) = \frac{M}{(4\pi t)^{3/2}\ (K_x K_y K_z)^{1/2}} \exp\left(\frac{-x^2}{4K_x t} - \frac{-y^2}{4K_y t} - \frac{-z^2}{4K_z t}\right) \qquad [6.16]$$

The results are shown in Figure 6.4b for both SEDTRAN and [6.15] for x, y and z directions.

5. One dimensional advection/diffusion: the one dimensional advection diffusion equation (terms 1, 2 and 5 in [6.1]) which is known as the lake thermocline model is solved for the step function, using the initial condition previously mentioned in part 2.b. The analytical solution is

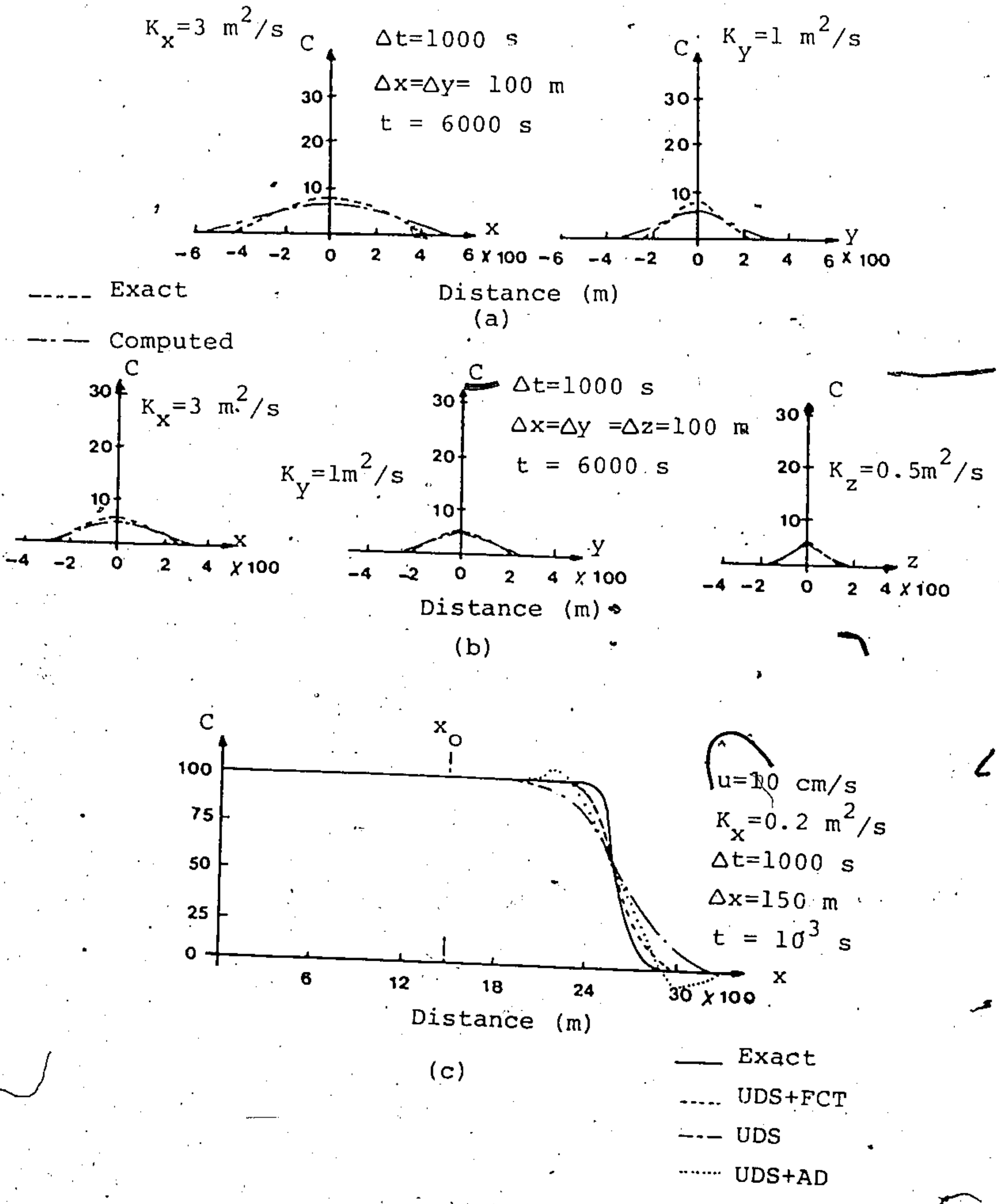

Figure 6.4 SEDTRAN verification, 2-D diffusion (a), 3-D diffusion (b) and 1-D advection/diffusion (c).

given by:

$$C(x,t) = \frac{C_0}{2} \{1 - \mathrm{erf}\,(\frac{((x - x_0) - ut)}{\sqrt{4K_x t}})\} \qquad [6.17]$$

Comparison between UDS, UDS and anti-diffusion without flux correction (UDS+AD), UDS+FCT and the exact solution is shown in Figure 6.4c. The artificial diffusion introduced by UDS, the new maxima and minima and the negative values associated with UDS+AD and the removal of the artificial diffusion by UDS+FCT can be seen in Figure 6.4c. The UDS+FCT removed 75% of the error introduced by UDS.

6. Two dimensional advection/diffusion: Siemons (1970), Smith et al. (1973) and Lam (1975) solved the two dimensional advection diffusion equation (terms 1, 2, 5 and 6 in [6.1]) for the initial concentration shown in Figure 6.5a. Figure 6.5b shows the results obtained by Siemon (1970) and Smith et al. (1973). The results of applying SEDTRAN using UDS, UDS+AD and UDS+FCT are shown in Figure 6.6a, b and c. Figure 6.6a shows that UDS does not produce negative concentration but introduces high artificial diffusion ($K_{art} = 9.4 \times 10^4$, $R_e = 4.7$). The UDS+AD removes the artificial diffusion and creates negative values, Figure 6.5b. The UDS+FCT removes the artificial diffusion without creating new maxima, minima or negative values.

Figure 6.7 summarizes the comparison between SEDTRAN and the analytical solutions of the first five verification cases, using different values of currents and diffusivies.

0	0	0	0	0	0	0	0	0
0	0	0	0	250	0	0	0	0
0	0	0	250	500	250	0	0	0
0	0	250	500	750	500	250	0	0
0	250	500	750	1000	750	500	250	0
0	0	250	500	750	500	250	0	0
0	0	0	250	500	250	0	0	0
0	0	0	0	250	0	0	0	0
0	0	0	0	0	0	0	0	0

(a) Initial concentration distribution

Siemons' solution (t= 2500 s)

0	0	0	0	0	0	0	0	-1	-11	0	1	1	1	0	0	0	0	0	0	0
0	-2	2	-3	3	-3	1	1	-4	5	-1	-6	11	11	8	0	-1	0	0	0	0
3	-5	7	9	10	-9	5	3	-14	21	-11	-21	98	169	80	13	-3	-1	0	0	0
2	-3	4	-6	7	-7	5	0	-9	18	-17	32	270	401	293	89	6	-3	0	-0	0
4	-5	7	-9	9	-7	1	5	-8	5	38	209	500	652	531	274	79	5	-3	0	0
1	-3	5	-8	11	-11	5	9	-23	43	165	395	704	843	733	480	217	53	1	-2	0

6	-9	4	-9	12	-10	4	10	-23	32	143	372	680	820	710	454	194	41	-2	-2	0
29	-3	7	-8	9	-7	2	4	-8	11	49	221	512	664	543	267	91	11	-2	0	0
14	0	4	-5	6	-7	5	-0	-10	32	270	400	272	88	6	-4	0	0	0	0	0
24	-1	7	-8	11	-10	6	4	-15	22	-11	-22	95	132	82	12	3	0	0	0	0
8	0	2	-3	3	-2	1	1	-4	5	-1	-6	11	18	8	0	0	0	0	0	0
0	0	0	0	0	0	0	0	0	0	0	1	-1	2	0	0	0	0	0	0	0

Smith' solution (t= 2500 s)

(b) Siemons and Smith solutions

Figure 6.5 Smith and Siemons results (2-D advection/diffusion), Initial concentration distribution (a) and concentration distribution at 2500 sec (b).

0	0	0	0	0	0	0	0	0	0	0	0	0	0	0	0
0	0	0	0	0	0	0	1	1	0	0	0	0	0	0	0
0	0	0	0	0	2	5	9	12	9	3	0	0	0	0	0
0	0	0	1	3	10	27	55	81	82	52	16	0	0	0	0
0	0	1	3	13	38	91	170	242	250	177	76	16	0	0	0
0	0	3	-11	38	100	211	352	462	468	357	199	75	15	0	0
0	1	6	23	71	175	338	521	645	645	520	334	168	61	12	0
0	0	3	11	38	100	211	352	462	468	357	199	75	15	0	0
0	0	1	3	13	38	91	170	242	250	177	76	16	0	0	0
0	0	0	1	3	10	27	55	81	82	52	16	0	0	0	0
0	0	0	0	0	2	5	9	12	9	3	0	0	0	0	0
0	0	0	0	0	0	0	1	1	0	0	0	0	0	0	0
0	0	0	0	0	0	0	0	0	0	0	0	0	0	0	0

(a) SEDTRAN using UDS

-0	0	0	-0	-0	0	-0	0	-0	0	-0	0	0	0	0	0
-0	0	0	-0	-0	0	0	-0	0	-0	0	-0	0	0	0	0
0	0	-0	-0	-0	0	1	1	-0	0	-0	0	-0	0	0	0
0	0	-0	-0	-0	2	9	15	6	-5	1	-0	0	-0	0	0
0	-0	-0	-0	1	14	59	120	115	21	-30	7	-1	0	-0	0
0	-0	-0	0	12	67	201	353	337	122	-23	-19	6	-1	0	-0
-0	-1	-1	9	61	207	443	626	568	319	84	-12	-19	6	-1	0
-0	-1	0	30	152	398	670	820	768	509	242	76	-12	-16	-5	-1
-0	-1	-1	9	61	207	443	626	568	319	84	-12	-19	6	-1	0
0	-0	-0	0	12	67	201	353	337	122	-23	-19	6	-1	0	-0
0	-0	-0	-0	1	14	59	120	115	21	-30	7	-1	0	-0	0
0	0	-0	-0	-0	2	9	15	6	-5	1	-0	0	-0	0	0
0	0	-0	-0	-0	0	1	1	-0	0	-0	0	-0	0	0	0
-0	0	0	-0	-0	0	0	-0	0	-0	0	-0	0	0	0	0
-0	0	0	-0	-0	0	-0	0	-0	0	-0	0	0	0	0	0

(c) ERCH using UDS+AD

0	0	0	0	0	0	0	0	0	0	0	0
0	0	0	0	0	1	0	0	0	0	0	0
0	0	0	0	4	10	11	0	0	0	0	0
0	0	0	3	19	70	102	90	27	0	0	0
0	0	2	14	73	223	316	301	132	0	0	0
0	1	11	60	215	474	569	543	348	69	0	0
0	2	27	145	403	692	765	739	540	239	56	0
0	1	11	60	215	474	569	543	348	69	0	0
0	0	2	14	73	223	316	301	132	0	0	0
0	0	0	3	19	70	102	90	27	0	0	0
0	0	0	0	4	10	11	0	0	0	0	0
0	0	0	0	0	1	0	0	0	0	0	0
0	0	0	0	0	0	0	0	0	0	0	0

(c) ERCH using UDS+FCT

Figure 6.6 SEDTRAN results (2-D advection/diffusion) at 2500 sec. for UDS (a), UDS+AD (b) and UDS+FCT (c).

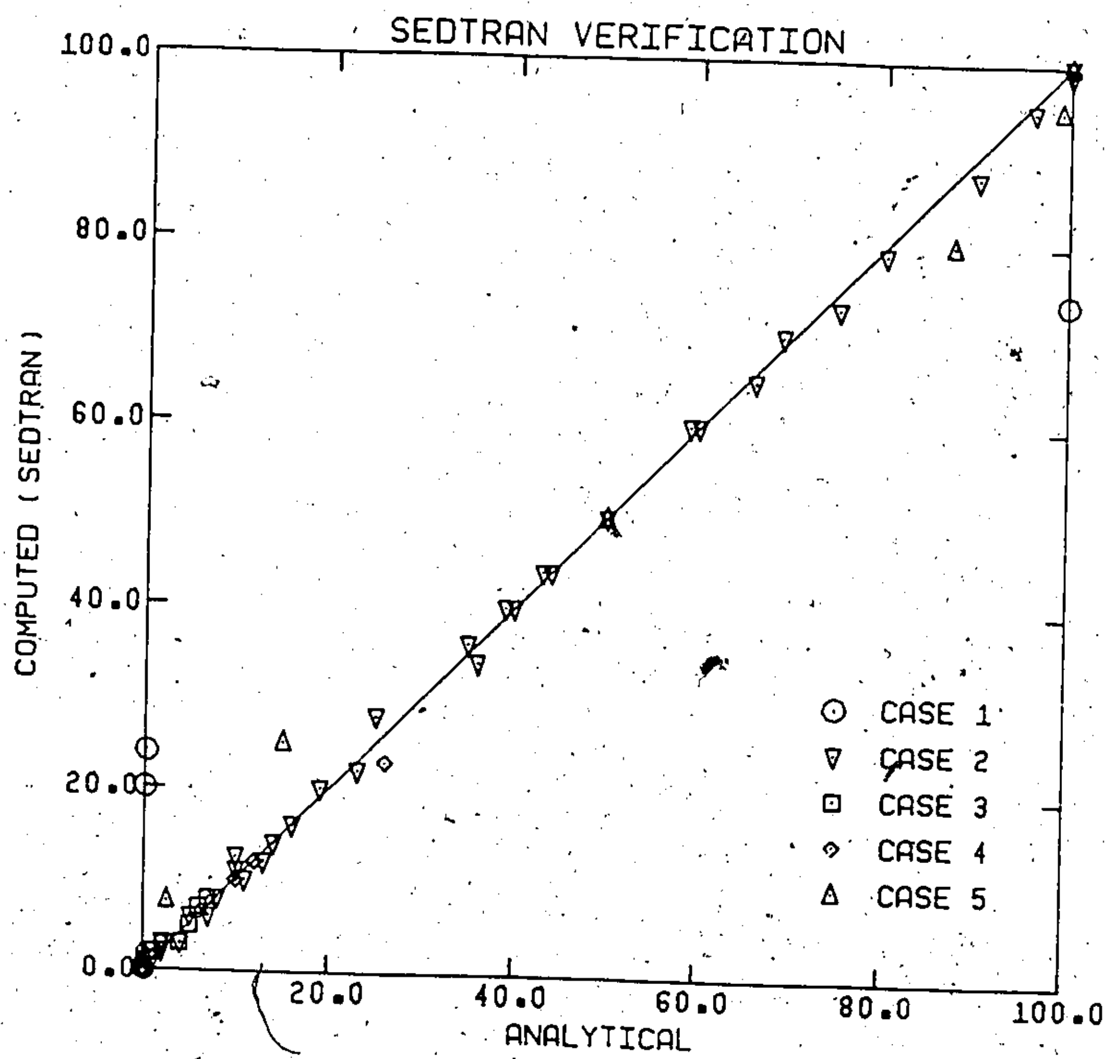

Figure 6.7 Comparison between SEDTRAN and analytical results.

6.4 SEDTRAN SENSITIVITY

In carrying out sensitivity analysis for SEDTRAN, a cross-section similar to the Lake Erie cross-section at Cleveland was used. The following parameters were varied: the three velocity components u, v and w; the diffusion coefficients K_x, K_y and K_z; and the sediment particle size. Table 6.1 summarizes the analysis. SEDTRAN was run for four prototype hours using $\Delta x = \Delta y = 400$ m, $\Delta z = 5$ m and $\Delta t = 300$ sec. The effect of changing the forementioned parameters on the maximum concentration and plume length (LP) parallel to the shoreline and width (WP) perpendicular to the shoreline at each level were studied. The maximum sediment concentration is important for an evaluation of the local effect of the pollutant source. The plume length and width are significant parameters to show the extent of pollution along the shoreline and the sediment penetration across the coastal boundary layer respectively. The initial values and the ranges of variability used in carring out the sensitivity analysis are typical values used in lake modelling.

Figure 6.8 shows the results of changing the shore-parallel and shore-perpendicular components. Figures 6.8a and d show that the maximum concentration at all levels decreases with the increase of u and v and vice-versa. The maximum concentration is highly sensitive to the low velocity range below 10 cm/sec and of low sensitivity to the high range. The plume length is highly sensitive to u and low sensitivity to v (Figures 6.8b and c), while the plume width is highly sensitive to v and of low sensitivity to u (figures 6.8c and f).

Figure 6.9 shows the effect of changing the vertical velocity w

TABLE 6.1 SEDTRAN SENSITIVITY PARAMETERS

Parameter	Initial value	Range of variability min	max
Shore-parallel velocity, u (cm/sec)	25	-12	50
Shore-perpendicular velocity, v (cm/sec)	12	6	25
Vertical velocity, w (cm/sec)	.01	-.06	.05
Shore-parallel diffusivity, K_x (cm^2/sec)	1.5×10^4	1.5×10^3	1.5×10^5
Shore-perpendicular diffusivity, K_y (cm^2/sec)	3.0×10^3	1.0×10^3	1.0×10^4
Vertical diffusivity, K_z (cm^2/sec)	20.0	0.0	100.
Particle size, D_s (mm)	.03	.003	.1

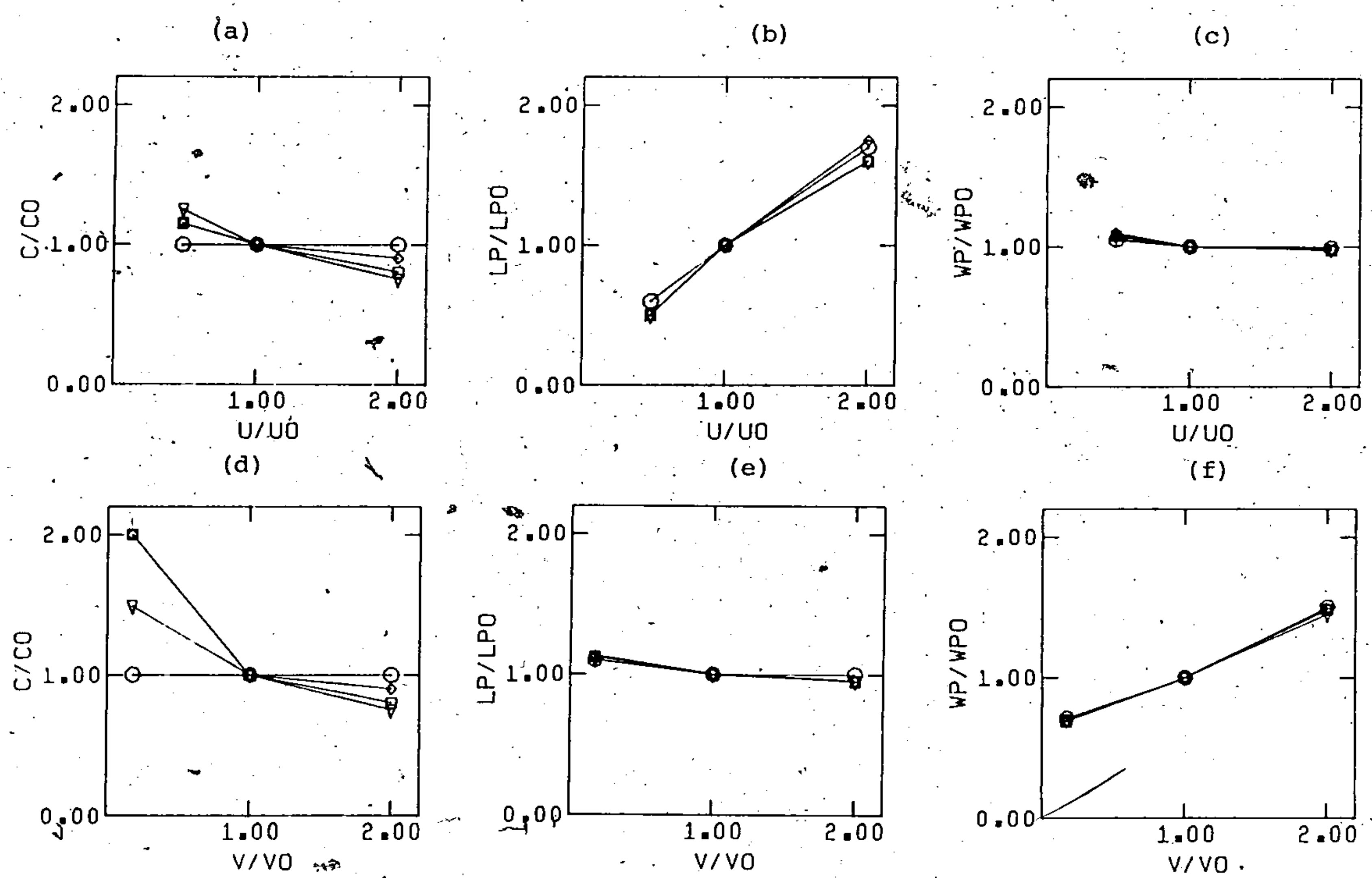

Figure 6.8 SEDTRAN sensitivity analysis.

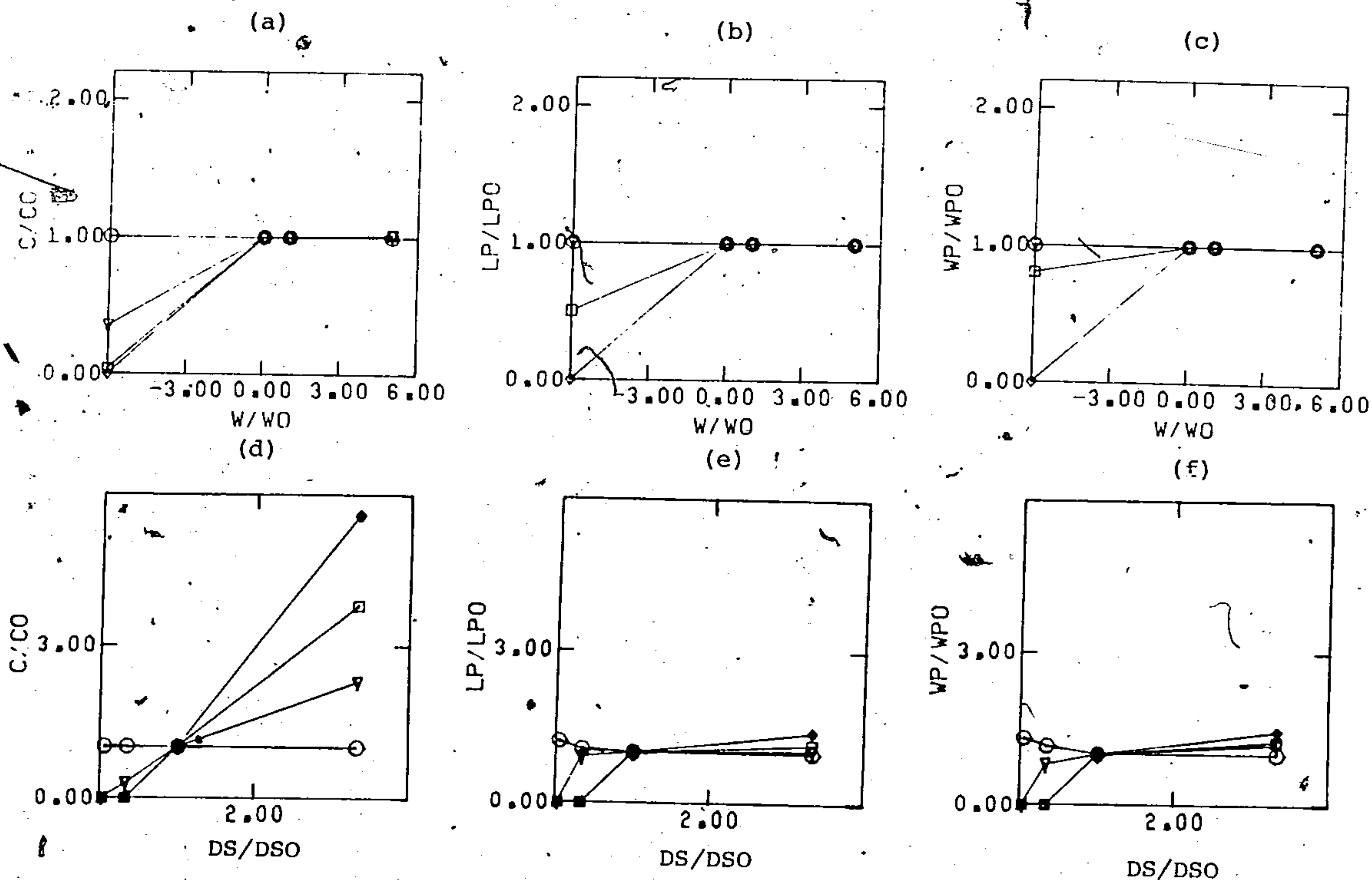

Figure 6.9 SEDTRAN sensitivity analysis.

and the sediment particle size D_s. For negative values of w (downwelling) the maximum concentration and the plume length and width were found to be insensitive, because the vertical flux was highly influenced by the initial value of the fall velocity. For positive values of w (upwelling) the sediment reaching the lower levels decreases dramatically (no sediment reaches the lower level at the end of the simulation time), hence the plume length and width decrease rapidly (Figures 6.9a, b and c).

The maximum concentration and the plume length and width were found to be highly sensitive to the change in the sediment particle size. The fall velocity is proportional to the square of the particle size, hence the vertical flux is highly influenced by the particle size. In Figures 6.9d ,e and f, decreasing the particle size causes a small increase in the plume length and width at the surface and a large increase at lower levels, and vice-versa.

Figure 6.10 shows the effect of changing the horizontal diffusion coefficients K_x and K_y. The plume width and length were found to be of low sensitivity to K_x and K_y respectively (Figures 6.10 c and e). The maximum concentration decreases with the increase ~~of~~ both of K_x and K_y (Figures 6.10a and d). The maximum concentration was found to be of low sensitivity to both of K_x and K_y. The plume width and length increases with the increase of K_x and K_y respectively. The sensitivity of the plume width to K_y is higher than that of the plume length to K_x (Figures 6.10b and f) because the advection dominates the diffusion more in the alongshore direction than the cross-shore direction. It is important to

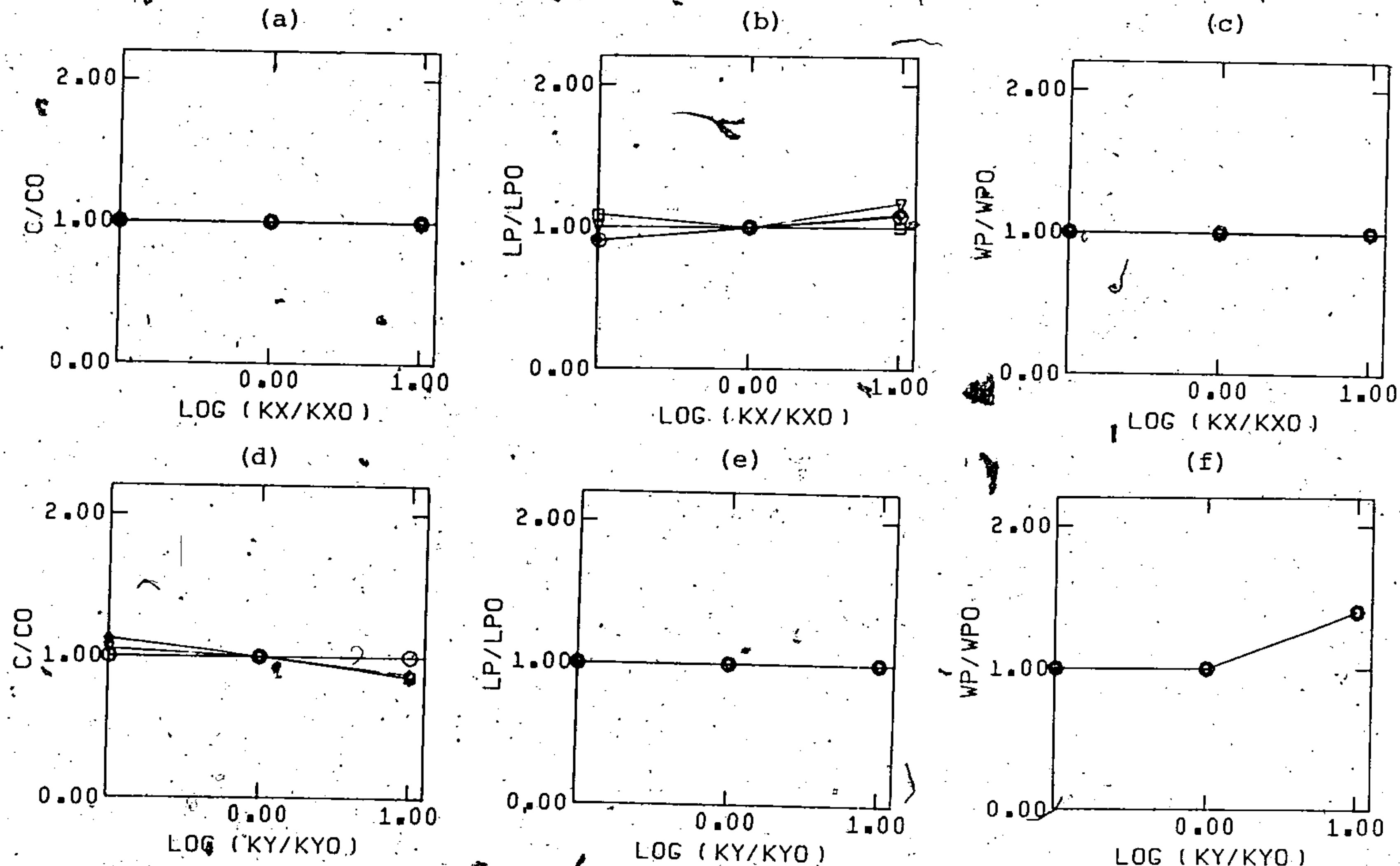

Figure 6.10 SEDTRAN sensitivity analysis.

note that in spite of the low sensitivity of the downstream concentrations (source downstream), the upstream concentrations were highly sensitive where a factor of change (a sensitivity factor) of 8 was observed.

Figure 6.11 shows the effect of the vertical diffusion K_z. The maximum concentration was found to be highly sensitive especially at the lower level where the downward sediment flux increases by the increase of K_z and vice-versa (Figure 6.11a). The plume length and width were found to be sensitive to K_z (Figures 6.11b and c).

6.5 SEDTRAN VALIDATION

Validation implies the comparison of model results to field measurements, to another model known to be accurate or some other adequate criteria to ensure that model productions agree with real data (James, 1978). The most accurate method of validation of a model is the comparison of responses from the verified model with corresponding field measurements. Calibration of empirical parameters to achieve proper results may be necessary in some cases. No complete data and observations existed in the coastal zone of Lake Erie in the vicinity of Cleveland for 1979. Several attempts were carried out to validate SEDTRAN.

6.5.1 Dye experiment

The first attempt was to generate a dye patch similar to that observed in Lake Ontario for the period June 27-29, 1972, (Murthy, 1976). Figure 6.12a shows the dye concentrations observed 7 hours and 26 hours

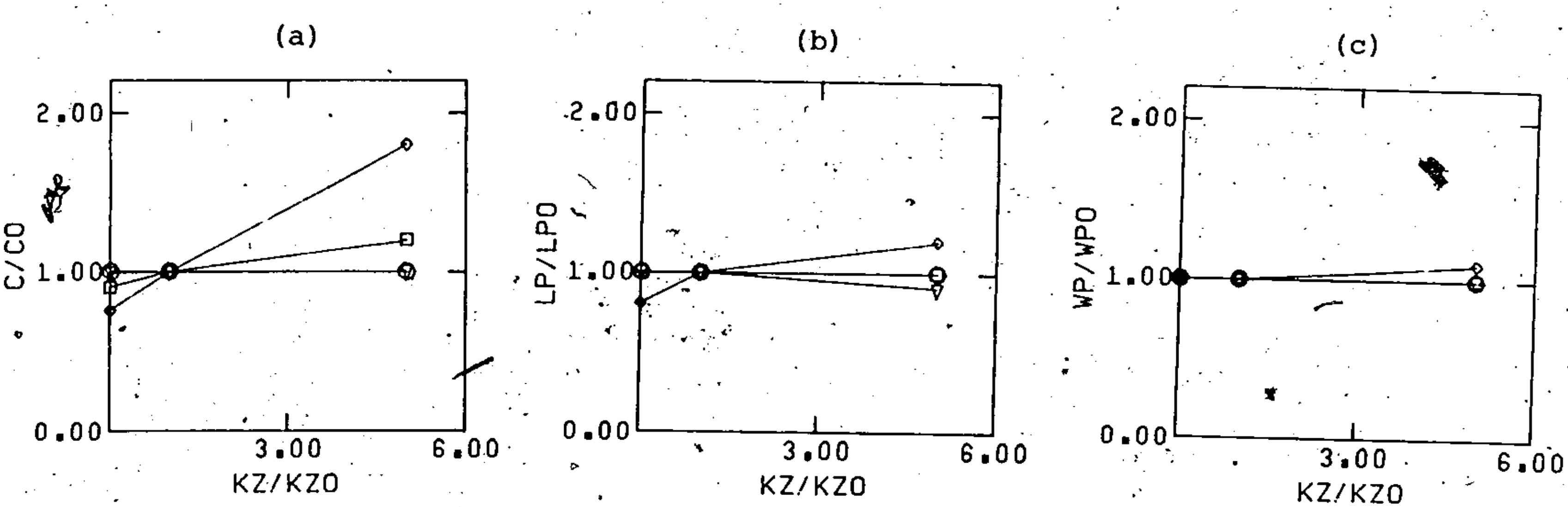

Figure 6.11 SEDTRAN sensitivity analysis.

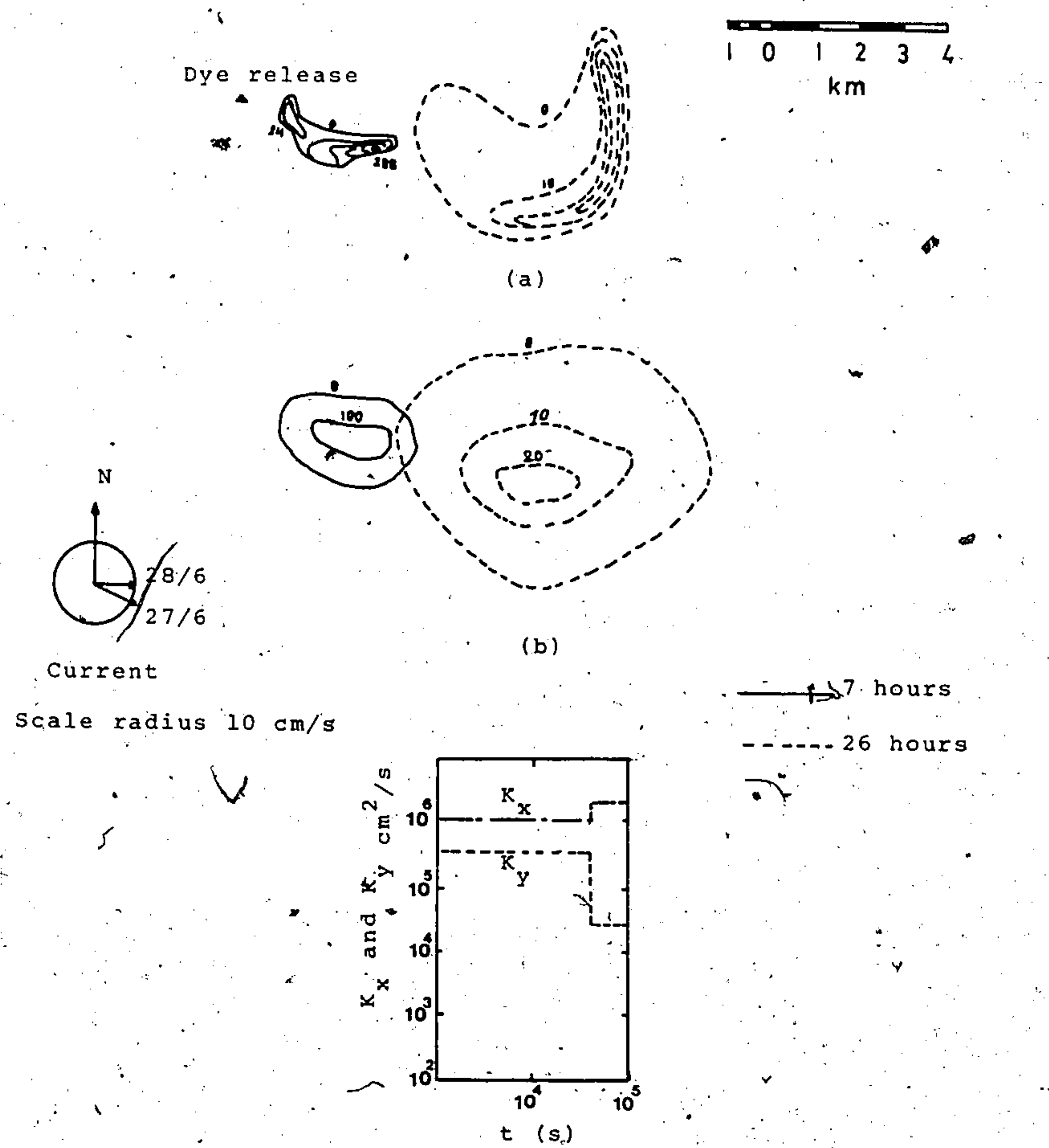

Figure 6.12 SEDTRAN validation: (a) observed dye plume (Murthy, 1976), (b) SEDTRAN results (UDS) and (c) diffusion diagram (UDS)

after dye release and the corresponding current vectors. To demonstrate (1) the effect of artificial diffusion in the case of a patch, and (2) the effect of the variability of the diffusion coefficient with time, SEDTRAN was run using UDS and UDS+FCT with constant $K_x = K_y = 2\times10^4$ cm^2/sec and UDS+FCT with both of K_x and K_y as functions of diffusion time. The results are given in Figures 6.12 and 6.13. Due to the high artificial diffusion introduced by UDS, the results show that the patch dimensions (length and width) are much larger than those observed and the concentrations are less than those observed as shown in Figures 6.12a and b. The effective diffusion coefficients are plotted in Figure 6.12c. The observed clockwise curvatures from the leading edge to the trailing edge and the higher concentrations in the leading edge, Figure 6.12a, are due to the vertical structure of the horizontal current (vertical current shear in the mean flow, wind-induced Ekman transport). Okubo (1971) and Murthy (1973) provide more details. The vertical structure of the current and it's variability with time were not available to input to SEDTRAN, therefore the actual patch shape is not expected to be properly generated by SEDTRAN. Figure 6.13a shows the results obtained by using UDS+FCT with constant $K_x = K_y = 2\times10^4$ cm^2/sec. The decrease in the patch dimensions and the increase in the concentrations due to the antidiffusion stage can be observed. The results obtained by Lam (1976), using UDS+FCT to simulate the actual plume are plotted in Figure 6.13b for 7 and 26 hours. It can be seen that SEDTRAN results are very close to Lam's results.

To demonstrate the effect of using variable diffusion coefficient,

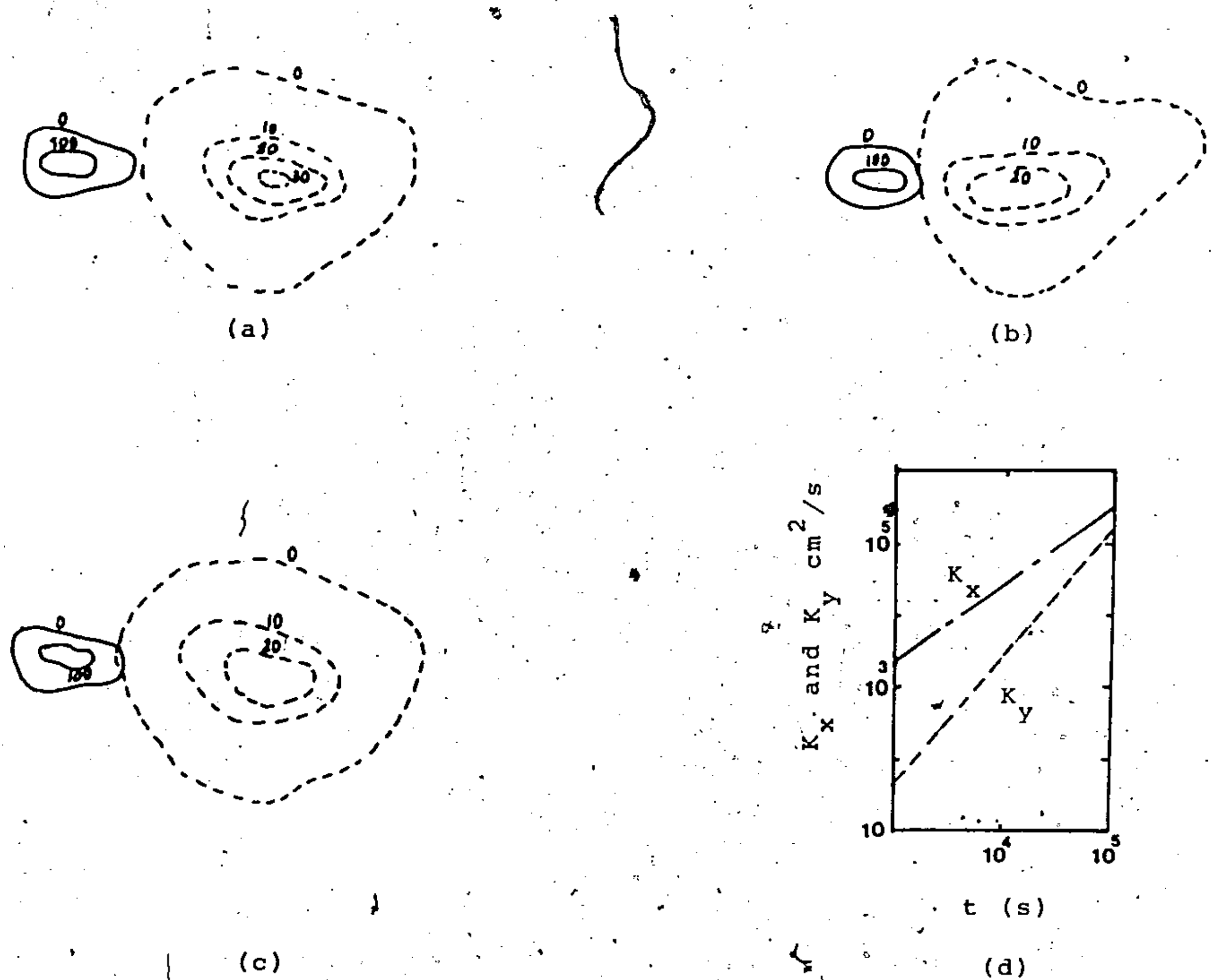

Figure 6.13 SEDTRAN validation: (a) SEDTRAN results (UDS+FCT), (b) computed dye plume (Lâm, 1976), (c) SEDTRAN results (UDS+FCT and time variable diffusivities) and (d) diffusion diagram (time variable diffusion coefficients)

the diffusion relations calculated from the actual patch concentrations (Murthy, 1976) were used. The diffusivities were converted to functions of time as follows:

$$K_x = 0.69\ t^{1.15}$$

$$K_y = 4.6 \times 10^{-4}\ t^{1.7} \qquad [6.18]$$

where t is the diffusion time. The diffusion diagram for K_x and K_y are plotted in Figure 6.13c. Figure 6.13d shows the results obtained using UDS+FCT with variable diffusivities in accordance with [6.18]. The concentrations at 7 hours in the case of variable diffusivities were less than those of constant diffusivities as shown in Figure 6.13c, while the concentrations were higher at 26 hours. In the case of variable diffusivities, K_x and K_y were lower than those of the constant diffusivities case before about 2 and 12 hours respectively, and higher after that.

6.5.2 Suspended solids

To the author's knowledge, the only suspended sediment concentrations (SSC) available in the vicinity of the Cleveland coastal zone for 1979 are the data collected by Heidelberg College Water Quality Laboratory (HCWQL), and reported by Richards (1981). During 1978 and 1979 HCWQL conducted a sampling program at different sites in the nearshore portion of Lake Erie, one of which was near Cleveland as shown in Figure 6.14. Water samples were taken at 1 m below surface and 1 m above bottom, but all SSC bottom samples were unsuccessful. During 1979

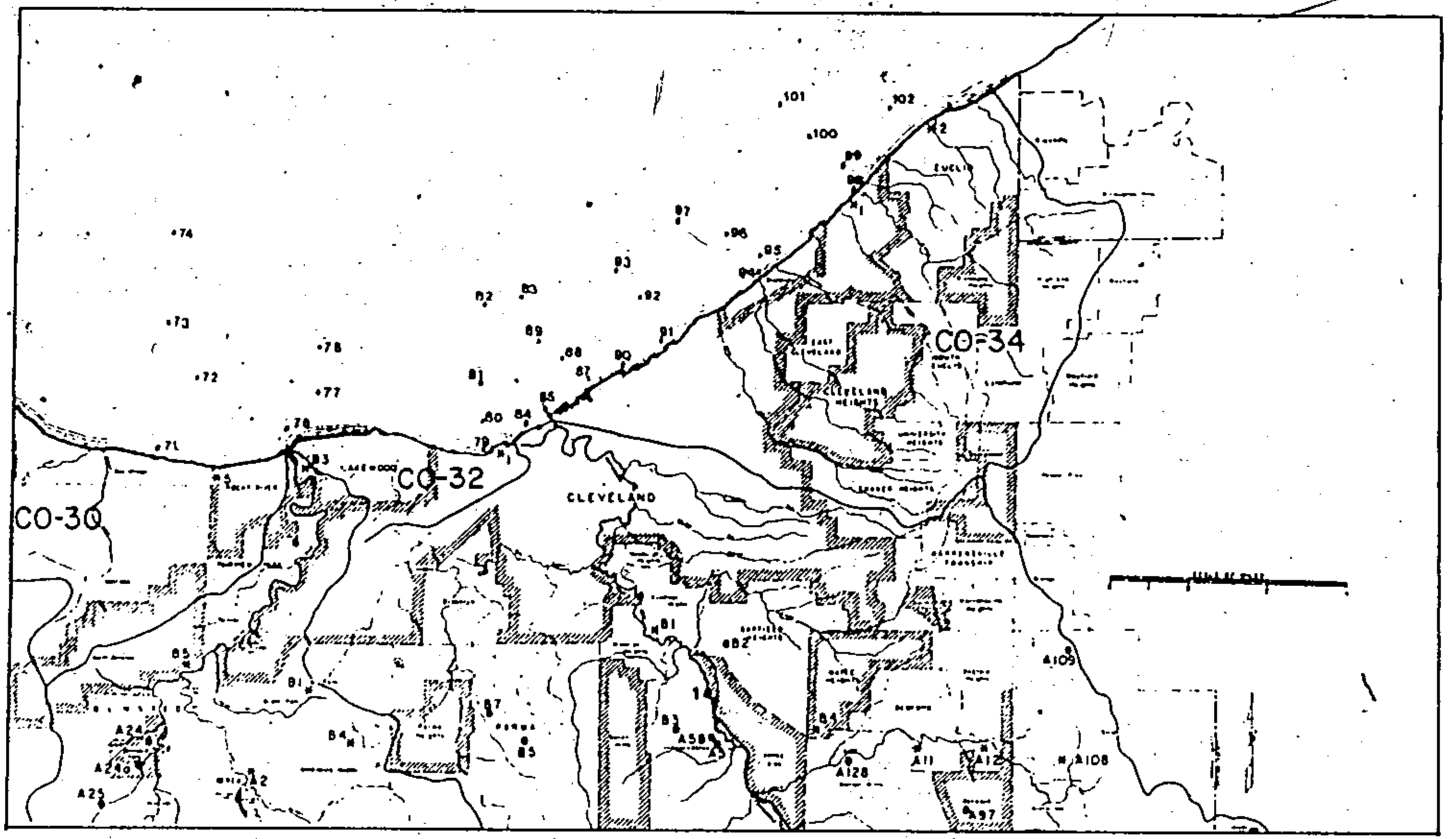

Figure 6.14 HCWQL sampling stations.

each station was to be sampled on each of four cruises. During each cruise, each station was to be sampled on three successive days. Table 6.2 summarizes all the available SSC data including the time of sampling for each station during the summer period.

The second data set which is relevant to this study is the daily average discharge and SSC published by the USGS (Water Data Report OH-79-2). The daily average discharge and SSC at several streams tributary to Lake Erie were reported for the period October, 1978 to September, 1979. Cuyahoga river which flows through Cleveland was one of the streams sampled. Sampling station 1, shown in Figure 6.14, was about 12 km upstream of the river mouth. The suspended sediment grain size distribution was reported only for one day (August 28, 1979). The daily average discharge and SSC for the four days mentioned earlier (Table 6.2) are summarized in Table 6.3.

The sediment data required to generate the sediment plume by SEDTRAN are the source location, SSC and sediment grain size distribution. The source location was assumed to be at the Cleveland harbour entrance station, about 1 km offshore (station 86). Because all the available measurements were taken at 1 m below the surface, the single point source is assumed to be located at the water surface. The effects of changing the source location and using more than one source are discussed later in this chapter. The source SSC is available (Table 6.2) for July 17 and August 24 1979. For the rest of the study period, the source SSC had to be estimated using the available data. Out of four measurements (April 17, July 17, August 24 and October 8, 1979) the observed SSC at the harbor entrance (station 86) was less than that of

Table 6.2: HCWQL suspended sediment data summary

Station	July 17, 1979		July 20, 1979		Aug. 24, 1979		Aug. 27, 1979	
Number	SSC mg/l	time	SSC mg/l	time	SSC mg/l	time	SSC mg/l	time
70	-1	-1	2.0	9:57	-1	-1	7.5	9:32
71	-1	-1	2.4	9:25	-1	-1	5.6	9:08
72	-1	-1	-1	-1	-1	-1	1.7	11:23
73	-1	-1	1.3	11:27	-1	-1	1.5	11:00
74	-1	-1	1.6	10:55	-1	-1	1.3	10:34
75	-1	-1	14.0	8:35	-1	-1	22.1	8:53
76	-1	-1	-1	-1	-1	-1	4.7	11:58
77	-1	-1	-1	-1	-1	-1	1.9	12:41
78	-1	-1	1.7	13:08	-1	-1	1.8	12:57
79	-1	-1	4.1	8:08	-1	-1	6.5	8:31
80	-1	-1	2.6	13:40	-1	-1	3.2	13:44
81	-1	-1	2.9	14:03	-1	-1	3.8	14:03
82	-1	-1	1.4	15:54	-1	-1	1.3	14:58
83	-1	-1	1.9	14:28	-1	-1	3.4	14:28
84	9.4	15:20	-1	-1	8.7	15:25	-1	-1
85	8.9	15:06	-1	-1	14.4	15:11	-1	-1
86	5.0	15:36	-1	-1	9.8	15:00	-1	-1
87	5.2	14:45	-1	-1	7.4	14:25	-1	-1
88	-1	-1	1.1	15:20	-1	-1	2.2	15:20
89	-1	-1	2.1	14:15	-1	-1	3.8	14:12
90	4.0	14:26	-1	-1	7.0	14:09	-1	-1
91	4.4	14:12	-1	-1	5.3	13:54	-1	-1

Table 6.2 continued

92	1.5	13:55	-1	-1	3.1	13:33	-1	-1
93	1.1	13:37	-1	-1	2.2	13:20	-1	-1
95	5.1	13:04	-1	-1	3.1	11:47	-1	-1
96	1.2	12:35	-1	-1	2.5	12:37	-1	-1
97	1.1	12:52	-1	-1	2.1	12:55	-1	-1
98	21.9	9:12	-1	-1	3.8	9:00	-1	-1
99	1.5	9:36	-1	-1	2.5	9:43	-1	-1
100	1.2	9:55	-1	-1	2.0	10.01	-1	-1
101	1.1	11:15	-1	-1	1.5	10:26	-1	-1
102	1.4	10:20	-1	-1	2.2	10:05	-1	-1

-1 no sample

Table 6.3: U.S. Geological Survey Water Data

Day, 1979	July 17	July 20	Aug. 24	Aug. 27
Daily average flow, cfs	370	242	1210	613
Daily average SSC, mg/l	17	16	267	36

the river mouth (station 85) by a factor of 2.

Relating the river mouth SSC to that of the river station (station 1) was a difficult task. Station 1 SSC were daily averages while that of station 86 was instantaneous. Relating the ratio between the instantaneous and the daily average concentrations to the daily average discharge is difficult due to the very small number of available measurements (the previously mentioned dates except October 8, 1979) and the erratic variability (Tables 6.2 and 6.3). Station 1 was located relatively close to the river mouth where about 10% of the total drainage area load was not measured, hence the sediment load is expected to increase. Toward the river mouth the velocity and the turbulence are expected to decrease due to the flat river slopes and the lake backwater effect. Hence the transport capacity and SSC are expected to decrease. In this study, in the absence of better information, the daily average SSC at Station 86 is assumed to be equal to that of Station 1. Based on the above discussion the source SSC is assumed to be constant for each non-sampled day and equal to 50% of that measured at Station 1. To obtain better estimates of the source SSC, a river hydrograph and pollutograph routing with sediment resuspension and deposition model would be required, which is beyond the scope of this study. For more detail refer to James and Elzawahry (1981).

For the lake sediment, size is the property that varies greatly. It has been shown in the SEDTRAN sensitivity analysis that the sediment particle size is the most critical parameter (Figure 6.9). The sediment grain size distribution was not available for any station sampled by

HCWQL. Based on the above discussion , the surficial sediment measurements of Lake Erie (Thomas et al., 1976 and Richards, 1981) and Cuyahoga river grain size distribution, given in Figure 6.15 was used in this study. The grain size distribution has about 40% clay, 40% fine silt and 20% medium silt.

To generate the sediment plume emanating from Cleveland for each of the four days (Table 6.2), ERCH and SEDTRAN were run. In each case ERCH was run for two consecutive days, one day before the day of simulation to remove the effect of the initial condition (state of rest), and the day of simulation. The same input parameters used to run ERCH (Chapter 5) were used except for the wind corresponding to each day. In running ERCH, a numerical time step of 15 minutes and an hourly average wind speed and direction were used. The currents were printed out every 6 hours and stored to be used for input to SEDTRAN.

Figure 6.16 shows the currents calculated by ERCH at 12:00 hours on July 17, 1979. Figure 6.16a is a plot of the contour lines of v, and shows a north-western near surface flow accompanied by return flow at about 8 m depth. Figure 6.16b presents the same plot as Figure 6.16a but for u, close to the shore, the entire layer was moving toward the south-west. Moving offshore a flow return at about 8 m depth was observed. Figure 6.16c shows a vertical upward nearshore current, about three orders of magnitude less than the horizontal current. Figure 6.16 presents a typical case of upwelling. Figure 6.17 shows the results obtained by SEDTRAN at 18:00 hours of July 17, using the currents at Figure 6.16. SEDTRAN was run using $\Delta x = \Delta y = 500$ m, $\Delta z = 2.5$ m, and $\Delta t =$ 300 sec. The values of K_z were obtained using [6.3] while K_x and K_y were

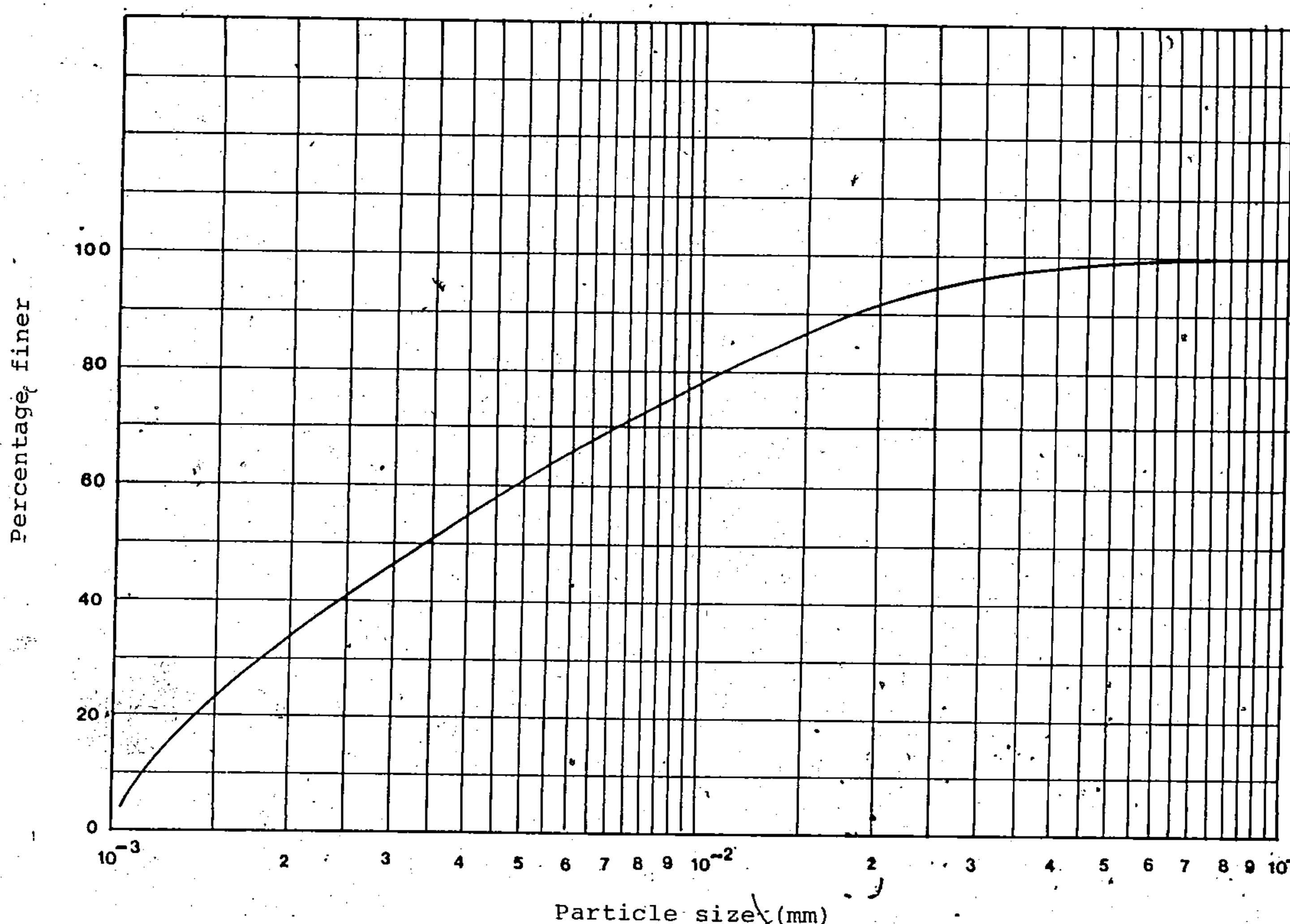

Figure 6.15 Sediment grain size distribution.

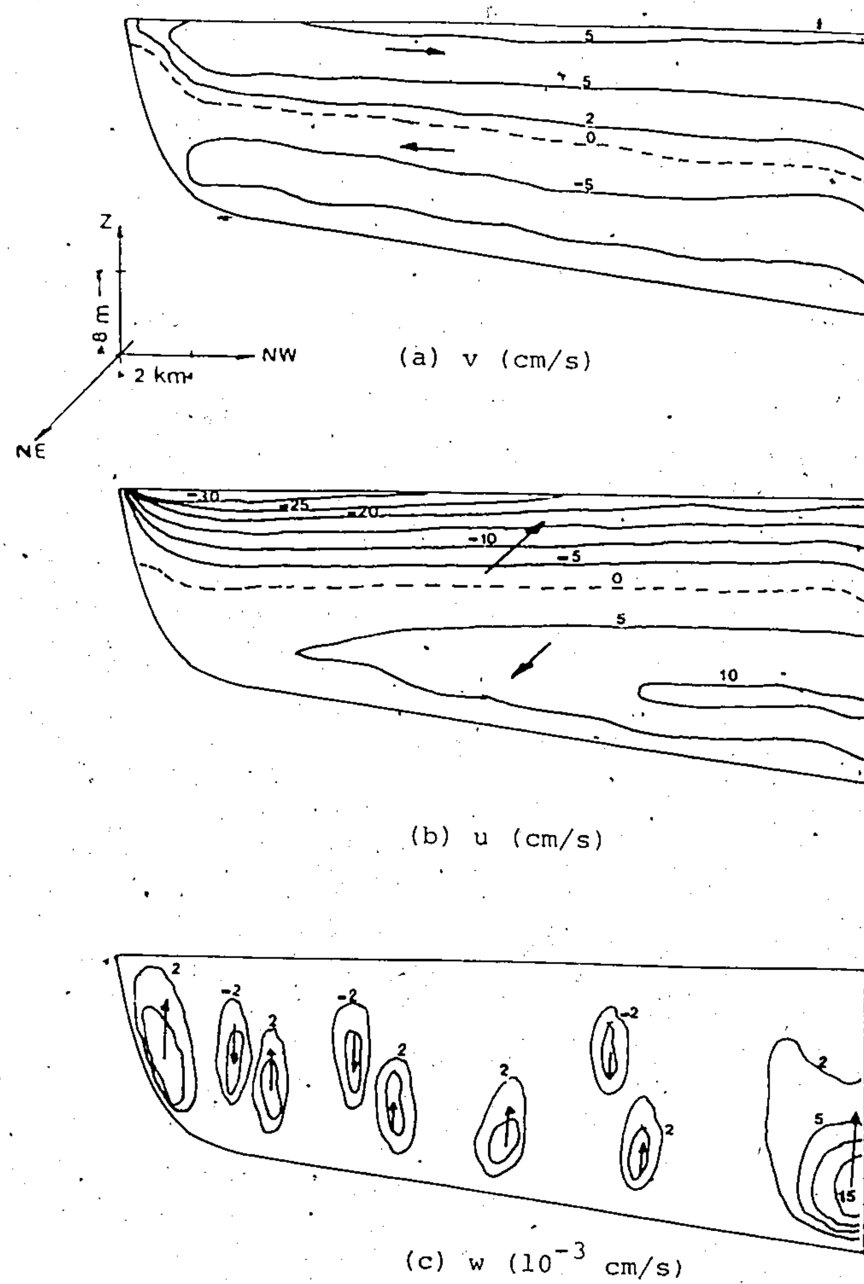

Figure 6.16 Computed flow profiles at 12:00 hours on July 17, 1979.

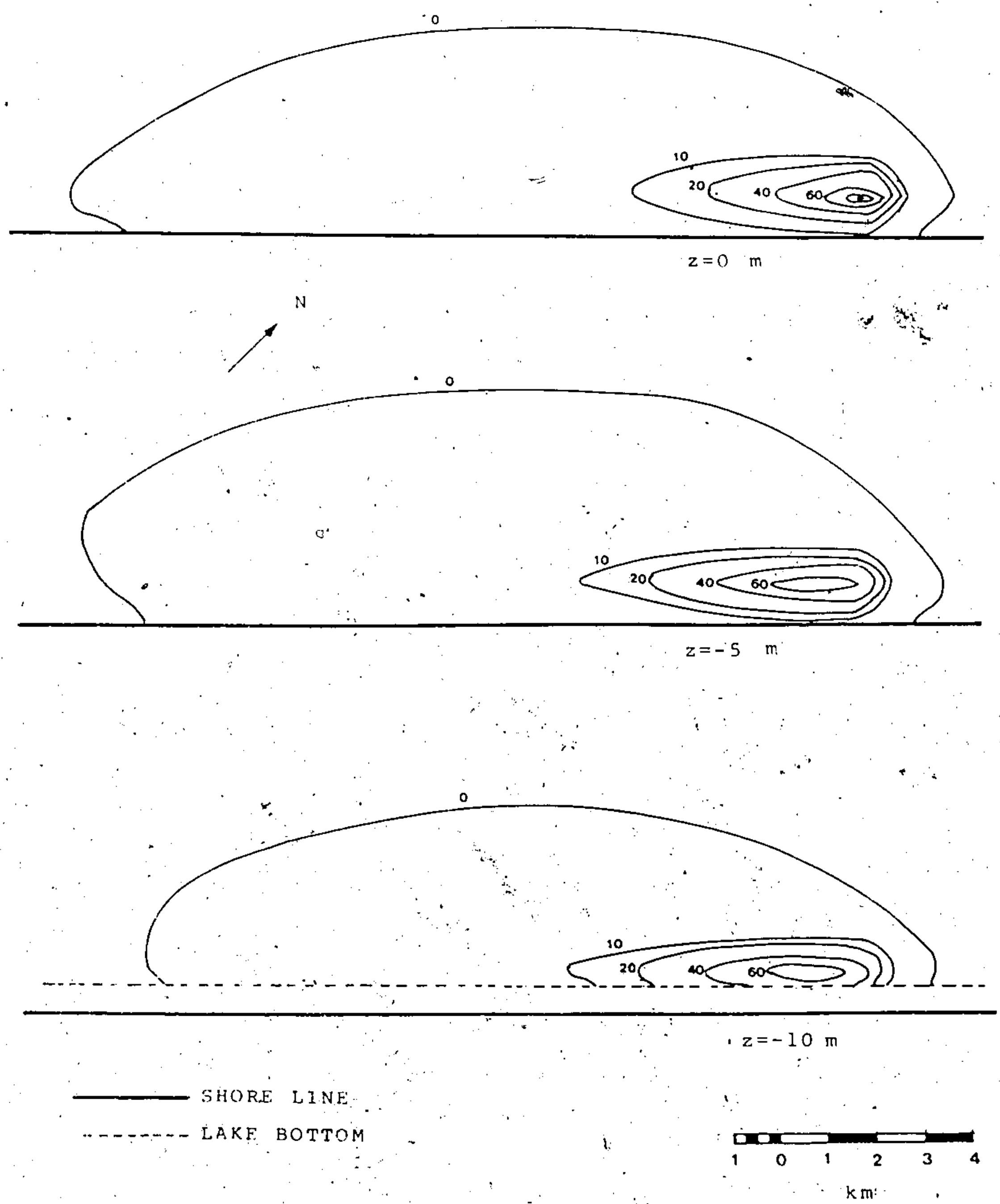

Figure 6.17 Computed SSC plume at 18:00 hours on July 17, 1979, point source at 1 km offshore and particle size of 0.02 mm.

assumed to be constants of $2x10^4$ and $5x10^3$ cm^3/sec respectively (Table 4.5). The fall velocity was obtained from [6.2] or Figure 6.1 , using the grain size distribution in Figure 6.15.

In the case of a plume in non-uniform flow such as Figure 6.16, the definition of the diffusion time [6.18] is difficult. Defining the diffusion time as the traveling time, in the case of a steady state plume, implies one fixed diffusion coefficient value for each time. This is only accurate at a distance from source equal to the product of the travelling time and the velocity. The other alternative is to use the diffusion coefficient as a function of a length scale or standard deviation of concentrations according to [4.10]. This procedure requires iterative techniques to keep consistency in the prediction of C and the definition of the diffusion coefficient. To obtain the value of the standard deviation: (1) the three dimensional flow pattern must be obtained; (2) tangents and perpendiculars along the stream lines are drawn; (3) using an interpolation scheme the concentrations are obtained at several points along the tangents and the perpendiculars; (4) the standard deviations are calculated ; (5) longitudinal and lateral diffusivities are obtained using the diffusion relations; (6) the values of K_x, K_y and K_z are obtained using the diffusion matrix; and (7) the values of K_x, K_y and K_z are obtained on the original grid using the interpolation scheme. This procedure is repeated in iteratively for each point at each time step. For more discussion refer to Lam et al. (1984). Use of this technique in SEDTRAN proved to be extremely complicated and expensive.

Figure 6.17 shows the horizontal lines of equal SSC relative to a source concentration 100 mg/l at different water depths. The plume was directed toward the south-west at all depths occupying a relatively narrow width. The zero concentration is equivalent to concentrations less than 0.1 mg/l. At the surface, the plume extended about 17 km and 4 km along and across the shore respectively. The plume length, width and concentration decreases with depth. The concentrations larger than 10% of the source concentration extended only to about 6 km and 1.8 km along and across the shore respectively. Most of the concentrations observed by HCQWL in July 17 (Table 6.2) were between 12 hours and 18 hours. Stations 84, 86, 87, 90 and 91 were excluded because they were located in theharbor. Figure 6.14 shows the four main sampled sources located at stations 75, 86, 94 and 98. There are also some other small unsampled creeks. The distance between stations 86 and 94 is about 10 km. Because the flow is assumed not to vary within such distance, ERCH would produce a similar plume to that of Figure 6.17 from station 94. Figure 6.17 shows that between 0% to 3% of station 94 concentration may be added to station 86 plume concentrations, while 0% to 6% of station 98 concentration may be added to station 94 plume concentrations. The concentration ratios between stations 94 - 95, 94 - 96, 98 - 99 and 98 - 100 were about 21%, 5%, 7% and 5% respectively, while the computed concentration ratios at similar distances from station 86 were about 24%, 3%, 8% and 0%.

Figure 6.18 shows the flow profiles at 18:00 hours on July 17, 1979. Figure 6.18a shows strong near-surface offshore flow accompanied by a broad return flow at about 5m depth. Figure 6.18b shows that close

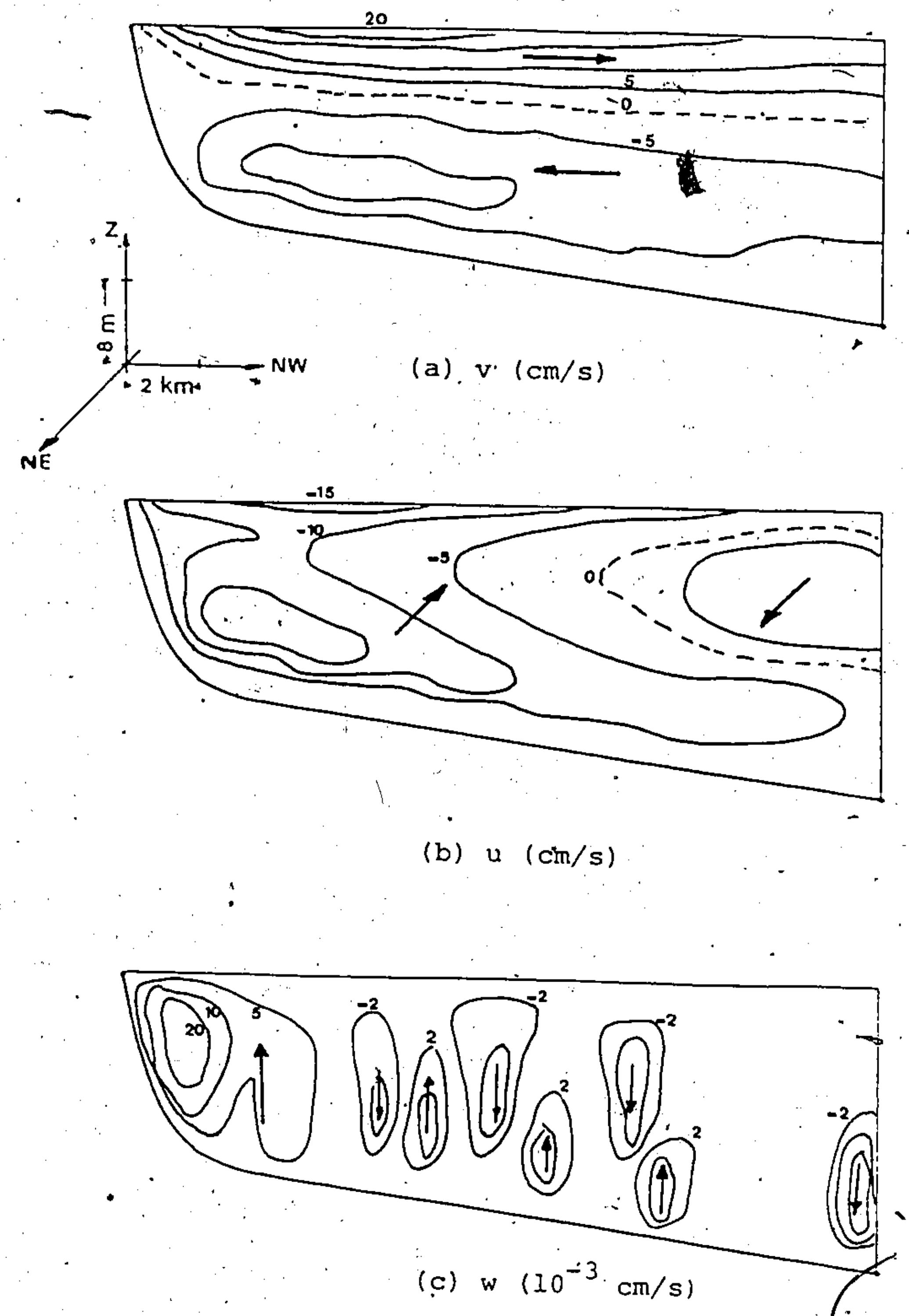

Figure 6.18 Computed flow profiles at 18:00 hours on July 17, 1979.

to the shore the entire layer was moving toward the south-west with relatively weak current, while far from shore a return flow can be observed. The plume computed at 0.00 hours on July 18, 1979 is shown in Figure 6.19. Due to the strong near-surface offshore component and the relatively weak shore-parallel current, the plume at the surface was almost offshore. The plume extended to about 12 km and 11 km along and across the shore respectively. Due to the effect of the onshore component at lower levels the plume was elongated in the alongshore direction occupying a relatively narrow width. This case presents a case of maximum penetration across the coastal zone.

Figure 6.20 shows the flow profiles at 12:00 hours on July 20, 1979. Figure 6.20a shows an almost zero shore-perpendicular component everywhere. Figure 6.20b shows that a weak near-surface north-western current was accompanied with return flow at about 2 m depth. Figure 6.20 represents a weak current event. Figure 6.21 shows how the plume at 18:00 hours on July 20 was slightly directed to the north-east at all depths. The plume covered about 6 km by 4 km along and across the shore respectively. The concentration ratios between stations 86 - 88 and 75 - 78 were about 14% and 12% respectively while those computed at similar distances from station 86 were about 8% and 0%.

Figure 6.22 shows the flow profiles at 12:00 hours on August 24. Figure 6.22a shows that onshore near-surface flow was accompanied by return flow at about 8 m depth. Figure 6.22b shows that the entire layer was moving to the north-east close to the shore with return flow at the intermediate range of the water column far from shore (about 10 km). The

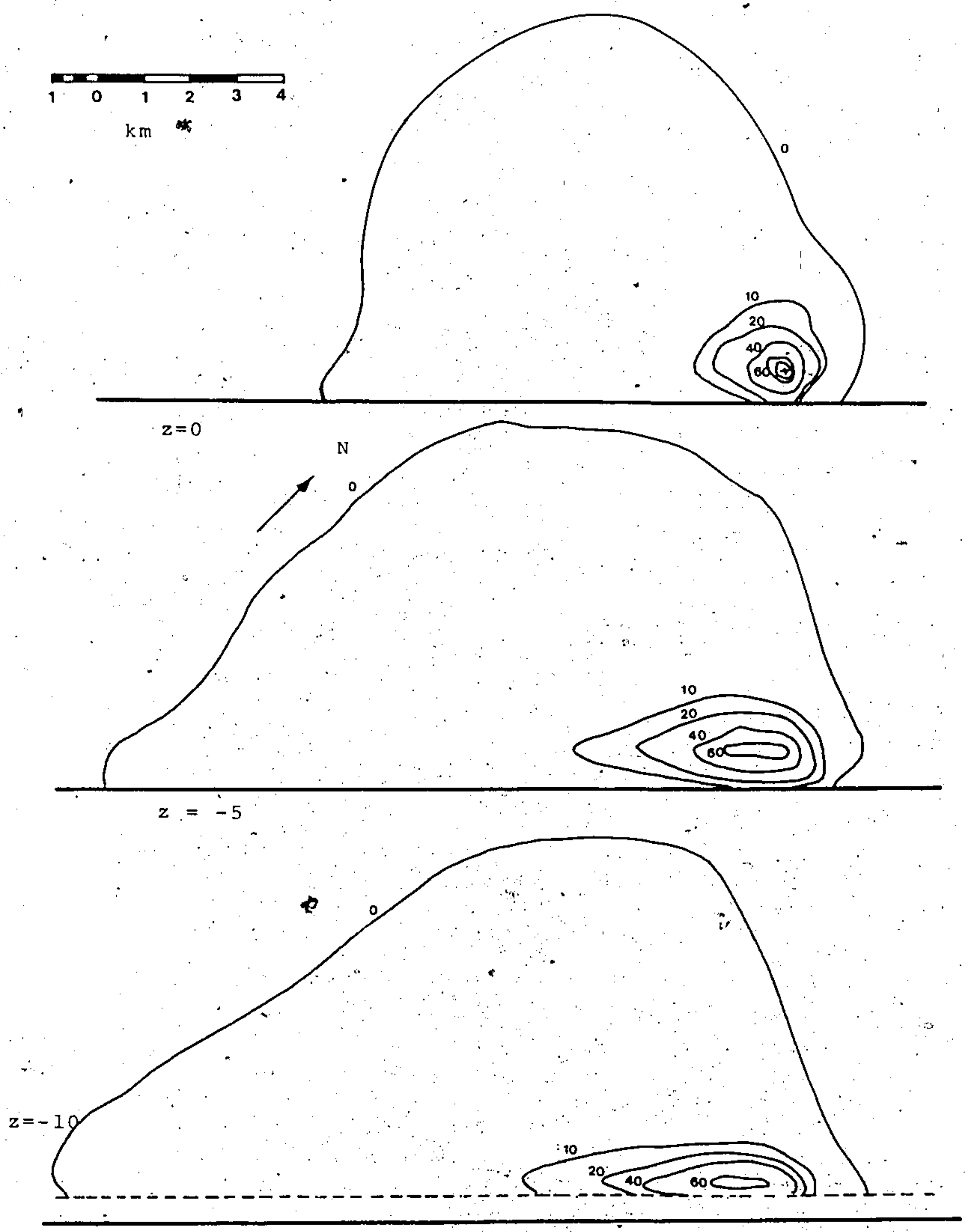

Figure 6.19 Computed SSC plume at 00:00 hours on July 18, 1979, point source at 1 km offshore and particle size of 0.02 mm.

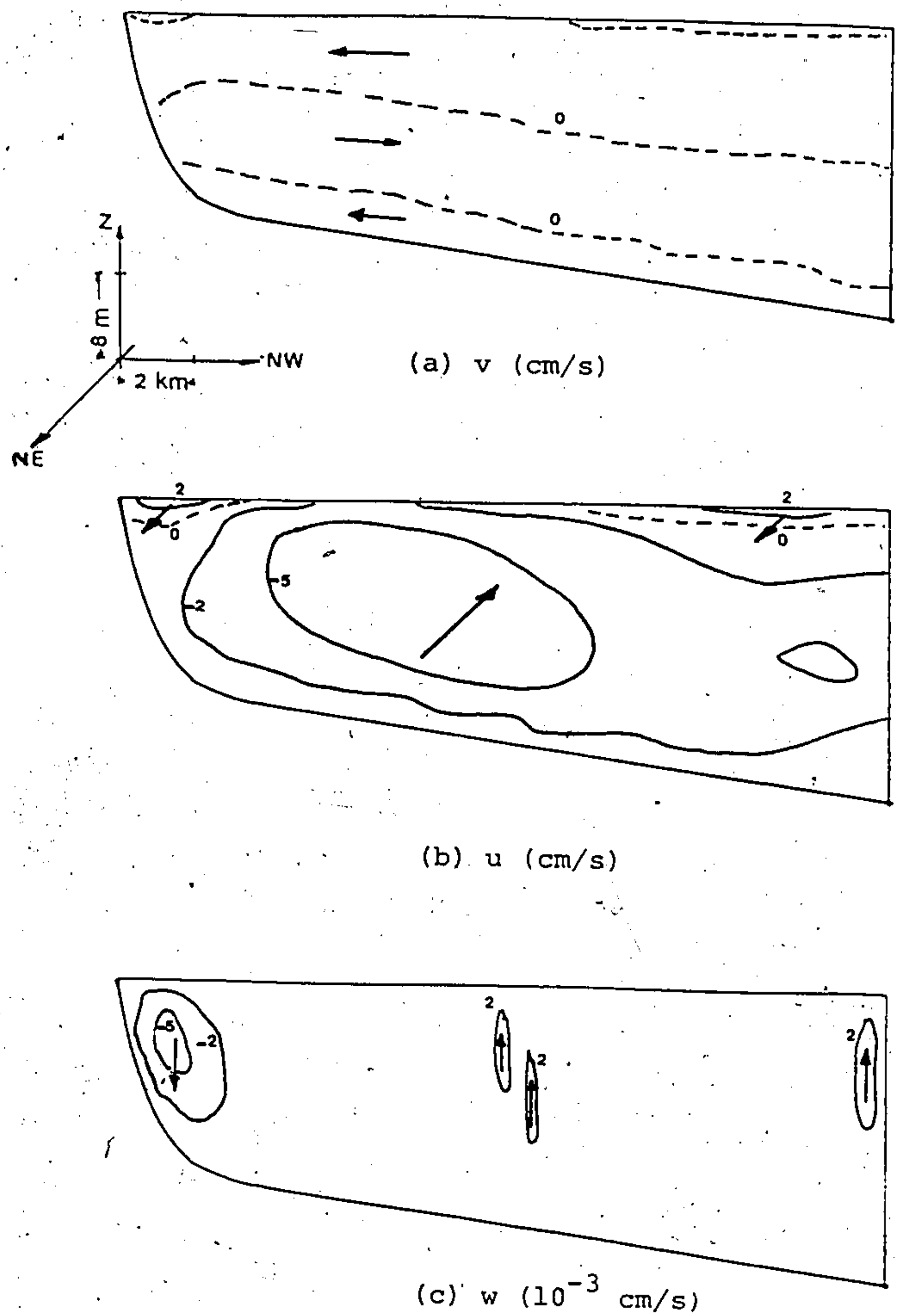

Figure 6.20 Computed flow profiles at 12:00 hours on July 20, 1979.

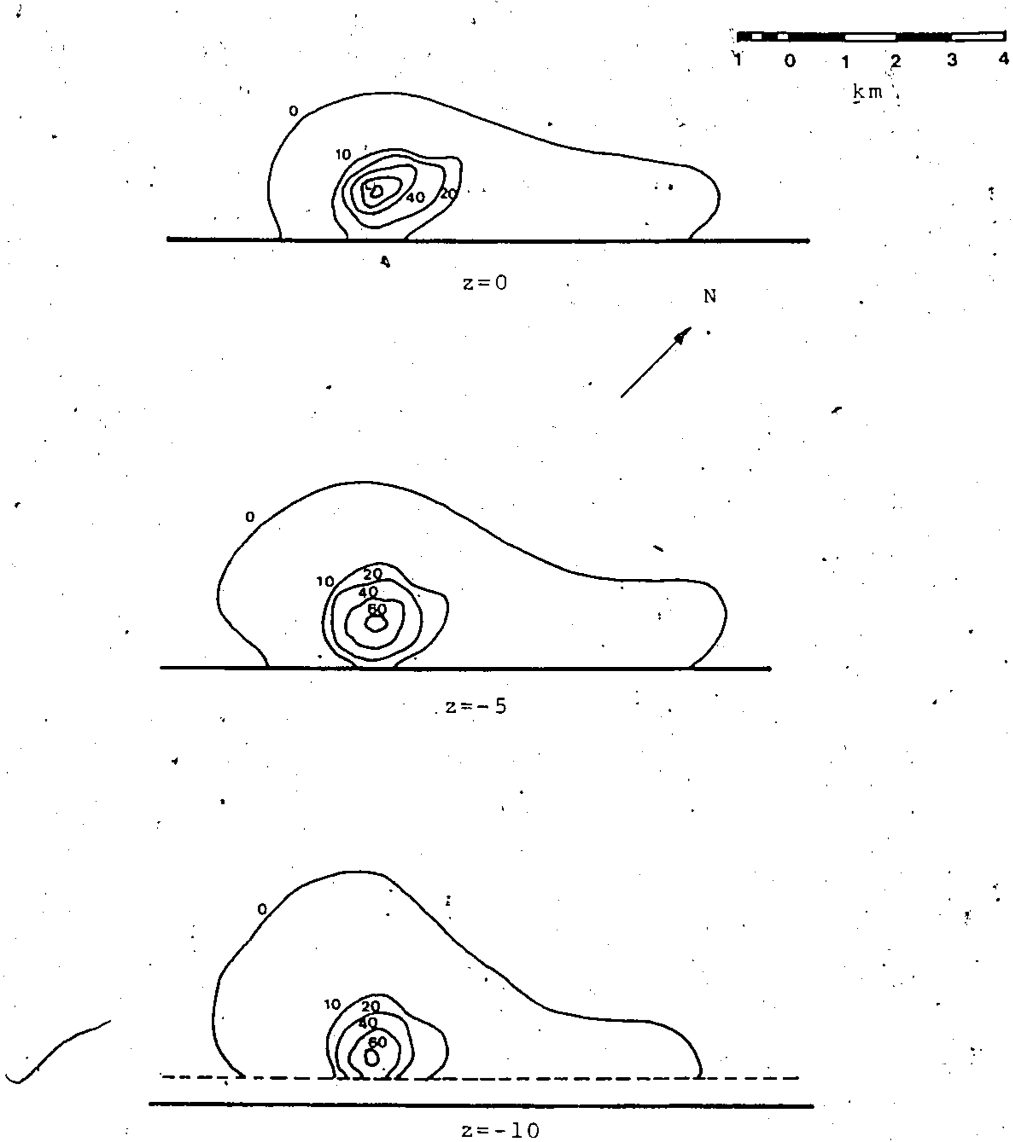

Figure 6.21 Computed SSC plume at 18:00 hours on July 20, 1979, point source at 1 km offshore and particle size of 0.02 mm.

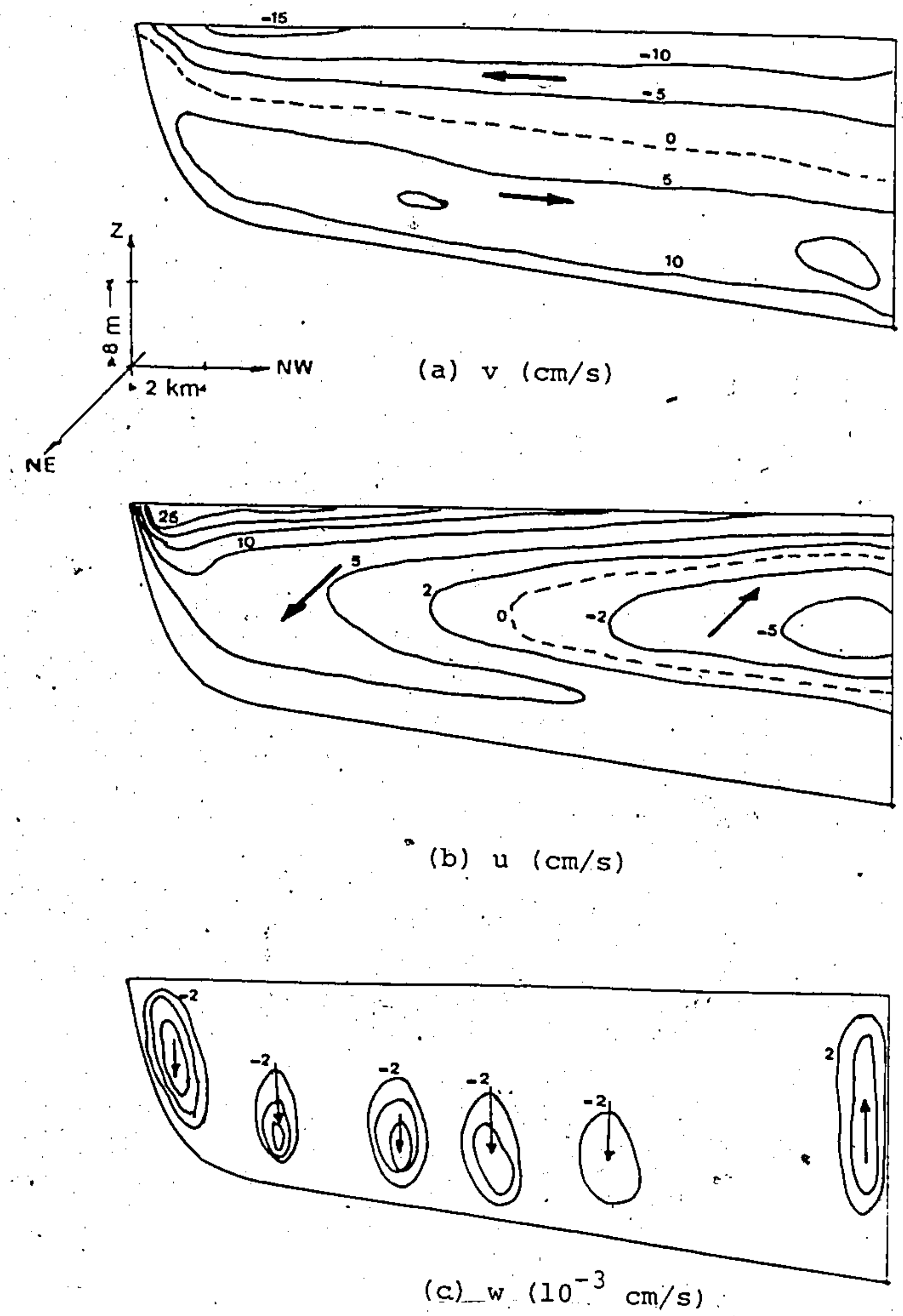

Figure 6.22 Computed flow profiles at 12:00 hours on August 17, 1979.

sediment plume at 18:00 hours on the same day is plotted in Figure 6.23. The plume was directed toward north-east. The plume occupied a narrow width at the surface and was wider at depth due to the near-surface onshore flow and the return flow at depth respectively. The concentration ratios between stations 92 - 86 and 95 - 94 were about 32% and 20%, while the corresponding computed concentration ratios were about 2% and 18%.

Figure 6.24 shows the flow profiles at 12:00 hours on August 27, 1979. Figure 6.24a shows an offshore near-surface component with flow return at about 5 m depth. Figure 6.24b shows a south-western nearshore surface current with flow return at an offshore distance of about 3 km. Figure 6.25 shows that the sediment plume at 18:00 hours on the same day, was directed toward the south-west. Figure 6.26 shows that the flow profiles at 18:00 hours on the same day were similar to those of Figure 6.25 except that the near-surface shore perpendicular and alongshore components are higher and lower respectively by a factor of 2. Figure 6.27 shows the sediment plume at 0.00 hours on August 28, 1979. At the surface, the plume covered an offshore distance of 9 km and a longshore distance of 5 km. Figure 6.27 shows another case of maximum penetration across the coastal zone.

The differences between the computed and observed concentrations and the high values at some stations remote from the source were due to resuspension of bottom sediments, variability of grain size distribution with time and the effect of the unsampled creeks. Hakanson (1982), estimated the percentage of a lake area that is dominated by erosion and transportation processes or accumulation processes from two parameters,

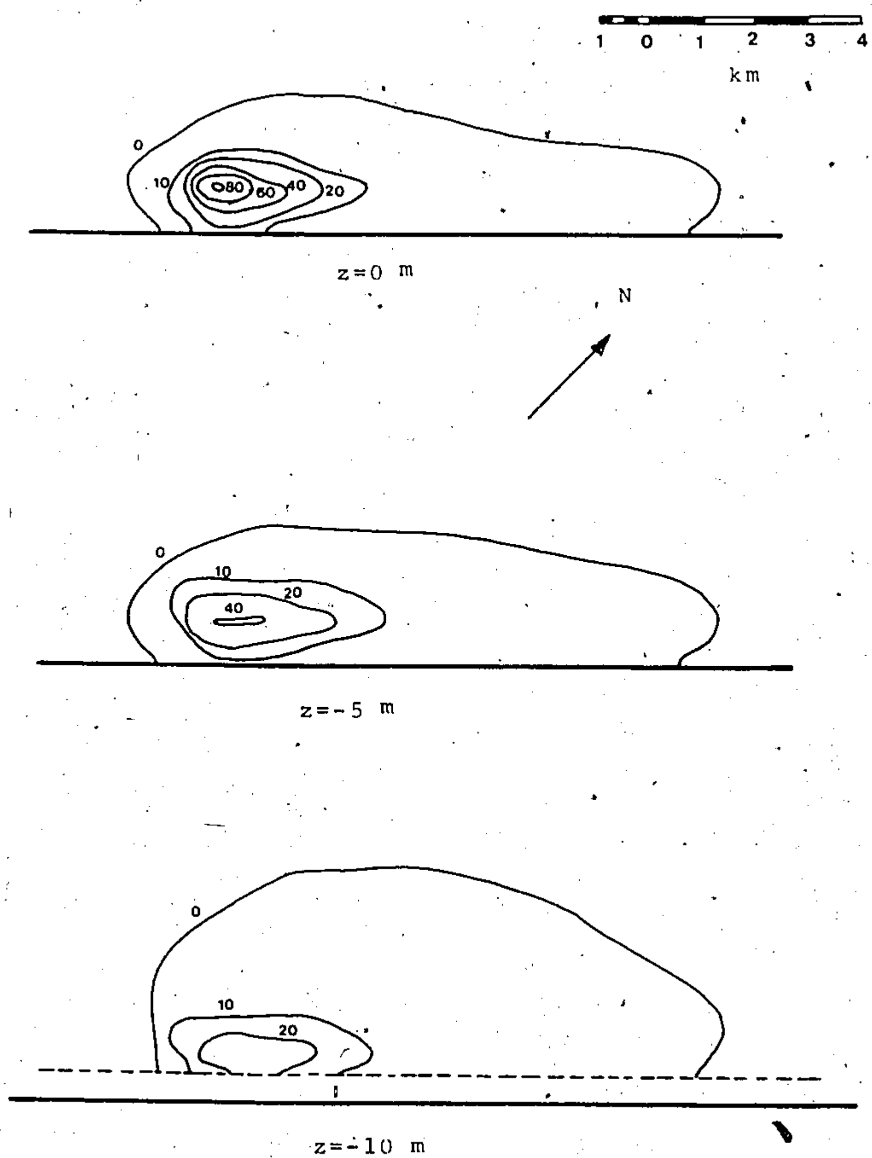

Figure 6.23 Computed SSC plume at 18:00 hours on August 24, 1979, point source at 1 km offshore and particle size of 0.02 mm.

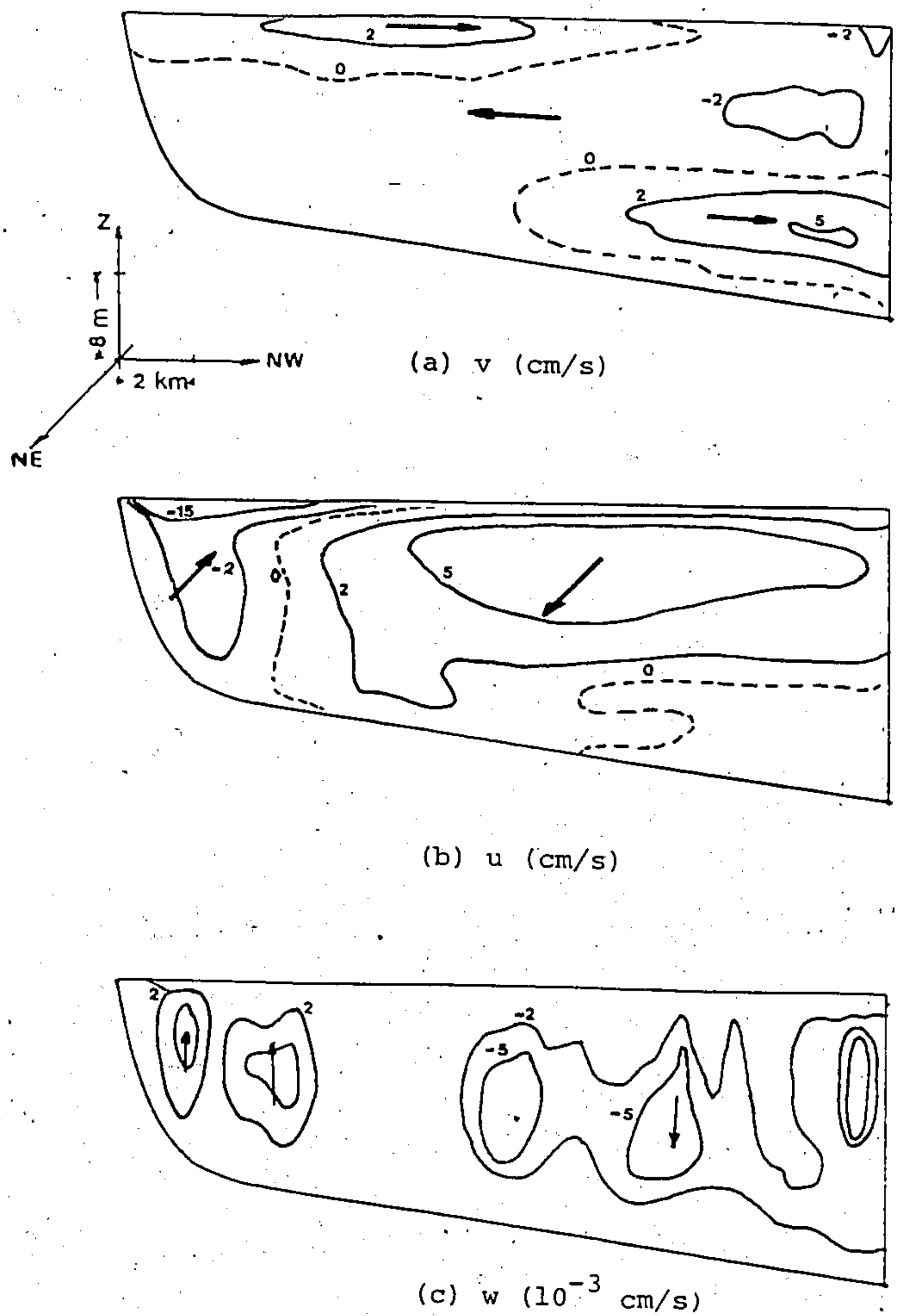

(a) v (cm/s)

(b) u (cm/s)

(c) w (10^{-3} cm/s)

Figure 6.24 Computed flow profiles at 12:00 hours on August 27, 1979.

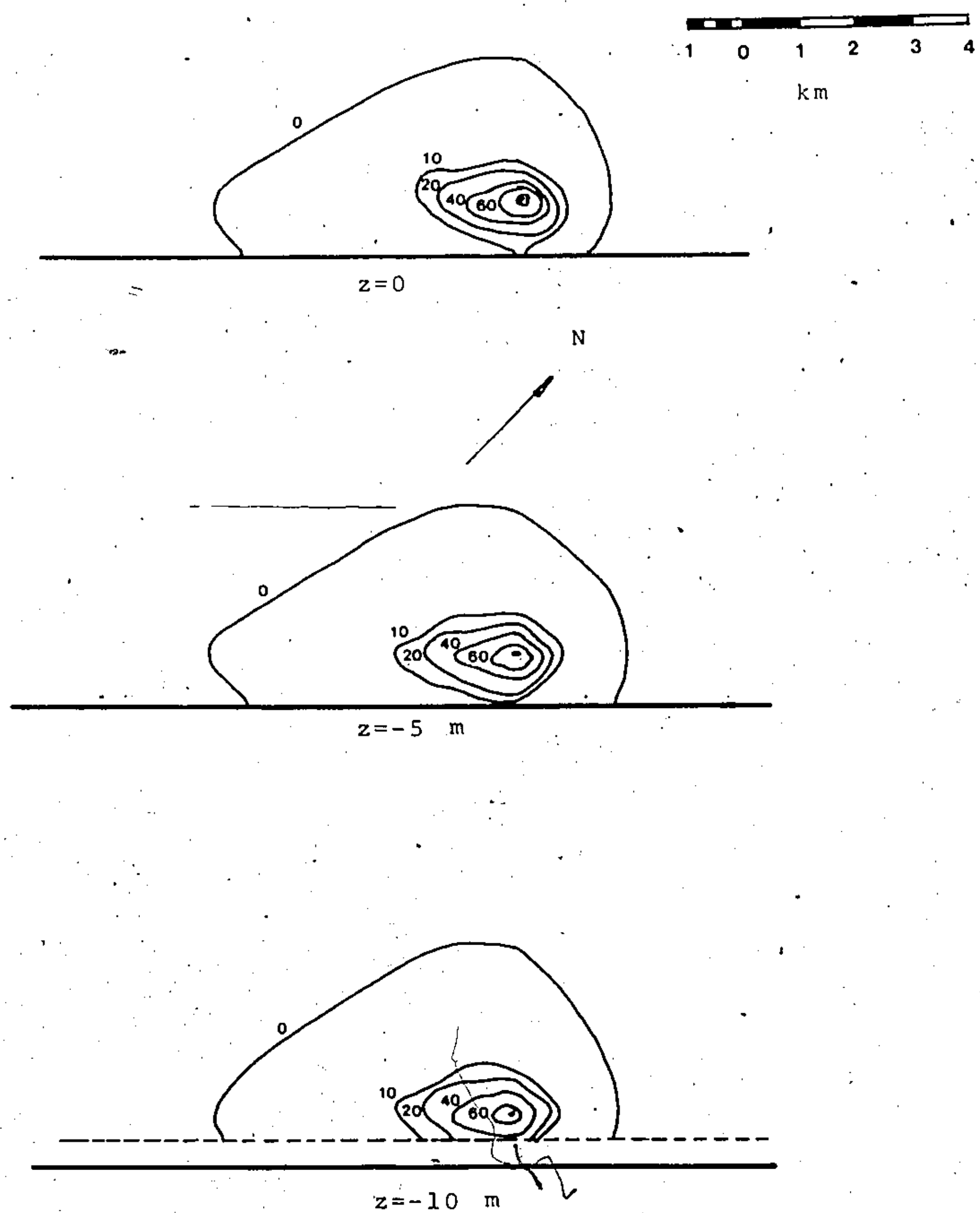

Figure 6.25 Computed SSC plume at 18:00 hours on August 27, 1979, point source at 1 km offshore and particle size of 0.02 mm.

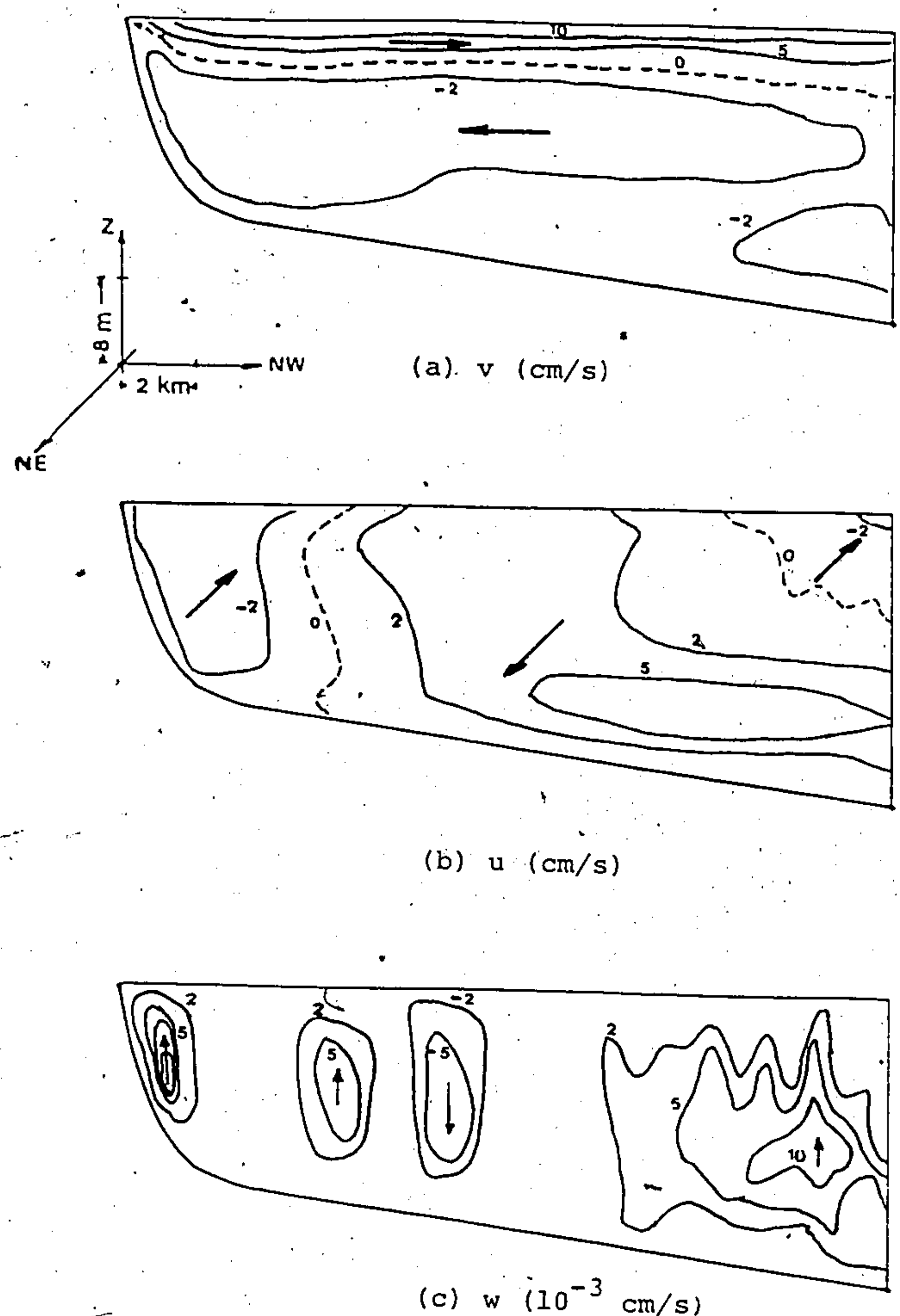

Figure 6.26 Computed flow profiles at 18:00 hours on August 27, 1979.

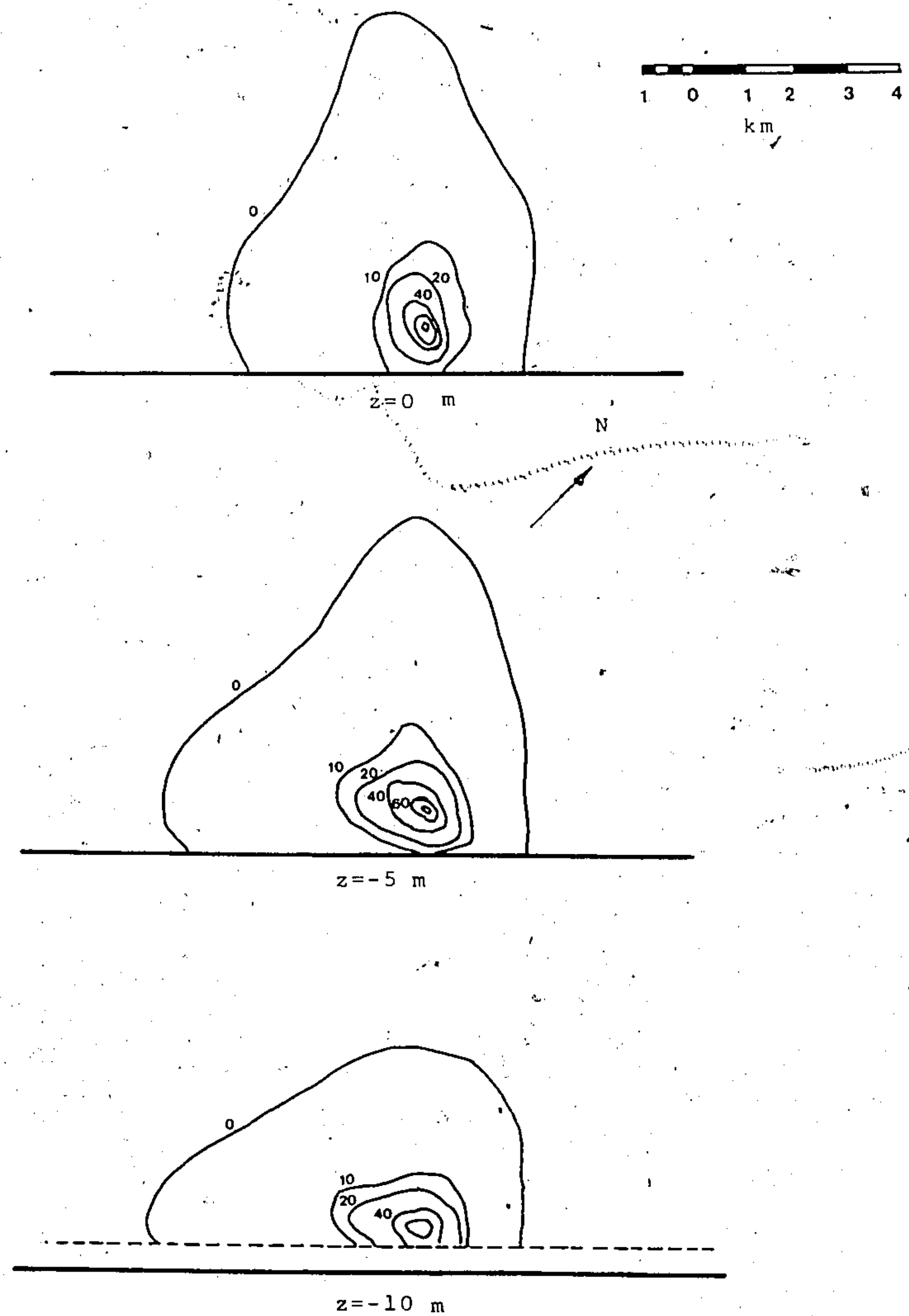

Figure 6.27 Computed SSC plume at 00:00 hours on August 28, 1979, point source at 1 km offshore and particle size of 0.02 mm.

lake area and mean depth. Hakanson (1982) studied Swedish lakes with areas up to only 5000 km^2 (Lake Erie central basin area is about 16000 km^2). Based on that study, resuspension activity in Lake Erie central basin is important. The shoreline hydrology is expected to produce high rain intensity runoff with short time duration, so errors in sampling timing may also affect the SSC distribution within the coastal zone.

6.6 SEDTRAN APPLICATIONS

To investigate the effect of coastal currents on the suspended sediment plume and patch, and the extent of suspended sediment in both coastal and offshore waters, several types of sediment-related activities were studied: (a) continuous dredging using side-caster dredge; (b) dumping of sediment spoils; and (c) river sediment loads. Those cases were simulated by running both ERCH and SEDTRAN.

6.6.1 Point source

For the case of dredging the harbor entrance or constructing a nearshore structure using suction dredging (side-caster dredge), a surface point source 1 km offshore was simulated. For disposal of heavy particles, a surface source is the worst case, since the entire water column is polluted. This case was simulated for the period July 1 to 5, 1979 when a strong shore parallel current persisted. The currents computed by ERCH were input to SEDTRAN using $\Delta x = \Delta y = 500$ m, $\Delta z = 2.5$ m, Δt=300 sec, K_x=2.6 x 10^4 cm^2/sec and K_y = 6 x 10^3 cm^2/sec. A grain size distribution similar to that of Figure 6.15 was also used. Figure 6.28

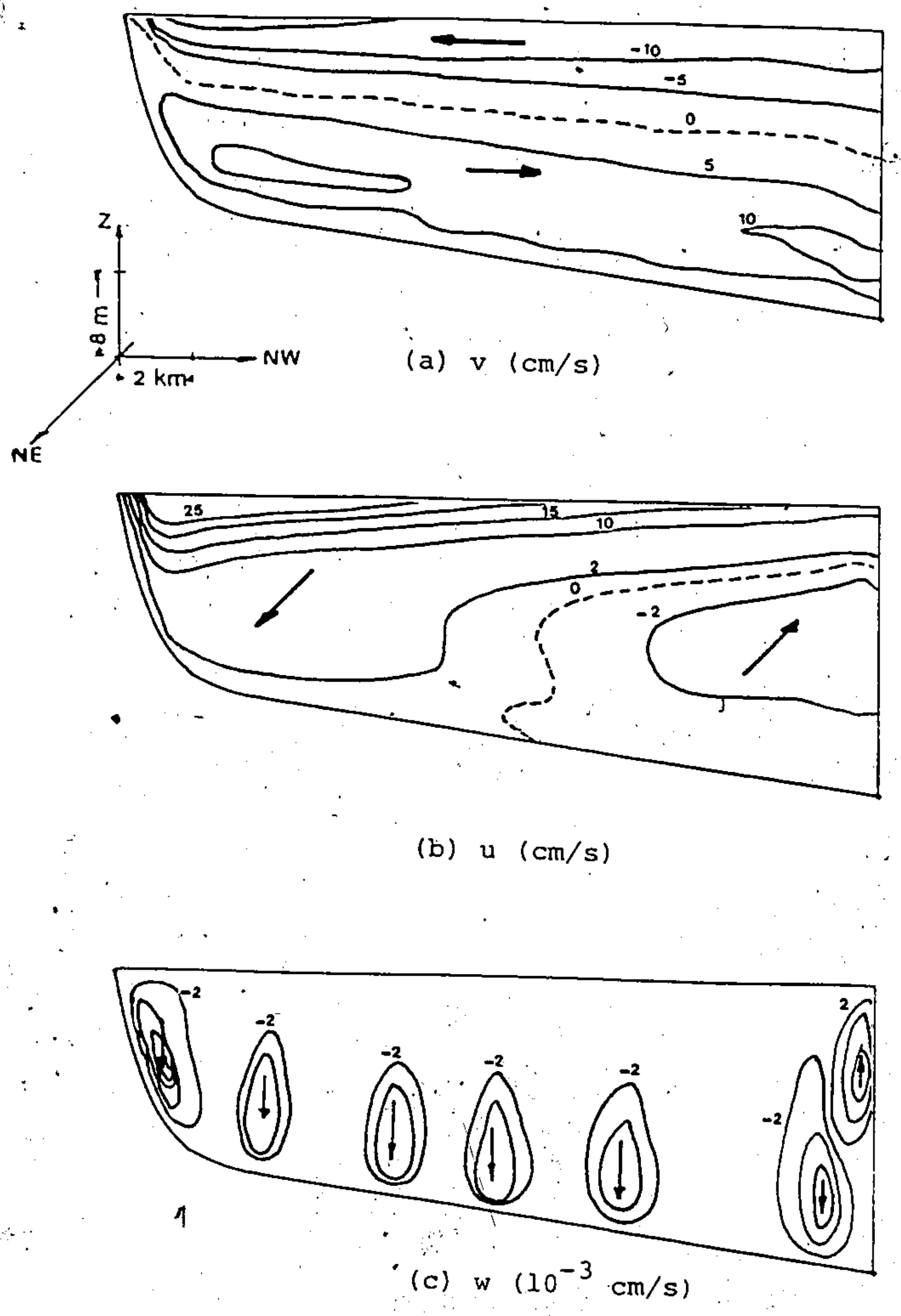

Figure 6.28 Computed flow profiles at 12:00 hours on July 1, 1979.

shows the flow profiles at 12:00 hours on July 1. Figure 6.28 shows a near-surface onshore component accompanied with return flow at 5 m depth, strong nearshore north-east flow with return flow at about 9 km offshore, and a downward nearshore current. Figure 6.29 shows the computed sediment plume at 18:00 hours on July 1. The plume was directed toward the north-east occupying a narrow width at surface and wider at depth. At the surface the plume extended about 10 km and 2 km along and across the shore respectively. At 10 m depth the plume also extended to the 10 km but 5 km across the shore.

Figure 6.30 shows the flow profiles at 12:00 hours on July 2. Figure 6.30 shows a strong near-surface onshore component accompanied by return flow at about 5 m depth, near-surface weak south-west current ~~with~~ return flow at about 4 m depth and a downward nearshore current. Figure 6.31 shows the computed sediment plume at 18:00 hours on July 2. The plume was directed toward the west at the surface and north at 10 m depth. The plume, at the surface, extended about 5 km and 2 km along and across the shore respectively, and about 7 km and 4 km at 10 m depth. At surface the 10% and 20% concentration covered about 1.5 km and 0.5 km of the shore respectively.

Figure 6.32 shows the flow profiles at 12:00 hours on July 3. Figure 6.32a shows a weak offshore component accompanied with return flow between 1.5 m and 5m depths only. Figure 6.32b shows a weak north-east current everywhere. Figure 6.32c shows several weak vertical eddies. Figure 6.33 shows the computed sediment plume at 18:00 hours on July 3. At all depths the plume was shifted toward north-east. At the surface,

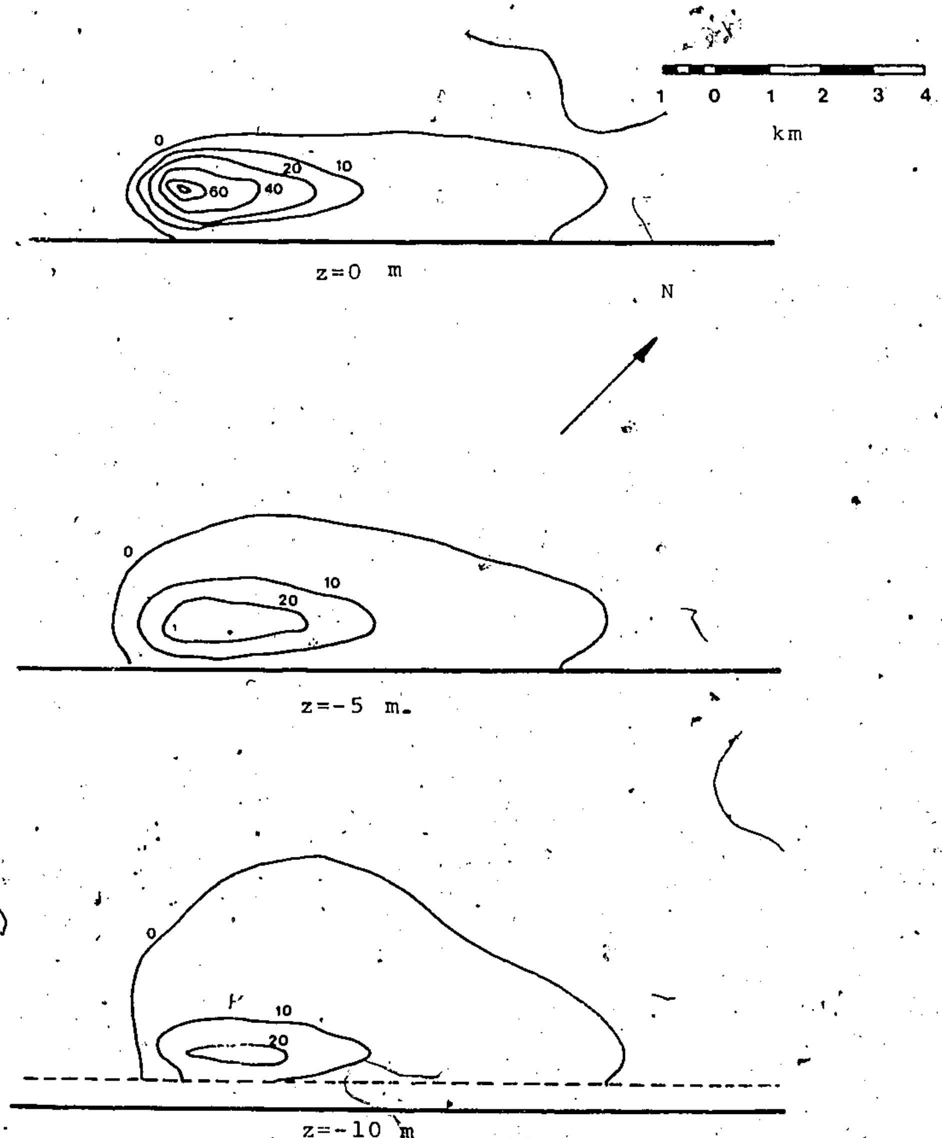

Figure 6.29 Computed SSC plume at 18:00 hours on July 1, 1979, point source at 1 km offshore and particle size of 0.02 mm.

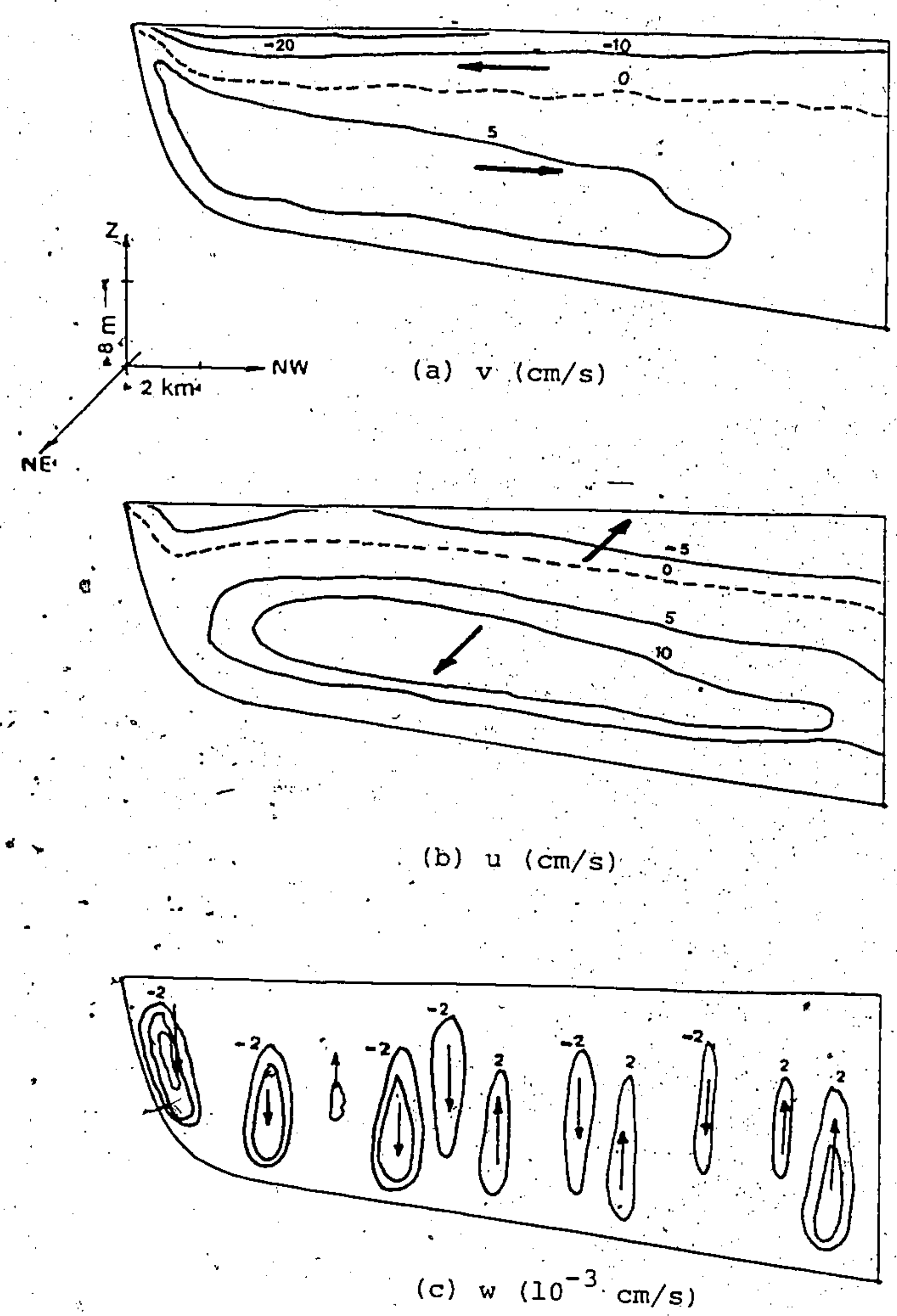

Figure 6.30 Computed flow profiles at 12:00 hours on July 2, 1979.

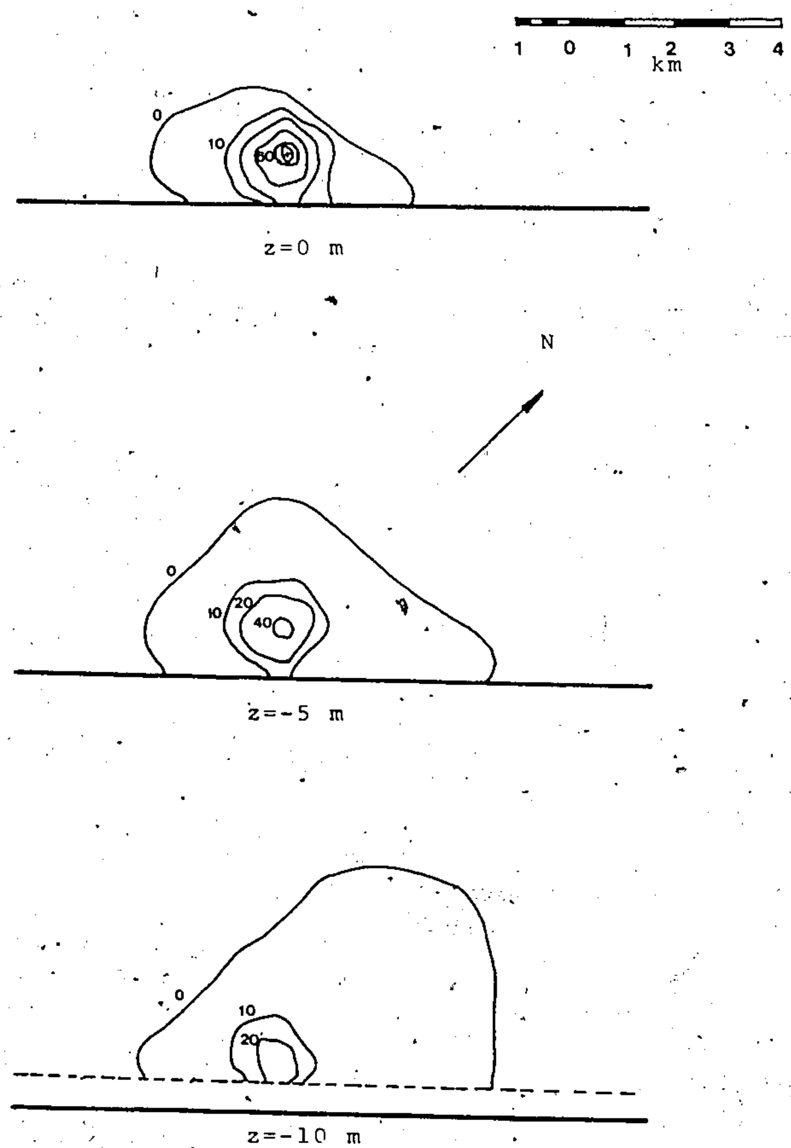

Figure 6.31 Computed SSC plume at 18:00 hours on July 2, 1979, point source at 1 km offshore and particle size of 0.02 mm.

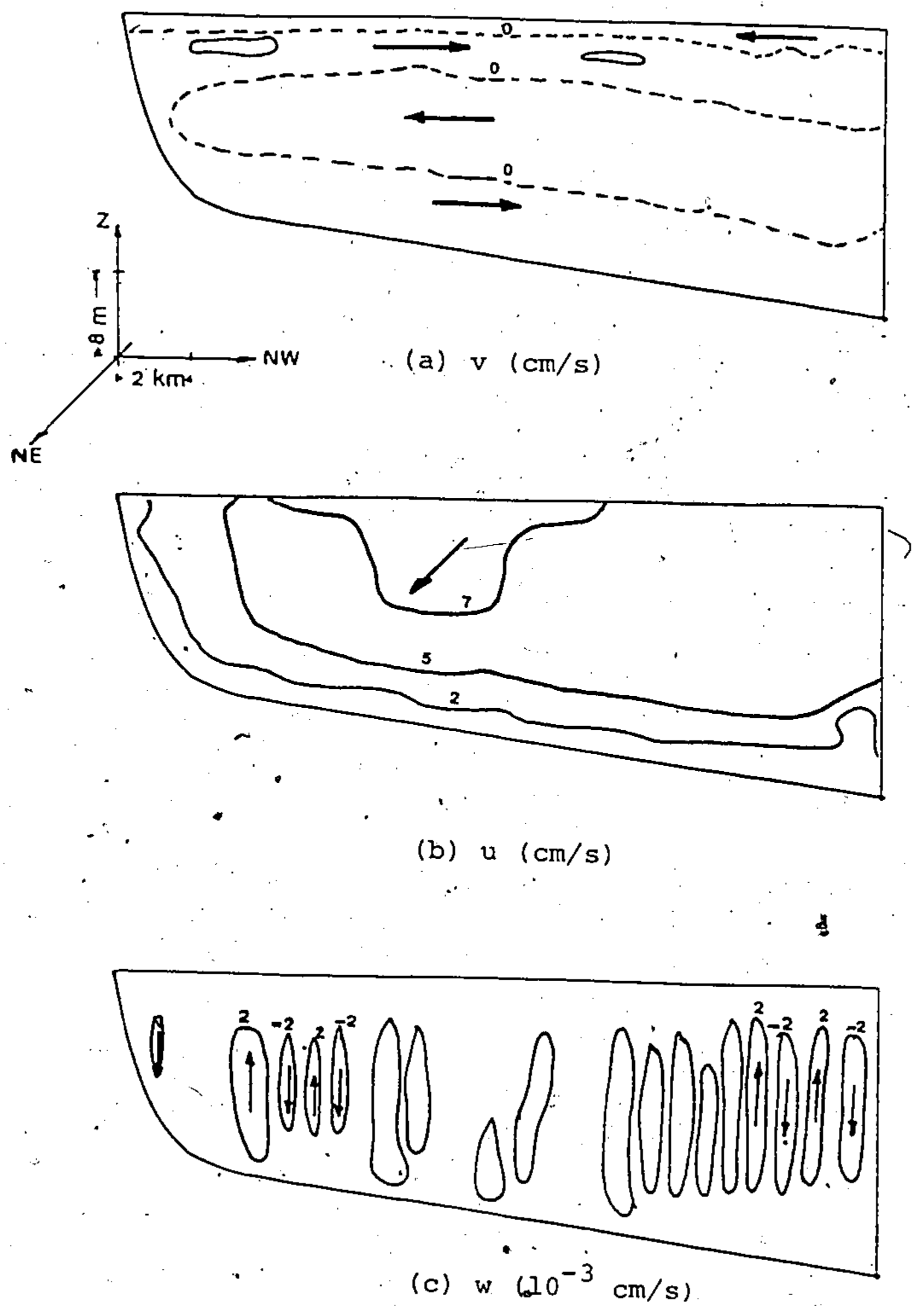

Figure 6.32 Computed flow profiles at 12:00 hours on July 3, 1979.

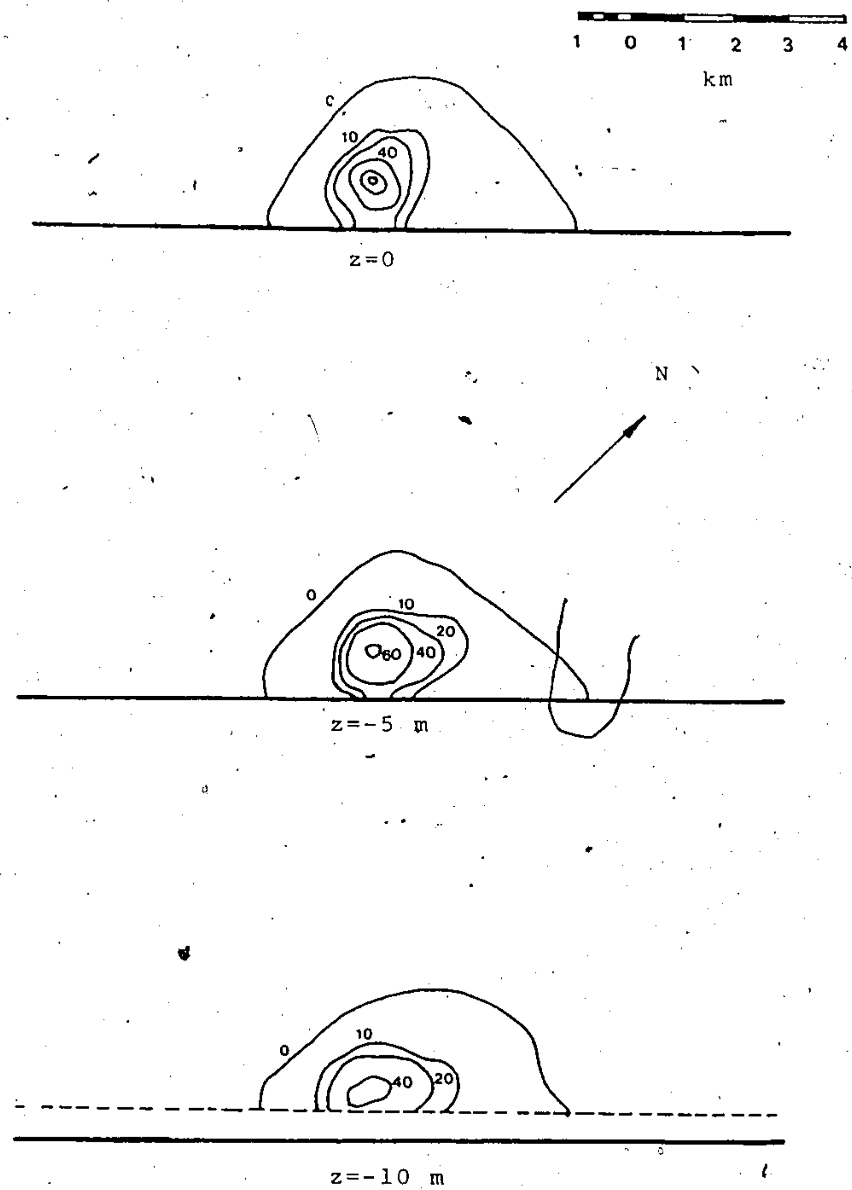

Figure 6.33 Computed SSC plume at 18:00 hours on July 3, 1979, point source at 1 km offshore and particle size of 0.02 mm.

the 10%, 20% and 30% concentrations covered about 1.5 km, 1 km and 0.5 km of the shore respectively, while only the 10% concentration covered about 1.5 km of the shore at 10 m depth.

Figure 6.34 shows the flow profiles at 12:00 hours on July 4. Both the shore-parallel and shore-perpendicular components reversed their directions to south-west and north-west respectively. Both components were accompanied with return flow at about 5 m depth. Figure 6.34c shows a nearshore upward current. The computed sediment plume at 18:00 hours on July 4 is plotted in Figure 6.35. At all depths the plume was directed toward the west, occupying a relatively wide band across the coastal zone. The plume extended to about 9 km and 7 km along and across the shore respectively. At surface the 40% concentration covered about 300 m of the shore.

Figure 6.36 shows the flow profiles at 12:00 hours on July 5. Figure 6.36a shows near-surface offshore component with return flow at about 5m depth. Figure 6.36b shows that, close to the shore, the entire layer was moving with a strong south-western current with a return flow below 5m depth 6 km offshore. Figure 6.36c shows a nearshore upward current. Figure 6.37 shows the computed sediment plume at 18:00 hours on July 5. At all depths the plume was directed toward the south-west, extending to about 13 km and 5 km along and across the shore respectively. At surface the 50% concentration covered about 250 m of the shore.

The flow profiles computed for the period July 1 to 5, 1979, show several current direction combinations for u, v and w with different magnitudes between weak and strong currents. The computed sediment

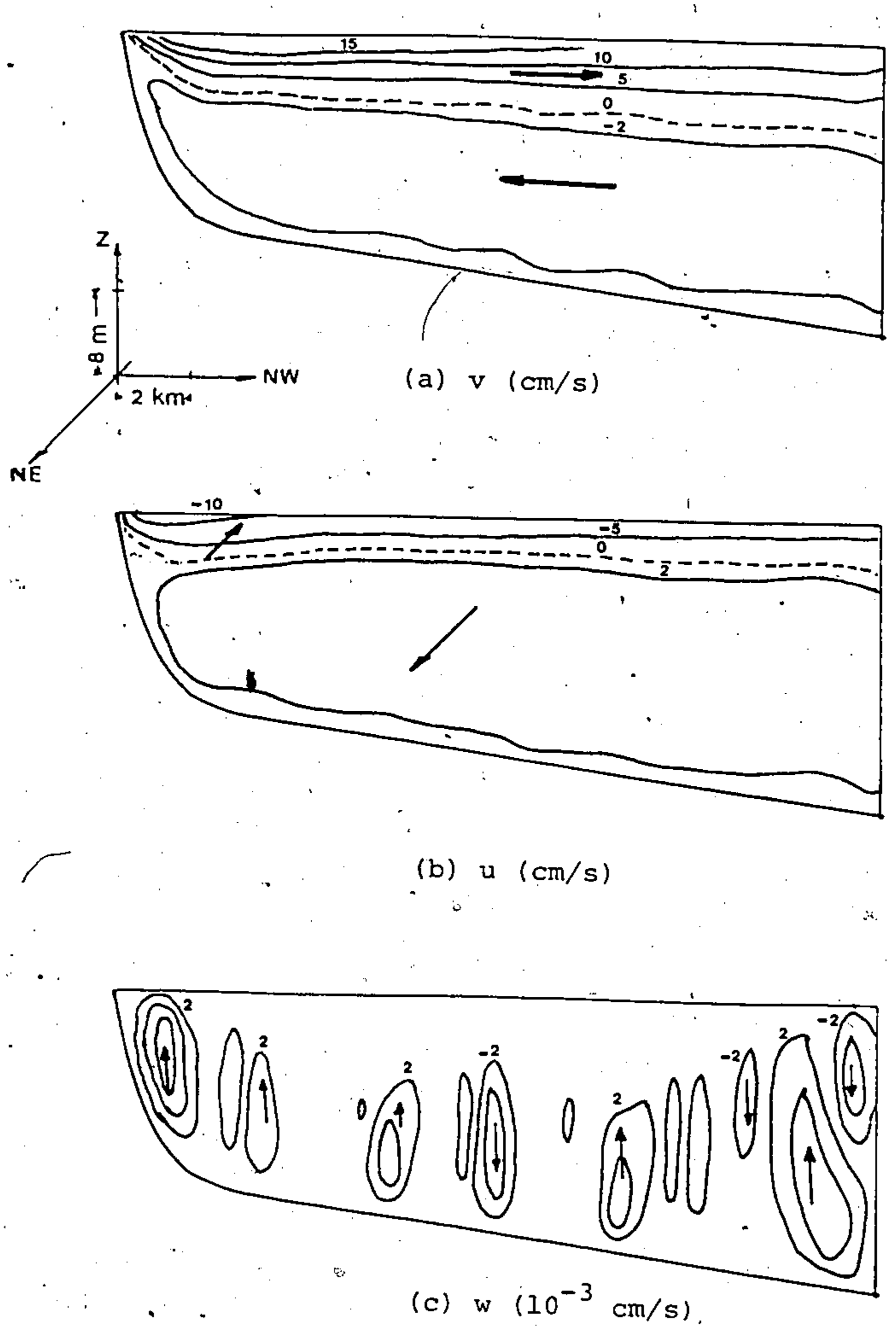

Figure 6.34 Computed flow profiles at 12:00 hours on July 4, 1979.

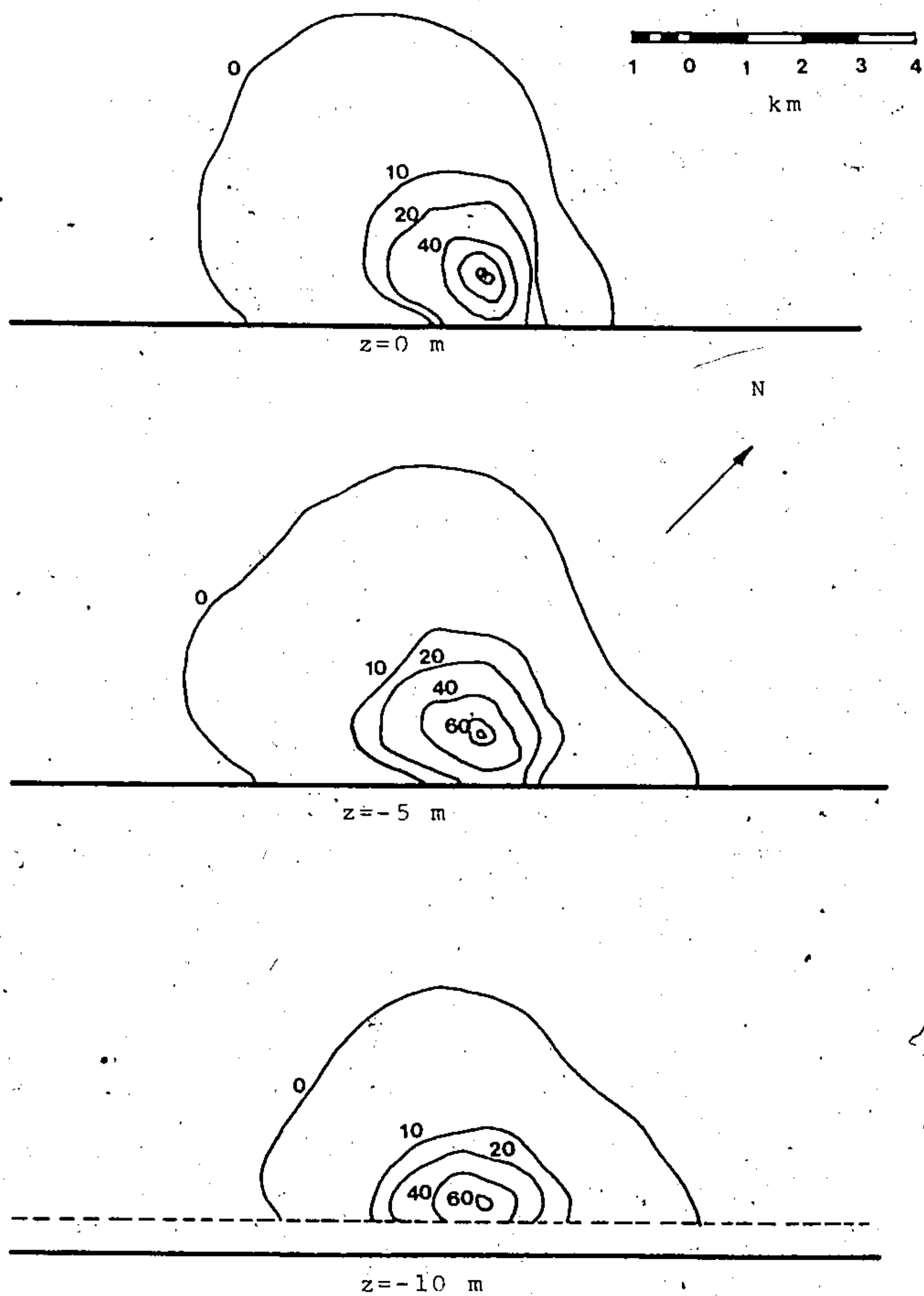

Figure 6.35 Computed SSC plume at 18:00 hours on July 4, 1979, point source at 1 km offshore and particle size of 0.02 mm.

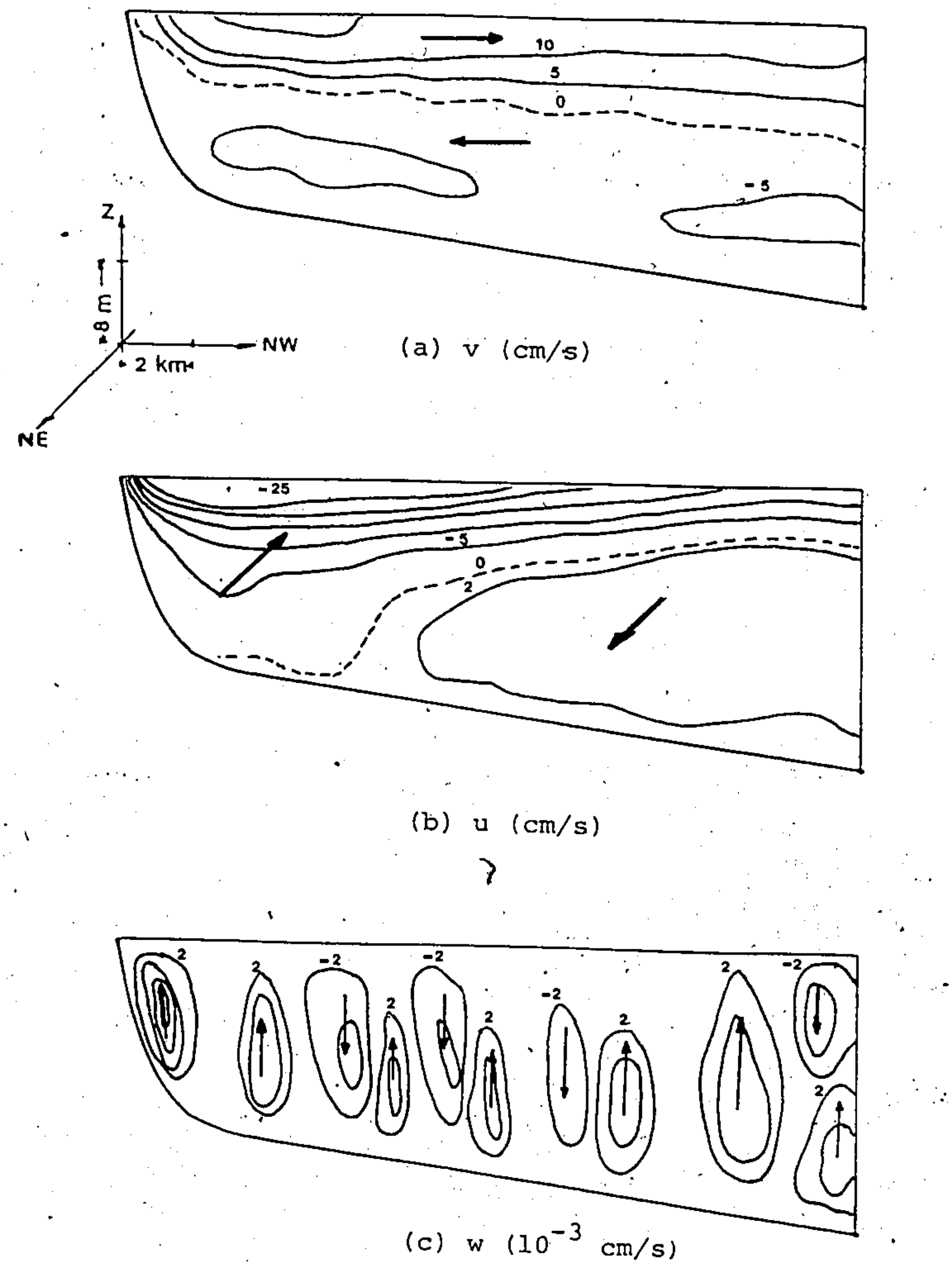

Figure 6.36 Computed flow profiles at 12:00 hours on July 5, 1979.

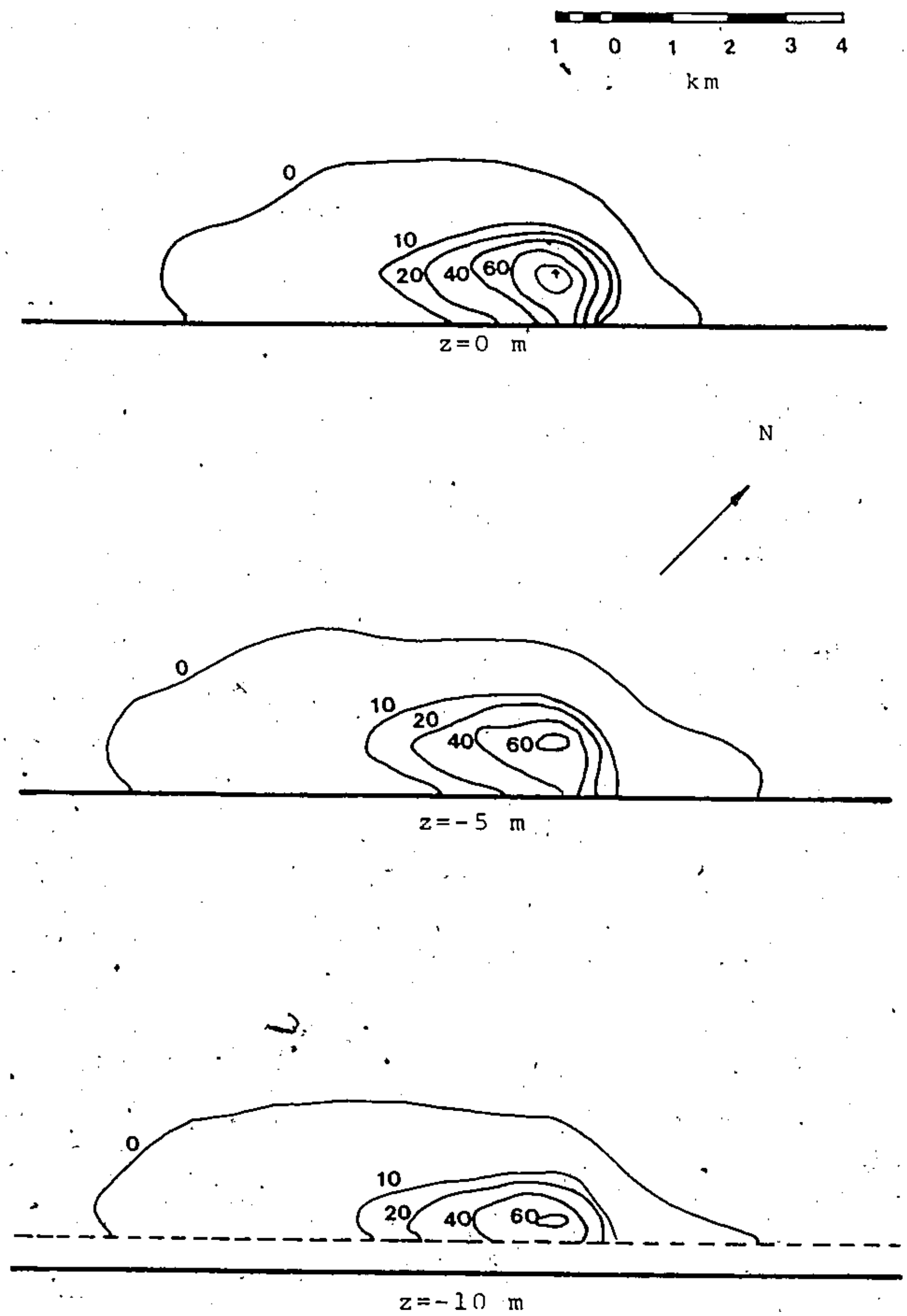

Figure 6.37 Computed SSC plume at 18:00 hours on July 5, 1979, point source at 1 km offshore and particle size of 0.02 mm.

plumes also show different shapes at different directions with increasing shoreline concentrations with time. The concentrations decreased as a function of distance from the source as is to be expected. The plume shapes and dimensions were not always similar for all depths, for example Figures 6.31 and 6.20. During the five day simulation the plume extended about 18 and the 10% concentration about 8 km and 2 km along and across the shore respectively. The maximum shoreline concentration was about 54% of the source concentration and covered about 250 m of the shore.

To study the effect of the source location across the coastal boundary layer, a surface point source located 3 km offshore was used. The flow profiles for August 24 were computed, Figure 6.22. The same parameters used earlier for the August 24 sediment plume (section 6.5) were used. Figure 6.38 shows the computed sediment plume at 18:00 hours on August 24. Due to the relative remoteness of the shore from the source, the plume was elongated in the horizontal mean current direction, and relatively wider than that of Figure 6.23. The plume extended about 10 km and 5 km along and across the shore line respectively, corresponding to about 0.83 and 1.66 of Figure 6.23. The maximum shoreline concentration was about 1% of the source concentration.

As mentioned earlier the most critical parameter is the sediment grain size. So two additional cases, representing fine sand and very fine silt, were studied. Figures 6.39 and 6.40 show the computed sediment plumes at 18:00 hours on August 24 for particle sizes of 0.1 mm and 0.005 mm respectively. In the case of the fine sand range (Figure 6.39), the plume covered a relatively smaller area at all depths, while

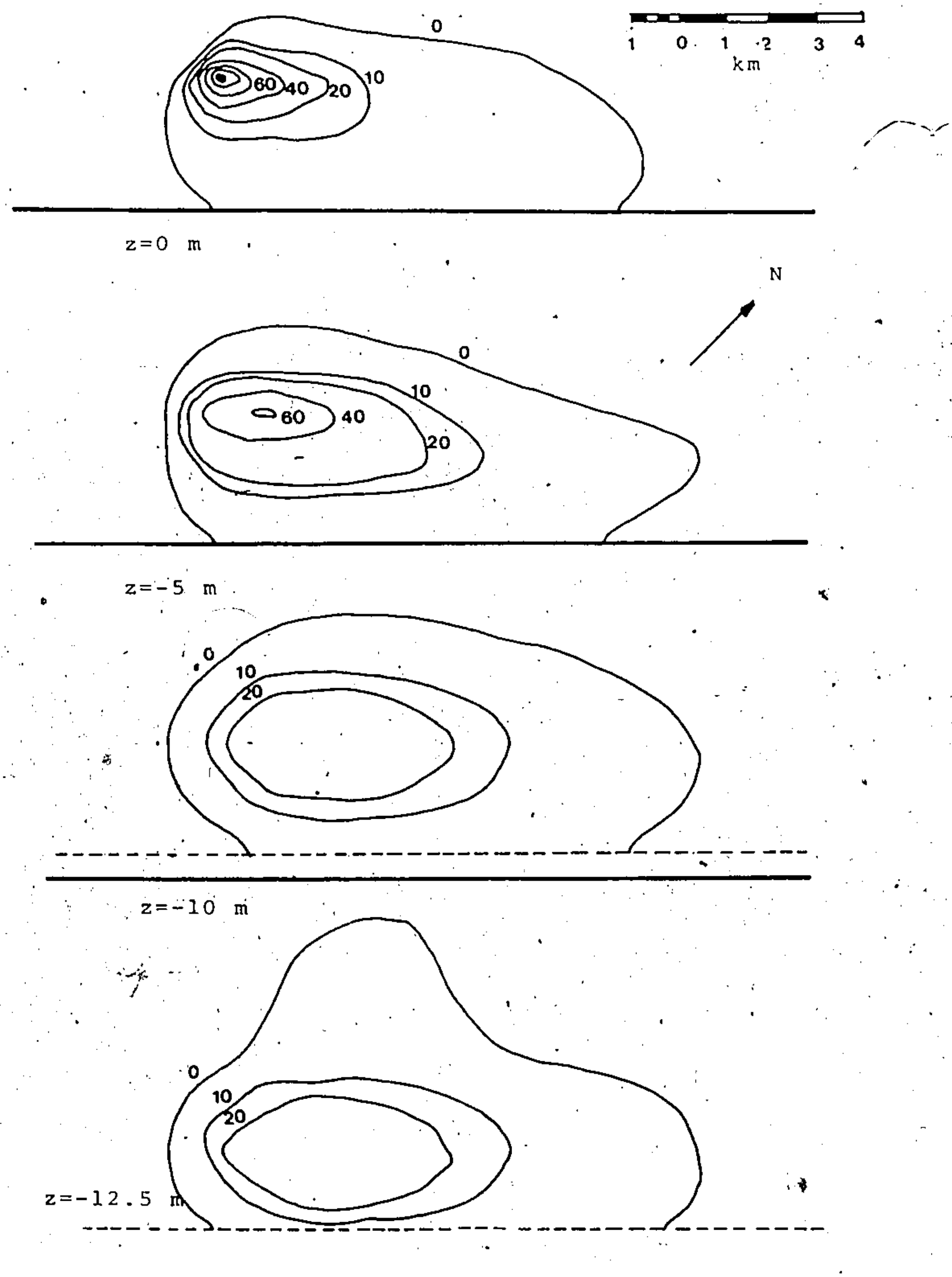

Figure 6.38 Computed SSC plume at 18:00 hours on August 24, 1979, point source at 3 km offshore and particle size of 0.02 mm.

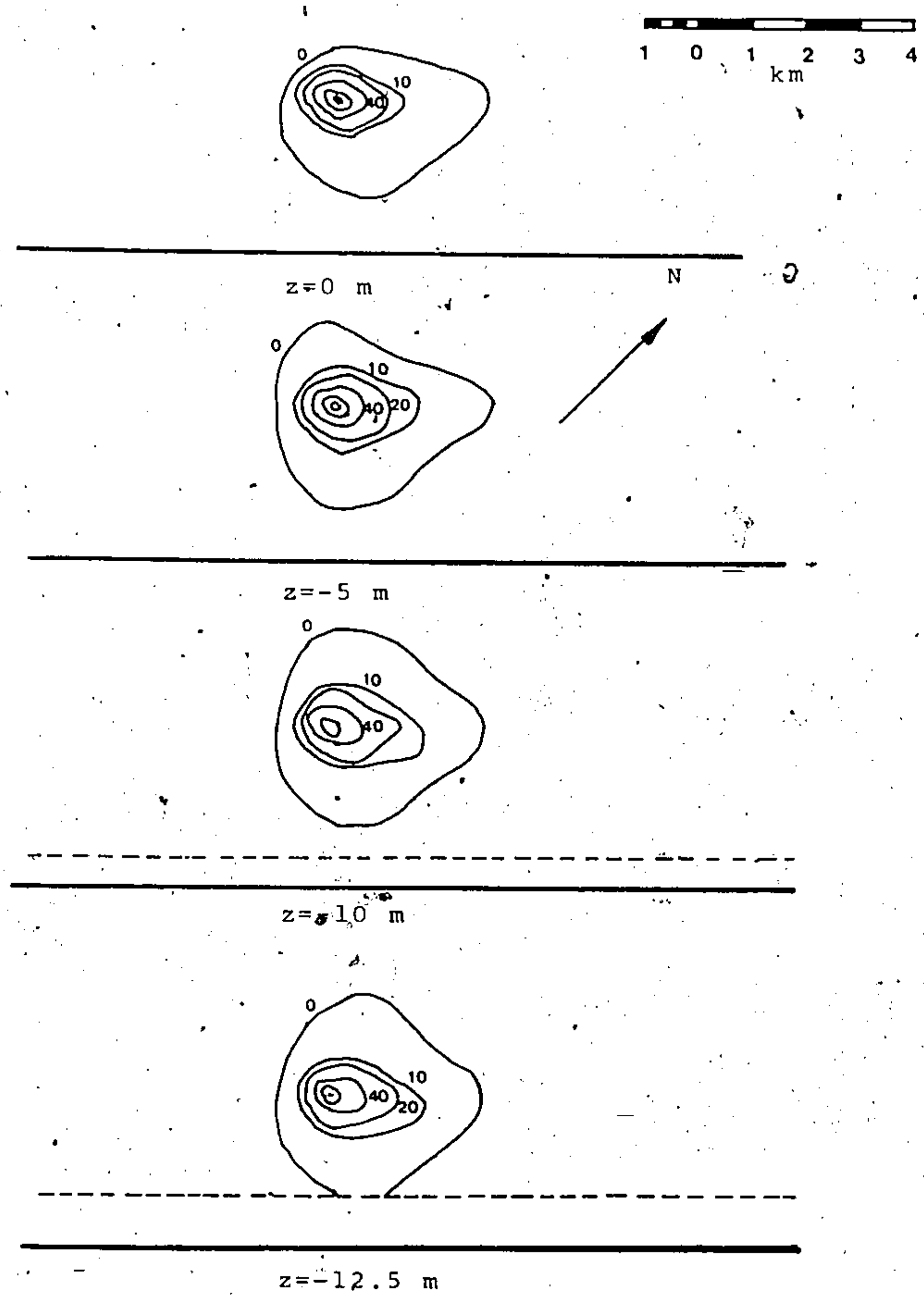

Figure 6.39 Computed SSC plume at 18:00 hours on August 24, 1979, point source at 3 km offshore and particle size of 0.1 mm.

the 0% concentration did not reach the shoreline. The plume extended to about 4 km and 3 km along and across the shore respectively. The concentrations computed at lower depths were relatively high, having a maximum value of 80% and 70% at 5 m and 10 m respectively.

Figure 6.40 shows that the plume computed using the very fine silt range was sensitive to the horizontal current. At the surface the plume covered about 18 km and 5 km along and across the shore respectively. The maximum shoreline concentration was about 2% of the source concentration. The concentrations at lower depths were relatively small, having a maximum value of about 17% and 3% at 5 m and 10 m depths respectively.

Dredging and dumping of dredge spoil is one of the most serious and frequent of the problematic activities which take place in coastal waters. Nearly all dredge spoil disposal sites in U.S. coastal waters are in the near shore areas, in water less than 30 m deep (Bishop, 1983). At the dredge site there is much turbulence and resuspension of sediment. If the sediments are polluted, resuspension can greatly increase the toxic materials concentration in the surrounding area. Despite this, the affected area is relatively confined. On the other hand the plume that develops during spoil dumping may have a more wide spread effect. Figures 6.23, 6.39 and 6.40 represent the impact zone of a side-caster dredge for three grain sizes that could be expected in dredge spoil.

6.6.2 Sediment patch

The transport of sediment particles dumped in the coastal zone was investigated by again assuming a surface instantanuous source located 3

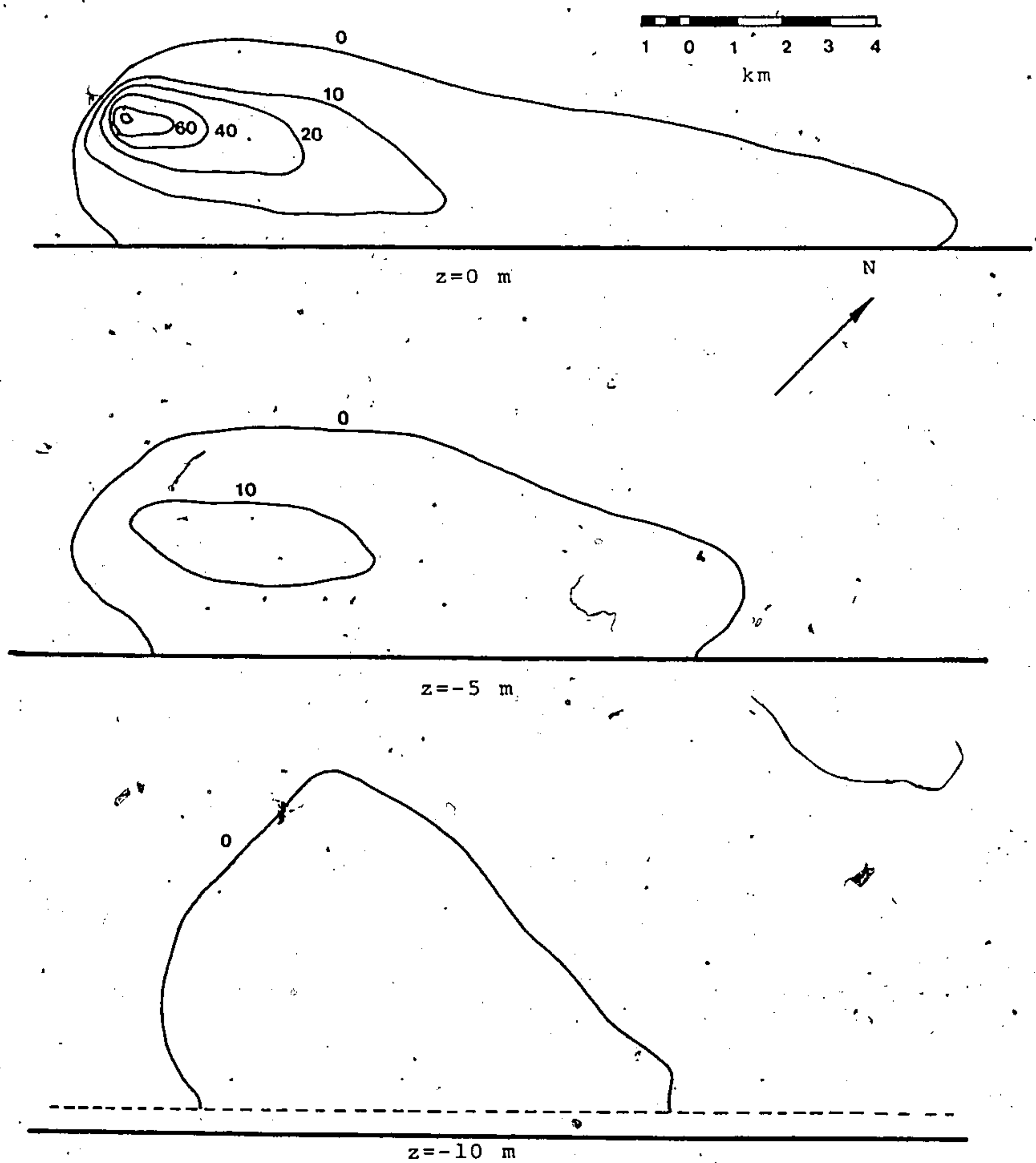

Figure 6.40 Computed SSC plume at 18:00 hours on August 24, 1979, point source at 3 km offshore and particle size of 0.005 mm.

km offshore. The sediment patch was simulated using the August 24 currents and the parameters for the particle size ranges given earlier. Figure 6.41 shows the computed sediment patch at 1:00 hours on August 24 for a particle size of 0.1 mm. Due to the high settling velocity (0.5 cm/sec), no sediment was found in the upper 5 m. Sediment was found below the 5 m depth with increasing concentrations downward. At the 5 m depth the patch extended about 2 km along and across the shore with maximum concentrations of 1% of the original dumped sediment concentration. At 10 m depth, the patch extended about 4 km along and across the shore respectively with maximum concentration of 9%. The centre of the gravity of the patch almost did not move, the flow being dominated by vertical advection (the settling term). One hour later, no sediment was found in the entire water column. Figure 6.42 shows the sediment patch at 3:00 hours on August 24 for a particle size of 0.02 mm. Sediment concentrations were found through the entire water column with a maximum concentration at 5 m depth, where the patch covered about 6 km and 3 km along and across the shore respectively, corresponding to about 4 km and 2km at 10 m depth. The centre of gravity of the patch moved about 2 km at the surface and the 5 m depth. Due to the decrease in the shore parallel component and the offshore flow return the centre of gravity of the patch was almost stationary at 10 m depth.

Figure 6.43 shows the sediment patch at 3:00 hours on August 24 for a particle size of 0.005 mm. The sediment concentrations were found only in the upper 5 m with a maximum concentration at the surface. The patch covered about 7 km and 3 km along and across the shore respectively

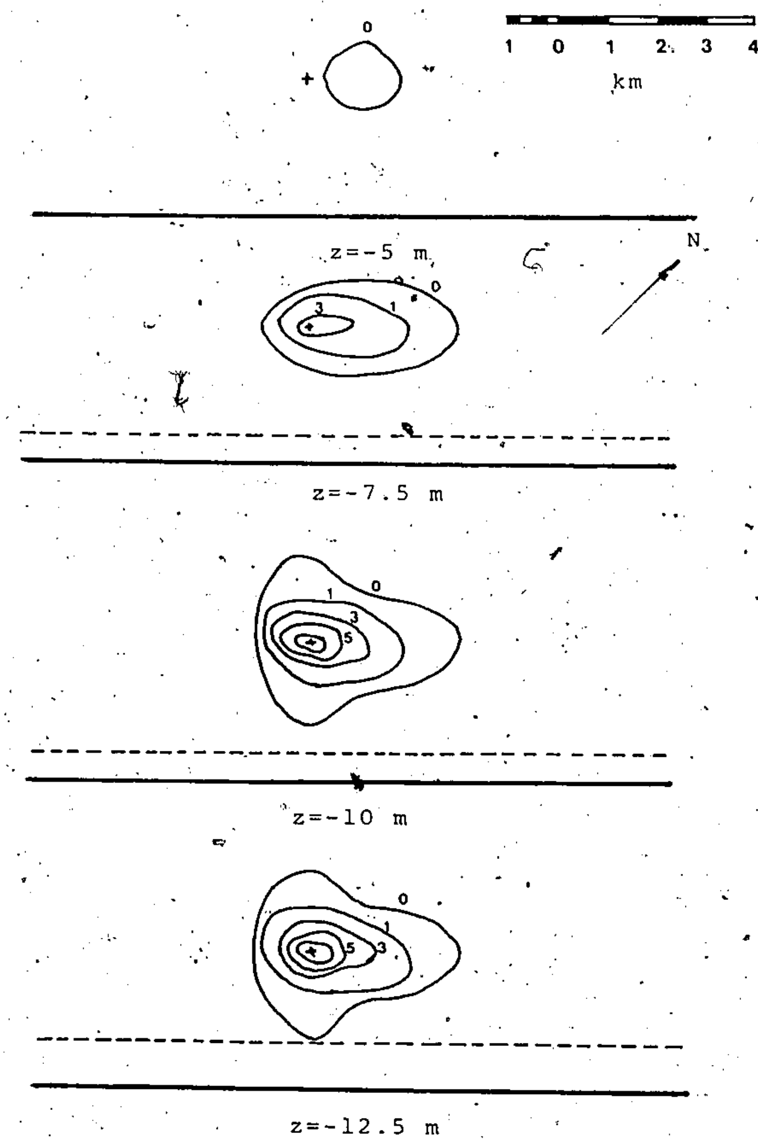

Figure 6.41 Computed SSC patch at 1:00 hour on August 24, 1979, point source at 3 km offshore and particle size of 0.1 mm.

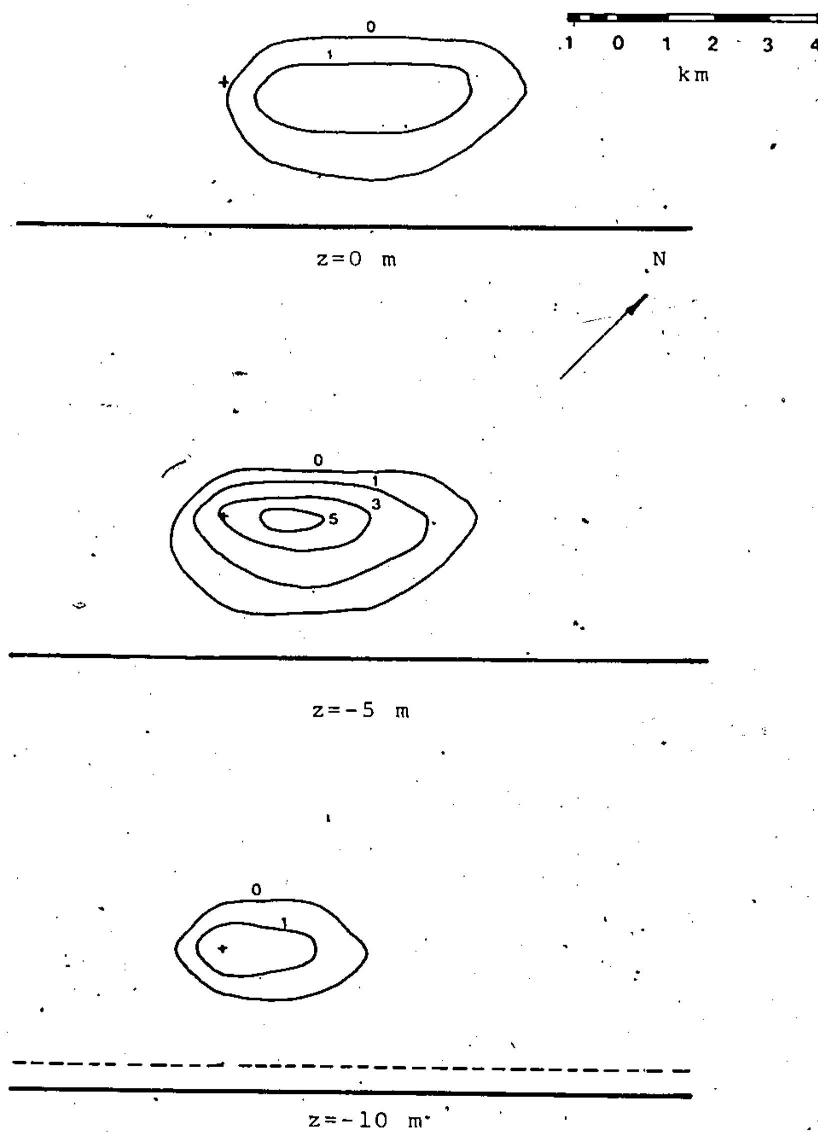

Figure 6.42 Computed SSC patch at 3:00 hour on August 24, 1979, point source at 3 km offshore and particle size of 0.02 mm.

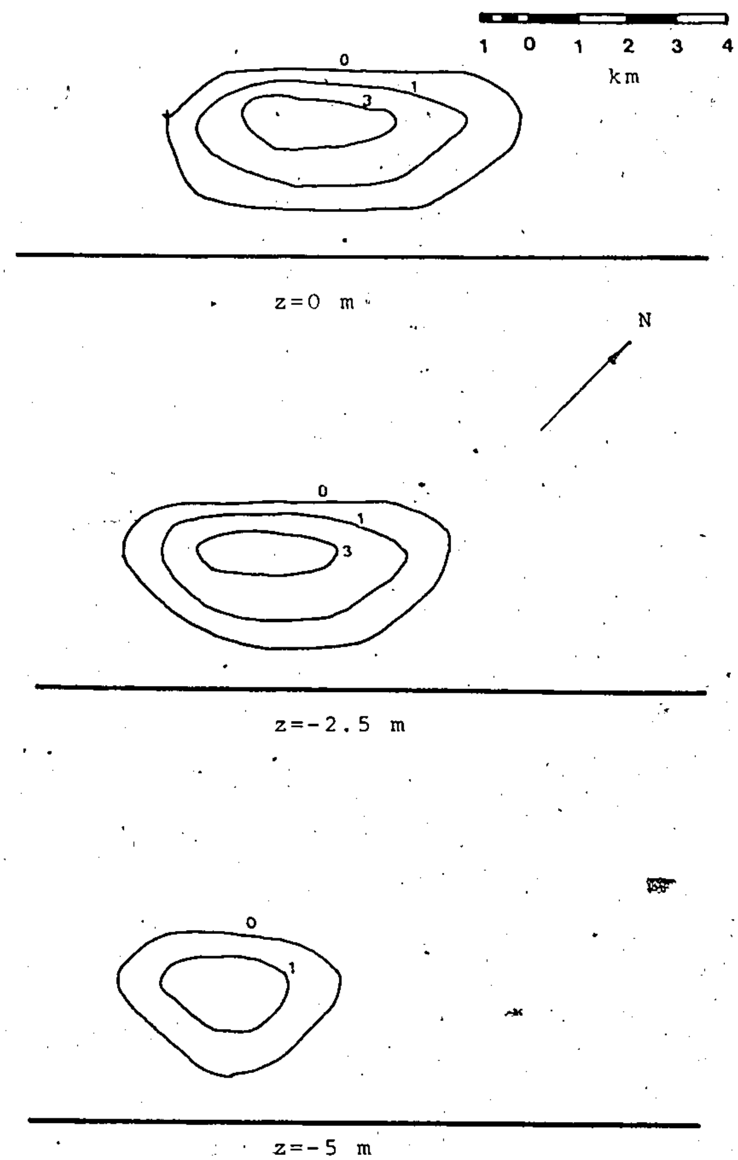

Figure 6.43 Computed SSC patch at 3:00 hour on August 24, 1979, point source at 3 km offshore and particle size of 0.005 mm.

at the surface, corresponding to 5 km and 3 km at 5 m depth. The patch centre of gravity moved about 2 km at the surface and 1.5 km at the 5 m depth. At 9:00 hours on August 24, no sediments were found in the water coloumn for a particle size of 0.02 and the 0.005 mm patch reached the shoreline at the surface with concentrations less than 0.04%. It is important to note that, though concentrations computed for the patch were much less than those of the plume, the initial patch concentration is usually much higher than that achieved by the continuous source concentration.

6.6.3 Vertical line source

Major sources of coastal water pollution are rivers, where runoff, industrial and waste loads are emitted. The annual average suspended sediment load from the Cuyahoga river is about 2 x 10^5 tons/year. Close to the river mouth the suspended sediment transport is influenced more by the river inertia than coastal currents. Rivers flow into the lake as a turbulent jet such that inertia decreases rapidly at distances about 16-20 times the river width. A vertical line source of 100 mg/l located 500 m offshore was used to simulate the river. The plume was computed using the August 24 currents for the three particle sizes given earlier.

Figure 6.44 shows the sediment plume at 18:00 hours on August 24 for a particle size of 0.1 mm. The plume is elongated in the alongshore direction at all depths occupying a very narrow width. The plume covered an alongshore distance of 5 km and an across-shore distance of 1 km with maximum shoreline concentration of 65% of the source concentration. Due to the bottom slope effect and the flow return, the plume extended 1.5 km

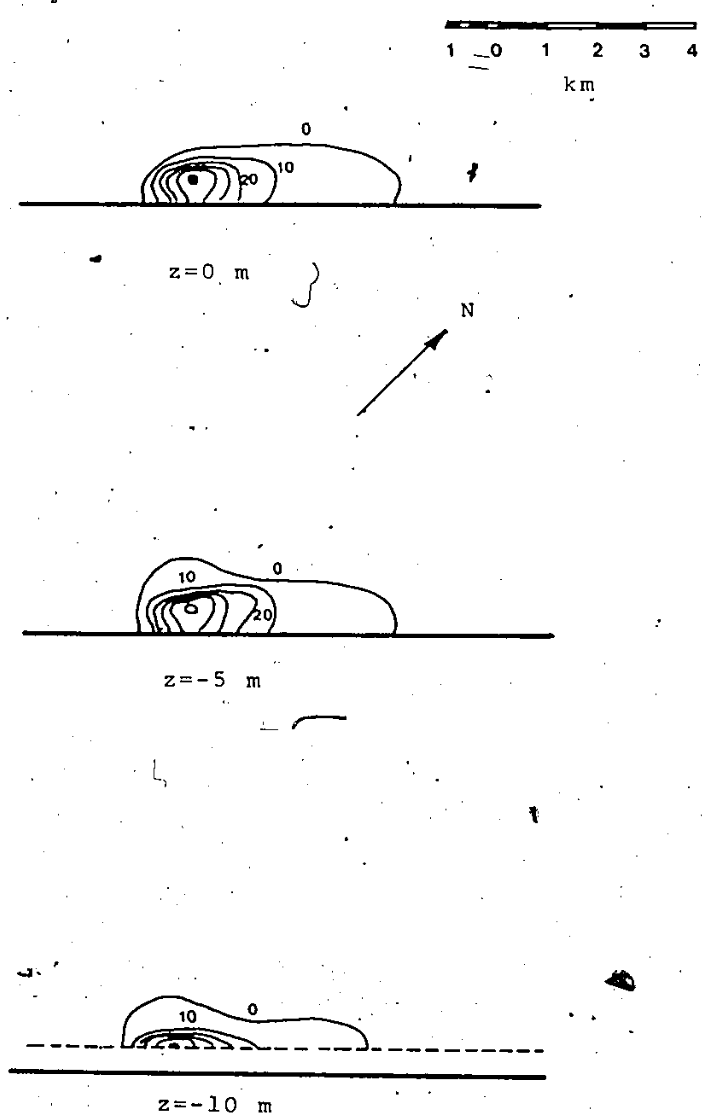

Figure 6.44 Computed SSC plume at 18:00 hours on August 24, 1979, vertical line source at 0.5 km offshore and particle size of 0.1 mm.

across the shore at 10 m depth. Figure 6.45 shows the sediment plume at 18:00 hours on August 24 for a particle size of 0.02 mm. At the surface the plume extended about 12 km and 1.5 km along and across the shore respectively with a maximum shoreline concentration of 65%. Similar plume shapes were found at lower depths but with decreased plume length and increased plume width. Figure 6.46 is the same as Figure 6.45 but for a particle size of 0.005 mm. Similar shapes can be observed with increased plume dimensions. At the surface the plume extended about 14 km and 1.5 km along and across the shore respectively.

6.6.4 Neutral density tracer

A surface point source located 1 km offshore was simulated using the August 24 currents and a zero fall velocity. This case may represent any conservative neutral density pollutant, for example Chloride. The computed plume at 18:00 hours on August 24 is plotted in Figure 6.47. At the surface, the plume extended about 14 km and 3 km along and across the shore respectively. The maximum concentrations at the 5 m and 10 m depths were about 9% and 4% of the source concentration. The plume extended in the alongshore direction about 1.16 times that of Figure 6.23.

6.7 THE INFLUENCE ZONE OF A NEARSHORE SOURCE

Based on the results for all the simulated cases and for some other cases not reported here (such as June 1-6), as well as the sensitivity analysis, an "influence zone" of a nearshore source (located

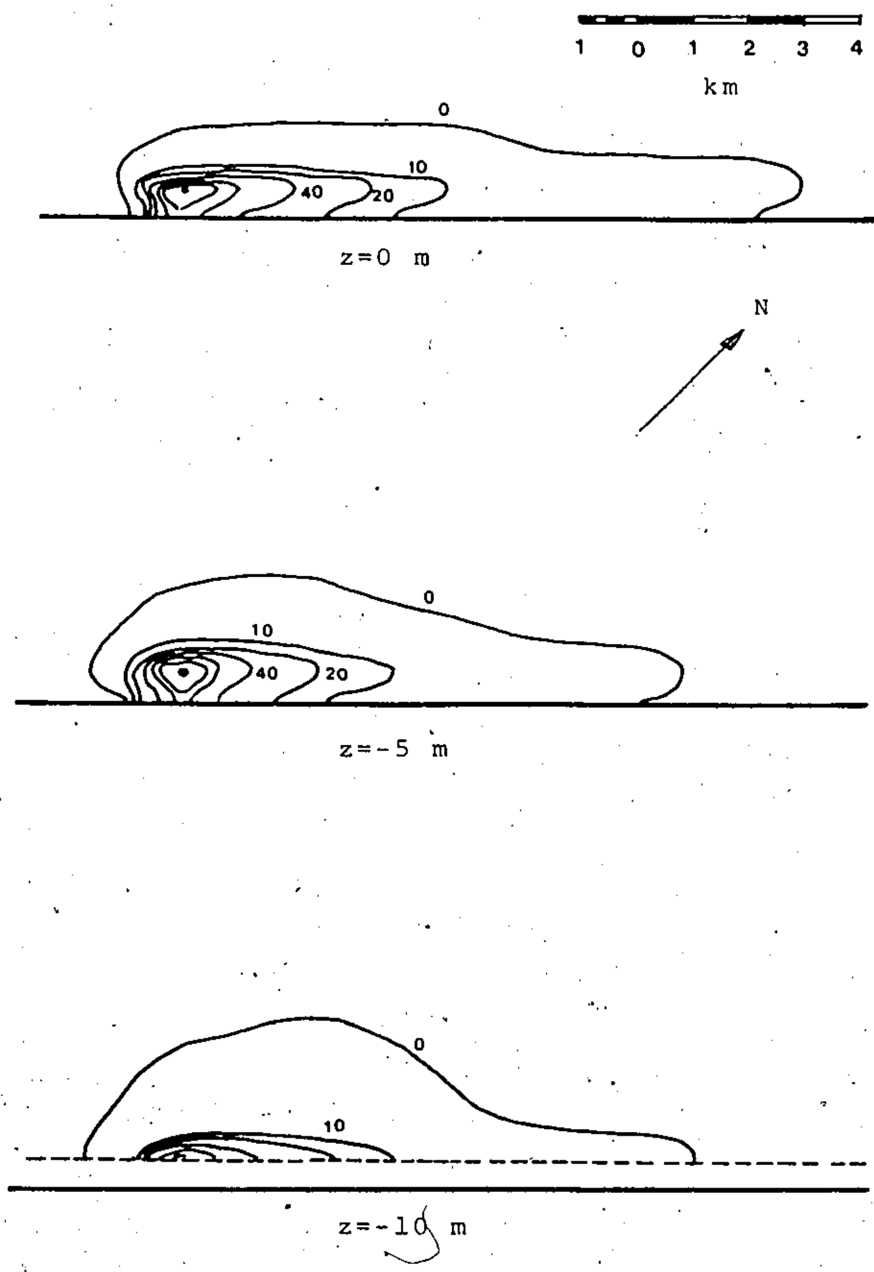

Figure 6.45 Computed SSC plume at 18:00 hours on August 24, 1979, vertical line source at 0.5 km offshore and particle size of 0.02 mm.

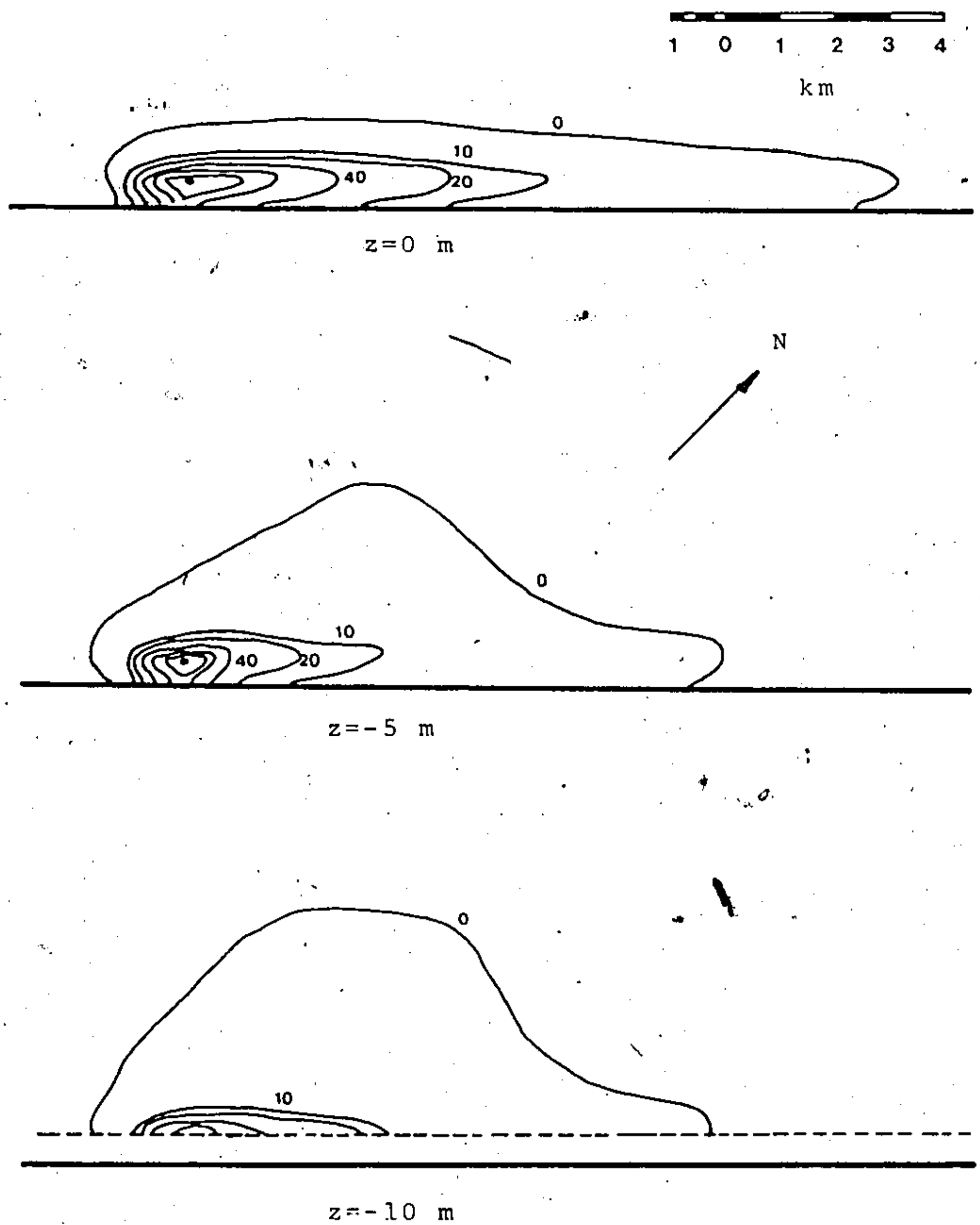

Figure 6.46 Computed SSC plume at 18:00 hours on August 24, 1979, vertical line source at 0.5 km offshore and particle size of 0.005 mm.

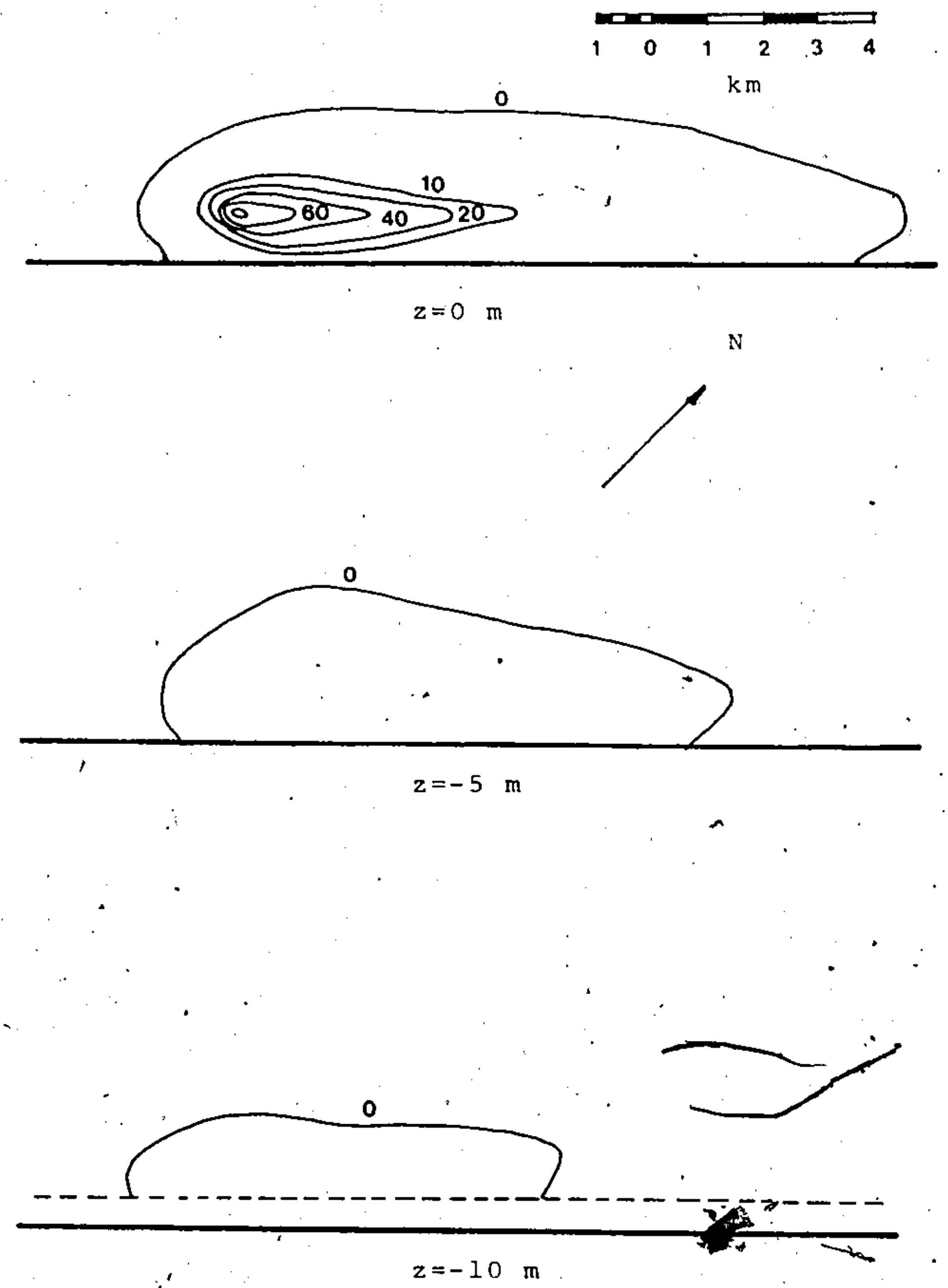

Figure 6.47 Neutral density plume at 18:00 hours on August 24, 1979, point source at 1 km offshore.

up to 3 km offshore) is plotted in Figure 6.48. The lines of constant percentage of source concentration represent the zone of effective pollution, for example in the region between the 10% line and the shoreline, the 10% concentration may be found for any flow regime that may exist and for any conservative (neutral or heavier density) substance. The same results were used again to find the spatial distribution of the sediment particle sizes across the coastal boundary layer. Figure 6.49 shows the settling areas of the three previous particle sizes. The results are in agreement with the distribution of percent-size fraction in surficial sediment in Lake Erie (Thomas et al., 1976) where the surficial sediment grain size distribution is about 80% sand and 20% silt up to 7 km off Cleveland and more than 60% clay beyond 15 km offshore.

To fully validate a water quality model such as SEDTRAN, pollutant sampling is recommended over an area similar to that given in Figure 6.48, but at horizontal and vertical incremental distances of the order of 1 to 8 km and 3 to 5 meters respectively. The horizontal distances offshore should follow the contour lines given in Figure 6.48. The sampling stations should to form transects parallel, 45 degrees and perpendicular to the shoreline. The observations must be frequent to cover different flow regimes and loading activities.

6.8 DISCUSSION AND CONCLUSIONS

Several typical sediment-related activities which may take place in the coastal boundary layer were simulated using ERCH and SEDTRAN (river flow to the coastal zone, continuous dredging and instantaneous

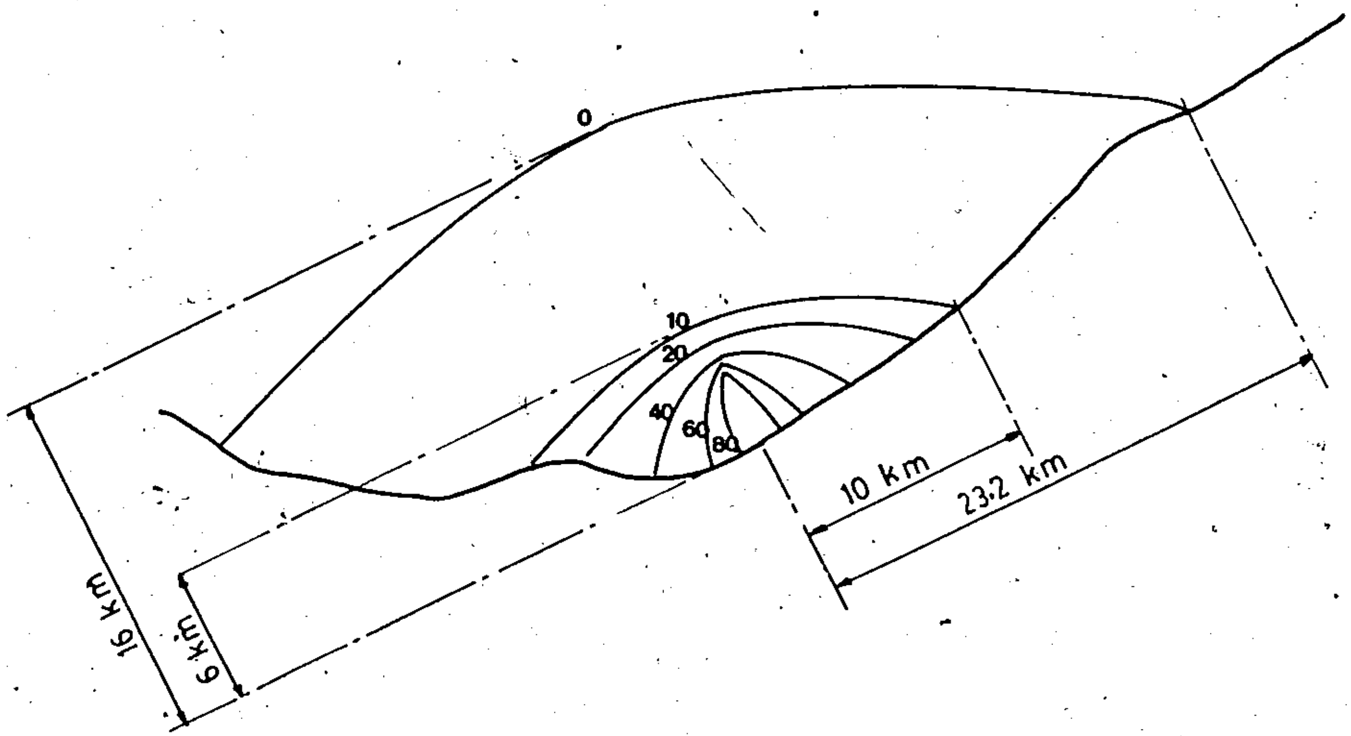

Figure 6.48 Influence zone of a source within 3 km offshore distance.

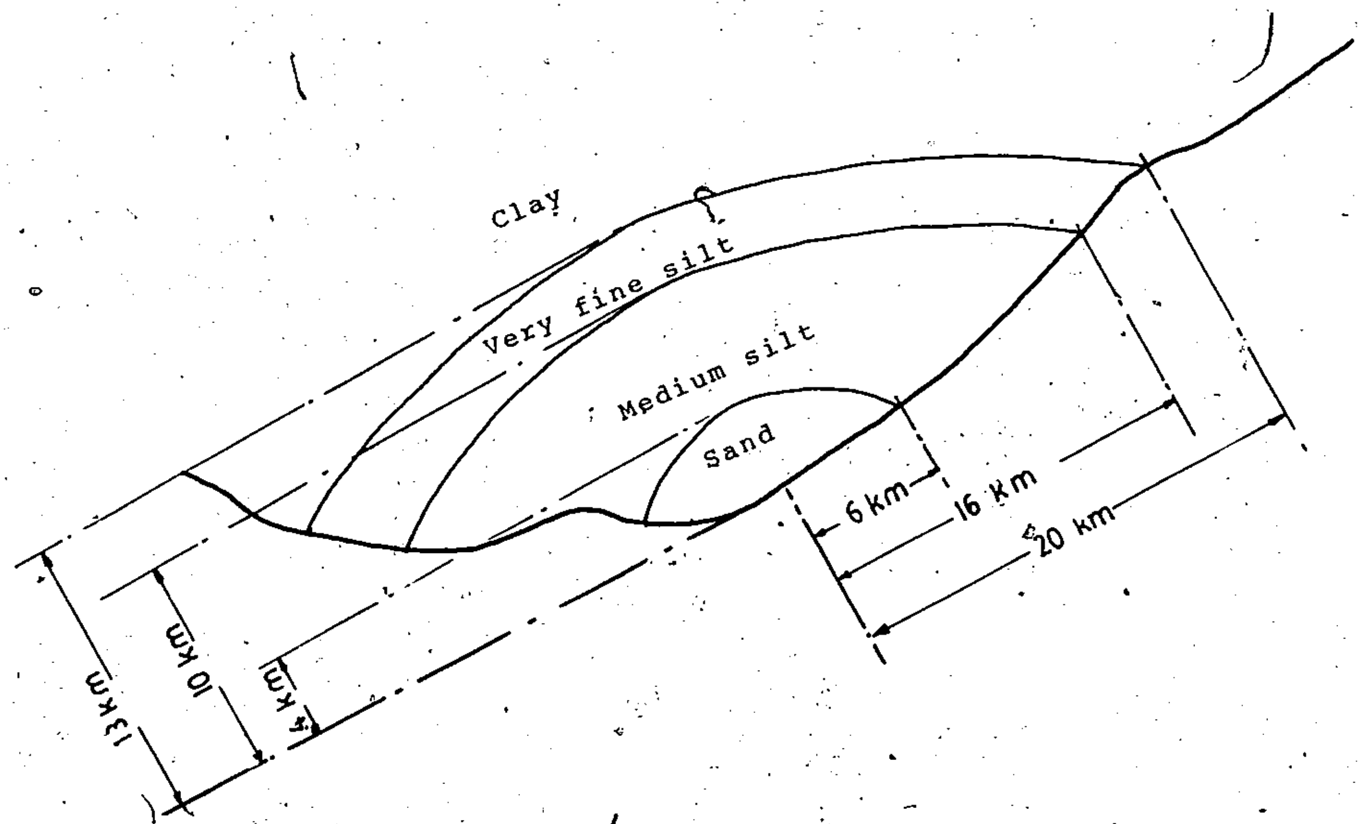

Figure 6.49 Spatial distribution of sediment grain sizes within the coastal boundary layer off Cleveland.

sediment dumping). All the cases were simulated in the nearshore area (within 3 km offshore). The suspended sediment concentration to a minimum value of 0.1% of the source concentration was tracked. The simulation included all the possible current combinations for the three typical sediment grain sizes: very fine silt, medium silt and fine sand. The results showed that, in most cases, concentrations more than 10% of the source concentration extended only to about 1/2 of the total plume length or width. The plume shape and dimensions were not constant at all depths, due to the vertical variability of the currents. The maximum distance of travel in the alongshore direction was at the surface, and was caused by the maximum near-surface shore-parallel current. The maximum penetration across the coastal zone was not always at the surface, especially in the cases of downwelling, where the offshore component takes place at depth. The maximum shore concentrations were due to the river sources. Figures 6.48 and 6.49 should prove useful for the design of offshore or nearshore projects such as a water treatment plant, recreation areas, harbour maintenance and nearshore dredging or dumping.

CHAPTER 7

SUMMARY AND CONCLUSIONS

Discharges into the coastal zones of the Great Lakes contain contaminated particulate and other materials of density greater than or equal to that of the lake water. The dynamic behavior of these particles in the coastal and offshore water is basic to an understanding of the removal processes (transport and particle settling). This study focuses on the effect of nearshore currents, diffusion and temperature patterns on these transport and removal processes. To the authors' knowledge, this is the first attempt to apply 3-dimensional transient mass transport model within the coastal boundary layer.

The dissertation is divided into three interrelated topics: (i) data analyses, (ii) hydrodynamic modelling, and (iii) transport modelling. The significant findings obtained in each part are listed below.

1. Data analysis

Wind, current and temperature data collected off Cleveland were subjected to detailed analyses. A computer program called ADVDIFF was developed to calculate the mean flow, horizontal turbulent length and time scales, horizontal diffusivities and kinetic energy. The program uses filtering techniques, spectral analyses and statistical analyses. Five episodes representing three different flow regimes which may exist in the coastal zone were chosen for the special analyses.

The results showed that the important time and length scales were

4900 seconds and 200 meters respectively. Coastal boundary layer characteristics were exhibited during strong shore-parallel episodes. The results showed an inner coastal boundary layer dominated by bottom and shore friction extending about 14 km from the shore. The entire coastal boundary layer extended over an offshore distance of 30 km or so. The shore-parallel exchange coefficients were greater than for onshore/offshore by a factor of six, indicating anisotropic turbulence structure in the coastal boundary layer. The regression equation obtained from plotting the diffusion coefficient against diffusion length-scale showed that linear length scale diffusion governs the diffusion in the coastal zone off Cleveland.

2. Hydrodynamic models

To generate coastal currents, a rigid-lid channel-type model was used with variable grid size, finer size nearshore. A mdoel originally developed by Simons (1983) was modified to include (a) nonlinear acceleration terms, and (b) two different forms of the vertical eddy viscosity, representing two different hypotheses for vertical transfer of momentum. The modified model is called ERCH. A two dimensional x-y model developed by Simons and Lam (1982) was also modified and used to justify part of the observations. This modified model is called ONELAY.

The hypothesis representing the effects of the wind and the surface and internal waves in the vertical eddy viscocity formulation gave better results than that representing only the wind. In the coastal zone the length scale decreases and the velocity and the velocity gradient increase rapidly, indicating the importance of the nonlinear acceleration term. Including the nonlinear acceleration terms in ERCH caused a reductions of up to 6 cm/s and 11 cm/s in the u and v components respectively. The results obtained by ERCH were in agreement with observations except in the case of a strong wind impulse from north-northeast. ONELAY gave better results than ERCH, but was still deemed to be inadequate for this study. ONELAY predicts the vertically integrated lake circulation during nonstratified periods.

3. Transport model

A computer program (SEDTRAN) was developed to predict sediment concentration distribution within the coastal boundary layer. To the authors' knowledge, SEDTRAN is the first 3-D transient mass transport model to use typical episodes of coastal currents in developing the temporal and spatial distribution of pollutants. SEDTRAN solves numerically the three dimensional time dependent mass transport equation including the settling term, using upwind finite difference with flux-corrected transport (UDS+FCT) for the advection terms. The model was verified against many numerical test examples, and partially validated using the available data set. The results showed that the artificial diffusion introduced by UDS is one order of magnitude higher than the actual diffusion. The UDS+FCT algorithm removed up to 75% of the error.

SEDTRAN was applied to certain cases of sediment acvtivity that may take place in the coastal zone. The results were used to define a representative zone influenced by a nearshore source. In most cases concentrations of more than 10% of the source concentration extended only up to about 1/2 of the total length and width of the plume. The plume shape and dimensions were not constant with depth due to the vertical variation of the horizontal currents. The maximum penetration of the plume across the coastal zone was not always at the surface, especially in downwelling cases where the offshore component takes place at depth. The maximum shore concentrations were computed for a river source. For any flow regime that may exist in the coastal boundary layer off Cleveland, the influence zone of a conservative (neutral or heavier density) substance from a source within 3 km offshore, extends to a maximum of 48 and 16 km along and across the shore respectively. Concentrations down to 0.1% of the source concentration were tracked.

The computation of an influence zone and the grain size spatial distribution by a 3-D transient mass transport model using typical episodes in the coastal boundary layer is a new potential interest to the Great Lakes management.

Recommendations for future research:

(1) Data analysis

This dissertation represents a step towards a comprehensive study of the transport and settling in the coastal zones of the Great Lakes. More research is needed to fully account for all the physical processes within the coastal zones of the Great Lakes.

More field observations within the coastal zones are needed to refine the relation between the Eulerian and Lagrangian frameworks, for example the relation between the Lagrangian and Eulerian correlograms (β coefficient) and the Stokes velocity. To fully validate water quality models within the coastal zones, extensive field programs sampling the different water quality parameters, are needed. Pollutant sampling is recommended over an area similar to that given in Figure 6.48, but at horizontal and vertical distances of the order of 1 to 8 km and 3 to 5 meters respectively. The observations must be frequent to cover different flow regimes and loading activities.

(2) Hydrodynamic models

Further investigation is needed to elucidate why the observed flow is more barotropic than predicted by ERCH and ONELAY. This may indicate that ERCH should be modified to include the spatial variability of the wind.

(3) Transport model

The sediment transport model (SEDTRAN) needs further improvement to include sediment resuspension processes and the length scale dependent diffusion coefficient. Finally, similar studies (all three phases covered) in this study should be applied to different coastal sites in the Great Lakes.

BIBLIOGRAPHY

Ahn, C.S. and P.F. Smith, 1972: "The first report of a study to forcast nuclear power plantseffects on oastal zones", U.S. Govt. printing Office Washington D.C.

Bishop, P.L., 1983: "Marine pollution and its control", McGraw-Hill Book Company.

Bengtsson, L., 1976: "Stocastic modelling of dispersion in the Lulea River", Sartryck Proc. 2nd IAHR conference: Stocastic Hydraulics, Lund.

Bengtsson, L., 1973: "Mathematical models of wind-induced circulation in a lake", Proc. Int. Symp. on Hudrology of lakes, Helsinki, 312-320.

Bengtson, L., 1978: "Wind induced circulation in lakes", Nordic Hydrology, 9:75-94.

Bennett, J.R., 1974: "On the dynamics of wind-driven lake currents", J. Phys. Oceanogr., 4:400-414.

Blanton, J.O., 1973: "Rates of vertical entrainment in stratified lakes", In Proc. Int. Symp. Hydrology of Lakes. Helsinki, Int. Assoc. Hydrol. Sci. Pupl. 109.

Blanton, J.O., 1974: "Some characteristics of nearshore currents along the north shore of Lake Ontario", J. Phys. Oceanogr., 4:415-424.

Blanton, J.O., 1975: "Nearshore lake currents measured during upwelling and downwelling of the thermocline in Lake Ontario", j. Phys. Oceanogr., 5:111-124.

Book, D.L., J.P. Boris and K. Hain, 1975: "Flux-corrected transport II: Generalization of the method", J. Comp. Phys., 18:248-283.

Book, D.L., J.P. Boris and S.T. Zalesak, 1981: "Flux corrected transport in: Finite difference techniques for vectorized fluid dynamics circulations" (ed. D.L. Book), pp. 29-55. Springer-Verlag Belin, 266 p.

Boris, J.P. and D.L. Book, 1973: "Flux-corrected transport I: SHASTA, A fluid transport algorithm that works", J. Comput. Phys. 11:38-69.

Bowden, K.F., Krauel, D.P., and R.E. Lewis, 1974: "Some features of turbulent diffusion from a continuous source at sea", Adv. Geophys., vol 18A, 315-329.

Boyarinov, P.M., 1981: "A case of upwelling in the southern part of Lake

Onega", Meteorologiya i Gidrologiya, 1:72-75.

Boyce, F.M., 1974: "Some aspects of Great Lakes physics of importance to biological and chemical processes", 19th Cong. of the International Association of Limnology (SIL), Winnipeg, Man., p. 689-730.

Boyce, F.M., 1977: "Response of the coastal boundary layer on the north shore of Lake Ontario to a fall storm. J. Phys. Oceanogr", 7:719-732.

Boyce, F.M., 1985: "Personal Communication, February 1985".

Boyce, F.M. and P.F. Hamblin, 1975: "A simple diffusion model of the mean field distribution of soluble material in the Great Lakes",J. Limnology and Oceanography, vol. 20(4) p.511-517.

Boyce, F.M. and C.H. Mortimer, 1978: "IFYGL temperature transects, Lake Ontario, 1972", Dept. Environ. Ottawa Tech. Bull. 100:315 p.

Birchfield, G.E. and D.R. Davidson, 1967: "A case study of coastal currents in Lake Michigan", Proc. 10th Cnf. Great Lakes Res. Un. Mich. Great Lakes Res. Division, 264-273.

Bull, J.A. and R. Farooqui, 1976: "Coastal zone limnological observations in Lake Huron and Bruce Nuclear Power Development, May-November, 1974", CCIW Report No. 17.

Bull, J.A. and D.E. Kaiser, 1980: "Coastal zone limnological observations in Lake ~~Huron~~ near Oshawa, May-November, 1972 and December 1973-March 1974", NWRI Report.

Bull, J.A. and C.R. Murthy, 1980: "Climatology and structure of coastal currents in Lake Ontario during the winter season", NWRI Report.

Callaway, R.J., 1974: " Subsurface horizontal dispersion of pollutants in open coastal waters", International symposium on discharge of sewage from sea outfalls, London.

Chaudri, N.M., 1971: "An improved numerical technique for solving multidimensional miscble displacement equations", Soc. Petrol. Eng. AIME J. 11(3):277-284.

Chen, C.L., 1971: "Sediment dispersion in flow with moving boundaries", J. Hydraulics Div., ASCE, Vol. 97, No. HY8, pp. 1181-1201.

Crank, J. and P. Nicolson, 1976: "A practical method for numerical evaluation of solutions of partial diffrential equations of the heat-conduction type", Proc. of the Cambridge Philosophical Society, 43(50) 50-67.

Csanady, G.T., 1967: "Large-scale motion in the Great Lakes", J. Geophys. Res., 72:4151-4162.

Csanady, G.T., 1968: "Wind-driven summer circulation in the Great Lakes", J. Geophys. Res., 73:2579-2589.

Csanady, G.T., 1972a: "Frictional currents in the mixed layer at the sea surface", J. Phys. Ocenogr., 1:263-270.

Csanady, G.T., 1972b: "The coastal boundary layer in Lake Ontario, Part II: The Summer-Fall Regime", J. Phys. Oceanogr., 2:168-176.

Csanady, G.T., 1972c: "Response of large stratified lakes to wind", J. Phys. Oceanogr., 2:3-13.

Csanady, G.T., 1973: "Turbulent diffusion in the environment", D. Reidel Publishing Company, Holland, 248 p.

Einstein, H.A., 1950: "The bed-load function for sediment transportation in open channel flows", U.S. Dep. Agric., Soil Conserv. Serv., T.B. No. 1026.

Ekman, V.W., 1905: "On the influence of the earth's rotation on ocean currents", Ark. Mat. Astron. Fys., Roy. Swed. Acad. Sci., 2(11):1-52.

Elzawahry, A.E., 1981: "Transient sediment deposition and resuspension in one-dimensional zone between an outfall and a recieving water", M.Eng. Thesis, McMaster University, Hamilton, Ontario, Canada., 146 p.

Elzawahary, A.E. and W. James, 1982: "Lake Erie winds, currents and temperatures in the vicinity of Cleveland, Ohio, May-December, 1979", Report to NWRI, Burlington, CHI publications.

Falkenmark, M., 1973: "Dynamic studies in Lake Velen", Int. Hydrological Decade, Sweden rep. 31.

Fischer, H.B., E.J. List, R.C.Y. Koh, J. Imberger and N.H. Brooks, 1979: "Mixing in inland and coastal waters", Acadimic Press, N.Y., 483 p.

Gedney, R.T., 1971: "Numerical calculations of wind-driven currents in Lake Erie", Ph.D. thesis, Case Western Reserve University, Cleveland, Ohio. 258 pp.

Gedney, R.T. and W. Lick, 1972: "Wind-driven Lake currents in Lake Erie", J. Geophys. Res., 77:2714-2723.

Gedney, R.T., W. Lick and F.B. Molls, 1973: "A simplified stratified lake model for determining effects of wind variation and eddy diffusivity", In Proc. 16th Conf. Great Lakes Res., 710-722, Int. Ass. Great Lakes Res., Ann Arbor, Michigan.

Gonella, J., 1971: "The drift current from observations made on the Bouee Laboratorie", Cah. Oceanogr., 23:19-33.

George,J.A. and R.B. Simpson, 1979: "The Waterloo finite element package, User's Guide. Rep. Proj. No. 606-03-03, Waterloo Res. Institute, U. of Waterloo, Ontario.

Graham, R.J., 1963: "Determination and analysis of a numerical smoothing weight", NASATR R-179, 28 p.

Hakanson. L., 1982: "Lake bottom dynamics morphometry: The dynamic ratio", Water Resources Res. Vol. 18 , No. 5:1444-1450

Happel, J. and H. Brenner, 1973: "Low Reynolds number hydrodynamics", Noordhoff International Publishing, Leyden, The Netherlands.

Hay, J.S. and F. Pasquill, 1959: "Diffusion from a continuous source in relation to the spectrum and the scale of turbulence", Adv. Geophys., 1959, 6, 345-364.

Healy, P.M., B.H. Moore and F.H. Don, 1980: "An operations summary; Lake Erie physics, 1979", NWRI unpublished report, 102 pp.

Heinrich, J., W. Lick and J. Paul, 1981: "Temperatures and currents in a stratified lake: a two dimensional analysis", J. Great Lakes Res., 7(3):264-275.

Hino, M., 1963: "Turbulent flow with suspended particles", Journal of the Hydraulics Division, ASCE, Vol. 89, No. Hy4, Proc. Paper 3579, pp. 161-185.

Hollan, E. and T.J. Simons, 1978: "Wind-induced changes of temperature and currents in Lake Constance", Arch. Meteor. Geophys. Bioklimatol., A27:333-373.

Howarth, M.J., 1981: "Instruments and methods", Deep-Sea Res. Vol. 28A, 601-607.

Hutter, K., Mysak, L.A., Heaps, N.S., Sunderman, J., Kielmann, J, Simons, T.J. and Mortimor, C.H., 1983: "Hydrodynamics of lakes", Springler-Verlag, N.Y.

James, W., 1978: "Developing hydraulics computer program", CHI Publication, Hamilton, Ontario, Canada.

James, W. and B. Eid, 1978: "A three-dimensional model of Hamilton harbour Incorporating spatial distribution of transient surface drag", Canadian J. of Civil Eng. CSCE, 5(4):479-488.

James, w. and A.E. Elzawahry, 1981: "Transient sediment deposition and resuspension in one-dimensional zone between an outfall and a recieving water", Proc. SWMM Users Group Meeting January 19-20, 1981, Austin, Texas.

Jordan, D.E. and J.A. Bull, 1977: "Coastal zone limnological observations in Lake Ontario at Bronte. June 1973-March 1974", CCIW Paper No. 18.

Jones, R.A., 1957: "A preliminary examination of the spectrum and scale of the vertical component at 2000 ft." Meteorol. Res. Committee (Londen), MRP. No. 1044.

Kaiser, D.E. and J.A. Bull, 1978: "Coastal zone limnological observations in Georgian Bay near Byng Inlet, November 1975 - November 1976", CCIW Paper No. 19.

Karamchandani, P. and L.K. Peters, 1983: "Analysis of the error associated with grid representation of point sources", Atmospheric Environment, 17(5):927-933.

Keller, H.B., 1971: "A new difference scheme for parabolic problems", B. Hummard ed., Acadimic Press, N.Y., pp 327-350.

Ketchum, B.H. and D.J. Keen, 1955: "The accumulation of river water over the continental shelf between Cape Cod and Chesapeak Bay", Deep-Sea Res. 3(suppl): 316-357.

Konyayeve, K.V. and G.I. Merinova, 1983: "Ocean-current spectra determined from the tracks of free-drifting floats in the POLYMODE experiment", Izvestiya, Atmospheric and Oceanic Physics, vol 19, No. 10.

Krasnoff, J.O. and R.L. Peskin,1971: "The Langevin model for turbulent diffusion", Geophysi. Fluid dynamics,2,123-146.

Kuehnel, R.O.W., C.R. Murthy, K.C. Miners, B. Kohli and Y. Hamdy, 1981: "A coastal dispersion model for effluent plumes", NWRI report, 128 pp.

Kullenberg, G., 1969: "Measurements of horizontal and vertical diffusion in coastal waters", Kungl. Vetenskaps- och Vitterhets-Samhallet Acta Geoph. 2 Goteborg, 52 pp.

Kullenberg, G., 1971: "Vertical diffusion in shallow waters", Tellus 23, 2:129-135.

Kullenberg G., C.R. Murthy and H. Westerberg, 1974: "Vertical mixing characteristics in the thrmocline and hypolimnion regions of Lake Ontario (IFYGL)", Proc. 17th Conf. Grat Lakes Res., 425-434.

Lam, D.C.L., 1976: "Comparison of finite-element and finite-difference methods for nearshore advection-diffusion transport models", Finite element in Water Resources, Gray et al., Princeton University, N.J., p. 1.15-1.29.

Lam, D.C.L. and R.W. Durham, 1984: "Finite element analysis of radioactive tritium patch and a waste heat plume observed near the Pickering nuclear power generating station, Lake Ontario", J. Grat Lakes Res. 10(1):59-67.

Lam, D.C.L. and C.R. Murthy, 1978: "Outfall diffusion models for the coastal zone", Proc. 16th Coastal Engineering Conf., Hamburg, Germany, A.S.C.E., N.Y., p. 2584-2597.

Lam, D.C.L., C.R. Murthy and K.C. Miners, 1981: "An inverse problem approach to modelling coastal effluent plumes", Adv. Water Resources, 4:185-190.

Lam, D.C.L., W.M. Schertzer and A.S. Fraser, 1983: "Simulation of Lake Erie water quality responses to loading and weather variations", Environment Canada, Inland Waters Directorat, Sci Ser No. 134, Ottawa, Ontario.

Lam, D.C.L., C.R. Murthy and R.B. Simpson, 1984: "Lecture notes on coastal and estuarine studies", Springer-Verlag publication, N.Y.

Lam, D,C.L. and T.J. Simons, 1976: "Numerical computaions of advection and diffusive transports of chloride in Lake Erie, 1970", J. Fish. Res. Board Can. 33:537-549.

Langlois, W.E., 1964: "Slow viscous flow", MacMillan, N.Y.

Liggett, J.J. and C. Hadjitheodorn, 1969: "Circulation in shallow homogeneous lakes", J. Hydr. Div., ASCE, 95, HY2, pp. 609-620.

Longuet-Higgins, M.S., 1969: "On the transport of mass by time-varying ocean currents", Deep-Sea Res., 16:431-447.

Martin, H.C. and G.F. Carey, 1973: "Introduction to finite-element analysis", McGraw-Hill, N.Y.

McNown, J.C. and P.N. Lin: "Sediment concentration and fall velocity", Proc. 2nd Midwestern Conf. on Fluid Mechanics, Ohio State University, Columbus, Ohio, pp. 401-411.

Masinger, F. and A. Arakawa, 1976: "Numerical methods used in atmospheric models", GARP Publ. Ser. No. 17 (W.M.O.) 64 p.

Molinari, R. and A.D. Kirwan, 1975: "Calculations of diffrential kinematic properties from Lagrangian observations in the western Caribbean Sea", J. Phys. Ocean. 5:461-368.

Munk, W.H. and E.K. Anderson, 1948: "Notes on the theory of thermocline", J. Mar. Res. 7:276-295.

Murthy, C.R., 1971: "An investigation of diffusion characteristics of the hypolimnion of Lake Erie", Proc. 14th Conf. Great Lakes Res.

Murthy, C.R., 1972: "Complex diffusion processes in coastal currents of a lake", J. Phys. Ocean., 2:80-90.

Murthy, C.R., 1973: "Horizontal diffusion in lake currents", Hydrology of lakes, International association for Great Lakes Res., p. 327-334.

Murthy, C.R., 1976: "Horizontal diffusion characteristics in Lake Ontario", J. Phys. Ocean., 6: 76-84.

Murthy, C.R. and B.C. Kenney, 1974: "Diffusion in coastal currents of large lakes", Rapp. P.-V. Reun. Cons. Int. Explor. Mer, 167:111-120.

Murthy, C.R. and J.O. Blanton, 1975: "Coastal zone climatological studies of the Laurentian Great Lakes", Proc. 2nd World Congress, Int. Water Resources Assoc., New Delhi, 5:431-448.

Murthy, C.R. and K.C. Miners, 1978: "Turbulent diffusion processes in the Great Lakes", Sci. Ser. 83:27, Inland Water Directorat, Dept. of The Environment, Ottawa.

Murthy, C.R. and D.S. Dunbar, 1981: "Structure of the flow within the coastal boundary layer of the Great Lakes", J. Phys. Oceanogr., 11:1567-1577.

Okubo, A., 1970: "Horizontal dispersion of flotable particles in the vicinity of velocity singularities such as convergences", Deep-Sea Res. Vol. 17, p. 445-454.

Okubo, A., 1971: "Remarks on the use of diffusion diagrams in modeling scale-dependent diffusion", Deep-Sea Res., 23:1213-1214.

Okubo, A., 1976: "Determination of Lagrangian deformations from analysis of current followers", J. Phys. Ocean., vol. 6, p. 524-527.

Okubo, A. and C.C. Ebbesmeyer, 1976: "Determination of vortocity divergence and deformation rates from analysis of drogue observations", Deep-Sea Res., 23:349-352.

Okubo, A., 1974: "Some speculations on oceanic diffusion diagrams", Rapp. P.-v. Reun cons. Int. Explor. Mer, 167:77-85.

Paul, J.F. and W. Lick, 1974: "A numerical model of thermal plumes and river discharges", In Proc. 17th Conf. Great Lakes Res., Int. Assoc. Great Lakes Research, pp.445-455.

Paul, J.F. and W, Lick, 1981: "A numerical model for three-dimensional, variable-density hydrodynamic flows, U.S. Environmental Protection Agency Report.

Pasquill, F.,1962: "Atmospheric diffusion", D. Van Norstrand Company Lt., London, England.

Platzman, G.W., 1963: "The dynamic prediction of wind tides on Lake Erie", Meteorol. Monogr. 4(26): 44 pp.

Peyret, R. and T.D. Taylor, 1981: "Computational methods in fluid flow", Springer- Verlag Berlin, 358 p.

Pollard, R.T. and R.C. Millard JR., 1970: "Comparison between observed and simulated wind generated inertial oscillations", Deep-Sea Res., 17:813-822.

Price, H.S., J.C. Cavendish and R.S. Varga, 1968: "Numerical methods of higher-order accuracy for diffusion-convection equations", Soc. Petrol. Eng. J., 243(3):293-303.

Proudman T. and J.R.A. Pearson, 1957: "Expansions at small Reynolds number for the flow past a sphere and a circular cylinder", J. Fluid Mech., 2:237.

Richards, R.P., 1981: "Chemical limnology in the nearshore zone of Lake Erie between Vermilion, Ohio and Ashtabula, Ohio, 1978-1979", HCWQL report, Ohio, USA.

Richtmyer, R.D., 1963: "A survey of difference methods for nonsteady fluid dynamics", NCAR technical note 63-2, Boulder, Colorado.

Richtmyer, R.D. and K.W. Morton, 1967: "Difference methods for initial-value problems", Second Edition, Interscience Publishers, J.Wiley and Sons, N.Y.

Roache, P.J., 1972: "Computational fluid dynamics", Hermosa publishers, Albuquerque, N.M.

Rouse, H., 1937: "Nomogram for the settling velocity of spheres", Division of Geology and Geography, Exhibit D of the report of the Commission on Sedimentation, 1936-37, National Research Council Washington D.C., pp 57-64.

Sasaki, Y., 1970: "Some basic formalisms in numerical variational analysis", Mon. Weather Rev., 98:875-883.

Saylor, J.H. and G.S. Miller, 1983: "Investigation of the current and density structure of Lake Erie", NOAA Technical Momerandum ERL GLERL-49.

Sherman, C.A., 1976: "A mass-consistent model for wind fields over complex terrain", UCRL-76171, Livermore, Cal.

Siemons, J., 1970: "Numerical methods for the solution of diffusion-advection equations", Publ. 88, pp. 1-32, Delft Hydraul. Lab., the Netherlands.

Simons, D.B. and F. Senturk, 1977: "Sediment transport technology", Water Resources Publications, Colorado, USA.

Simons, T.J., 1971: "Development of numerical models of Lake Ontario", Proc. 14th Conf. Great Lakes Res. Int. Assoc. Great Lakes Res., pp. 654-669.

Simons, T.J., 1972: "Development of numerical model of Lake Ontario, Part 2", 15th Conf. Great Lakes Res. Int. Aassoc. Great Lakes Res.

Simons, T.J., 1973a: "Comparison of observed and computed currents in Lake Ontario during Hurrican Agnes, June, 1972", In Proc. 16th Conf. Great Lakes Res., IAGLR, 16:831-844.

Simons, T.J., 1973b: "Development of three-dimensional numerical models of the Great Lakes", Scientific Report No. 12, CCIW, Burlington, Ontario.

Simons, T.J., 1974: "Verification of numerical models of Lake Ontario: Part I Circulation in Spring and Early Summer", J. Phys. Oceanogr. 4:507-523.

Simons, T.J., 1976: "Continuous dynamical computation of water transport in lake Erie for 1970", J. Fish. Res. Board Can., 33:371-384.

Simons, T.J., 1980a: "Verification of seasonal stratification models", Departmental report, Institute for meteorology and Oceanography, University of Utrecht, the Netherlands, 12 pp.

Simons, T.J., 1980b: "Circulation models of lakes and inland seas", Can. Bull. Fish. Aquat. SCI.203:146p.

Simons, T.J., 1983: "Pesonal communication, Fortran Coding of Channel-type model"

Simons, T.J. and D.C.L. Lam, 1980: "Some limitations of water quality models for large lakes: a case study of Lake Ontario", Water Resour. Res., 16:105-116.

Simons, T.J., and D.C.L. Lam, 1982: "Documentation of a two-dimensional x-y model package for computing circulation and pollutant transport", Lecture notes of course CE754, McMaster University, Hamilton, Ontario.

Simons, T.J., F.M. Boyce, A.S. Fraser, E. Halfon, D. Hyde, D.C.L. Lam, W.M. Schertzer, A.H. El-Shaarawai, K. Wilson and D. Warry, 1979: "Assessment of water [illegible]lity simulation capability for Lake Ontario" Environment Canada, [illegible] Water Directorate, Sci. Ser. No. 111, Ottawa, Ontario, 220 p.

Simpson, R.B., 1981: "[illegible]PACK implementations using external storage for Crank Nicolson and extrapolated backwards Euler method", Rep. Proj. No.

004-20, Waterloo Research Institute, U. of Waterloo, Ontario.

Smith, R.L., 1974: "A description of current, wind and sea/level variations during coastal upwelling off the Oregon coast, July-August, 1972", J. Geophys. Res., 79:435-443.

Smith, I.M., R.V. Faraday and B.A. O'Connor: "Rayleigh-Ritz and Galerkin finite element for diffusion-convection problems", Water Resources Res., 9(3):593-606.

Snodgrass, W.J. and C.R. O'Melia, 1975: "Predictive model for phosphours in lakes", Environmental Science and Technology, 9:937-943.

Stokes, G.G., 1874: "On the theory of oscillatory waves", Trans. Cambridge Phil. Soc., 8:441-445.

Taylor, G.R., 1921: "Diffusion by continuous movements", Proc. London Math. Soc., Ser.2,20,196.

Thomas, R.L., J.-M. Maquer and A.L.W. Kemp, 1976: "Surficial sediment of Lake Erie", J. Fish. Res. Board Can. 33:385-403.

Tukey, J.W., 1950: "The sampling theory of power spectrum estimates", Symp. Application of Autocorrelation Analysis to Physical Problems, Woods Hole, Mass., Office of Naval Research, Washington, D.C.

Vasseur, B., L. Funkquist and J.F. Paul, 1980: "Verification of a numerical model for thermal plumes", Sverigeo Meteorolgiska och Hydrologiska Institute, ISSN 0347-7827, Norrkoping Sweden.

Vollenweider, R.a., 1975: "Input-output models", Schweiz Z. Hydrol, 37:53-84.

Watters, R.Z., G.F. Carey and D.F. Winter, 1978: "Temperature computation for temporate lakes", Appl. Math. Modelling, 2:41-48.

Weenink, M.P. and P. Groen, 1958: "A semi-theoretical, semi-empirical approach to the problem of finding wind effects on water levels in a shallow partly-enclosed sea", Konink1. Ned. Akad. Wetenschap. Proc., B61, 198-213 (Summarized on p. 632 of Groen, P. and W. Groves, 1962: "Surges. The Sea, Vol. I, M. N. Hill, Ed. N.Y., Interscience.)

Wellander, P., 1957: "Wind action on shallow sea, some generalizations of Ekman's theory", Tellus 9:47-52.

Zaltev, R., R. Berkowicz and L.P. Prahm, 1983: "Testing subroutines solving advection-diffusion equations in atmospheric environments", Computer and fluids, Vol 11, 1:13-38.

APPENDICES

APPENDIX A

ENERGY SPECTRUM

The Eulerian energy spectrum can be obtained from the correlogram ($R_E(t)$ vs t) by the Fourier transform relation,

$$F(n) = 4\int R_E(t).\cos 2\pi nt.dt \qquad (/cps)$$

or

$$E(n) = 4\,\overline{u^2} \int R_E(t).\cos 2\pi nt.dt \qquad (cm^2\ s^{-2}/cps) \qquad [A.1]$$

where the plot of F(n) against n forms the energy spectrum curve and E(n) against n may be refered to as spectral density.

For N observations of x_i with averaging interval Δt, the first step is to form covariances Q_k of the values x_i (i=1,1,3,...,N) for successive values of lag $k\Delta t$, as follows,

$$Q_k = \frac{1}{N-k}\left[\sum_{i=1}^{N-k} x_i x_{ik} - \frac{1}{N-k}\sum_{i=1}^{N-k} x_i \sum_{i=1}^{N-k} x_{i+k}\right] \qquad k=0,1,\ldots,m \qquad [A.2]$$

Since Q_k is known only at the m+1 specific lags it follows that the spectrum is determined only for specific frequency bands centred at n=0, $1/2m\Delta t$, $2/m\Delta t$,...., $1/2\Delta t$. The fourier transform of [A.1] is accordingly evaluated in series form, with frequency n replaced by $h/2m\Delta t$ and time-lag t by $k\Delta t$, as follows:

$$L_0 = \frac{1}{2m}[Q_0 + Q_m] + \frac{1}{m}\sum_{k=1}^{m-1} Q_k$$

$$L_h = \frac{1}{m} Q_0 + \frac{2}{m} \sum_{k=1}^{m-1} Q_k \cos \frac{kh\pi}{m} + \frac{1}{m} Q_m \cos \pi h$$

$$h = 1,2,\ldots,(m-1)$$

$$L_m = \frac{1}{2m} [Q_0 + (-1)^m Q_m] + \frac{1}{m} \sum_{k=1}^{m-1} (-1)^k Q_k \qquad [A.3]$$

in which it is implicit that $\sum_{h=0}^{m} L_h$ is equal to Q_0, the variance of the series.

The quantities L_h are related to F(n) by the equation

$$L_h = F(n) Q_0 \Delta t \qquad [A.4]$$

where $\Delta n = 1/4m\Delta t$ for the end values (L_0, L_m), otherwise $\Delta n = 1/2m\Delta t$.

The values of L are smoothed by means of a 3-term weighted average (Tukey, 1950) as follows:

$$U_0 = 0.54L_0 + 0.64L_1$$
$$U_h = 0.54L_h + 0.23(L_{h-1} + L_{h+1}) \quad \text{for } h = 1,2,\ldots,(m-1)$$
$$U_m = 0.54L_m + 0.46L_{m-1} \qquad [A.5]$$

Tukey (1950) suggested that the number of lags be small enough that $m < N/15$ where $6 < m < 30$.

APPENDIX B

LOW-PASS FILTER

Graham (1963) designed a low-pass filter with the following functional definition:

$$H(\omega) = H(-\omega)$$

$$H(\omega) = 0; \quad |\omega| \geq \omega_t \text{ (the termination frequency)}$$

$$H(\omega) = 1; \quad |\omega| \leq \omega_c \text{ (the cuttoff frequency)}$$

$$H(\omega) = \frac{1}{2} \{ \cos [(\frac{\omega_c + \omega}{\Delta \omega}) \pi] + 1 \}; \quad -\omega_t \leq \omega \leq -\omega_c$$

$$H(\omega) = \frac{1}{2} \{ \cos [(\frac{\omega - \omega_c}{\Delta\omega}) \pi] + 1 \}; \quad \omega_c \leq \omega \leq \omega_t$$

$$\Delta\omega = \omega_t - \omega_c \qquad [B.1]$$

where $H(\omega)$ is the gain function of frequencies ($-\infty$ to $+\infty$), $\omega = 2\pi f$, f is is frequency and t is time. The gain function is shown in figure (B.1)

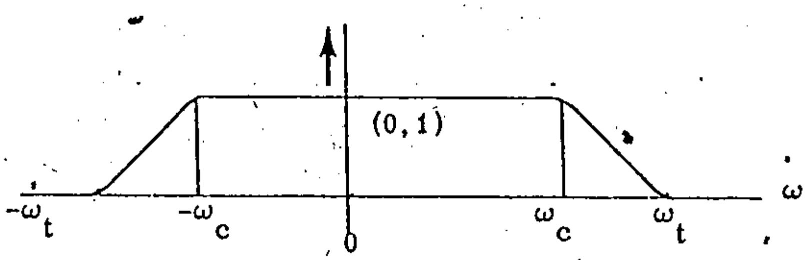

Figure B.1

The inverse Fourier transformation is applied to the basic low-pass filter [B.1] i.e.,

$$h(t) = \frac{1}{2\pi} \int_{-\infty}^{\infty} e^{i\omega t} H(\omega)\, d\omega \qquad [B.2]$$

The weight function derived from the inverse Fourier transformation is defined in time domain to be:

$$h(t) = \frac{\pi}{2t} \; \frac{\sin \omega_t t + \sin \omega_c t}{\pi^2 - (\omega_t - \omega_c)^2\, t^2} \qquad [B.3]$$

This is the basic function from which the numerical smoothing weights are derived. To obtain weights from this function the following constants must be defined:

1. The number of weights desired. This number must be odd.
2. The sampling interval of the data (Δt).
3. The cutoff and termination frequencies (ω_c and ω_t).

To obtain weights evaluate h(t) at distict points, h_n, where $h_n = \Delta t h(t_n)$; $t_n = n\Delta t$; $n= 0, \mp 1, \ldots, \mp N$.

To keep maximum error of the frequency gain in the interval ($0 \leq f \leq f_c$); at approximately 1%, set $N(\Delta t)\,(f_t - f_c) \geq 2$; at approximately 1/2 %, set $N(\Delta t)\,(f_t - f_c) \geq 3$.

The actual functional filter output is given as foloows:

$$H(\omega) = h_0 + 2 \sum_{1}^{N} h_n \cos n\Delta t\omega \qquad [B.5]$$

Figure (B.2) shows the actual functional filter output using n=73, Δt=20 minute, f_t= 0.083 and f_c= 0.0416 cph.

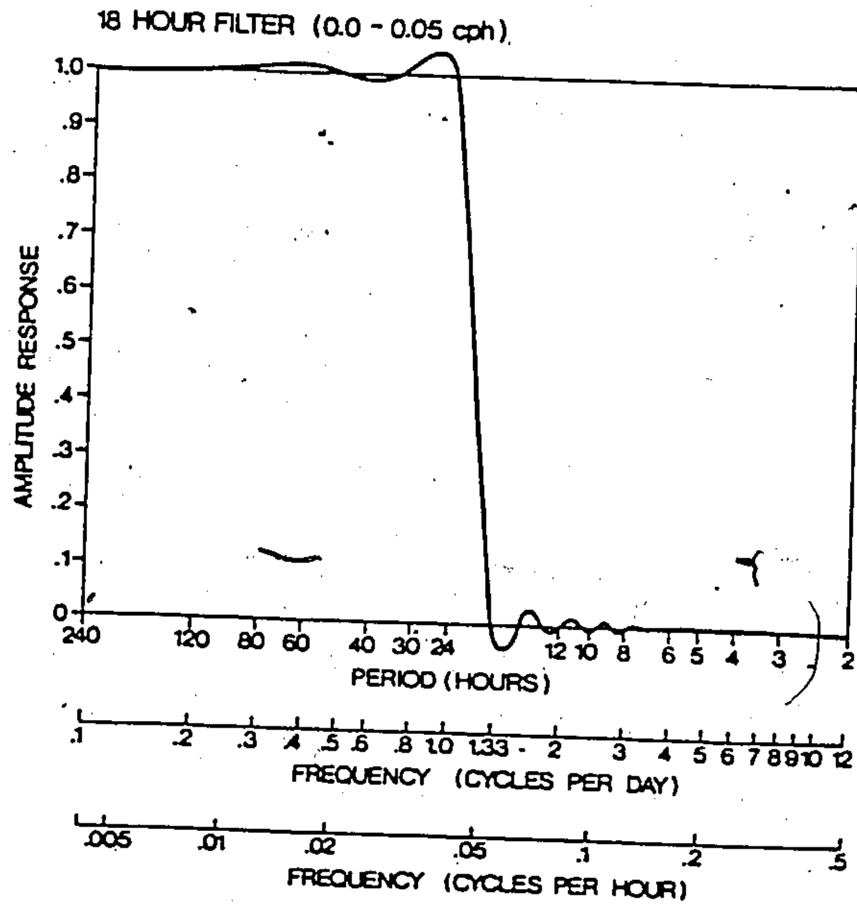
18 HOUR FILTER (0.0 - 0.05 cph)
AMPLITUDE RESPONSE
1.0
.9
.8
.7
.6
.5
.4
.3
.2
.1
0
240 120 80 60 40 30 24 12 10 8 6 5 4 3 2
PERIOD (HOURS)
.1 .2 .3 .4 .5 .6 .8 1.0 1.33 2 3 4 5 6 7 8 9 10 12
FREQUENCY (CYCLES PER DAY)
.005 .01 .02 .05 .1 .2 .5
FREQUENCY (CYCLES PER HOUR)

Figure B.2

APPENDIX C

LIST OF NOTATIONS

a	= diffusion parameter used to define K with the diffusion time.
A	= cross-sectional area of the lake (cm^2)
A_B	= vertical eddy viscosity at lake bottom (cm^2/s)
A_o	= vertical eddy viscocity in the absence of stratification (cm^2/s)
A_s	= surface vertical eddy viscocity (cm^2/s)
A_x, A_y, A_z	= eddy viscocities in the x, y and z directions respectively (cm^2/s)
B	= bottom stress coefficient.
c	= diffusion parameter for length scale diffusion model.
C	= effluent concentration (ppm)
C_1, C_2	= empirical constants.
C_D	= drag coefficient.
Cn	= Courant number.
D	= empirical constant of the same order of magnitude as the wave length of surface wave (cm).
D_s	= sediment particle diameter (mm).
f	= Coriolis parameter (10^{-4} s^{-1})
F	= vertical flux per unit area
g	= gravity acceleration (cm/s^2)
H	= water depth (cm)
i_x, i_y	= turbulence indices in the x and y directions

respectively.

K_s	= surface eddy diffusivity (cm^2/s)
K_x; K_y, K_z	= eddy diffusivities in the x, y and z directions respectively (cm^2/s)
K_{art}	= artificial (numerical) diffusion coefficient (cm^2/s)
L	= length scale of eddy diffusion (cm).
L_s	= length scale calculated by Taylor (1921) assumption (cm)
L_{sx}, L_{sy}	= length scales in the x and y directions respectively (cm)
m	= power index (superscript) used in diffusion time eddy diffusion model.
n	= power index of the length scale diffusion model.
N^2	= Brunt-Vaisala frequency (s^{-2})
p	= pressure ($gm/cm\ s^2$)
p_e	= external (barotropic) pressure ($gm/cm\ s^2$)
p_i	= internal (baroclinic) pressure ($gm/cm\ s^2$)
p_s	= external pressure at air/water interface ($gm/cm\ s^2$)
q	= diffusion velocity (cm/s)
R_E	= Eulerian autocorrelation coefficient.
R_i	= Richardson number.
R_e	= Reynolds cell number.
S	= integrated speed in cm/s^{-1}
t	= time (s)
T	= temperature (^oC)
TC	= subscript denotes valus at thermocline.
T_o	= reference temperature (4 ^oC)

T_s = time scale (s)

T_{sx}, T_{sy} = time scales in the x, y directions respectively (s)

u, v, w = fluid velocities in the x, y and z directions respectively (cm/s).

$\bar{u}$, $\bar{v}$, $\bar{w}$ = mean velocities in the x, y, z directions respectively (cm/s)

u′, v′, w′ = fluctuation velocities in the x, y, z directions respectively (cm/s).

u_o = surface velocity (cm/s)

u_b, v_b = bottom velocities in the x, y directions respectively (cm/s).

U, V = vertically integrated velocities in the x, y directions respectively (cm^2/s^2)

w_s = settling or fall velocity (cm/s)

W = wind speed (m/s)

x, y, z = orthogonal coordinates.

α = thermal expansion coefficient ($^oC^{-2}$)

β = Hay and Pasquill (1959) coefficient.

φ = angle from north to local shore line (degrees)

η = elevation of the water surface above the mean level (cm)

ξ = energy dissipation rate (cm^2/s^3)

ρ = fluid density (gm/cm^3)

ρ_o = reference watewr density at 4^oC.

ρ_s = suspended sediment density (gm/cm^3)

γ = empirical constant.

θ = instantaneous direction of current in degrees measured clockwise from north.

σ	=	the standard deviation of the concentration distribution (cm).
σ_1, σ_2	=	empirical constants.
τ	=	time lag (s)
τ_w	=	wind stress (gm/cm s^2)
τ_{bx}, τ_{by}	=	bottom shear stresses in the x, y direction respectively (cm^2/s^2)
τ_{wx}, τ^{wy}	=	wind shear stresses in the x, y directions respectively (cm^2/s^2)
τ^{zx}	=	shear stress in the x direction across a plane perpendicular to z.
Δx, Δy, Δz	=	spatial increments in the x,y and z directions respectively.
Δt	=	time increment (s)
μ	=	dynamic vescocity of the fluid.